Room-Temperature Deposition of DLC Films by an Ion Beam Method, Reactive Magnetron Sputtering and Pulsed Laser Deposition: Process Design, Film Structure and Film Properties

Mag. rer. nat. Markus Kahn

Being a thesis in partial fulfilment of the requirements for the degree of a

Doctor of Montanistic Sciences (Dr. mont.)

at the University of Leoben

Leoben, November 2009

AFFIDAVIT

I declare in lieu of oath, that I wrote this thesis and performed the associated research myself, using only literature cited in this volume.

Leoben, November 2009

ACKNOWLEDGEMENT

Primary thanks must go to my doctoral thesis supervisor Prof. Dr. Christian Mitterer from the Department of Physical Metallurgy and Materials Testing, University of Leoben for fruitful scientific discussions and the supervision of this thesis. Further thanks go to my company supervisor Dr. Wolfgang Waldhauser and DI Elmar Brandstätter from the Laser Center Leoben for offering me the opportunity of this research position and for scientific discussions. I also thank Prof. Dr. Christian Teichert from the Institute for Physics, University of Leoben, for acting as a referee for this thesis.

For providing analytical facilities and co-authorship in scientific publications I must especially thank Dr. Miha Cekada from Jožef Stefan Institute in Slovenia and Dr. Thomas Schöberl from Erich Schmid Institute of Materials Science of the Austrian Academy of Sciences. Additional thanks for collaboration must go to Dr. Nicola Menegazzo and Prof. Dr. Boris Mizaikoff from the Georgia Institute of Technology, School of Chemistry and Biochemistry. My thanks also go to Dr. Christoph Bauer, Institute of Earth Sciences, Department of Mineralogy and Petrology, University of Graz.

I send my thanks to all colleagues at Laser Center Leoben. I express my particular thanks to Ms. Roswitha Berghauser for her patient assistance with the process equipment and for her friendship.

~

I must thank Miriam Baumgartner for all her love, lenity and support during these years!

Financial support of this work by the Austrian Federal Ministry of Traffic, Innovation and Technology, the Austrian Industrial Research Promotion Fund (FFG), the Government of Styria, Forschung Austria and the European Union is highly acknowledged.

SCIENTIFIC PUBLICATIONS INCLUDED IN THE THESIS

Publication 1:

M. Kahn, M. Cekada, T. Schöberl, R. Berghauser, C. Mitterer, C. Bauer, W. Waldhauser, E. Brandstätter, Structural and mechanical properties of diamond-like carbon films deposited by an anode layer source, Thin Solid Films 517 (2009) 6502.

Publication 2:

M. Kahn, M. Cekada, R. Berghauser, W. Waldhauser, C. Bauer, C. Mitterer, E. Brandstätter, Accurate Raman spectroscopy of diamond-like carbon films deposited by an anode layer source, Diamond Relat. Mater. 17 (2008) 1647.

Publication 3:

M. Kahn, N. Menegazzo, B. Mizaikoff, R. Berghauser, J.M. Lackner, D. Hufnagel, W. Waldhauser, Properties of DLC and nitrogen-doped DLC films deposited by DC magnetron sputtering, Plasma Processes Polym. 4, S1 (2007) 200.

Publication 4:

M. Kahn, M. Cekada, T. Schöberl, H. Parizek, B. Raninger, R. Berghauser, W. Waldhauser, E. Brandstätter, DLC films deposited at room-temperature by reactive magnetron sputtering and by an anode layer source – a comparative study, Proceedings of the 17th Plansee Seminar 2009, Vol. 2, HM 40/1.

Publication 5:

M. Kahn, S. Paskvale, M. Čekada, T. Schöberl, W. Waldhauser, C. Mitterer, E. Brandstätter, P. Pelicon, Relation between structural/topological disorder and mechanical properties of hydrogenated DLC films, *submitted*

Publication 6:

M. Kahn, W. Waldhauser, C. Mitterer, T. Koch, A. Pauschitz, E. Brandstätter, M. Roy, Nanoindentation and nanoscratch behaviour of room-temperature reactive pulsed magnetron sputtered DLC films-correlations with film structure, *submitted*

UNPUBLISHED RESULTS:

N. Menegazzo, M. Kahn, R. Berghauser, W. Waldhauser, B. Mizaikoff, Application of nitrogen-doped diamond-like carbon films as novel optically transparent electrodes for multi-reflection IR-ATR spectroelectrochemistry, *Collaborative effort which generated preliminary data that showed a potential chemical application of nitrogen-doped diamond-like carbon films*

TALKS AND POSTER PRESENTATIONS AT INTERNATIONAL CONFERENCES

M. Kahn, M. Cekada, T. Schöberl, H. Parizek, B. Raninger, R. Berghauser, W. Waldhauser, E. Brandstätter, DLC films deposited at room-temperature by reactive magnetron sputtering and by an anode layer source – a comparative study, Plansee Seminar 2009, May 25 – May 29, 2009, International Conference on High Performance P/M Materials – 17th Plansee Seminar 2009, Reutte (Austria)

M. Kahn, M. Čekada, T. Schöberl, R. Berghauser, C. Mitterer, C. Bauer, W. Waldhauser, E. Brandstätter, Structural and mechanical properties of diamond-like carbon films deposited by an anode layer source, 35th International Conference on Metallurgical Coatings and Thin Films (ICMCTF 2008), April 28 – May 2, 2008, San Diego (California, USA)

M. Kahn, M. Cekada, N. Menegazzo, C. Bauer, B. Mizaikoff, R. Berghauser, W. Waldhauser, E. Brandstätter, Structural and Surface Properties of DLC and Nitrogen-doped DLC Films Deposited by DC Magnetron Sputtering, Symposium on Reactive Sputter Deposition, December 6 – December 7, 2007, Leoben (Austria)

M. Kahn, N. Menegazzo, B. Mizaikoff, R. Berghauser, J.M. Lackner, D. Hufnagel, W. Waldhauser, Properties of DLC and nitrogen-doped DLC films deposited by DC magnetron sputtering, International Conference on Plasma Surface Engineering, September 11 – September 15, 2006 Garmisch (Germany)

M. Kahn, M. Cekada, R. Berghauser, W. Waldhauser, C. Bauer, E. Brandstätter, Structural properties of diamond-like carbon films deposited by an anode layer source, 3rd Euroschool on Complex Metallic Alloys, 26 May – 31 May, 2008 Ljubljana (Slovenia)

M. Kahn, M. Cekada, W. Waldhauser, R. Berghauser , C. Bauer, C. Mitterer, E. Brandstätter, Accurate Raman Spectroscopy of Diamond-Like Carbon Films Deposited by Employing an Anode Layer Source, 18th European Conference on Diamond, Diamond-Like Materials, Carbon Nanotubes and Nitrides (Diamond 2007), 8 September – 15 September 2007, Berlin (Germany)

TABLE OF CONTENTS

1. BACKGROUND INFORMATION AND INTRODUCTION 1
2. DIAMOND-LIKE CARBON FILMS - OVERVIEW 5
2.1. OUTLINE 5
2.2. KINETIC ASPECTS DURING GROWTH – SUBPLANTATION/THERMAL SPIKE AND DOWNHILL CURRENT MODEL 7
2.3. DEPOSITION TECHNIQUES 13
2.3.1. Outline 13
2.3.2. Ion beam deposition 15
2.3.3. Pulsed laser deposition 17
2.3.4. Magnetron sputtering deposition 18
3. TYPES OF DIAMOND-LIKE CARBON FILMS – OVERALL PROPERTIES AND APPLICATIONS 19
3.1. OUTLINE 19
3.2. THE ta-C and ta-C:H FILMS 20
3.3. THE a-C:H FILMS 21
3.4. THE ELEMENTAL DOPED DIAMOND-LIKE CARBON FILMS 22
4. STRUCTURE AND HYDROGEN CONTENT OF DIAMOND-LIKE CARBON FILMS AND SELECTED ASPECTS OF FILM CHARACTERISATION 24
4.1. OUTLINE 24
4.2. ATOMIC AND ELECTRONIC STRUCTURE – CLUSTER MODEL 26
4.3. SELECTED ASPECTS OF DLC FILM CHARACTERISATION 28
4.3.1. Elemental content analysis by ERDA/RBS 28
4.3.2. Surface free energy determination 30
5. RAMAN SPECTROSCOPY OF DIAMOND-LIKE CARBON FILMS 34
5.1. OUTLINE 34
5.2. THE D-MODES AND G-MODES 35
5.3. INTERPRETATION OF RAMAN SPECTRA 37
5.3.1. Spectrum fitting 37
5.3.2. The three-stage model 39
5.3.3. The intensity ratio I_D/I_G 40
5.3.4. The full width at half maximum of the G-band - FWHM (G) 41
5.3.5. The dispersion of the G-band with excitation wavelength – Disp. (G) 41
5.3.6. The photoluminescence background in visible Raman spectroscopy 42
5.4. RAMAN SPECTROSCOPY OF NITROGENATED DIAMOND-LIKE CARBON FILMS 44
5.5. SELECTED APPLICATIONS OF RAMAN SPECTROSCOPY WITHIN THE OWN WORK 45
5.5.1. Laser pulse fluence versus variations in Csp^3–Csp^3 bonding content of UV-PLD deposited a-C and ta-C films 45
5.5.2. Process development of Si-a-C:H films guided by structural Raman analysis 46
5.5.3. The structural evolution of ion beam deposited ta-C:H films grown at varied angles of incidence from 0 to 90° 48
5.5.4. The relation of Raman band parameters and mechanical properties of ion beam deposited (t)a-C:H films ...49
6. SUMMARY AND CONCLUSIONS 51
7. REFERENCES 53
8. OWN PUBLICATIONS 59
9. APPENDIX-EXPERIMENTAL DETAILS 162

1. BACKGROUND INFORMATION AND INTRODUCTION

A coating is a thin solid matter, which allows the adaptation of a surface in a fashion to provide desired properties different from the surface properties of the bulk material. The coated bulk material is called substrate in thin film technology.

The surfaces of a substrate can be coated and/or modified. The modification is a tuning of the microstructure near to the surface of the substrate material by application of laser beams, ion beams, plasma-techniques, UV and synchrotron radiation [1]. Typically, the modification of the microstructure is a gradient like tuning of the desired surface properties towards the depths of the bulk material. Another common way to generate a new surface with tuned properties is to combine surface modifications and coating processes. In this case, a plasma modified surface is coated with a desired thin film. The combination of those techniques is mainly applied to enhance the adhesion of the thin film to the substrate. Thin films can be applied by the use of a single film, a double layer film, a gradient film or films in multilayer and composite assembling. Multilayer designs or composites with a single film thickness or composite diameter below 100 nm are called nanostructured films [2,3].

Surface modification and thin film development by physical vapour deposition (PVD) and plasma assisted chemical vapour deposition (PA-CVD) methods starts with the selection of the plasma modification and coating equipment, which is installed in a vacuum chamber. This step is followed by the process design and deposition experiments. The investigation of the structural, chemical and physical properties of the modified and coated surfaces plays the most important role during process development. Surface modification and film development are strongly associated with the substrate material. Usually, the substrate material is determined by the application of the whole substrate/thin film assembling, whereas the surface modification or the film is dedicated to tune the given surface of the bulk material. This implies, that plasma processes have to be chosen in a fashion to meet the demands for the final product as well as to be applicable to the given substrate material. To prevent thermal and/or radiation damage from plasma processes on sensitive substrates are major challenges in thin film and plasma technology. Especially polymers are sensitive to thermal damage, and therefore, the process temperature should be kept as low as possible when cleaning or coating polymer surfaces with plasma techniques.

Another technical problem occurs when coating insulating polymers or even any insulating material: Insulating samples cannot be conventionally direct current (DC) biased during deposition. Biasing the substrates is a conventional way to tune the film properties by ion bombardment during growth. Non-conductive substrates can be biased with pulsed direct current (DC) (up to several 100 kHz) and radiofrequency (RF) (typically 13.56 MHz) power generators. A pulsed or radio frequency bias voltage is applied in PA-CVD and mostly during magnetron sputtering to ensure proper plasma conditions on the substrate in order to deposit dense films [4,5]. Pulsed or radio frequency bias applied to substrates causes elevated process temperatures of >100°C. Heavy ion bombardment of the substrate surface causes the elevated temperatures due to the excess kinetic energy.

The deposition temperature plays a prominent role in the growth of diamond-like carbon films (DLC). DLC films present a meta-stable amorphous form of carbon with a significant percentage of Csp^3–Csp^3 bonds. Due to an extremely broad field of possible physical and chemical properties gained by different deposition processes and process parameters as well as the use of alloying and doping elements, applications can be found in almost all fields of technology and life science (semiconductor and electronic industry, energy industry, biochemistry, biology, medicine, analytical chemistry, food industry, etc.).

Since DLC is a metastable matter with carbon atoms in sp^2 and sp^3 hybridisation, deposition temperatures higher than 150°C, as well as irradiation with energetic photons and particles, create the energetically preferable aromatic sp^2 clusters in the carbon network. This observation is supported by results reported in various articles dealing with the role of the deposition temperature during growth of DLC films [6-13]. Researchers noted a decrease of the Csp^3–Csp^3 fraction, density, residual stress, electrical resistivity, optical gap and an increase in roughness at deposition temperatures higher than 150°C when growing tetrahedral DLC films (ta-C).

Ta-C films have the highest Csp^3–Csp^3 fraction of all DLC films, and show thus the strongest diamond-like character supported by having the highest density, residual stress, electrical resistivity and optical gap of all DLC films [4]. Therefore, these films are deposited at room temperature when strong mechanical properties are required in the application. The behaviour does not change significantly, when depositing hydrogenated tetrahedral DLC films (ta-C:H) and hydrogenated DLC films (a-C:H). Elevated deposition temperatures cause aromatic sp^2 clusters to increase in the carbon network. Therefore, the demand of applying DLC films on temperature sensitive substrates coincidences in principle with the general requirement of lower deposition temperatures in order to control the Csp^3–Csp^3 fraction in the films. Thus, DLC differs substantially from most thin film systems (borides, carbides, nitrides, oxides, metals etc.) where higher deposition temperatures are mandatory to ensure the growth of preferred nano-crystalline or crystalline film structures [14].

For a controlled DLC deposition, the kinetic energy of the condensing carbon and hydrocarbon ions and neutrals plays the most important role [4]. The kinetic impact of ions on the growing DLC film causes variations in the Csp^3–Csp^3 bonding in the growing film and is therefore responsible for the diamond-like character of these films. An ion energy of 100 eV/C^+ is known to increase the Csp^3–Csp^3 fraction to its possible maximum, forming ta-C films [6-7,15-18]. It is not always clear, if the DLC film with the highest Csp^3–Csp^3 bonding fraction is adequate in application. However, the ion energy represents the most effective parameter to control the structure of DLC during the growth and can therefore ensure proper process results if assessable and easy to control in the selected process. From this discussion, mass selected ion beam deposition (MSIBD) would be the most preferable technique for DLC deposition. In MSIBD, a carbon ion beam is formed by an ion source from a graphite target, which is thereafter accelerated up to 40 keV. Neutrals will be filtered out with a magnetic filter followed by retarding the ions to the desired ion energy for film growth [6-7,9,19-23]. This technique allows the deposition of virtually every amorphous carbon system (from graphite like to diamond-like), but has the major and serious drawback of a deposition rate of $\sim 10^{-2}$ $nm \cdot min^{-1}$ [4], which almost prevents the application of MSIBD as an industrial coating process.

Similar to MSIBD, pulsed laser deposition (PLD), working at a wavelength in the ultraviolet range, has the potential to control easily the ion energy of carbon ions, which is linearly related to the pulse fluence [24,25]. Considering assets and drawbacks of PLD, a higher deposition rate up to several $nm \cdot min^{-1}$ has to be noted for this technique, whereas the area, which can be homogeneously coated with one laser beam is only less than one cm^2. PLD by employing infrared laser radiation enables even higher deposition rates and coating areas. However, a drawback of PLD is the formation of particulates and droplets in the films, which result from intense laser bombardment of the graphite target. Particulates are microscopic parts of the target, which do not undergo any vapour or plasma state. Droplets are melted aggregates of the target material. The formation of these defects is a major challenge in DLC coating technology. The use of a solid carbon source for DLC growth like in PLD, magnetron sputtering and arc discharge will unavoidably result in the formation of defects in the deposited DLC films. From these named techniques, magnetron sputtering has the potential to grow the most homogeneous DLC films [4] with the smallest number of defects originating from the target, when the process is properly tuned. Moreover, magnetron sputtering is a very common DLC deposition technique applied in industry since it allows ease of scale up [26-35].

Deposition of metal-carbide containing DLC films with magnetron sputtering was proved by various scientists. Sputtering is the preferable process for the deposition of these nanostructured films, since the metals can be incorporated by the evaporation of metal targets in an argon (Ar)/hydrocarbon discharge, where the hydrocarbon gas acts as the precursor for the growth of the DLC matrix [36-40]. The drawback of conventional DC, pulsed DC and RF magnetron sputtering is the low rate of ionised species to neutrals in the plasma and the low kinetic energy of the carbon species [4].

Besides the discussed deposition techniques, ion beam methods have the potential to combine the needs of controllable ion energy of carbon species, controllable and if required low substrate temperature, acceptable deposition rate and basically a defect free nature of the deposited films [41]. Veerasamy et al. [41] reported in 2003 on the use of a newly developed ion beam source for the deposition of very thin ta-C:H films onto glass substrates. The authors claimed excellent adhesion of the ta-C:H coatings on the glass substrates, caused by the initial effect of implantation of carbon into the glass surface, enabling the growth of a diffuse interfacial carbon-glass layer [41]. Therefore, such a source can in principle be used for surface modification as well as for DLC deposition. This source can work with discharge voltages from ~500 V to several thousands of Volts enabling mean ion energies of accelerated carbon species from ~100 to ~1000 eV. Ion implantation and film growth can be realized with one aggregate. Moreover, the ion beam source enables plasma cleaning by sputtering the contaminants, oxides and adsorbed hydrocarbons on the substrate surface. In this case, the ion beam source is operated with Ar and/or oxygen (O_2) [41] as process gas. The work from Veerasamy et al. [41] is the only scientific article dealing with the direct deposition of DLC films using this special type of ion beam source. Zhurin et al. [42] have given a detailed review on the physics of closed drift ion beam sources - the synonym for ion beam sources. In general, the electric field, which accelerates the ions, is established by an electron current guided by a magnetic field [42]. The electrons in the magnetic field follow a closed drift path, which is eponymous for these devices. The anode layer thruster has its origin in the acceleration of electrons from the cathode to the anode, increasing the electron temperature, which results in a sharp decrease in plasma potential, so that the ion generation and acceleration take place in the form of a thin layer near the anode,

giving the source its name - anode layer source [42]. In thin film technology, anode layer sources are typically used for Ar or O_2 plasma cleaning of substrates.

The present work consequently investigates the structure of DLC films deposited by employing an anode layer source. Additionally, magnetron sputtering of carbon and silicon targets evaporated in Ar/acetylene (C_2H_2) process gas atmosphere is investigated. DLC films deposited by infrared PLD (IR-PLD; λ=1064 nm) and ultraviolet PLD (UV-PLD; λ=248 nm) are investigated further within the thesis. Consequently, Raman spectroscopy as the most important technique for the direct characterisation of the bonding structure of DLC films and related carbons [43-46] is a major part of the present thesis and will be used to provide the basic understanding of process parameters and their influence on the structure of the room-temperature deposited DLC films.

Furthermore, as too weak adhesion, too high coating process temperatures and improper diamond-like carbon structure formation etc. on different types of substrates represent still major challenges in DLC coating technology, the present thesis investigates the applicability of the developed films on different substrates.

Therefore, the aims of the present thesis are defined as follows:

- Development of new process variants of PVD and ion beam deposition processes by employing an anode layer source ion beam process, pulsed laser deposition and reactive magnetron sputtering for the deposition of diamond-like carbon films well adherent on temperature sensitive substrates (coating temperature should be kept well below 100°C)
- Identification of tailoring process parameters and subsequent process tuning in a fashion to obtain highly defect free films with unique properties on different kinds of substrates (silicon, glass, aluminium-alloys, fluorine-polymers, polymers, steels, ZnSe-crystals)
- Investigation of the deposited films due to their structural, chemical, mechanical, surface and surface chemistry properties
- Correlation of process parameters with film structure in order to achieve basic process understanding
- Subsequent correlation of film structure with film properties (hydrogen barrier properties, surface topography, surface energy) in order to achieve a scientific basis for future studies
- Provide scientific basis for Raman spectroscopy of carbon phases and enlighten the relation between Raman band parameters of DLC films and their mechanical properties

Chapters 2 to 4 of the present thesis give a short overview of the types of DLC films, their structure and chemistry, deposition techniques as well as known applications, acting as the framework to the scientific publications found at the end of the thesis. The present thesis represents a cumulative work of own scientific papers. Where possible, selected examples of the own research are discussed in brief. Chapter 5 deals exclusively with Raman spectroscopy of carbon based films. Chapter 6 provides the summary and conclusions to the thesis.

2. DIAMOND-LIKE CARBON FILMS - OVERVIEW

2.1. OUTLINE

DLC is a meta-stable amorphous form of carbon with a significant percentage of Csp^3–Csp^3 bonds [4]. Carbon is able to exist in three hybridisations, which are sp^3, sp^2 and sp^1. Only in sp^3 hybridisation, the four valence electrons of carbon with its electronic configuration $2s^2 2p^2$ are each located in a sp^3 orbital. This sp^3 orbital makes a strong σ-bonding to a neighbouring atom forming a tetrahedral, three dimensional bonding from the carbon atom. In sp^2 hybridisation, three of the four valence electrons will be found in three in-plane trigonal sp^2 orbitals. The fourth electron is entering a $p\pi$ orbital, which is directed normal to the plane of the trigonal sp^2 orbitals. The trigonal sp^2 orbitals form strong σ-bonds, whereas the electron in the $p\pi$ orbital forms a weaker π bond with one or more neighbouring atoms.

The overall sp^3 content in the films can be varied from 5 % [47] to 88 % [15,16,47]. When introducing atomic hydrogen (electronic configuration: 1s) in the films, Csp^3–H1s and Csp^2–H1s bonds are partly formed. Since diamond and polyethylene have per definition both 100 % sp^3 carbon hybridisation, it is clear that the term overall sp^3 content, often found in literature, can be understood as the sum of Csp^3–Csp^3 and Csp^3–H1s bonds.

Indeed, the presence of hydrogen causes the overall sp^3 content of a-C:H and ta-C:H coatings to be rather equal at 60 to 75 at.%, but causes the hardness of these two types of films to be very different. The ta-C:H films may reach a hardness up to 50 GPa [48], whereas polymeric a-C:H films with the same overall sp^3 bonding content have a hardness of less than 10 GPa [49]. The investigation of the influence of the hydrogen content and the structural disorder on the nanohardness and reduced modulus values of ion beam source deposited films was a major part of the present thesis (*Publication 5*). The results of these studies revealed an authentic relation between the clustering of the sp^2 phase and the Csp^3–Csp^3 bonding content with the mechanical properties of the investigated films.

Hydrogen has a further important effect, influencing the optical gap of the DLC coatings [49]. Hydrogen induces the optical gap to increase up to 4 eV for polymeric a-C:H films [49]. Hydrogen causes the density of DLC films to decrease [49]. Koidl et al. [49] reported on hydrogen contents of 30-40 at.% with a corresponding total sp^3 fraction of 40 % for a-C:H films and found a hydrogen content of 40-50 at.% for polymeric a-C:H films with a total sp^3 fraction of 60 %. Ta-C:H films show a maximum hydrogen content of 30 at.% while the total sp^3 fraction reaches 70 % [48]. From these data, it can be derived, that the population of Csp^3–Csp^3 bonds is much higher in ta-C:H films compared to a-C:H and polymeric a-C:H films. In polymeric a-C:H films, Csp^3–H1s bonds dominate typically the DLC structure. Indeed, during the own research it was found, that the deposited a-C:H coatings can contain up to 28 at.% hydrogen. Even more hydrogen was detected in silicon alloyed a-C:H coatings (Si-a-C:H), showing up to 34 at.% hydrogen. Furthermore, the own research revealed, that the deposition of hydrogen free a-C coatings by applying pulsed DC magnetron sputtering of graphite is almost impossible under room-temperature deposition conditions. The sputtered films show at least 13 at.% hydrogen.

Bringing clarity in the bonding regimes of DLC films, the ternary phase diagram of diamond, graphite and hydrogen was introduced by Jacob and Moller [50]. Figure 2.1 displays the ternary phase diagram published by Ferrari and Robertson in 2004 [51].

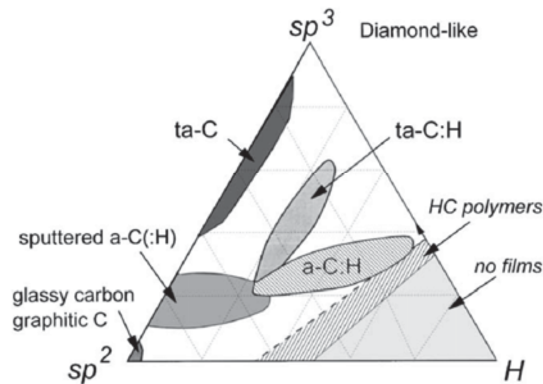

Figure 2.1. Ternary phase diagram of bonding in amorphous carbon-hydrogen alloys [51].

The ternary phase diagram is bordered in the right corner by polyacetylene showing 50 at.% sp^2 hybridisated carbon atoms bound to 50 at.% hydrogen in Csp^2–H1s bonds and polyethylene showing theoretically 100 % sp^3 hybridisation by having 33.3 at.% carbon and 66 at.% hydrogen (Csp^3–H1s bonding). Referring to this, it was found during the own research, that small additions of C_2H_2 up to 20 % (v/v) to the sputtering plasma during reactive pulsed DC sputtering of graphite results in favoured formation of Csp^2–Csp^2 and Csp^2–H1s bonds, whereas higher concentrations of 30 % C_2H_2 in the sputtering plasma tend to form an increased population of Csp^3–H1s bonding in a-C:H films (*Publication 4*).

Ferrari and Robertson further stated that the Csp^3–Csp^3 bonding content controls the elastic constants of the films [51]. Additionally, films with the same Csp^3–Csp^3 bonding content and hydrogen content can have different optical and mechanical properties due to different sp^2 clustering, different sp^2 orientation and cross sectional nano-structure [51]. The clustering of the sp^2 phase as a fourth axis in the ternary phase diagram should be added in order to further enlighten the link between structure and physical properties of DLC films [51]. Since clustering of the sp^2 phases beneath other important structural properties can be investigated with Raman spectroscopy, all articles presented in the thesis deal besides other aspects with the clustering of the sp^2 phase, and discuss the results in terms of possible relations to physical properties.

Changing from structure/property relations to applications of DLC films, it has to be noted, that even this unique combination of properties adjustable by deposition techniques and deposition properties gained the huge number of application fields, where these films can be found. The semiconductor and electronic industry, energy industry, biochemistry, biology, medicine, analytical chemistry and food industry can be named in a not exhaustive list [4,5]. Mostly, DLC films are applied as wear and corrosion protective coatings for magnetic storage media [4,5]. Very thin films with less than 4 nm thickness are applied on magnetic disks and heads [52]. However, in order to increase the storage density, even thinner coatings, ideally as thin as 1 nm are required in the future to coat data storage media. These films must be atomically smooth, dense and in principle defect free. Films of the system a-C:N and a-C:H are not able to be applied with a thickness of 1 nm.

The roughness of these films is in the range of the required film thickness and therefore prevents growth of dense films. Highly Csp^3–Csp^3 bonding films grown with high ion energy deposition methods are required for such applications. The film roughness is a function of the Csp^3–Csp^3 content and the ion energy. A roughness of ~0.1 nm is mandatory on data storage disks [52]. Additionally, the roughness has to be independent of the film thickness. During the own research, it was found, that ion beam deposited films with thicknesses between 50 to 200 nm show root mean square (RMS) roughness values of down to 0.1 nm. Structurally, these films are ta-C:H and nitrogen containing ta-C:H films. It is assumed, that these ion beam deposited films are applicable in data storage technology as ultra thin wear and corrosion protection for hard disk drives.

Due to the chemical inertness, DLC films could also protect biological implants against corrosion and serve as diffusion barriers. DLC films were considered as coating on metallic and polymeric bio-components to improve their biocompatibility [53-55].

2.2. KINETIC ASPECTS DURING GROWTH – SUBPLANTATION/THERMAL SPIKE AND DOWNHILL CURRENT MODEL

Fundamental research on the kinetic and thermal aspects during growth of ta-C films was done by Lifshitz et al. [6,13,19] and Robertson [17,18,56-69]. Lifshitz et al. proposed that the growth of ta-C is sub-surface, which suggests the deposition process as a shallow implantation. This process was denoted as the subplantation model. Robertson further proposed that the subplantation creates a metastable increase in density in the growing DLC film. This changes the local bonding to Csp^3–Csp^3.

In contrast to the work from Lifshitz et al. [6,13,19] and Moller [60], where a preferential displacement of the sp^3 hybridisated atoms to sp^2 sites was published, Robertson proposed, that such a displacement is not needed for a high Csp^3–Csp^3 bonding character of the films. Only sub-surface growth in a restricted volume is needed to get Csp^3–Csp^3 bonds [4]. The subplantation model was proven by various numerical and analytical simulations [61-67]. However, the suppression of Csp^3–Csp^3 bonding at higher ion energies and higher deposition temperatures is still a problem in the subplantation model.

In the kinetic energy range of deposition techniques, *i.e.* 0-1000 eV, carbon ions loose their energy mainly by collisions with solid matter. The cross-section of collisions decreases, when the ion energy is raised. At a specific ion energy the ion can pass through an interstice, causing the ion to penetrate the surface layer. This ion energy is called penetration threshold, E_p. Consequently, the displacement threshold E_d is the minimum energy of an incident ion needed to displace an atom from a bonded site, creating a permanent vacancy-interstitial pair. This raises the kinetic energy of an ion by E_B (surface binding energy) when it enters the surface [56-58]. The net penetration threshold for free ions is given by [4]:

$$E_p \approx E_d - E_B \quad (2.1)$$

The net penetration threshold is ~32 eV for carbon [4]. Applying this model to carbon ions incident on an amorphous carbon surface, a low energy ion will not have enough energy to enter the surface, and will stay at

its lowest possible energy state which is sp^2 hybridisation [56-58]. An ion with energy higher than E_p will penetrate the surface entering a sub-surface interstitial site. This causes an increase of the local density in the growing film. Subsequently, the surrounding carbon atoms will reform around the incident atom. Robertson et al. assumes, that atomic hybridisations will adjust to the increased local density and will become sp^2 if the density is low and sp^3 if the density is high, respectively [56-58].

At higher ion energies, the incident ion penetrates deeper into the surface, transferring about 30 % of its energy to atom displacements [68]. The excess energy is transferred to heat. The collision time of the ions is 10^{-13} s, the thermalisation time is 10^{-12} s and the relaxation time is 10^{-10} s [4]. Thermalisation and/or relaxation allow the excess density to relax to zero. If the ion energy is high enough, this will cause a loss of sp^3 carbon atom hybridisation. Subplantation is a process, where incident ions penetrate the surface and densify the film. Some ions end up at the surface as sp^2 bonded fraction and cause the film to grow. This means, that a subsurface densified layer grows covered by a lower density layer consisting of mainly sp^2 hybridisated atoms, which will consequently be transferred continuously to a certain population of sp^3 hybridisated atoms by the energy of the incident ions still reaching the surface of the film. The flux of penetrating ions back to the surface is proportional to a driving force, which is the fraction of interstitials below the surface. Penetration may occur directly or only by knock-on of ions or atoms with a certain kinetic energy. At an incident ion energy of 100 eV/C^+, the carbon sp^3 hybridisation in the films reaches the maximum [4 and references therein]. The thermal spike model, represented in equation 2.2 allows the calculation of that certain energy optimum.

$$\frac{\Delta_\rho}{\rho} = \frac{f\phi}{1 - f\phi + 0.016(E_i / E_0)^{5/3}} \qquad 2.2$$

In equation 2.2, ρ is the density of the sp^2 hybridisated carbon atoms, $\Delta\rho$ is the density increase, $f\Phi$ is the ion flux with the fraction Φ, E_i is the ion energy and E_0 is the diffusion activation energy. Figure 2.2 shows that equation 2.1 gives a rough representation of the variation of the sp^3 content for ta-C films deposited by filtered cathodic vacuum arc deposition technology (FCVA) [16,57].

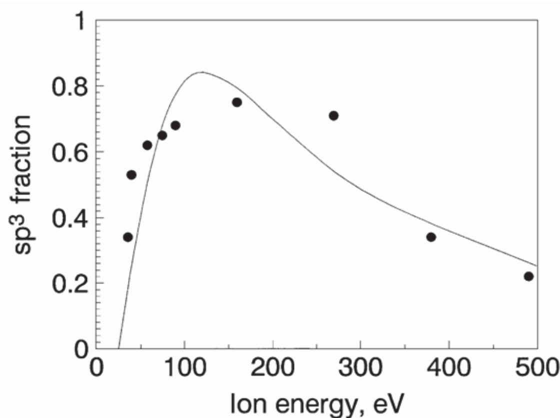

Figure 2.2. Comparison of calculated sp^3 fraction (grey line) with FCVA deposited ta-C according to the subplantation/thermal spike model (2.1) published by Fallon et at. [16]

Practically the shallow decline of the sp^3 fraction is found to range over a large ion energy region from ~90 to ~250 eV (Figure 2.2). A lower value of E_0 applied in equation 2.2 will bring theoretical and practical results to more agreement. E_0 was fixed at 3.1 eV by Fallon et al.[16].

The subplantation/thermal spike model also accounts for the density found in ta-C:H films deposited from acetylene (C_2H_2). C_2H_2 has two carbon atoms in sp^1 hybridisation, which will fragment into two carbon atoms during impact with the surface. The kinetic energy is shared equally between them [4]. The hydrogen atoms take only little energy because of conservation of momentum [4]. The penetration and densification will occur for each carbon atom separately and independently (Figure 2.3).

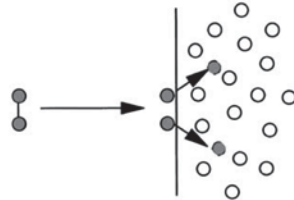

Figure 2.3. Subplantation for a C_2H_2 molecule impacting on the growing carbon film surface [after 4].

A rather small energy must be subtracted from E_i to break the three bonds (one σ and two times π) in the C_2H_2 molecule. The relaxation step will occur as a single event for the molecular ion, since the spikes of the two carbons atoms will overlap [4]. Therefore, C_2H_2 as kinetic particle will show a much steeper decline in densification compared to mono-atomic ions, found during deposition of ta-C films [4]. Figure 2.4 shows this behaviour by comparing again theoretical results corresponding to equation 2.2 with experimental data.

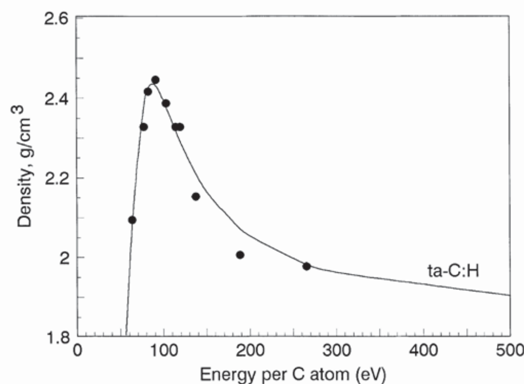

Figure 2.4. Comparison of calculated density (grey line) with ion beam deposited ta-C:H from Weiler et al. [48] according to the subplantation/thermal spike model (equation 2.2) published by Fallon et at. [16].

The calculated values of the density as a function of the ion energy coincide very well with experimental data for the deposition of ta-C:H [48]. Highly tetrahedral Csp^3–Cps^3 rich films can be deposited by using exclusively C_2H_2 as process gas in ion beam processes [4]. It is also reported by Conway et al. [69], that C_2H_2 is the favoured precursor for growing ta-C:H with plasma beam methods. They report, that depositions, where methane as carbon source is used, do not grow authentic ta-C:H films and the character is less tetrahedral.

However, the subplantation/thermal spike model has several limitations [4]. In order to improve the subplantation/thermal spike model to meet the experimental data from a wide field of deposition techniques following details have to be taken into account:

- The different dependence of carbon sp^3 fractions on the ion energy in the FCVA and in the MSIBD, which has been attributed to the slower growth rate in MSIBD
- The transition temperature to sp^2 bonding, being 400 to 500 K [6,7,70], despite the temperature in a thermal spike being 10^6 K
- The variation of the transition temperature for the sp^3 formation with ion energy [70]
- The variation of the transition temperature with instantaneous growth rate [71,72]

The study of high kinetic energy ion beam deposited films by applying an anode layer source was besides the investigation of low energy DLC deposition with magnetron sputtering the main task of the present thesis. Subsequently, in four scientific publications, aspects of the applied ion beam method itself as well as a discussion of structural, chemical and mechanical properties of the grown films is given (*Publications 1, 2, 4 and 5*).

Own results showed that the ion beam deposited films follow the subplantation/thermal spike model. The Csp^3–Csp^3 bonding content in the studied films reach a maximum when working with the lowest possible discharge voltage of 1 kV applied to the source. This discharge voltage corresponds to the lowest possible ion energy. It was found, that increasing the discharge voltage yields films with less tetrahedral character and with less Csp^3–Csp^3 bonding content. It is important to mention, that even for Ar as plasma gas, a discharge voltage of 1 kV corresponds to a mean ion energy of 450 eV, whereas the highest possible discharge voltage of 3 kV corresponds to 750 eV measured at a pressure of $1.3 \cdot 10^{-3}$ mbar [73]. The applied discharge voltage relates in a linear fashion to the $Ar^{(+)}$ ion energy in the discharge range from 1 to 3 kV. The real ion energy, which is present at the surface, is not known and hardly accessible. It is assumed, that the relation between discharge voltage and kinetic carbon ion energy is similar to the dependence of kinetic energy observed for $Ar^{(+)}$ ion energy. Higher discharge voltages correspond to higher kinetic carbon ion energies. The correlation between the discharge voltage (ion energy) and Csp^3 hybridisation of the deposited films suggests, that the lowest applied discharge voltage of 1 kV results in a kinetic carbon energy, higher than the kinetic energy which is needed to grow DLC films with highest Csp^3–Csp^3 bonding character (~100 eV at the growing film surface).

Lifshitz [6] reported on charging effects on insulating substrate materials, due to the formation of a retarding potential, reducing the kinetic energy of incident particles or ions. He further reports on the formation of rougher and much more graphitic DLC films deposited with MSIB on quartz substrates compared to films, which where deposited on silicon wavers at the same ion energy of 120 eV [6]. The charging of insulating substrates is a result of the bombardment of the surfaces with charged carbon species and cannot be ignored for MSIBD and also for other ion beam deposition techniques.

Veerasamy et al. [41] found the highest hardness values for mean ion energies of ~750 eV per carbon atom for films deposited on soda-lime glass. They did not observe any drop in hardness and tetrahedral character of the deposited films when working with ion energies up to 1 keV per carbon atom. The ta-C:H films in their study were deposited with a linear ion beam source, which is constructed according to the principles of an anode layer source, similar to the source, which was used in this thesis. Veerasamy et al. [41] reported a completely inverse trend of the Csp^3–Csp^3 bonding content as a function of the mean ion energy per carbon atom

compared to all reported studies [4 and references therein] as well as the data obtained during this thesis. They named two possible reasons for explaining their higher Csp^3–Csp^3 bonding character of the DLC films deposited at elevated ion energies: First, the presence of hydrogen during the film growth may delay the onset of graphitisation which is caused by thermal spikes at high energies. Second, the charging of the film surface can also reduce the effective energy of the incident ions. It is very likely, that the ion energies reported by Veerasamy and co-workers [41] are not real ion energies present on the film surface. The charging of the insulation glass substrates due to bombardment with carbon ions damps the ion energy of incident carbons dramatically. This is a good example pointing out the difficulties in the estimation of the real ion energy present on a growing DLC film surface.

Some ion beam and plasma beam sources show a low ion/neutral ratio of 2 to 10 % in the carbon flux [4]. The kinetic energy of non-charged carbon species has a similar influence on the structure formation of DLC films as the ion energy of charged species [4]. For the own research, an almost linear relation between the discharge voltage-being directly proportional to the kinetic energy and the Csp^3–Csp^3 fraction, the nanohardness and the reduced elastic modulus detected for the deposited films is evident. Films deposited at the lowest discharge voltage show in accordance to the spectroscopic data the highest nanohardness (36±1 GPa), stress (-2.34±0.2 GPa) and reduced elastic modulus (180±4 GPa). The elucidation of the influence of the structural disorder and hydrogen content on the mechanical properties of the ion beam deposited ta-C:H films is potentially the most important finding during the present thesis (*Publication 5*).

The angle of incidence of the bombarding species on the DLC surface has a crucial impact on growth effects of the films [6]. The penetration depth of carbon ions or neutrals is a function of their angle of incidence, where a beam with the same ion energy shows a lower penetration at a glancing angle of incidence. This reduces the effective ion energy. Due to the fact, that most deposition systems as well as the geometry of the substrates prevent a normal angle of incidence of carbon species, the effective ion energy is again hardly known. From this discussion, one can see, that the ion energy of a deposition system is a rather theoretical value, which can be significantly influenced by the type of substrates (conductivity), their geometry, their manipulation through the beam and the ion/neutral ratio of the beam. In the present thesis, the structural evolution of ion beam deposited ta-C:H films grown at varied angles of incidence from 90° to 0° (perpendicular to the major beam axis and parallel to the major beam axis) was studied with Raman spectroscopy. Since Raman spectroscopy was identified as the most appropriate way to determine the clustering of sp^2 phases and the structural disordering (equivalent to changes in Csp^3–Csp^3 bonding content), the deposited films are evaluated in terms of these parameters as a function of the angle of incidence of energetic carbon species. The results are summarised in chapter 5.5.3 of the present thesis.

Many practical three-dimensional shaped substrates also prevent a constant distance between the ion source and the coating surface. A non-constant kinetic species flight distance to the substrates will result in a different film structure formation at different distances due to differences in kinetic energy of the incident ions or neutrals. Within this context, the survey of the influence of static, oscillated and rotated deposition on the structural properties of ion beam deposited films was part of the thesis (*Publication 1 and 2*). The clustering of sp^2 hybridised carbon phases, the disorder of sp^2 hybridised carbon phases and the hydrogen content of the

films was investigated as a function of the relative position to the major beam axis of the ion source. The results made clear, that the knowledge of structural formation on different positions relative to the ion beam source plays a crucial role during process development.

Corresponding to the kinetic aspects of the ion beam deposition method, the influence of mixing Ar with C_2H_2 in ion beam processing on the structure of ta-C:H films was investigated in detail during the thesis. With a mixture of 15 sccm C_2H_2 and 5 sccm Ar, subsequent graphitisation converting Csp^3–Csp^3 bonds to Csp^2–Csp^2 bonds was recognised with Raman spectroscopy. The tetrahedral bonding character of the corresponding film grown without Ar added to the carbon precursor was converted partly to clustered sp^2 phases. The degree of clustering is proportional to the ion energy of Ar^+ ions accelerated from the ion beam source to the growing film. Higher ion energies of Ar^+ ions show subsequent a higher degree of graphitisation and clustering of sp^2 phases. This behaviour can be interpreted as the result of the high energy ion bombardment by heavy Ar^+ ions (~450 to 750 eV) during film growth, reducing the disordered character and Csp^3–Csp^3 bonding content in the film by relaxation processes forming energetically preferable sp^2 ring like carbon structures (*Publication 1*).

Coming to the role of the deposition temperature during growth of ta-C films, temperatures higher than 150°C show as mentioned previously, clustering of sp^2 phases. This clustering is accompanied by a decrease of the Csp^3–Csp^3 fraction, density, residual stress, electrical resistivity, optical gap and an increase in roughness [6-13]. Lifshitz [6] sees the origin for this effect in the increased mobility of carbon species, which migrate to the surface of the DLC film. In his opinion, the growth at high deposition temperatures is controlled by surface processes. The surface processes favour a sp^2 rich film. In contrast, consistent with the subplantation/thermal spike model, room temperature deposition causes the carbon interstitials to become immobile, trapping carbon species which have penetrated the surface, resulting in higher stressed and sp^3 hybridised rich films. The surface roughening is directly associated with the growth of graphitic clusters at higher deposition temperatures.

The roughness of ta-C:H and ta-C films, being typically around 0.15 nm, increases up to several nm at deposition temperatures higher than 150°C. Note, that even very Csp^3–Csp^3 bonding rich films can be deposited at low ion energies of 10 to 20 eV when cooling the substrates to -200°C [74-77]. This indicates the existence of very shallow sp^3 configurations that are frozen at sufficiently low temperatures and are stabilised by coverage of the bombarding carbon species [13]. In summary, scientists see the reason for growth of graphitic films in increased mobility at higher temperatures resulting in migration of carbon atoms to the surface. The bombarding of the surface with high energetic carbon ions and neutrals increases the deposition temperature continuously during deposition. An equilibrium temperature, which is sufficiently lower than the transition temperature for ta-C deposition of 150°C should be realised for controlled and homogeneous DLC growth. Within this regard, all deposition experiments carried out during the thesis were performed at substrate temperatures lower than typically 80°C. More frequently, depositions were carried out at a substrate temperature of 50°C. The transition temperature is a well defined temperature [4], where transformations of the film pop-up sharply, meaning a rather uninfluenced growth up to temperatures of 100 to 150°C is likely.

DLC is an ultra-smooth material with roughness values down to 0.1 nm [4 and references therein]. In 2005, Moseler and co-workers [78] reported on a possible reason for such ultra-smoothness of these films. They explain the ultra-smoothness of DLC films by an atomistic/continuum multiscale model. At the atomic scale, so-called downhill currents formed by the impact of carbon ions cause an erosion of hills into neighboring hollows, causing the smoothness at a continuum scale. A similar behaviour is reported for ultra-smooth amorphous silicon films bombarded with low energy Ar^+ ions [79,80]. Their quantum and classical molecular dynamics simulations indicate that in ion beam deposition of DLC there is a tendency towards sub-nm crater formation in the immediate neighbourhood of the impact point, which leads to an increase of the local interface curvature. An efficient damping of the surface fluctuations is achieved through impact-induced downhill currents, eroding the hills into neighbouring holes.

Lateral transport processes like bulk-diffusion do not play any role in the deposition of DLC films at room-temperature [78]. A saturation of the surface roughness at ultra-smooth levels for ion energies higher than 120 eV is reported. Moseler et al. [78] also proved ion energies of 30 eV to be high enough for the growth of ultra-smooth film surfaces caused by the generation of downhill currents. Indeed, ta-C:H films grown within this work with a discharge voltage of 1 kV (lowest ion energy) show roughness values of ~0.1 nm. Films deposited by using the highest possible ion energy established by a discharge voltage of 3 kV show equal roughness values. These ion beam deposited films are ultra-smooth and are therefore comparable to ta-C and ta-C:H films deposited by MSIBD and can compete with smoothest films ever reported.

Beneath ion energy/roughness relationships, own results obtained with reactive unbalanced magnetron sputtering of silicon in Ar/C_2H_2 process atmospheres revealed a clear relation of the quantitative roughness parameters of the Si-a-C:H films and the C_2H_2 concentration in the process gas mixture. A concentration of 4 % C_2H_2 results in a very smooth DLC film with a roughness of 0.25 nm which was increased to 1 and 1.5 nm by using 8 and 10 % C_2H_2, respectively. The addition of 4 % C_2H_2 to the process gas atmosphere results in the first clear formation of diamond-like carbon structures. At 8 to 10 % C_2H_2, the structure of a-C:H was distinctly formed.

2.3. DEPOSITION TECHNIQUES

2.3.1. Outline

The first DLC films were deposited by Aisenberg and Chabot [81] by ion beam deposition. Since it is the kinetic energy of carbon ions or neutrals, which is responsible for the formation of sp^3 hybridised carbon atoms, the deposition methods should be categorized due to their potential kinetic energy of carbon atoms or ions impinging on the growing film. The kinetic energy of carbons can be either gained by electrostatic acceleration (ion beam methods) or momentum transfer by collision with energetic species simultaneously within the deposition process (ion plating by external ion beam source or by application of a bias voltage to the substrates) [13]. Momentum transfer with noble gas atoms is rather ineffective, due to massive elemental weight differences between e.g. Ar^+ ions and carbon atoms. However, the impact ion energy of Ar^+ ions on the growing film should be chosen very carefully, since too high energies tend to graphitise the DLC and makes

therefore the control of structure very difficult. Own studies have revealed a clear influence of impinging Ar^+ ions on the growing DLC film surfaces (*Publication 1 and 6*).

The carbon ion energy is highest for ion beam deposition methods (10 eV to 40 keV) [13] and pulsed laser deposition (10 eV to ~150 eV) [4]. Magnetron sputtering is known for lowest ion energies of carbon species of zero to several tens of eV [13]. DLC deposition techniques of all varieties of DLC deposition principles except PA-CVD are available at the Laser Center Leoben. The techniques are of complex nature in terms of [after 6]:

- the distribution of energetic species involved
- the energy of carbon species and their angle of incidence
- the ambient pressure during deposition
- the substrate temperature
- the gradient of substrate temperature during room-temperature conditions
- the carbon source (solid target or ion source) to substrate distance
- the purity of target materials and process gases
- the vacuum chamber base pressure
- the deposition rate
- the kind of substrate manipulation
- the electric potential of the substrate holding device (grounded, floating potential, biased)

It is clear, that this list is rather incomplete, and there are several other factors, which can influence the DLC film structure or properties achieved with a chosen deposition system. It is very important to note, that the kind of substrate manipulation (static, oscillation, 1-fold rotation, 2-fold rotation, 3-fold-rotation) has a major impact on the structure and properties of DLC films. When possible, it should be avoided to coat in static mode on technical products, since not any deposition system is able to provide an energy-homogeneous distribution of carbon species involved in film growth. The ion beam source used in the experiments during the thesis shows mean ion energies of 450 to 750 eV for Ar^+ ions, corresponding to discharge voltages of 1 to 3 kV [73]. The peak ion energy present at a distance of 10 cm from the ion source detected directly in the center of the beam is as high as 1100 eV and can be as low as 10 eV at other positions out of the beam (for a process pressure of $1.3 \cdot 10^{-3}$ mbar) [73]. In static deposition mode, such an energy spread will result in films with a fundamentally different DLC structure as a function of the lateral distance to the major ion beam source axis. This was investigated in detail by the evaluation of clustering of sp^2 phases, structural disorder and hydrogen content of the deposited films as a function of the horizontal position perpendicular to the major beam axis of the ion beam source. Fundamental relations were obtained, which are discussed in two publications presented in chapter 8 of the present thesis (*Publication 1 and 2*).

A brief overview of the deposition techniques applied during the thesis is given below. Since the DLC deposition with the applied ion beam source is rather novel, the physics behind this aggregate will be described in more detail.

2.3.2. Ion beam deposition

In general, ion beam sources accelerate carbon ions electrostatically via a bias voltage through a grid towards the substrate. The ions can be either produced by a sputtering plasma or an arc discharge from a graphite target. Alternatively, as for example in the 'Kaufman' source, a hydrocarbon gas is ionised in a plasma, giving electrostatically accelerable ionised carbon species [82]. Also in MSIBD a hydrocarbon gas can be used as carbon source [7]. A carbon ion beam is accelerated and a magnetic filter separates charged from neutral species for film growth with a desired ion energy [6-7,9,19-23] in MSIBD. A sharply defined carbon ion flux with controlled ion energy and a typical energy spread of maximal 10 eV in the resulting beam is ideal for scientific work on energy-structure relationships. Doping of the films can be easily achieved by using reactive gases containing doping elements or by the use of dual beam MSIBD systems [83]. The low deposition rate of ~10^{-2} nm·min^{-1} [4] is the major drawback of this technique.

Dealing with ion beam methods it has to be mentioned, that if the source is operated with a hydrocarbon gas, in principle defect-free films can be deposited. This is especially mandatory for applications of the DLC films as gas barrier coatings or coatings on artificial implants. Therefore, ion beam methods present the only group of DLC deposition techniques, where the kinetic energy is easily accessible and no solid carbon source can be used. A so-called anode layer source was used for the direct deposition of DLC films in this thesis. Figure 2.5 shows a cross-section of this special ion beam source. Experimental details to the deposition of DLC films with this source are summarised in chapter 9 of the thesis. The use of such a source is rather novel in direct DLC deposition and was first reported in 2003 [41].

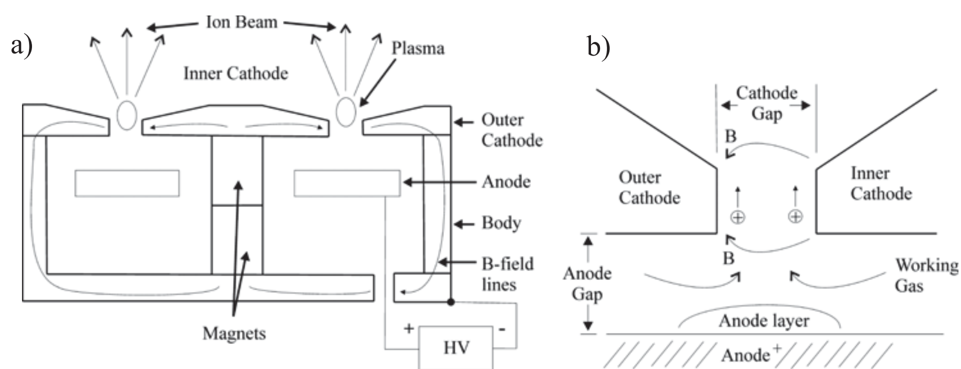

Figure 2.5. a) Cross-section of the anode layer source ALS340 from Veeco Instruments showing the main components of the source body and electrical circuit points [after 73]. **b)** Working principle of the anode layer source [after 73].

Such an anode layer source has no electrostatic grid conventionally used in other ion beam principles and can work without a beam neutralising electron emitter, since the beam is highly neutralised. The low floating potential of less than -20 V detected for this source is a big advantage when coating non-conductive substrates, due to minimisation of charging effects.

The physical principle behind this source is the closed drift theory [42]. Most ions produced in closed field ion beam sources are singly charged [42]. The reason for this behaviour is that when an atom loses an electron, there is usually enough electric energy to remove the ion from the discharge plasma, before other collisions with other electrons can further ionise it. Multiply charged ions are usually the result of single collisions of

electrons that were sufficiently energetic to remove two or more electrons from a neutral atom. In addition to the required electrons with a sufficient energy, the cross sections for multiple ionisation in a single collision are small compared to the single ionisation process. The efficient operation of closed-drift ion beam sources is based upon the reduced mobility of plasma electrons across a magnetic field. The magnetic field in a source is predominantly in the radial direction. Figure 2.6 shows the circumferential motion of electrons in a closed drift ion source.

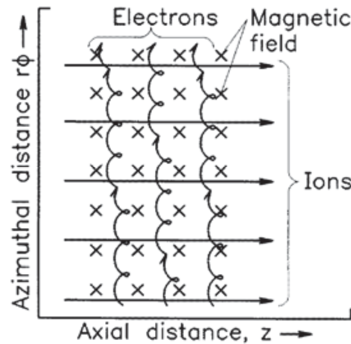

Figure 2.6. Circumferential motion of electrons in closed-drift ion source [42].

Ions enter the closed-drift region and are accelerated into the beam. This is an azimuthally electron drift shown in Figure 2.6. This drift is normal to the applied electric and magnetic field and constitutes therefore a Hall current. The axial electron current density is the result of collisions of electrons with other electrons, ions, neutrals, and the wall of the discharge region and discharge fluctuations in the plasma. Because of the reduced electron mobility normal to the magnetic field, it is possible for the plasma to withstand a substantial strength of electric field while conducting only a small electron current density. Under these conditions, the electric field mainly supplies energy to the ions increasing their directed kinetic energy. If the electron drift in Figure 2.6 will be obstructed, a secondary electric field will be generated. The secondary electric field will result in a component of the electron drift parallel to the applied electric field, and therefore increased electron conduction. For a sufficient operation of a closed-drift ion source, it is important, that the electron drift motion takes place without obstacles, *i.e.* in a closed drift path. Electrons are trapped inside the closed-drift region, where most of the accelerating electric field exists. The rate of their departure from this layer is low enough that they are continually replaced by electrons supplied by the cathode and by secondary electrons from the ionisation of neutrals. Therefore, one can speak of quasineutrality within the closed drift region as well as within the ion beam outside the ion source. There is an important part of the closed-drift region, in which quasineutrality is not satisfied when the anode layer source is operated in vacuum. The plasma is diluted into the vacuum, causing the non-quasineutrality. An anode layer source has a short discharge channel, where regions of ionisation and acceleration practically coincide. The acceleration is concentrated in a thin plasma layer on the anode of the source (Figure 2.5).

Due to the physics of the source, the energy and current of the ion beam cannot be monitored directly on the power supply. The effective ion energy for Ar at $1.3 \cdot 10^{-3}$ mbar varies between 450 and 750 eV, corresponding to discharge voltages between 1 and 3 kV [73]. It is assumed, that the relation between discharge voltage and ion energy is similar for Ar and C_2H_2. During routine operation, the process pressure is similar for Ar and

C_2H_2 operation. The total gas flow has no relation to the ion energy of accelerated ions [41]. As discussed previously, the effective ion energy present on the growing DLC film is not known. Since the beam is highly neutralised, one can assume, that charging effects on non-conducting substrates are limited.

2.3.3. Pulsed laser deposition

PLD is an elegant way for the deposition of kinetically controlled DLC films in the system ta-C, ta-C:H, a-C and a-C:H. Doping or alloying with several elements is possible via using reactive gases during deposition as well as by applying alloyed targets. The PLD method was reviewed by Voevodin and Donley [24] and Siegal et al. [25]. In PLD of DLC films, a laser is ablating the graphite target under high vacuum conditions or inert gas or reactive gas process atmosphere. The energy distribution of carbon species depends on the laser pulse fluence applied for deposition. A linear relationship between laser pulse fluence present on the ablation spot and the average kinetic energy of carbon species is evident (Figure 2.7).

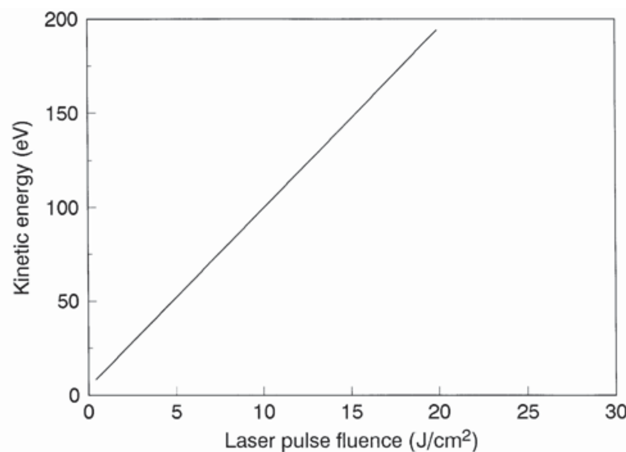

Figure 2.7. Average ion energy of ablated carbon ions versus laser pulse fluence for excimer laser PLD [24].

Therefore, in PLD, the dependence between kinetic carbon species energy and Csp^3–Csp^3 bonding fraction in the deposited films is similar to MSIBD or FCVA. Since PLD can be processed without inert gas under high vacuum conditions, the films have a very low level of contaminants when using graphite targets of high purity. The kinetic energy of carbon species in the plume is also dependent on the wavelength of the applied laser. In general, short intense laser pulses with an excimer laser working at a wavelength of 248 nm give an intense plasma with controllable ion energy. The physics behind excimer lasers is comprehensively described in reference [84]. Processes involved in the laser ablation are: adsorption of photons, formation of free electrons, adsorption of electrons, fast heating up by electron-phonon interaction, flash evaporation, formation of a plasma and expansion of the cloud of ablated species [84]. The ablated species are determined by the high intensity nanosecond laser pulses resulting in the input of a large amount of energy in a very short time. The high temperatures being necessary for flash evaporation, lead to the high kinetic energies of the ablated atoms and ions. Pulsed lasers with wavelengths of 248, 532 and 1064 nm are available at the Laser Center Leoben. A detailed description of the excimer laser (λ=248 nm) and the Nd:YAG laser (λ=532 or 1064 nm) used in the present work is given in chapter 9. DLC films in the system a-C and a-C:H were studied by scientists of the Laser Center Leoben in 2003 [85]. During the present thesis, a-C, a-C:N and ta-C films were studied. The structural properties of the excimer laser deposited DLC films were evaluated in terms of the laser pulse

fluence. An almost linear relation between laser pulse fluence and Csp^3–Csp^3 content in the deposited films detected by structural disordering was found. The results of these studies are presented in chapter 5.5.1 of the present thesis. Beneath the fact, that defect-free films are not achievable, the effective area which can be homogeneously coated with one excimer laser beam is as small as one cm^2. However, it is postulated, that up-scaling the deposition area by use of multiple laser beams is possible, but difficult.

2.3.4. Magnetron sputtering deposition

Magnetron sputtering is known to be the most industrially applied DLC coating process [26-35]. Sputtering is the ejection of atoms or clusters from a target material caused by momentum transfer of incident inert gas ions, usually Ar^+ ions [4]. Mostly DC or RF discharges are used to provide a glow discharge on the target which is evaporated. The target acts as the cathode. RF fields are used to sputter non-conductive materials. Magnetron sputtering is used to enhance the sputtering yield of the target material. Magnetrons can be categorised into balanced and unbalanced types. In balanced magnetron sputtering all magnetic field lines are closed between inner and outer magnets, forming a closed magnetic loop. In unbalanced magnetron sputtering, the magnetic field lines are partly not closed and expand therefore towards the substrate to some extent. The unbalanced field is achieved by using stronger inner or outer magnets. Figure 2.8 represents the schematic diagram of an unbalanced magnetron sputtering process.

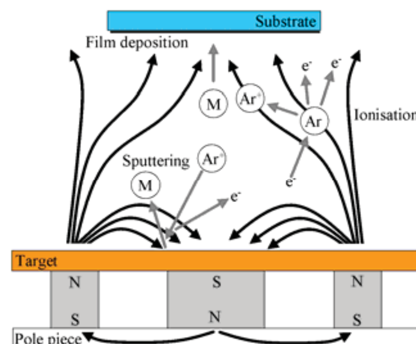

Figure 2.8. Principle of unbalanced magnetron sputtering deposition, M…target atom, Ar…argon atom, Ar^+…argon ion, e^-…electron [after 87].

The sputtering plasma expands towards the substrate surface due to the escape of secondary electrons on the partly open magnetic field lines. Ionisation of inert gas atoms is caused by collisions with electrons. This ion flux improves the film properties [86-91]. The substrate holding device, which faces the sputtering target, can be grounded, negatively or positively charged. By means of reactive magnetron sputtering, the deposition of nitrogen doped DLC films as well as the hydrogenation of DLC films is possible. Metal-carbide containing a-C:H films can be deposited by sputtering a metal target in inert gas/hydrocarbon gas mixtures [36-40]. The fraction of neutral carbon species is known to be almost 100 %, that's why sputtered a-C and a-C:H films are not the hardest [4]. Due to momentum transfer of impinging Ar^+ ions accelerated by a bias voltage applied to the substrate, film quality can be improved to some extent. Too high energy of Ar^+ ions as well as high deposition temperatures will result in graphitisation of the deposited DLC films.

3. TYPES OF DIAMOND-LIKE CARBON FILMS – OVERALL PROPERTIES AND APPLICATIONS

3.1. OUTLINE

The ternary phase diagram of diamond, graphite and hydrogen (Figure 2.1) was introduced by Jacob and Moller [50]. They proposed to divide DLC films into four groups of films, whose properties can be categorised and range in rather narrow fields in the ternary phase diagram. The four groups are ta-C, ta-C:H, a-C:H and rather graphitic non-hydrogenated DLC (a-C).

Caused by their high Csp^3–Csp^3 bonding content of 80 to 88 %, ta-C films exhibit some extreme properties like a hardness of up to 88 GPa [92] and an elastic modulus of up to 800 GPa [7], reflected in a density similar to that of diamond of ~3.26 $g \cdot cm^{-3}$ [93]. Ta-C films show a very high intrinsic stress of up to -13 GPa [94]. The high internal stress limits the possible applicable thickness of ta-C films often to less than 1 µm [7]. On the other hand, ta-C films show a low roughness of ~0.1 nm and due to their high wear resistance, they can be applied even thinner compared to other DLC films systems in applications where wear resistance is required. Ta-C films show a wear rate being typically 100 to 1000 times lower than that of a-C:H coatings. The wear rate of ta-C films is in the range of 10^{-9} $mm^3N^{-1}m^{-1}$, whereas a-C:H films display a wear rate of 10^{-6} to 10^{-7} $mm^3N^{-1}m^{-1}$ [95]. The a-C:H films are known for their extremely low friction coefficients of down to 0.02, whereas ta-C films show lowest friction coefficients around 0.1 [95]. A-C:H films are soft and show a hardness of 10 to 20 GPa, which can be mainly tailored with their hydrogen content ranging from 30 to 40 % [4]. The a-C films are quasi non-hydrogenated DLC films, meaning that their hydrogen content is very low. A-C films are typically deposited by magnetron sputtering and are usually graphitic.

Another class of DLC are ta-C:H films, which can keep a fixed hydrogen content while their properties are mainly tailored by variations in the Csp^3–Csp^3 content [96]. They can have a hardness of 50 GPa [48], and their elastic modulus reaches 300 GPa [97]. Ta-C:H films bridge the properties of ta-C and a-C:H films. Their hydrogen content lies between 25 and 30 at.% [96]. Within this regard, the properties of ion beam deposited ta-C:H films were extensively studied within the present thesis (*Publications 1, 2, 4 and 5*). *Publication 4* represents a comparative study of a-C:H and ta-C:H films.

DLC film properties can be improved by alloying the material with fluorine, boron, nitrogen and various metals [98-102]. For example, the application of nitrogen-doped DLC (a-C:N) as thin film electrodes was initially reported by Yoo et al. [103] and Yee [104] who demonstrated that ta-C films, doped with ~ 10 at.% nitrogen, displayed electrochemical properties similar to those of highly boron doped diamond. Within this regard, a-C:N films were also investigated within the present work. Structural properties and the wetting behavior of magnetron sputtered a-C:N films are presented in *Publication 3* and the electrochemical properties of PLD deposited a-C:N films are discussed in *Unpublished Results*. CrC/a-C:H films were studied by Gassner et al. [36,37], who used reactive direct current magnetron sputtering of chromium in the presence of methane for the deposition of nanostructured films which display tailored properties in tribological applications. Moreover, it is reported that the incorporation of silicon into a-C:H films stabilises the sp^3 bonding, reduces the stress, makes the friction coefficients independent from relative humidity, improves

adhesion on metal substrates and increases the thermal stability and optical gap [105-115]. Therefore, Si-a-C:H films were additionally studied within the present thesis. The results of these investigations are discussed in chapter 5.5.2 of the present thesis.

In general, the tailoring of DLC film properties is mainly a question of the applied coating process and its kinetic energy of carbon species involved in film growth. Ta-C and ta-C:H films can only be deposited with deposition techniques, where the kinetic energy of carbon species is controllable and typically higher than ~30 eV, whereas a-C and a-C:H films can be deposited with a wide range of deposition techniques.

On the following pages, the mainly applied deposition techniques as well as frequently observed applications for the films studied within the present thesis are briefly discussed. Additionally, the landmark properties of these films and the most important process parameters controlling the film growth are presented.

3.2. THE ta-C and ta-C:H FILMS

The properties of ta-C films have been studied intensively in the literature [4 and references therein]. Since ta-C films are deposited at room-temperature, the structure of these films is mainly a function of the ion energy of carbons involved in film growth [4]. These films are deposited with high ion energy deposition techniques like MSIBD, FCVA and UV-PLD [4 and references therein].

The structural network of ta-C films is defined by the connectivity of sp^3 hybridised carbon atoms, meaning that here sp^2 clusters act as defects in the network [4]. In ta-C, there are only a limited number of sp^2 clusters present, which are formed by a few atoms. Therefore, the band gap is determined by the size of these very small graphitic clusters and the degree of their distortion [4]. Authentic ta-C films are almost hydrogen free [4]. Therefore, deposition under high vacuum conditions is mandatory for ta-C growth. Ta-C films exhibit very low roughness values of ~0.1 nm. The roughness of these films was found to be strongly related to the ion energy applied for deposition [94]. Figure 3.1 shows the evolution of the surface roughness as a function of the ion energy of C^+ ions [94].

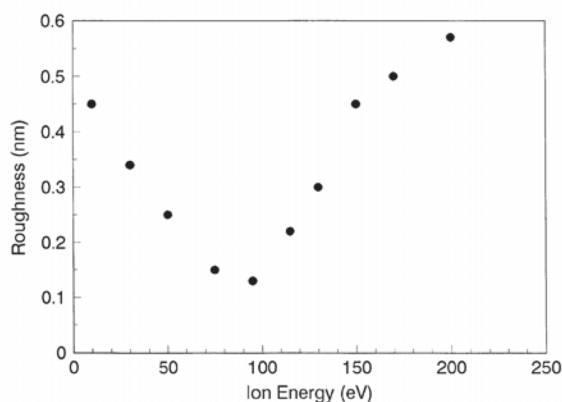

Figure 3.1. Variation of roughness with ion energy for ta-C [94].

It can be seen in Figure 3.1, that lowest roughness values can only be obtained within a very narrow carbon ion energy range from ~80 to 110 eV. Chapter 2.2 of the present thesis describes in detail the origin for such ultra-smooth film growth. Accurate process control with respect to the ion energy present on the substrates is

necessary to obtain ultra-smooth films. Authentic ta-C films are rarely applied in industrial applications due to their high deposition costs, provoked by high costs of coating equipment and low deposition rates.

In contrast, ta-C:H films are frequently applied as wear resistant coating on magnetic discs and heads [52]. In parallel work to the present thesis, the deposited ta-C:H films where also found to excel as hydrogen barrier coatings. Similar to ta-C films, ta-C:H films are also known for their very low roughness, down to 0.1 nm. Therefore, dense films with low thickness can be applied for example in data storage technology. Own results revealed, that the low roughness values of these films can be obtained within a wider range of kinetic carbon energies present during film growth. Within the present work, ion beam deposited films grown with the lowest possible discharge voltage of 1 kV display a RMS roughness of ~0.1 nm, which was not influenced when increasing the discharge voltage up to 3 kV. The kinetic energy of carbons species emitted from the source is assumed to be in direct relation to the discharge voltage, ranging from ~450 to 750 eV [73]. These ion beam deposited films are applicable in data storage technology as ultra thin wear and corrosion protection for hard disk drives. Ta-C:H films can be further deposited by MSIBD, FCVA, ion beam methods and high density plasma reactors [4 and references therein]. The properties of ta-C:H films are tailored by the kinetic energy of carbon species involved in film growth, as discussed in *Publications 1,2,4* and *5*.

It is important to mention, that the source gas for ta-C:H deposition should be C_2H_2. Deposition from methane gives films with less tetrahedral character [69]. The hydrogen content in these films is lower than in a-C:H films and lies between 25 to 30 at.% [96]. Ta-C:H films can have a maximum overall sp^3 hybridised fraction of 75 %, enabling these films to have a significantly higher percentage of Csp^3–Csp^3 bonds in their structural network, showing subsequently significantly higher hardness and improved other mechanical properties compared to a-C:H films with a similar sp^3 hybridised fraction. *Publication 4* presents a comparison of ion beam deposited ta-C:H and reactive magnetron sputtered a-C:H films, whose properties are described in the following chapter of the thesis. Of further importance is the fact, that there is no polymeric regime in ta-C:H coatings, meaning that softer films are graphitic rather than polymeric (*Publication 5*). The hydrogen content in these films is too low to form polymeric chains [4]. Within this context, own results revealed, that ta-C:H films vary their overall sp^3 content (Csp^3–Csp^3 + Csp^3–H1s bonds) only by variations in the Csp^3–Csp^3 bonding content, whereas an increasing overall sp^3 content in a-C:H films is reflected in an increase of the population of Csp^3–H1s bonds (*Publication 4*). *Publication 5* comprehensively examines the relation between structure and mechanical properties of the ion beam deposited ta-C:H films studied within the present thesis.

3.3. THE a-C:H FILMS

Properties of a-C:H films have been studied by many scientists [4 and references therein]. Rather similar to other DLC films, their properties can be tuned by the kinetic energy of carbon species involved in film growth. In addition, the hydrogen content plays an important role when tuning the structure of these films. As mentioned previously, higher hydrogen contents of 30 to 40 at.% result in the polymerisation of these films. Therefore, hydrogen is preferentially bonded to sp^3 hybridised carbon atoms, forming Csp^3–H1s bonds [4]. Application of high bias voltages results in decreased hydrogen contents in these films as presented in *Publication 6*. It is clear, that the loss of hydrogen results in a lower overall sp^3 fraction, consequently almost

reflected only in a loss of Csp^3–H1s bonds. The a-C:H films can be deposited with all DLC deposition techniques, being PACVD the most popular. If these films are deposited by magnetron sputtering, PLD, MSIBD or FCVA, hydrogen or a hydrocarbon gas has to be introduced into the coating chamber simultaneously during carbon evaporation.

In a-C:H films, the Csp^3 sites form a continuous network of C–C bonds. Most carbon atoms are bonded to one or more hydrogen atoms [4]. A large part of the sp^3 bonding in a-C:H is caused by the saturation of carbon with hydrogen, forming a polymeric network. This behaviour was noted for a-C:H films which were grown at elevated C_2H_2 contents during reactive pulsed magnetron sputtering of graphite. In *Publication 6*, the influence of the C_2H_2 content in the process gas mixture on the nanomechanical and nanoscratch properties of these a-C:H films is studied.

As mentioned, *Publication 4* addresses the main structural and mechanical differences between a-C:H and ta-C:H films deposited within the present work. It was found, that during magnetron sputtering of graphite in the presence of C_2H_2, the size of sp^2 clusters was slightly increased by increasing the C_2H_2/Ar-ratio from 0 to 0.25. Sputtering at the highest C_2H_2/Ar ratio of 0.43 resulted in the formation of significantly more Csp^3–H1s bonds in the structure. The increase in Csp^3–H1s bonding fraction was accompanied by an increase in the hydrogen content to 28 at.% (C_2H_2/Ar-ratio of 0.43), whereas the hydrogen content was found to be 23 at.% when sputtering with a C_2H_2/Ar-ratio of 0.25. This described observation is in good agreement with literature [4]. The behaviour clearly identifies the sputtered coatings deposited in the present work as authentic a-C:H coatings, showing a high concentration of Csp^3–H1s bonds at elevated C_2H_2 concentrations used for deposition (*Publications 4 and 6*).

Due to their excellent friction behaviour, a-C:H films are mainly applied as low friction film systems [4]. Due to hydrogen release at elevated temperatures, these films should only be applied in low temperature applications. Within this regard, Gassner et al. [37] reported on a hydrogen release from CrC/a-C:H films at approximately 200°C in vacuum. The hydrogen release is associated with a collapse in the structure into a mostly sp^2 bonded network [5].

3.4. THE ELEMENTAL DOPED DIAMOND-LIKE CARBON FILMS

For elemental doped or alloyed DLC films the tailoring of the film properties follows significantly other process conductions compared to the ion energy controlled ta-C and ta-C:H films. Rather similar to the tailoring of the properties of a-C:H films by their hydrogen contents, elemental doped and alloyed DLC film properties are almost determined by their foreign elemental content.

Within the present thesis, nitrogen or silicon were mixed to the a-C and a-C:H film matrix in order to tailor mainly their surface properties or electrical conductivity (*Publication 3 and Unpublished Results*). It has to be mentioned for the present work, that the foreign elemental contents of these studied films are rather not present at doping elemental concentrations and were found to be at least ~6 at.% silicon in Si-a-C:H films, ~10 at.% nitrogen in magnetron sputtered a-C:N films and at least ~6 at.% nitrogen in PLD deposited a-C:N films.

Publication 3 and the *Unpublished Results* deal with the properties of a-C:N films, studied within the present work. The process development of Si-a-C:H films guided by Raman analysis is described in Chapter 5.5.2.

In principle, all known DLC deposition techniques can be applied for the growth of elemental alloyed DLC films (PA-CVD, PLD, MSIBD, ion beam methods and magnetron sputtering). The element of interest has to be either alloyed to the used target or can also be introduced into the chamber via reactive gases containing the element(s) of interest. In the present case, *i.e.* under room-temperature deposition conditions, nitrogen causes the sp^2 clusters in the films to increase in size with increasing nitrogen content detected in the films (*Publication 3 and Unpublished Results*). The *Unpublished Results* describe the development of an a-C:N film for the application as an electrode in multi-reflection mid-infrared attenuated total reflectance (IR-ATR) spectroelectrochemistry. There, a-C:N coatings were deposited using IR-PLD, involving the ablation of a high purity graphite target in the presence of nitrogen. Nitrogen was found to induce clustering of graphite-like carbon phases which resulted in enhanced conductivity of the films, as required for electrochemical applications.

The clustering of graphite-like phases induced by the addition of nitrogen was monitored with Raman spectroscopy. A percentage of 33 % nitrogen in the process gas mixture resulted in films with highest structural order and highest sp^2 cluster size, while still retaining typical diamond-like character and IR transmittance. The resulting films deposited at the highest nitrogen flow contain approximately 9 at.% nitrogen, and were chosen for the spectroelectrochemical studies. The electrochemical activity of IR-PLD fabricated a-C:N films was verified using the $Ru(NH_3)^{3+/2+}$ redox couple and demonstrated to be comparable with that of other conventional carbon-based electrodes (*Unpublished Results*).

4. STRUCTURE AND HYDROGEN CONTENT OF DIAMOND-LIKE CARBON FILMS AND SELECTED ASPECTS OF FILM CHARACTERISATION

4.1. OUTLINE

The structural characterisation of DLC films is complex and complicated due to the amorphous nature of the material. As previously mentioned, carbon exists in three hybridisations (sp^1, sp^2 and sp^3). The σ bonds of all carbon sites and C–H bonds form occupied σ states in the valence band and empty σ^* states in the conduction band, separated by a wide σ-σ^* gap [116]. The π bonds of sp^2 and sp^1 sites form filled π states and empty π^* states, with a much narrower π-π^* gap [117,118]. The generally most accepted model for atomic structure of DLC was introduced by Robertson [117,118]. His model is based on the properties of the σ and π bonds. Upon maximising the π bonding energy, the sp^2 sites form π bonded clusters within the sp^3 bonded matrix. The size of those clusters is determined by the band gap. Later on, it was found, that the sp^2 cluster size in DLC is overestimated in this model [119-121].

Consistent with the ternary phase diagram of DLC (Figure 2.1), the structural characterisation focuses strongly on the ratio of sp^2 and sp^3 hybridisation of carbon atoms and the hydrogen content of the films. Distinguishing between Csp^3–Csp^3 and Csp^3–H1s bonding character is the main problem occurring in structural analysis of DLC films. The most applied method to measure the sp^3 content is electron energy loss spectroscopy (EELS). However, EELS measurements are difficult in hydrogenated DLC films and require careful fitting to produce the sp^3 values in these films [4]. Hydrogenated DLC films with the same overall sp^3 content can have different optical and mechanical properties due to different sp^2 clustering, different sp^2 orientation, cross sectional nano-structure [51] and a different ratio of Csp^3–Csp^3 and Csp^3–H1s bonds. Indeed, the physical properties of hydrogenated DLC films are usually not related to the mainly probed overall sp^3 content.

Nuclear magnetic resonance spectroscopy (NMR) is able to probe the carbon Csp^3–Csp^3 bonding fraction in hydrogenated DLC films [122-130]. It is the most direct measurement of the Csp^3–Csp^3 fraction by C^{13} NMR. Only a few reports deal with C^{13} NMR of DLC films due to the complex interpretation of the data and the large sample sizes which are needed for the analysis.

Raman spectroscopy has the drawback of complex interpretation of the spectra, but offers the great advantage in that it probes the overall sp^3 content (Csp^3–Csp^3 and Csp^3–H1s) and at the same time the Csp^3–Csp^3 content in hydrogenated DLC films [96]. Raman band parameters are in direct relation to structural, optical and physical properties [51,131,132]. Although Raman spectroscopy does not allow the generation of the exact fraction of Csp^3–Csp^3 bonds for example, comparing the band parameters to literature gives good estimates. Most importantly, the Raman parameters can be used alone when comparing DLC samples together within a series of experiments. Moreover, Raman spectroscopy is able to probe the order/disorder, *i.e.* clustering of the carbon structure [51]. As mentioned previously, the clustering of the sp^2 phase as a fourth axis in the ternary phase diagram should be added in order to further enlighten the link between structure and physical properties of DLC films [51]. Therefore, Raman spectroscopy is able to fully characterise the carbon structure of DLC

films. Alternatively, Raman spectroscopy can also be used to quantify the hydrogen content of DLC samples with hydrogen contents over ~20 at.% [51].

In addition to Raman spectroscopy and infrared spectroscopy, hydrogen contents of DLC films are commonly determined by elastic recoil detection analysis (ERDA) [4]. This method requires nuclear facilities, but has the major advantage of offering the possibility to reveal the quantitative values of the hydrogen and carbon and other elemental contents if a Rutherford backscattering (RBS) signal is additionally recorded. Therefore, highly accurate full elemental quantification can be done within one measurement at one measurement spot in hydrogenated DLC films.

Electron spectroscopy for chemical analysis (ESCA) is used frequently for elemental quantification [4], but the values have to be corrected if hydrogen is present in the investigated DLC films, since with X-ray photoelectron spectroscopy (XPS), the detection of hydrogen is not possible. XPS is highly surface sensitive, which means, that the analysis is restricted only to a few atomic layers on the DLC surface. Therefore, surface contaminants play an important role in XPS analysis.

Mechanical properties of DLC films (hardness, elastic modulus, elasticity) are mostly determined by nanoindentation [133-136], where a small diamond-tip is progressively forced into the film and the force-displacement curve is measured. Especially, when DLC films are used as protective coatings, mechanical properties play an important role [137-147]. However, it is to be stressed, that the hardness values reported for example for ta-C films with a ~90 % Csp^3–Csp^3 bonding content vary from 45 to 88 GPa in literature [47,92,94,148], indicating, that nanoindentation measurements are complex in terms of indentation size effects [149] and effects from the substrate [150,151].

Coming to the investigation of surface properties of DLC films, a number of methods are used to characterise the roughness, surface energy and the surface constituents of these films. Due to its high resolution, atomic force microscopy (AFM) should be used to characterise the surface topography of DLC films, since these films show roughness values of significantly less than 10 nm [4-6]. Due to its versatility, the sessile drop method [152,153] is preferable for the determination of the surface free energy of DLC films, since it can in principle be applied to various shaped DLC coated technical products. There the surface free energy is probed by dropping small volumes of liquids with different free surface energy on the surface of interest. Other methods require dipping a test-body coated with the desired film, which has to be measured, into the liquids. Within this work, the surface free energy and/or the water contact angle was investigated for the film systems Si-a-C:H, a-C:N, a-C, a-C:H and ta-C:H.

Adhesion of DLC films has also to be studied, since it has the highest impact in commercial applications. DLC films are known for their lack of adhesion to various types of substrates [4]. Lack of adhesion is caused almost exclusively by the high intrinsic stresses which are present in these films. Properties such as a hardness value of up to 88 GPa [92] and an elastic modulus of up to 800 GPa [7], authenticate ta-C as the most stressed DLC film system showing a very high intrinsic stress of up to -13 GPa [94]. As previously stated, the high internal stress limits the possible applicable thickness of ta-C films often to less than 1 µm [7]. A film will delaminate

when the energy per unit volume due to the stress exceeds the surface fracture energy per surface [4]. For a given stress, this sets an upper limit for the film thickness. An important film deposition process step is proper substrate cleaning in order to ensure a proper film adhesion. This is usually done by Ar^+ ion bombardment. The Ar^+ ion bombardment can be achieved either via a glow discharge directly applied to the substrates or as in the case of the present work this can be done by the use of an ion beam source (e.g. anode layer source). This source offers the great advantage, that the Ar^+ acceleration to the substrate is almost independent from the substrate conductivity, which is in contrast to the typically applied glow discharge etching method, where a DC or pulsed DC electric field is applied to the conductive substrates to form an etching plasma. Moreover, the application of an intense glow discharge etching procedure will result in high substrate temperatures. Therefore, whenever a glow discharge etching procedure was applied, the etching parameters were chosen in a fashion to keep the substrate temperature well below 100°C (*Publication 3*).

Within the present thesis it was found, that a discharge voltage of 1 kV applied to the ion beam source together with an Ar flow rate of 15 sccm and an O_2 flow rate of 5 sccm gives excellent results of DLC film adhesion on substrates made of for example polyimide, polyvinylchloride, polyethylene, polyethylenetherephtalat, etc.. The adhesion of the deposited films on austenitic steels and aluminium alloys was also found to be excellent (pre-treatment was carried out by applying a discharge voltage of 2 kV at an Ar flow rate of 20 sccm). It is assumed, that the reason for the excellent adhesion of the DLC films on these soft substrates is a stress relief due to the possible relaxation of the film [4]. Intrinsic stresses of the deposited film systems are investigated in *Publications 1, 2 and 4*.

On the following pages, selected aspects on the characterisation of DLC films are discussed. The presented analytical techniques and concepts appeared to be very important within the work and were found to be not frequently applied in DLC research.

Raman spectroscopy was extensively applied to all deposited DLC film systems and appears therefore as an independent chapter in the thesis. New trends in Raman spectroscopy of carbon phases as well as selected own applications of Raman spectroscopy are presented in chapter 5. The potential of this analytical technique as process development guiding tool is discussed. The cluster model, which appears to be the basis for the structural analysis of DLC films, is discussed in the following chapter of the thesis.

4.2. ATOMIC AND ELECTRONIC STRUCTURE – CLUSTER MODEL

The cluster model is the basis to understand the bonding configurations and the electronic structure in DLC. Robertson [4] proposes a simple description of the electronic structure and the bonding in DLC [4], as described in the following:

The Huckel approximation is used for treating the σ and π states separately [116]. The σ and π states lie at different energies and the π states lie in an orthogonal plane to the σ bonds and sp^2 sites, so that their interaction is small [117,118]. The main effect is that π bonding favours a clustering of sp^2 sites because of the energy gain compared to a random distribution of sp^2 and sp^3 sites. An arbitrary network of π states forms a

half-filled band. The binding energy of the occupied states is lowered if one creates a gap in this band at the Fermi level (E_F). Robertson proposes that further effects can be deduced by analogy to the behaviour of organic molecules [116,117]. The following list outlines the landmarks of Robertson's cluster model [116].

- Any cluster will tend to have an even number of π orbitals, or otherwise there is a half-filled state at the E_F, which lowers the binding energy. The unpaired state at the E_F is a coordination defect.
- A pair of sp^2 sites tends to align their π states parallel, to maximise the π interaction, as in ethylene.
- The sp^2 sites tend to form planar clusters, to maximise the π interaction.
- Three pairs of ethylene-like C=C units tend to group into a six-fold ring, as in benzene. This gains an aromatic stabilisation energy, as the π electrons are now delocalised over the ring.
- A further small energy gain occurs if the six-fold benzene rings condense into graphitic sheets.
- Odd-member or eight-fold rings are not favoured, as these usually give rise to states near E_F, which reduces the binding energy.

The cluster model proposes, that sp^2 clusters are arranged in a planar fashion, which are embedded in the sp^3 hybridised matrix [116]. The arrangement of the sp^2 sites controls the electronic properties and the optical gap, because their π states lie closest to E_F, while the sp^3 fraction controls the mechanical properties, as corroborated in *Publication 5* of the present thesis. The cluster model arises from the weak, long range attraction of π sites [116], which can be probed by Raman spectroscopy. This again verifies Raman spectroscopy as the most important structural analysis tool, since with Raman spectroscopy it is possible to figure out the changes in sp^2 clusters size, while also be in relation to changes in the carbon sp^3 content.

Following the cluster model proposed by Robertson, the band gap of the aromatic clusters has a very simple form. The most stable planar, compact clusters have a band gap E_g given below in equation 4.1:

$$E_g \approx \frac{2\gamma}{M^{1/2}} \quad 4.1$$

There, γ is the nearest neighbour $V(pp\pi)$ interaction, and M the number of six-fold rings in the cluster. M can be related to the cluster diameter or in-plane correlation length L_a as $M \sim L_a^2$, so that

$$E_g \approx \frac{2\gamma}{L_a} \quad 4.2$$

Equation 4.1 says that the band gap depends only on the π states of sp^2 states and it varies inversely with the cluster diameter. This applies only to undistorted clusters. Thus, the gap depends only on the sp^2 configuration and not on that of other atoms such as hydrogen [117].

As mentioned previously, the cluster model proposed by Robertson overestimates the sp^2 cluster size [119-121], *i.e.* the structural order in as deposited films. This is because the ion-dominated deposition processes, which are needed to stabilise sp^3 bonding, also introduce a large disorder energy. This disorder

energy is comparable to the stabilisation energy of forming larger clusters. The clusters must be quite large to give band gaps of the size found by experiments [4]. Such clusters are not found experimentally in as-deposited a-C and a-C:H, and can only be found in thermally annealed DLC samples [4]. A more accurate schematic of a carbon DLC network is shown in Figure 4.1.

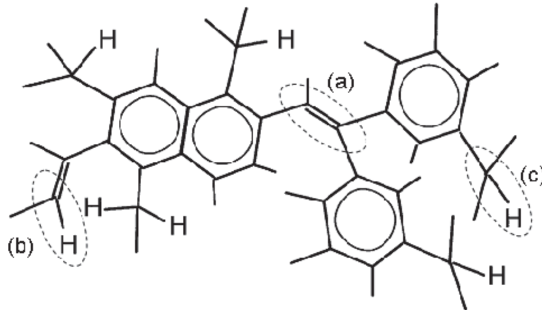

Figure 4.1. Schematic of sp^2 clusters in a-C:H [after 94]. Examples for Csp^2–Csp^2 (a), Csp^2–H1s (b) and Csp^3–H1s (c) bonds are shown.

More likely, the cluster model provides a reasonable description of micro-crystalline graphite and annealed DLC films. Figure 4.1 shows, that in a-C:H films the sp^2 sites are mainly arranged in small olefinic chains and conjugated systems. It can also be seen, that the Csp^3 fraction is low in authentic a-C:H films. Therefore, in this kind of films, Csp^2–Csp^2, Csp^2–H1s and Csp^3–H1s bonds form the structural network (Figure 4.1).

From this discussion, one can imagine, that accurate interpretation of analytical results gained from DLC films and their proper connection to the authentic structure present in an investigated film is time consuming and far from satisfaction.

4.3. SELECTED ASPECTS OF DLC FILM CHARACTERISATION

4.3.1. Elemental content analysis by ERDA/RBS

The knowledge of the hydrogen content in the deposited DLC films is of great importance for the present thesis. Except of the deposited ta-C and a-C:N films, whose hydrogen content is assumed to be very low due to their Raman band contour, all deposited films contain hydrogen in a significant concentration. As the ternary phase diagram of sp^3 and sp^2 hybridised carbon and hydrogen allows us to classify DLC films, the knowledge of hydrogen contents is necessary for a complete analysis of a hydrogenated DLC film. ERDA is accepted as the most appropriate method to determine the hydrogen content in DLC films. The formalism developed for this purpose was first established by L'Ecuyer et al. [154], who showed in 1976 the analytical capabilities of ERDA. ERDA is based on the detection of light nucleus recoil from a target bombarded by energetic ions [155]. The energy of a recoil nucleus E_1 is defined through the following equation [155]:

$$E_1 = E_0 \frac{4M_1M_2}{(M_1+M_2)^2}\cos^2\Theta \qquad 4.3$$

There, E_0 is the projectiles particle initial energy, M_1 and M_2 are the masses of the projectile and the target atom and Θ is the recoil angle. Figure 4.2 shows schematically the collision between an incident ion M_1 and a target atom M_2.

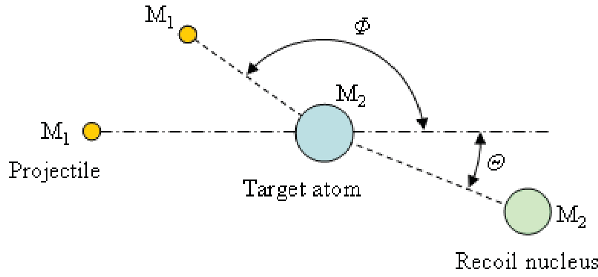

Figure 4.2. Schematic of the collision between an incident ion M_1 and a target atom M_2 [after 155].

The geometry of the collision is characterised by the relation between the scattering angle Φ (RBS) and the recoil angle Θ (ERDA) [155]:

$$\cos^2\Theta = \frac{(M_1M_2)^2 - (M_1\cos\Phi \pm \sqrt{(M_2{}^2 - M_1{}^2\sin^2\Phi)})^2}{4M_1M_2} \qquad 4.4$$

Within the present thesis, ERDA/RBS measurements were performed at the 2 MV tandetron accelerator at the Jozef Stefan Institute in Ljubljana. There, a lithium (^{7}Li) ion beam with an energy of 4.2 MeV was used for ERDA [156].

In order to accurately determine the number of impact ions, El Bouanani et al. [157] developed an in-beam charge-collection device, consisting of a tungsten mesh enclosed by two negatively biased annular electrodes and a shaping slit. Further information on this device can be found in reference [157]. This device was also used for the measurements within the present thesis. The aim of the mesh charge collector set behind the shaping slit was to measure the number of ions hitting the target [157]. The bias on the electrodes was set to -800 V in order to suppress the secondary electron current from the mesh. The beam normalisation parameter of the measured spectra *i.e.* the number N of ions hitting the sample multiplied by the detector solid angle Ω_{RBS}, is proportional to the charge q collected by the mesh charge collector [156]:

$$N\Omega_{ERDA} = R_q \qquad 4.5$$

The coefficient R was calibrated by measuring the RBS yield from thin standard targets. The measured RBS and ERDA spectra were analyzed using SIMNRA code [158].

The investigations of ta-C:H films deposited with the anode layer source revealed, that the hydrogen content had not been changed significantly by application of discharge voltages between 1 and 3 kV. For a discharge of 1 kV the hydrogen content was found to be 21.2 at.%, whereas discharge voltages of 2 and 3 kV showed hydrogen contents of 22 at.% and 23.5 at.%, respectively. These data were of importance for *Publication 5*,

where the influence of the structure and the hydrogen content on the nanomechanical properties of a-C:H films was studied. Combination of resonant Raman spectroscopy with the ERDA/RBS data revealed, that these films follow accurately the tetrahedral regime displayed in the ternary phase diagram shown in Figure 2.1.

Investigations of Si-C:H films deposited by reactive RF unbalanced magnetron sputtering of silicon in the presence of C_2H_2 in the process gas mixture showed, that these films can be categorised to polymeric a-C:H films. In particular, the ERDA measurements revealed increasing hydrogen contents when increasing the C_2H_2 concentration in the chamber from 4 to 10 %, corroborating the trends derived from Raman spectroscopy. Sputtering in 4 % C_2H_2 showed a hydrogen concentration of 23 at.%, whereas the use of 8 % C_2H_2 showed a hydrogen concentration of 33.7 at.% in the film. By further increasing the C_2H_2 concentration in the chamber to 10 %, a hydrogen concentration of 34 at.% was observed. It can be concluded from Raman and ERDA data, that these films represent highly hydrogenated a-C:H samples.

RBS studies further revealed that the carbon content of the investigated films increases with increasing C_2H_2 content in the chamber, being in line with the trends of increasing sp^2 clustering derived by Raman investigations. Si contents were found to decrease with increasing C_2H_2 concentrations in the chamber. ERDA/RBS data are summarised in Table 5.1. Chapter 5.5.2 gives a overview of the results obtained from the Si-a-C:H films.

4.3.2. Surface free energy determination

The knowledge about the surface free energy of the deposited DLC films was one main task of the present thesis. The surface energy and the wetting properties of the films were determined by the sessile drop method [152,153]. Herewith, a small drop of a chosen test liquid with a small volume is displaced on the DLC film of interest. Depending on the surface properties, *i.e.* surface energy of the tested surface, the drop will form a defined contact angle at the air-solid-liquid interface, which is schematically shown in Figure 4.3. The contact angles of different test liquids are used to determine the surface energy of the DLC films.

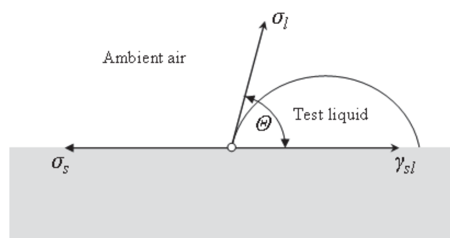

Figure 4.3. Test liquid on a sample surface showing the contact angle Θ and vectors σ_S, σ_l and γ_{Sl}.

In order to calculate the surface free energies, the model of Owens, Wendt, Rabel and Kaelble (OWRK-theory) was used. In this theory, the surface free energy is divided in a dispersive (σ_s^D) and polar component (σ_s^P). [152,153]. Following equation 4.6, the contact angle Θ depends on three vectors as shown in Figure 4.3. These three vectors are: the surface tension of the DLC film (σ_s); the surface tension of the liquid (σ_l) and the interfacial tension of the liquid and the DLC film (γsl) (Figure 4.3).

$$\sigma_s = \gamma_{sl} + \sigma_l \cos\Theta \quad 4.6$$

Upon insertion of the contact angles of minimal two liquids with known σ_l^P and σ_l^D in equation 4.7 [152,153] and a plot of y to x, σ_s^P and σ_s^D of the surface energy of the DLC films can be determined by the use of a linear regression.

Here, y is $\frac{(1+\cos\Theta)\sigma_l}{2\sqrt{\sigma_l^D}}$; k is $\sqrt{\sigma_s^P}$; x is $\sqrt{\frac{\sigma_l^P}{\sigma_l^D}}$ and d is $\sqrt{\sigma_s^D}$.

The square of k yields σ_s^P and the square of d yields the value for σ_s^D.

$$\frac{(1+\cos\Theta)\sigma_l}{2\sqrt{\sigma_l^D}} = \sqrt{\sigma_s^P}\sqrt{\frac{\sigma_l^P}{\sigma_l^D}} + \sqrt{\sigma_s^D} \quad 4.7$$

Figure 4.4 shows the experimental setup used for the determination of the surface energy of the deposited DLC films within the present thesis.

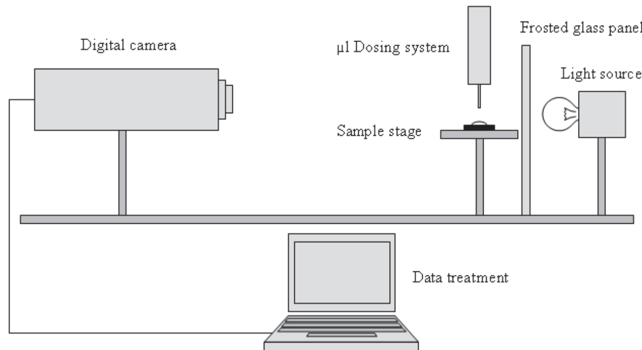

Figure 4.4. Experimental setup for surface energy determination of DLC films installed at the Laser Center Leoben.

The investigation of the surface free energies of the deposited DLC films brought out important results during the present thesis. As mentioned in *Publication 3*, the water contact angle increases with storage time post deposition for a-C and a-C:N films. This phenomenon is known [4 and References therein] and is attributed to a passivation of surface dangling bonds. Results shown in *Publication 3* revealed, that this passivation of the DLC films surface stabilises within a storage time of 24 hours counted from opening the deposition chamber after the deposition process. Further studies on this effect showed, that a significantly elongated storage time of 1000 days in atmosphere did not further increase the water contact angle, indicating that the passivation process is indeed completed within 24 hours post deposition.

An a-C:H film, which was deposited by reactive pulsed DC magnetron sputtering of graphite showed a similar behaviour, noted by a saturation of the contact angle of water after 24 hours post deposition. Figure 4.5 shows the results of this investigation.

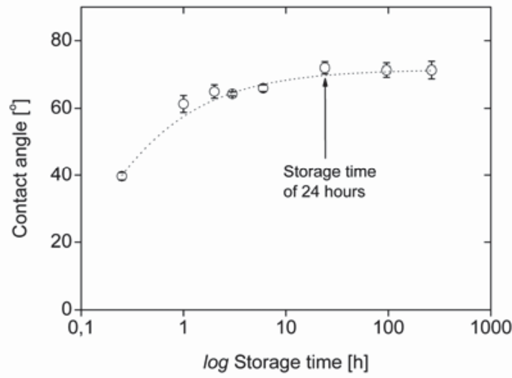

Figure 4.5. Water contact angle versus storage time of an a-C:H film deposited by reactive pulsed DC magnetron sputtering of graphite on a glass slide.

Further observation of the surface energy values showed, that σ_s^P decreases from ~19 mN·m^{-1} to ~6 mN·m^{-1} upon storage for 11 days. Consequently, the surface energy decreases from 57 mN·m^{-1} to 46 mN·m^{-1}. Figure 4.6 predict graphically the variation in σ_s^P, σ_s^D and σ.

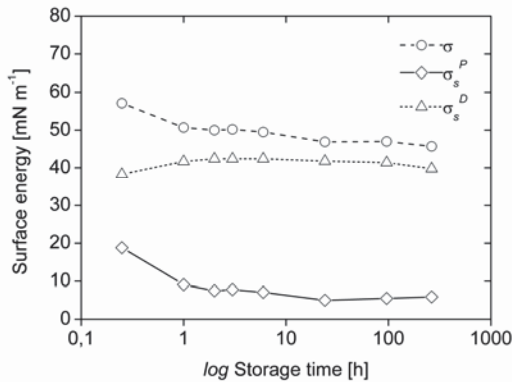

Figure 4.6. σ_s^P, σ_s^D and σ as a function of the storage time of an a-C:H film deposited by pulsed DC magnetron sputtering of graphite on a glass slide.

Consistent with the trends observed for the water contact angle, significant changes are observed only within 24 hours of storage after deposition. The experiments further verified, that the changes in the first 24 hours of storage are almost only reflected in a decrease σ_s^P, which can be interpreted as passivation of polar groups on the DLC surface. Considering this behaviour, investigations on the surface properties of DLC films were carried out on films which were stored for 24 hours in order to achieve a stable surface chemistry. Surface properties found within a storage time of 24 hours are not of practical interest.

Surface energy values of ta-C:H and a-C:H films are compared in *Publication 4*. There, it was found, that σ is rather similar for these two film systems and changes are only reflected in the contact angle for water. Interestingly, a bias support of -100 V during pulsed DC magnetron sputtering of graphite with Ar as process gas showed enhanced contact angles of 90°, compared to 80° detected for the grounded sample. Surface energy measurements revealed average values in the range of 46 mN m^{-1} for a-C:H films deposited by magnetron sputtering. σ_s^P did not exceed 2.5 mN m^{-1}. Therefore, the surface energy showed high dispersive character for the investigated a-C:H films. The measured values agree well to literature, and were found to be typical for a-C:H coatings [4]. The surface energy measurements on films deposited by applying the anode layer source revealed average values in the range of 41 mN m^{-1}, where σ_s^P was around 4.3 mN m^{-1}. Therefore,

also here the surface energy showed high dispersive character for all films deposited. No dependence of process parameters on surface energy and wetting properties were found for the a-C:H and ta-C:H films.

This contrasts significantly to the investigated Si-a-C:H films, where it was found, that σ_s^P can be effectively tailored by variations in the C_2H_2 concentration during reactive RF unbalanced magnetron sputtering of silicon. The development of these films is summarized in chapter 5.5.2 of the present thesis. It can be seen, that via increasing the C_2H_2 concentration in the chamber from 4 to 8 and 10 % in the process gas mixture, a decrease of σ_s^P from 17 to 8 and 4 $mN \cdot m^{-1}$ was possible, while σ showed a high value of ~50 $mN \cdot m^{-1}$ for 4 % C_2H_2 in the chamber, which was decreased to ~40 mN m^{-1} for C_2H_2 concentrations of 8 and 10 %. Considering Raman, ERDA and RBS data from these films (Table 5.1), it is possible to derive the trend, that a loss of silicon contents and a gain in hydrogen contents are the origin for the reported decrease in σ_s^P for these films.

In summary, all investigations showed that the surface energy or the water contact angle can be effectively tuned with addition of nitrogen and silicon into the DLC matrix. The surface energy of non-doped film systems like a-C:H and ta-C:H was found to be barely tailorable by variations in the process parameters while the carbon structure of these films could be effectively tuned by appropriate process parameters.

5. RAMAN SPECTROSCOPY OF DIAMOND-LIKE CARBON FILMS

5.1. OUTLINE

The Raman effect, first described by Chandrasekhara Venkata Raman [159], has its origin in the inelastic scattering of photons on the molecule being probed [160]. His work on scattering of light on molecules was honoured in 1930 with the Nobel Prize in Physics. In Raman spectroscopy, the probed sample is irradiated with monochromatic light. About one of 10^7 photons collides with a molecule and gives off some of its energy to the molecule. Thereby, the light appears as scattered light with lower energy compared to the energy of the primal light irradiating the sample. The scattered light with lower energy (lower frequency) is called Stokes-scattering. It is also possible, that energy is transmitted from the molecule to the photon. This phenomenon is called Anti-Stokes scattering. However, Raman active are molecules whose polarisability is anisotropic. Raman spectroscopy represents a standard structural characterisation technique for any carbon system. It is non-destructive and allows an insight in the structural parameters by means of [after 51]:

- Identification of the structural class of carbon films (ta-C, ta-C:H, a-C:H, a-C, polymeric a-C:H, a-C:N, a-C:H:N, ta-C:H:N, graphite, diamond etc.) due to the spectral shape of their active Raman bands.
- Measure of the degree of order/disorder in the carbon film structure, *i.e.* the clustering of the sp^2 phase
- Measure of the orientation of the sp^2 phase
- Identification of variations in the Csp^3–Csp^3 bonding content
- Identification of variations in the Csp^3–H1s bonding content
- Identification of variations in the Csp^2–H1s bonding content
- Estimation of hydrogen contents >20 at.%

Therefore, the Raman spectra depend on [51]:

- The clustering of the sp^2 phase
- The bond-length and bond-angle disorder of carbon bonds
- The presence of sp^2 rings or chains
- The sp^2/sp^3 hybridised carbon fraction

All carbons show their dominating features in the spectral range of ~800 to 2000 cm^{-1}: The so-called D-band, which is present at ~1360 cm^{-1}, the G-band present at ~1560 cm^{-1} and the T-band present at ~1060 cm^{-1} [51 and references therein]. The T-band can only be observed in ultraviolet (UV) excitation, whereas the G-band and D-band is present in booth visible and UV excitation. The T-band is due to Csp^3 vibrations [161-164]. The G-band and D-band are due to vibrations of sp^2 sites [51]. The G-band has its origin in the bond-stretching of all pairs of sp^2 atoms in rings and chains and the D-band originates from the breathing modes of sp^2 carbon rings [165-169]. In the visible Raman spectra, the cross-section of sp^2 hybridised phases is 50 to 250 times higher than that of the sp^3 phases [170,171]. Therefore, visible Raman spectra of DLC films do not show any signals originating from the sp^3 hybridised phase. Visible Raman spectra depend directly on

the configuration of the sp^2 phase and only indirectly on the sp^3 phase [51]. Only Raman spectroscopy allows an insight in the clustering of sp^2 phases. As mentioned previously, Raman band parameters are in direct relation to structural, optical and physical properties of DLC films [51,131,132]. Furthermore, it also allows an insight in the structure of a-C:N films [51].

In most cases the sp^2 fraction varies consistently with the sp^3 fraction [after 51]. However, in some cases (high temperature deposition, annealing after deposition, unfiltered deposition processes, low dose ion-implantation) the sp^2 configuration can be changed independently from the sp^2/sp^3 ratio [51]. Ferrari and Robertson [166] call this phenomenon hysteresis or non-uniqueness [166]. Therefore, the interpretation of Raman spectra can be quite complex and time consuming. Typically, spectra fitting and interpretation consumes almost all time of a Raman analysis.

It has also been reported, that fluorinated DLC films and metal incorporated DLC films can be easily probed with Raman spectroscopy in a similar fashion to un-doped films by considering the effect on the sp^2 clustering of the hetero atoms and using the rules for the interpretation of Raman spectra similar to a-C (ta-C) and a-C:H (ta-C:H) films. Moreover, possibly present nitrides/carbides (CNx/MeCx) in the amorphous carbon matrix can be detected with Raman spectroscopy, too.

Raman spectroscopy with a broad range of excitation energies was applied to all deposited DLC films systems (a-C, a-C:H, ta-C, ta-C:H, a-C:N, Si-a-C:H, polymeric a-C:H). It was found, that all structural properties could be addressed with Raman spectroscopy. Moreover, Raman spectroscopy was found to be an effective structural characterisation tool during process development. Alternating the working steps, coating experiment and subsequent Raman spectroscopic analysis was found to be the most appropriate way of process tuning. Therefore, it can be concluded, that Raman spectroscopy is of inherent importance in DLC research. On the following pages, a short overview on the Raman band formation in DLC, a summary of interpretation rules in particular for a-C:H films, as well as selected own examples of Raman spectroscopy applications are given.

5.2. THE D-MODES AND G-MODES

Raman is light scattering by the change in the polarisability χ due to a lattice vibration [160].

$$\chi(k) = \chi_0 + \frac{d\chi}{dq} Q(k,q) \qquad 5.1$$

There, χ is the polarisability at wavevector k and Q represents the amplitude of a phonon wavevector q. This change in polarisability causes an inelastic scattering of an incident photon (ω, k) into the scattered photon (ω', k') (ω is the phonon frequency) [4]. The Raman cross-section C can be expressed as [4]:

$$C = k\left(\frac{d\chi}{d\omega}\right)^2 \qquad 5.2$$

The polarisation can occur by excitation of the electronic ground state into virtual states at energy *E* or into real states at *E* [4]. The latter is called resonant Raman [160]. Raman spectra of disordered carbons are in strong contrast to single crystals [166]. The vibrational density of states (VDOS) of disordered carbon with variations in sp^3 contents consist of very smooth and broadened features [172,173]. The Raman spectra do not follow the VDOS of the sp^2 sites [4]. The reason for this behaviour is that the matrix element has a much stronger effect than in σ bonded networks. So, the Raman spectrum is controlled by the order of the sp^2 sites and not their fraction [166].

Due to the higher cross-section of sp^2 hybridised carbons originating from π states, the spectra of disordered carbons are dominated by the D-bands and G-bands. In particular, the π states are of lower energy than the σ states and so they are much more polarisable [117]. This causes for example the Raman spectrum of even ta-C with a sp^2 fraction of only 10 to 15 at.% dominated by signals originating of sp^2 vibrations [4]. The G-mode of graphite at 1581 cm^{-1} has E_{2g} symmetry [166]. The vector of the G-mode is shown in Figure 5.1a.

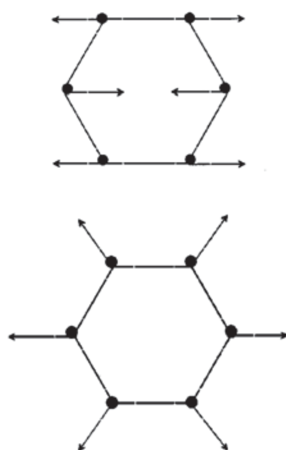

Figure 5.1a. Carbon motions in the G-mode. The G-mode is due the relative motion of sp^2 atoms and can be found in chains as well [166].

Figure 5.1b. Carbon motions in the D-mode. The D-mode is also called breathing mode [166].

The G-mode involves the in-plane bond-stretching motion of pairs of sp^2 hybridised carbon atoms [166]. This mode does not require the presence of six-fold carbon rings and occurs at all sp^2 sites. It is always present around 1500-1630 cm^{-1}. The D-mode present at ~1360 cm^{-1} is a breathing mode of A_{1g} symmetry involving phonons near the K zone boundary. The motion of carbon atoms in the D-mode is shown in Figure 5.1b. The D-mode is forbidden in perfect graphite and becomes visible only in disordered carbons [166]. The presence of this mode is strictly related to the presence of six-fold rings [166] and disorder. G-modes and D-modes tend to suppress modes of other symmetries [4]. Tuinstra and Koenig [165] noted that the intensity ratio of the D-mode and the G-mode (intensity ratio I_D/I_G), varies inversely with the in-plane correlation length L_a or grain size of the graphite.

$$\frac{I_D}{I_G} = \frac{c}{L_a} \tag{5.3}$$

There, *c* is the Raman coupling coefficient (*c* (515 nm)~44 Å) [166]. This means, that the intensity ratio I_D/I_G is proportional to the number of rings at the edge of a grain present in disordered carbons [4]. Since the G-band is due to all sp^2 sites, but the D-band is only due to six-fold rings, the intensity ratio falls as the number of

rings per cluster falls and the fraction of chain-like molecules is raised [4]. For DLC films, however, the Tuinstra-Koenig relation (equation 5.3) is not valid. Therefore, Robertson proposes to use equation 5.4 instead of equation 5.3.

$$\frac{I_D}{I_G} = cL_a^{\ 2} \qquad 5.4$$

The structure of DLC films can be enlighten by critical evaluation of the following Raman band parameters [4]:

- Intensity ratio I_D/I_G
- Position of the G-band (Pos. (G))
- Full width at half maximum of the G-band (FWHM (G)
- Shift, *i.e.* dispersion of Pos. (G), with excitation energy (Disp. (G))

To see how these Raman band parameters can be linked to the structure of DLC films, the following pages deal with the relation of these band parameters to the structural, mechanical and chemical properties of DLC films. Selected examples of own research with Raman spectroscopy are located at the end of this chapter.

5.3. INTERPRETATION OF RAMAN SPECTRA

5.3.1. Spectrum fitting

In order to provide a basis for the interpretation of Raman spectra, it must be clarified, how the obtained spectra should be fitted. In general there are two options for fitting Raman spectra: (1) an all symmetric Gaussian fit and (2) a Lorentzian line shape for the D-band and a Breit-Wigner-Fano (BWF) line shape for the G-band. The rather unknown BWF-function is given in equation 5.5 [4].

$$I(\omega) = \frac{I_0[1 + 2(\omega - \omega_0)/Q\Gamma]^2}{1 + [2(\omega - \omega_0)/\Gamma]^2} \qquad 5.5$$

There, I_0 is the band intensity, ω_0 is the band position, Γ is the FWHM and Q^{-1} is the coupling coefficient. Within this regard, these two options of Raman-band fitting were studied within the present work. It was found, that the fully symmetric Gaussian fit works well for all DLC films studied. Especially, within accordance to literature, the BWF line shape does not work very well for strongly hydrogenated DLC films, due to the influence of the background on the coupling coefficient. The BWF line shape tends to adjust its asymmetry to reproduce the photoluminescence slope present in these samples.

In order to compare the results obtained by a double Gaussian fit and a combination of a Lorentzian line shape for the D-band and a BWF line shape for the G-band, the ta-C:H films deposited with the ion beam source were studied in detail. It was found, that the overall observed trends in a series of experiments with respect to the intensity ratio I_D/I_D, FWHM (G) and Pos. (G) are not influenced by the mentioned fitting methods. It is

important to note, that the BWF line shape gives much higher values for FWHM (G), due to its asymmetry, and therefore, also the intensity ratio I_D/I_G was found to be almost zero for the ion beam source deposited ta-C:H films (*Publication 1 and 4*). In a similar fashion it was found, that an asymmetric Gaussian line shape for the G-band tends to behave in the same way, by showing the tendency to reproduce the D-band. An example for a double symmetric Gaussian fit and a combination of a Lorentzian line shape for the D-band and a BWF line shape for the G-band is shown in Figures 5.2a and 5.2b.

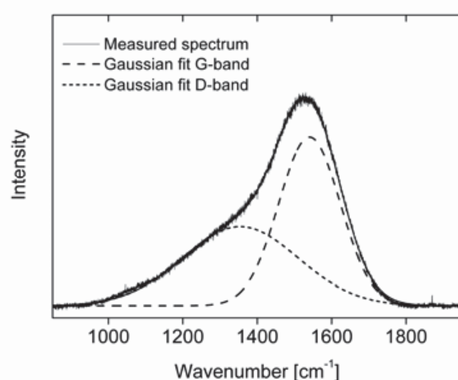

Figure 5.2a. Exemplary double Gaussian fit for the D-band and the G-band for a ta-C:H film deposited with the ion beam source used within this work.

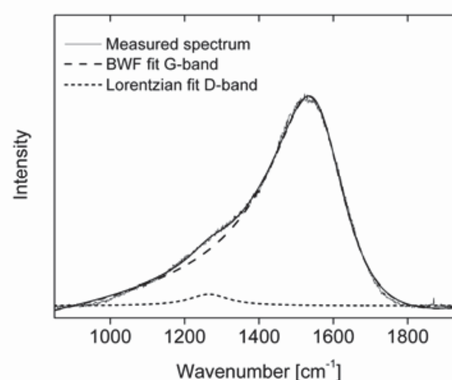

Figure 5.2b. Exemplary fit by applying a Lorentzian line shape for the D-band and a BWF line shape for the G-band for a film deposited with the ion beam source used within this work. Data reduction was applied for this set of raw data.

It can be clearly seen, how the BWF line shape tends to reproduce the D-band, resulting in a significantly higher FWHM (G) and a significantly lower intensity ratio I_D/I_G (Figure 5.2b). Since fully symmetric Gaussian line shapes work better in the presence of a background and a large number of scientific articles deal with the trends of Raman band parameters fitted with Gaussian functions, it was concluded to fit the obtained spectra within the present thesis with Gaussian functions for the D-band and the G-band.

The fitting procedure decided should be consistently applied within a set of DLC films. A proper fitting procedure with high accuracy will always show similar trends compared to other fitting methods. The studies should yield the same trends but the absolute numbers with respect to intensity ratio I_D/I_G, FWHM (G) and Pos. (G) can be different. Therefore, attention must be focused on the fitting procedure reported in a scientific article, when comparing own results with literature. Moreover, it is not always clear, if the intensity ratio I_D/I_G is the ratio of the band heights or band areas. The broadening of Raman bands of amorphous carbons is a function of the disorder being a measure of the Csp^3 content, and the information about the less distorted aromatic rings which are preferably probed with the intensity ratio I_D/I_G lies in the height of the bands [166]. Therefore, the present work uses band height intensity ratios I_D/I_G (except in *Publication 3*), since from the above discussion it can be derived, that authentic trends in clustering of sp^2 phases will be smeared out by using the area ratio.

5.3.2. The three-stage model

Dealing with the interpretation of the trends in D-bands and G-bands, Ferrari et al. [97] found, that it is possible to classify the spectra of disordered carbons within a three stage model of increasing disorder (Figure 5.3). The three stages are [97]:

Stage 1: perfect single-crystalline graphite to nano-crystalline graphite
Stage 2: nano-crystalline graphite to sp^2 a-C
Stage 3: sp^2 a-C to sp^3 a-C (ta-C)

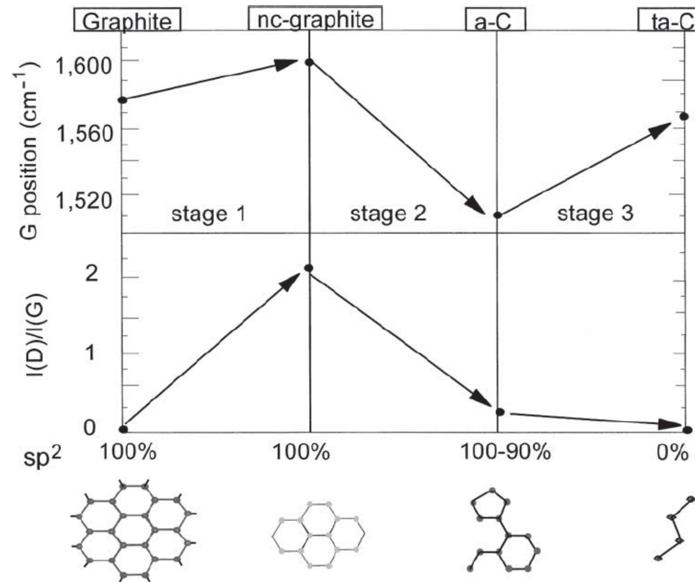

Figure 5.3. Schematic variation of Raman G-band wavenumber and the intensity ratio I_D/I_G with the degree of disorder [after 97]. The variation in G-band position and intensity ratio I_D/I_G refers to an excitation wavelength of 512 nm and fitting procedure by applying a Lorentzian line shape for the D-band and a BWF line shape for the G-band.

Stage 1 corresponds to the structural change from perfect graphite to nano-crystalline graphite. The main changes in the Raman spectrum are the following [after 166]:

- The G-band moves from 1581 to ~1600 cm^{-1}.
- The D-band appears and the intensity ratio I_D/I_G increases
- The Pos. (G) is not dispersive, *i.e.* it has similar positions in spectra taken at varied excitation energy.

The origin of these variations is explained in detail in Reference [166]. The main structural change in stage 1 is the passing from a mono-crystalline material to a poly-crystalline material [166].

Stage 2 corresponds to the structural change from nano-crystalline graphite to a-C. Here, defects are progressively introduced into the graphite layer, causing the phonon modes to soften, particular for the G-band [166]. The end of stage 2 corresponds to a completely disordered, almost fully sp^2 bonded a-C network. This structure consists of distorted six-fold rings [166]. The main changes in the Raman spectrum are the following [after 166]:

- The G-band decreases from 1600 cm^{-1} to 1510 cm^{-1}.
- The intensity ratio I_D/I_G decreases.
- The Pos. (G) disperses with excitation energy.

The intensity ratio I_D/I_G is proportional to the number and clustering sp^2 carbon rings [166]. The main effect in stage 2 is disordering, decreasing the number of ordered rings, reflected in a decrease of the intensity ratio I_D/I_G.

Stage 3 corresponds to the structural change from a-C to ta-C. Here, the sp^3 content increases from ~10 % to ~85 % [166]. The sp^2 sites change gradually from rings to chains. The main changes in band parameters are [after 166]:

- The G-band increases from ~1510 to 1570 cm^{-1}.
- The intensity ratio I_D/I_G decreases and is very low or zero.
- The Pos. (G) disperses with excitation energy.

The structural evolution from stage 1 to stage 3 is called amorphisation trajectory or disordering trajectory and the structural evolution from ta-C to single-crystal graphite is called ordering trajectory.

5.3.3. The intensity ratio I_D/I_G

In order to interpret the results obtained within the present thesis, the three stage model which is based on changes in non-hydrogenated DLC films is expanded to the structural evolution in hydrogenated DLC films. Moreover, it was attempted to link the Raman band parameters to mechanical properties, since there is an increasing interest in the relation of Raman band parameters and mechanical properties of non-hydrogenated and hydrogenated DLC films.

The I_D/I_G ratio, assigned to vary with the overall sp^3 content (Csp^3–Csp^3 + Csp^3–H1s) in a-C:H films, is zero for ta-C and polymeric a-C:H [96]. Since the I_D/I_G ratio is a parameter which probes the amount of ring-like sp^2 clusters in DLC films, it enables the prediction that in ta-C and polymeric a-C:H films no sp^2 rings are present. The presence of hydrogen causes the overall sp^3 content of a-C:H and ta-C:H to be approximately equal at 60 to 70 at.%, but causes the hardness of these two types of films to be very different. The ta-C:H films may reach a hardness up to 50 GPa [4], whereas polymeric a-C:H films with the same overall sp^3 content have a hardness of less than 10 GPa [4]. From these data, it is clear, that the I_D/I_D-ratio cannot in general relate to mechanical properties of a-C:H films. On the other hand, the I_D/I_G ratio describes the sp^2 cluster size and is therefore a useful parameter in structural analysis of DLC films. As mentioned previously, Ferrari and Robertson [51] stated that the Csp^3-Csp^3 bonding content controls the elastic constants of the films, but films with the same Csp^3–Csp^3 bonding content and hydrogen content can have different optical and mechanical properties due to different sp^2 clustering, different sp^2 orientation and cross sectional nano-structure [51].

5.3.4. The full width at half maximum of the G-band - FWHM (G)

The FWHM (G), as a parameter of structural disordering of sp^2 phases, has to be taken into account when one is hoping to find a relation between Raman band parameters and mechanical properties. Structural disorder arises from the bond angle and bond length distortions in DLC. The FWHM (G) is small when sp^2 clusters are more defect-free and ordered, and a higher FWHM (G) is thus indicative for an increase in disorder. The effect originates in the higher bond length and higher bond angle distribution in disordered materials. Since Csp^3-Csp^3 bonds are responsible for the structural disorder in the probed sp^2 hybridisated carbon fraction of the films, this parameter is in direct relation with the Csp^3–Csp^3 bonding content, density and mechanical properties [96]. Figure 5.4 shows that the density and the elastic modulus correlate with FWHM (G) [96].

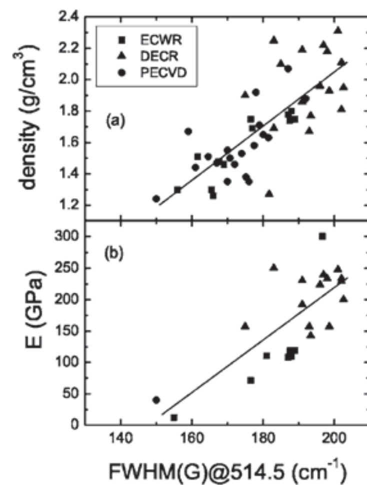

Figure 5.4. Density and elastic modulus as a function of FWHM (G) measured at 514.5 nm for DLC films prepared by different deposition techniques [96].

However, the data show a huge spread. The investigation of the relation between Raman band parameters and mechanical properties is a major part of the present thesis (*Publication 5*). The identified relations between structure and nanomechanical properties are highly accurate and allow an insight in the structural formation of a-C:H films as a function of the kinetic carbon ion energy during growth. It was found, that the FWHM (G) relates in all cases with the elastic modulus and the nanohardness of the investigated films. Moreover, *Publication 5* clearly shows, that in special cases, where Disp. (G) is directly proportional to the nanohardness and the elastic modulus and the intensity ratio I_D/I_G is inversely proportional to the nanohardness and the elastic modulus, one can assume to be in the tetrahedral regime, meaning that changes in the overall sp^3 contents are only reflected by changes in the Csp^3–Csp^3 bonding content in the films. The studies also show, that the film elasticity varies in an exponential relation with FWHM (G) respectively with the Csp^3-Csp^3 bonding content. The lowest detected FWHM (G) is accompanied with lowest elasticity or highest plastic behaviour of the film, whereas highest values of FWHM (G) relate to a high elasticity (*Publication 5*).

5.3.5. The dispersion of the G-band with excitation wavelength – Disp. (G)

Disp. (G) is a measure of the topological disorder [96]. Topological disorder arises from the size and shape distribution of sp^2 clusters [96]. Samples with a sp^2 phase entirely constituted of fully π delocalised rings, do not show any Disp. (G) [96] and therefore Disp. (G) is zero.

The Disp. (G) arises from the resonant selection of sp^2 chains of different sizes at different excitation energies [96]. Highest values for Disp. (G) are around 0.4 for ta-C and polymeric a-C:H [96]. Therefore, the Disp. (G) is proportional to the overall sp^3 content (Csp^3–Csp^3 + Csp^3–H1s) in a-C:H films [96]. Depending on the hydrogen content, two different structural regimes can be observed for a-C:H films [96]:

(1) At hydrogen contents lower than 25-30 at.%, the structural and topological disorder vary parallel to the amorphisation trajectory and are related to the Csp^3–Csp^3 content.

(2) If the hydrogen content is higher than 25-30 at.%, structural and topological disorder have opposite trends, meaning that at higher hydrogen concentrations, the overall sp^3 content can still increase but not the Csp^3–Csp^3 content. In this case, Csp^3–H1s bonds are formed augmented in the polymeric a-C:H films.

Figure 5.5 shows, that FWHM (G) relates to Disp. (G) in a directly proportional fashion if the films follow the tetrahedral regime (<25-30 at.% hydrogen) (line 1), whereas for the inversely proportional relation where a decreasing FWHM (G) is associated with an increase in Disp. (G), the films can be classified as polymeric a-C:H films (>25-30 at.% hydrogen) (line 2) [96].

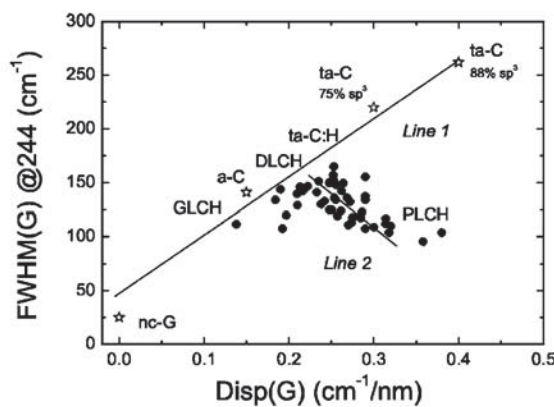

Figure 5.5. Correlation between Disp. (G) and FWHM (G) measured at 244 nm [96].

The relation from Figure 5.5 was also proved for the ta-C:H films deposited within the present thesis. It was found, that for visible and UV excitation, an increasing FWHM (G) is in line with an increasing Disp. (G) (*Publication 5*). Thus, these films follow accurately the tetrahedral regime as shown in Figure 5.5. Changes in the overall sp^3 content are reflected exclusively in changes of the Csp^3–Csp^3 bonding content.

5.3.6. The photoluminescence background in visible Raman spectroscopy

A typical signature of hydrogenated DLC films in visible Raman spectroscopy is the increasing photoluminescence background for higher hydrogen contents [96 and references therein]. The photoluminescence effect originates from the hydrogen saturation of non-radiative recombination centers [121,174]. The ratio between the slope m of the fitted linear background and the intensity of the G-band, m/I_G, can be empirically used as a measure of the hydrogen content of the investigated films [96 and references therein]. For hydrogen contents over 40-45 at.%, the photoluminescence background overshades the Raman

signal when using visible excitation. With UV excitation, the Raman spectra are not influenced by the severe photoluminescence effects in high hydrogen containing samples. Figure 5.6 shows the gain in m/I_G ratios for a series of hydrogenated DLC samples with hydrogen contents between ~20 and ~45 at.% [175].

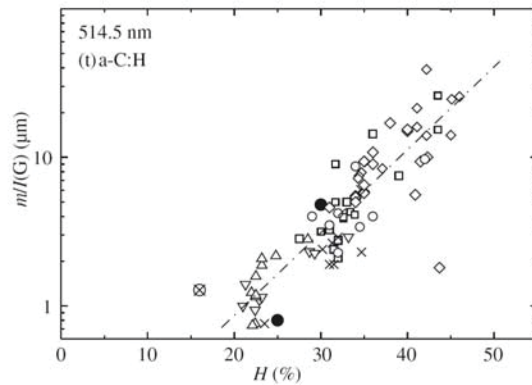

Figure 5.6. m/I_G as a function of the hydrogen content for a-C and ta-C films [175].

By applying equation 5.6, the hydrogen content can easily be calculated from the m/I_G ratio [175]. This is a highly economic alternative to ERDA in order to determine the hydrogen content in DLC films. The method is limited to hydrogen concentrations greater than ~20 at.%. For hydrogen contents lower than ~20 at.% no photoluminescence background is observed in the Raman spectrum.

$$H[at.\%] = 21.7 + 16.6 \log\left\{\frac{m}{I_G}[\mu m]\right\} \qquad 5.6$$

The photoluminescence effect was studied within the present thesis. Results of these investigations can be found in *Publications 1 and 2*. Spectra shown in Figure 5.7 taken from a highly hydrogenated reactive pulsed DC magnetron sputtered a-C:H film are recorded with visible and UV excitation within the present thesis. The photoluminescence effect seen in the slope in Figure 5.7a for visible excitation is completely absent for UV excitation (Figure 5.7b).

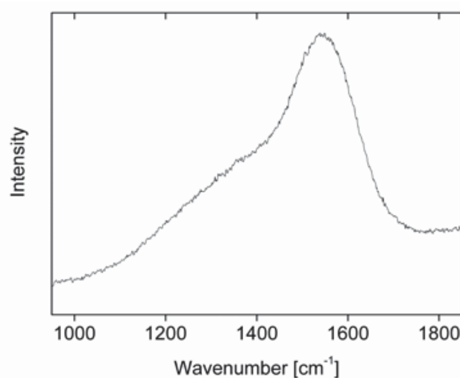

Figure 5.7a. Spectrum taken from an a-C:H film with a hydrogen content of 28 at.% at an excitation wavelength of 532 nm.

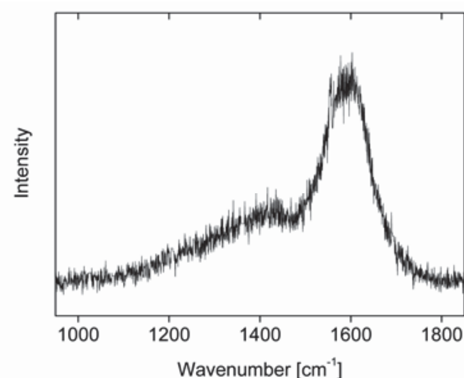

Figure 5.7b. Spectrum taken from the sample from Figure 5.8a with an excitation wavelength of 325 nm. The high noise in the spectrum is due to the low laser power applied on the sample, since for UV excitation carbon is very sensitive to annealing.

ERDA investigations revealed a hydrogen concentration of 28 at.% for this a-C:H film. Therefore, UV excitation is in particular useful if a sample cannot be measured with visible excitation due to overshading of the Raman bands caused by severe photoluminescence.

In conclusion, it can be remarked, that if the hydrogen content is lower than ~25 at.%, the Raman spectra can be interpreted in a similar fashion to a-C films [96]. If hydrogen is introduced in a-C, it breaks bonds and increases disorder. This is reflected in an increase of the Disp. (G). The size of graphitic clusters decreases and so the intensity ratio I_D/I_G decreases with increasing hydrogen content. That is the reason, why the intensity ratio I_D/I_G is in direct relation to the overall sp^3 content in a-C:H films. If hydrogen is introduced in ta-C, this increases the order and clustering of the structure [96]. Thus, Disp. (G) and FWHM (G) decrease as seen for ta-C:H, whose FWHM (G) is remarkable lower than for ta-C. The intensity ratio I_D/I_G increases for increasing hydrogen contents in ta-C.

If the hydrogen content is greater than ~25 at.%, the size of graphitic clusters is dramatically decreased [96]. The sp^2 phase is still topologically disordered, but the structural disorder reflected in FWHM (G) is lowered (Figure 5.5). However, hydrogen contents higher than ~25 % link the sp^3 and sp^2 phases together, resulting in easy interpretation of visible Raman spectra, due to limitation of hysteresis effects [4 and references therein].

5.4. RAMAN SPECTROSCOPY OF NITROGENATED DIAMOND-LIKE CARBON FILMS

The a-C:N films were studied in *Publications 3* and in the *Unpublished Results*. Raman spectra of a-C:N films can be interpreted in a similar fashion to a-C films [51]. The vibration frequencies of C–C and C–N bonds lie very close to each other. Therefore, it is not possible to figure out trends in the C–C and C–N bonding structure separately by applying Raman spectroscopy. Some important notes should be added for the interpretation of spectra taken from a-C:N films. Ferrari and Robertson [51] report on a G-band downshift with increasing nitrogen content in DLC for UV excitation, whereas for visible excitation an up shift of the signal is expected. The up shift of the G-band in visible excitation is due to a sp^2 clustering induced by nitrogen [51].

Ferrari and Robertson [51] also stress particular attention on the differences for carbon nitrides in Raman spectra due to their deposition technique. For room temperature deposition, stage 2 carbons (Figure 5.3) are known for increasing sp^2 clustering connected with a rise in the Pos. (G) (for visible Raman) for increasing nitrogen contents [51]. A typical example for that is shown in Figure 5.8a (*Unpublished Results*), where the up-shift of the G-band is observed for increasing nitrogen content in the investigated films. There the nitrogen content was probed by XPS and was found to be 9 at.% for the a-C:N film. Figure 5.8b (*Unpublished Results*) shows, how the structural order in a-C:N films is increased by an increasing nitrogen concentration in the process gas mixture. The disorder/order in the DLC structure is as previously mentioned probed by the FWHM (G). A lowering of FWHM (G) is associated with a higher degree of order in the DLC structure.

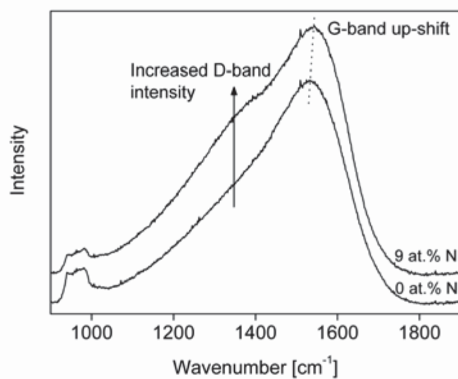

Figure 5.8a. Raman spectra as a function of the nitrogen concentration in the films. The small features around 900 cm^{-1} originate from the silicon substrate.

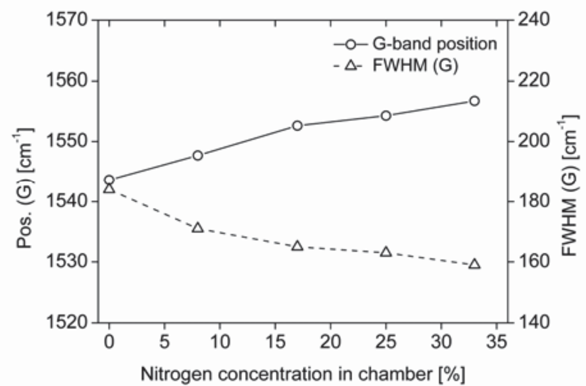

Figure 5.8b. Position of the G-band and FWHM (G) as a function of the N_2 concentration in process gas mixture.

For samples deposited at deposition temperatures higher than ~200°C a general increase in hardness is known with the addition of nitrogen. In this case, the addition of nitrogen does not cause more sp^2 clustering, but causes more cross-linking and therefore an increase in disorder. This type of carbons are known as stage 2 carbons (Figure 5.3) with increasing amorphisation showing a decreasing Pos. (G) for visible and UV excitation with increasing nitrogen concentration in the films [51]. The observed increase in hardness is not necessarily gained by an increase in the Csp^3 content in these films [51]. Films of stage 2 with increasing amorphisation were not studied within the present thesis.

5.5. SELECTED APPLICATIONS OF RAMAN SPECTROSCOPY WITHIN THE OWN WORK

5.5.1. Laser pulse fluence versus variations in Csp^3–Csp^3 bonding content of UV-PLD deposited a-C and ta-C films

UV-PLD is known for the deposition of ta-C films [4]. The kinetic energy of the carbons in the UV-PLD plasma relates in a linear fashion to the laser pulse fluence present in the focus which is located on the target surface [4]. Figure 2.7 shows the kinetic energy of carbon species versus laser pulse fluence on the graphite target. It can be seen, that the ideal kinetic energy for the growth of ta-C of ~100 eV can be reached when applying a pulse fluence of ~10 $J\cdot cm^{-2}$. Therefore, experiments with increasing laser pulse fluence from ~5.5 $J\cdot cm^{-2}$ to ~11 $J\cdot cm^{-2}$ were carried out within the present thesis. The resulting films were investigated by means of Raman spectroscopy. Figure 5.9 shows the variation of FWHM (G) as a function of the laser pulse fluence on the graphite target.

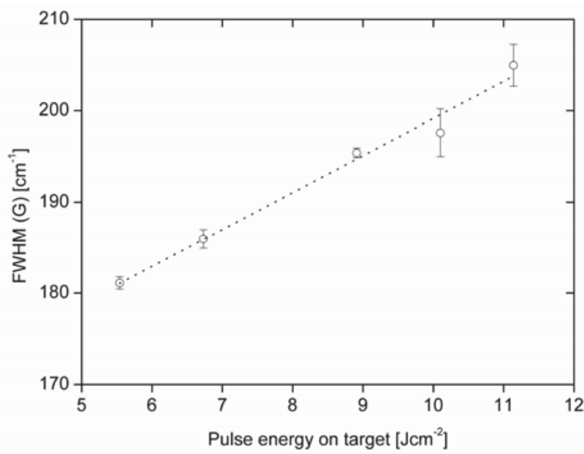

Figure 5.9. FWHM (G) versus laser pulse fluence on the target for PLD with λ=248 nm. Experimental details are listed in the appendix of the present thesis.

An almost linear relationship between the pulse fluence and the FWHM (G) is noted for the experiments. Since the FWHM (G) strongly related to the Csp^3–Csp^3 content, it is evident that the laser pulse fluence is under the described experimental setup in direct relation to the structure of the films. The high FWHM (G) of 205±2 cm^{-1} is indicative for an authentic ta-C structure of the investigated film deposited at the highest pulse fluence on the target. The observed finding of an increased Csp^3 fraction with increasing laser pulse fluence, *i.e.* carbon ion energy, agrees well with various articles cited in reference [4].

5.5.2. Process development of Si-a-C:H films guided by structural Raman analysis

An alternative approach of depositing Si-a-C:H films was investigated and is discussed in terms of structural and chemical properties of the deposited films. Deposition was carried out with an unbalanced magnetron sputtering cathode equipped with a Si target powered with a radiofrequency discharge using argon/acetylene (Ar/C_2H_2) process gas mixtures. In the following, the guiding of process development of Si-a-C:H films with Raman spectroscopy is discussed. The first diamond-like carbon bands in the Raman spectrum were found for a C_2H_2 concentration of 4 % in the process gas. These bands were intensified in its cross section by using 8 and 10 % C_2H_2 in the process gas atmosphere. Figure 5.10 shows the Raman spectra of the investigated films as a function of the C_2H_2 content in the process gas. From Figure 5.10 it can be concluded, that the C_2H_2 dissociation and subsequent film growth is highly effective in the applied RF discharge.

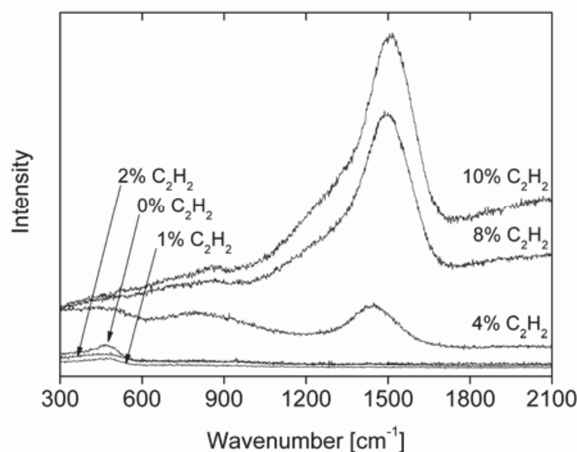

Figure 5.10. Raman spectra taken at 532 nm excitation wavelength from films deposited with 0 to 10 % C_2H_2 in the process gas mixture.

The following trends were noted when carefully fitting the Raman spectra with two Gaussian functions:

- The intensity ratio increases with the C_2H_2 concentration in the sputtering plasma from 0.1 for the film sputtered in 4 % C_2H_2 to 0.32 and 0.37 for films sputtered in 8 and 10 % C_2H_2.
- The FWHM (G) decreases with the C_2H_2 concentration in the sputtering plasma from 186 cm^{-1} for the film sputtered in 4 % C_2H_2 to 184 cm^{-1} and 181 cm^{-1} for films sputtered in 8 and 10 % C_2H_2.
- The m/I_G ratio increased via increasing the C_2H_2 concentration in the deposition chamber up to 3 µm (C_2H_2 concentration was varied from 4 to 10 % and the slope of the background was determined between 800 and 2000 cm^{-1}).

Table 5.1 summarises the Raman band parameters of the investigated films deposited with 4 to 10 % C_2H_2.

Table 5.1. Raman band parameters and hydrogen and silicon contents of the investigated Si-a-C:H films

C_2H_2 concentration [%]	**Intensity ratio I_D/I_D [-]**	**FWHM (G) [cm^{-1}]**	**Hydrogen content [at.%]**	**Silicon content [at.%]**
4	0.1	186	23.0	25.0
8	0.32	184	33.7	8.4
10	0.37	181	34.0	6.0

Interpretation of these spectral observations reveals that an increasing C_2H_2 content in the process gas results in an increasing content of Csp^2–Csp^2 and Csp^2–H1s bonds in the investigated films. This means, that sp^2 carbon clusters increase with increasing C_2H_2 content. A similar trend can be extracted from the variations in the FWHM (G), where higher C_2H_2 concentrations are connected with a higher order of sp^2 phases of the a-C:H matrix. Increased ordering of sp^2 phases can be understood as increased graphitisation of the films.

Evolution of the Raman spectra background slopes showed enhanced values varying with the C_2H_2 content in the process gas. The Raman spectra indicate a hydrogen content of 30 to 35 at.% for the film deposited with 10 % C_2H_2 in the process gas mixture. ERDA investigations revealed increasing hydrogen contents when increasing the C_2H_2 concentration from 4 to 10 %, corroborating the trends derived from Raman spectroscopy. Sputtering in 4 % C_2H_2 yielded a hydrogen concentration of 23 at.%, whereas the use of 8 % C_2H_2 showed a hydrogen concentration of 33.7 at.% in the film. By further increasing the C_2H_2 concentration to 10 %, a hydrogen concentration of 34 at.% was detected. Due to the observed high hydrogen contents, films sputtered in 8 and 10 % C_2H_2 can be classified to the group of polymeric a-C:H coatings. RBS studies further revealed that the carbon content of the investigated films increases with increasing C_2H_2 content in the process gas, being in line with the trends of increasing sp^2 clustering derived by Raman investigations. A concentration of 4 % C_2H_2 in the process gas atmosphere results in a carbon content of 52 at.%, whereas increasing the C_2H_2 concentration to 8 and 10 % results in carbon contents of 57.9 and 60 at.%, respectively. Si contents were found to decrease with increasing C_2H_2 concentrations. For a process gas mixture containing 4 % C_2H_2, 25 at.% Si were detected in the film. By increasing the C_2H_2 percentage to 8 and 10 %, Si contents of 8.4 and 6.0 at.% were found in the investigated films. The ERDA/RBS data are summarised in Table 5.1. Structural

and chemical data collected from the deposited films authenticate the applied deposition process as highly controllable by the C_2H_2 concentration in the deposition chamber. From this investigation it can be seen, that the primal observations made by Raman spectroscopy resulted in the successful development of Si-a-C:H films. It can be concluded, that process development guided by Raman spectroscopic analysis is highly economic and effective. Further investigations with AFM revealed that these films are ultra smooth and show a RMS roughness of down to 0.25 nm.

5.5.3. The structural evolution of ion beam deposited ta-C:H films grown at varied angles of incidence from 0 to 90°

As mentioned previously, the angle of incidence of the bombarding species on the DLC surface has a crucial impact on growth effects of the films [6]. The penetration depth of carbon ions or neutrals is a function of their angle of incidence, where a beam with the same ion energy shows a lower penetration at a glancing angle of incidence. This reduces the effective ion energy for film growth. Therefore, the influence of the angle of incidence was studied for the high energy ion beam deposition process applied within the present thesis. The deposited films are kinetically controlled DLC films. The resulting films grown at 10 angles of incidence (90° to 0°) were investigated by Raman spectroscopy. The results of this investigation are presented in Figure 5.11.

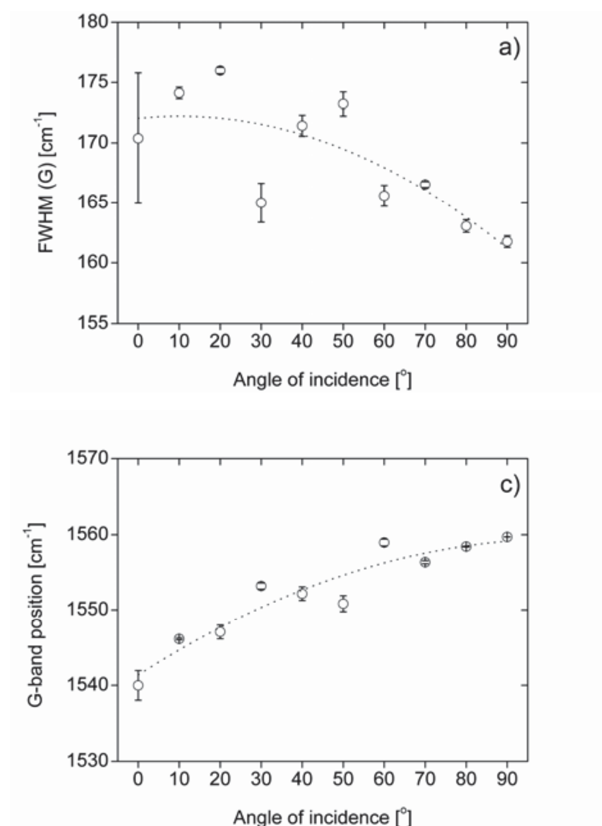

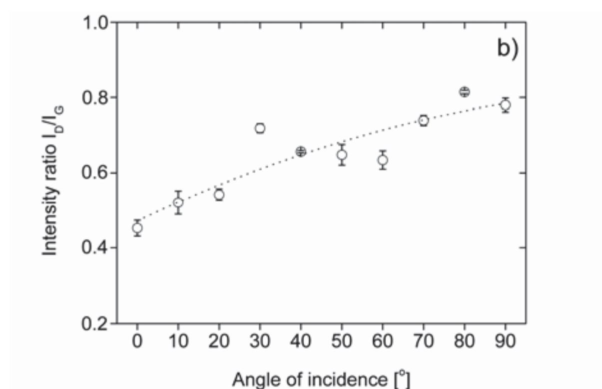

Figure 5.11.a Relation of FWHM (G) and the angle of incidence. 0° corresponds to full off-axis deposition (parallel orientation to the assumed direction of accelerated carbon species). Subsequently, an angle of 90° relates to perpendicular orientation of the sample to the assumed direction of accelerated carbon species. **b)** Intensity ratio I_D/I_G as a function of the angle of incidence and **c)** Pos. (G) as a function of the angle of incidence. Ion beam deposition parameters: discharge voltage: 3 kV; C_2H_2 flow: 20 sccm; process pressure: $1.3 \cdot 10^{-3}$ mbar. Substrates were kept static in front of one beam positioned in the center of the beam axis.

It can be clearly seen, that off-axis deposition results in elevated Csp^3–Csp^3 bonding contents (Figure 5.11a to 5.11c). In accordance to the findings in *Publications 1 and 2*, the applied discharge voltage of 3 kV results in an kinetic carbon species energy being in the range of 750 eV. This energy is too high for growth of films with a maximum Csp^3–Csp^3 bonding content. This is the reason, why films become more dominated by the

Csp^3-Csp^3 bonding content when lowering the discharge voltage, *i.e.* the kinetic carbon species energy (*Publications 1 and 2*). As a consequence of this discussion, it is clear, that the Csp^3–Csp^3 bonding content must be increased, when applying deposition angles lower than 90°, reducing the penetration depths and effective kinetic energy of carbon species. In contrast, Lifshitz [6] reports on a rise in Csp^2–Csp^2 bonding contents, *i.e.* graphitisation for films grown with an ion energy of ~100 eV at glancing angles, *i.e.* substrates orientated in parallel to the direction of accelerated carbon species.

Combining the results of the own studies with those of Lifshitz [6] leads to the conclusion, that a very high ion energy will result in films with higher Csp^3 contents at glancing angles, whereas if the ion energy is set to the ideal value for growth of ta-C films (~100 eV), glancing angles will result in sufficiently too low ion energies for growth of highly tetrahedral films. In this case, the Csp^3 content is decreased at glancing angle deposition.

5.5.4. The relation of Raman band parameters and mechanical properties of ion beam deposited (t)a-C:H films

In *Publication 1* and *2* it was shown, how a-C:H and ta-C:H films can be deposited with an anode layer source. There, it was found, that the structure and the mechanical properties of the deposited films can be tailored effectively by the discharge voltage applied to the source, *i.e.* the kinetic energy of carbon species involved in film growth.

Later it was recognised, that the knowledge about the relation between Raman band parameters and the mechanical properties of the films is of importance to understand the structural evolution mechanism of ta-C:H films. Therefore, a comprehensive study, employing ERDA/RBS, dual wavelength Raman spectroscopy and nanoindentation was carried out. The results of this investigation are presented in *Publication 5*. Here, only the landmarks of this publication are presented in brief.

The study revealed, that FWHM (G) $^{532\ nm}$, a measure of the Csp^3–Csp^3 bonding content as well as Disp. (G) relates to mechanical properties (Figures 5.12a and 5.12b). The nanohardness (H) and reduced elastic modulus (E) increases almost linearly with increasing FWHM (G)$^{532\ nm}$ as seen in Figure 5.12a. H and E increase with Disp. (G) (Figure 5.12b). Furthermore, H and E decrease with increasing intensity ratio $I_D/I_G{}^{532\ nm}$ (Figure 5.12c). The elasticity (H^3/E^2) was found to increase in an exponential fashion with FWHM (G), *i.e.* the Csp^3–Csp^3 fraction (Figure 5.13).

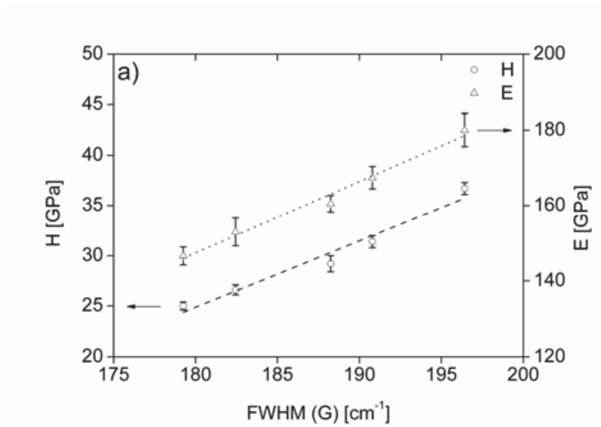

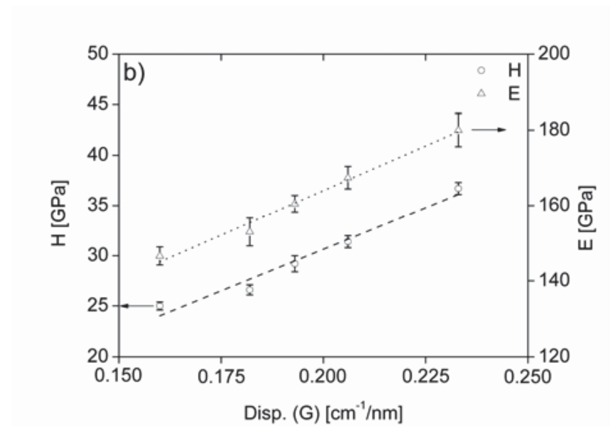

Figure 5.12a. H and E as a function of FWHM (G) determined an excitation wavelength of 532 nm.

Figure 5.12b. H and E as a function of Disp (G).

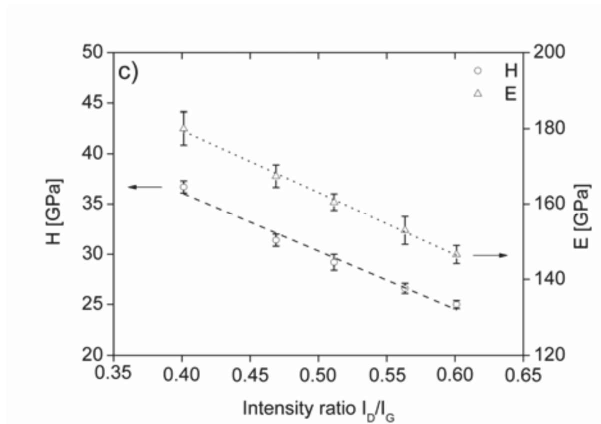

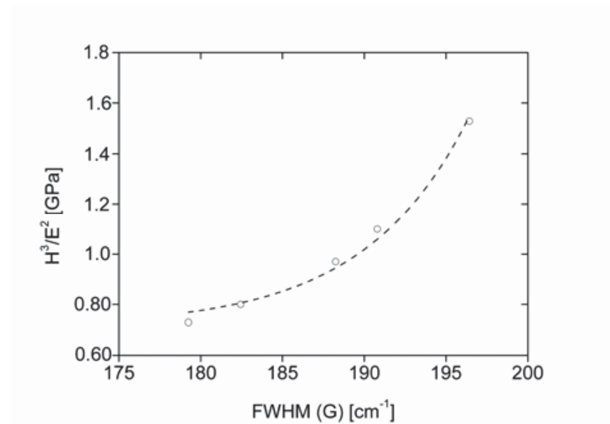

Figure 5.12c. H and E as a function of the intensity ratio I_D/I_G determined with an excitation wavelength of 532 nm.

Figure 5.13. H^3/E^2 as a function of FWHM (G) determined with an excitation wavelength of 532 nm.

The reason for the distinct relations is assumed to be the similar hydrogen content detected for all investigated films (22.2±1.2 at.%), allowing the Csp^3–Csp^3 bonding fraction to emerge independently from Csp^3–H1s bonds. This can be seen in Figure 5.14. In the tetrahedral regime (almost no variations in hydrogen content), the FWHM (G) increases with Disp. (G). Figure 5.14 is the man result of *Publication 5*.

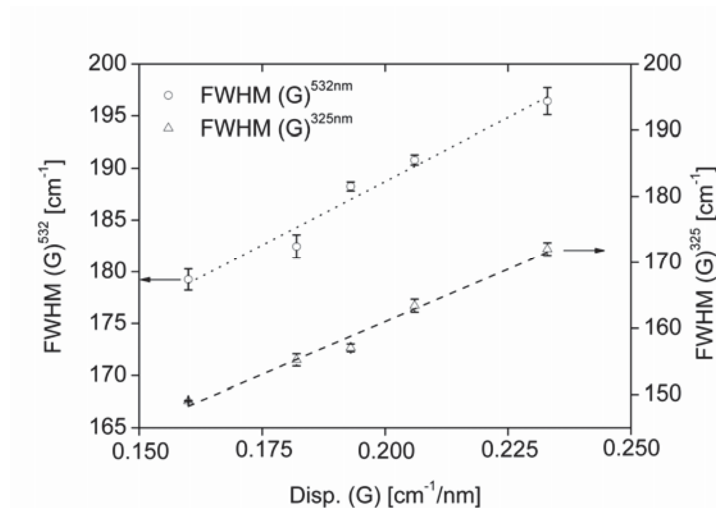

Figure 5.14. Correlation between Disp. (G) and FWHM (G) for excitation wavelengths of 532 nm and 325 nm.

6. SUMMARY AND CONCLUSIONS

The process design and the investigation of the film structure and film properties of room-temperature deposited DLC films was the objective of the present thesis. Films within the structural systems of: a-C, a-C:H, ta-C, ta-C:H, polymeric a-C:H and Si-a-C:H were deposited at substrate temperatures of well below 100°C. Via proper film deposition process tuning it was possible to tailor the structural, chemical, mechanical, tribological, surface topographical and surface chemical properties of these DLC films systems. The structure and elemental chemistry of the deposited films was investigated by Raman spectroscopy, XPS, ERDA and RBS. Hardness, elastic moduli, elasticity and the tribological behaviour of the films were studied by application of the nanoindentation and nanoscratch method. Surface topography and surface energy was determined by AFM and the sessile drop technique.

In order to meet the objective of the thesis, the deposition methods infrared PLD (IR-PLD; λ=1064 nm), ultraviolet PLD (UV-PLD; λ=248 nm), ion beam deposition as well as reactive balanced and unbalanced magnetron sputtering of graphite and silicon were studied. It was found, that for high kinetic ion energy film deposition processes, *i.e.* UV-PLD and ion beam deposition, the structure and properties of the film varieties ta-C and ta-C:H can be controlled solely by the kinetic energy of carbon species involved during film growth. For deposition techniques being typically known for low ion energies like IR-PLD and magnetron sputtering, process tuning involves the study of bias voltages as well as sputtering gas/reactive gas flow optimisation.

Process optimisation for high ion energy deposition techniques was done by adjustment of the discharge voltage applied to the ion beam source or by adjustment of the laser pulse fluence, both parameters found to be closely related to the effective ion energy for film growth. Within this regard it was found, that especially the angle of incidence of kinetic carbon species involved in film growth for the deposition of ta-C:H films has a crucial impact on the structural evolution of these films. Via investigation of glancing angle or acute angle deposition with the ion beam source, it was found, that angles of incidence lower than 90° favour an increased population of Csp^3–Csp^3 bonds in the film, when the ion energy is set typically higher than the ideal ion energy level for growth of tetrahedral, *i.e.* high Csp^3 hybridised, carbon films. Therefore, under the deposition conditions of acute angles, the effective ion energy present on the growing film is significantly decreased. These finding further shows the difficulties that emerge when coating three dimensional shaped technical products, where the angle of incidence of kinetic carbon species bombarding the growing film is variable. For IR-PLD deposited and reactive magnetron sputtered DLC films, the process is almost singularly controlled via the reactive gas flow, *i.e.* the C_2H_2 or N_2 concentration, in the process gas mixture. Here it was found, that during unbalanced magnetron sputtering of graphite or IR-PLD, the presence of N_2 induces ordering in the a-C:N structure, *i.e.* graphitisation occurs. For balanced sputtering of graphite in the presence of high concentrations of C_2H_2, a favoured formation of Csp^3–H1s bonds, *i.e.* polymerisation of the a-C:H structure, is noted. In contrast, the investigation of the structural evolution of Si-a-C:H films revealed an increased tendency of clustering of sp^2 phases at elevated C_2H_2 concentrations in the chamber during reactive unbalanced RF magnetron sputtering of a silicon target. ERDA investigations revealed an increasing hydrogen content from 23 to 34 at.% when increasing the C_2H_2 concentration in the process gas mixture from 4 to 10 %.

The structural evolution of ion beam deposited ta-C:H films with varied discharge voltages, *i.e.* carbon ion energies, was of particular importance for the present thesis. Here, Raman spectra showed that an increased discharge voltage yields decreased structural disorder, *i.e.* a lower Csp^3–Csp^3 hybridised fraction of carbon atoms in the films. By elevating the discharge voltage from 1 to 3 kV, the FWHM (G) decreases from 194±0.2 cm^{-1} to 183±0.7 cm^{-1}, meaning that the formation of sp^2 hybridised carbon atoms is favoured. Films deposited at the lowest discharge voltage show in accordance to the spectroscopic data the highest nanohardness (36±1 GPa), stress (-2.34±0.2 GPa) and reduced elastic modulus (180±4 GPa). During these studies it was recognised, that the connection between Raman band parameters and mechanical properties is of importance to understand the structural evolution in ta-C:H films. The study revealed, that mechanical properties relate to FWHM (G), being a measure of the Csp^3-Csp^3 bonding content, and Disp. (G), being a measure of the overall sp^3 content in a-C:H films. The nanohardness and reduced elastic modulus increase almost linearly with increasing FWHM (G) and Disp. (G). Analysis of these observations resulted in a reliable answer for the distinct relations of Raman band parameters and the mechanical properties of the studied films. The reason for the distinct relations is the similar hydrogen content detected for all investigated films (22.2±1.2 at.%), allowing the Csp^3–Csp^3 bonding fraction to emerge independently from Csp^3–H1s bonds. In special cases, *i.e.* in the tetrahedral structural evolution regime, mechanical properties relate to Raman band parameters usually associated with the overall sp^3 content (intensity ratio I_D/I_G and Disp. (G)), too. Structural evolution of ta-C:H films can be easily controlled via a plot of FWHM (G), measured at any excitation wavelength against the Disp. (G), representing a Raman band parameter associated to be proportional to the overall sp^3 content (Csp^3–Csp^3 + Csp^3–H1s bonds) in hydrogenated DLC films. If FWHM (G) increases with increasing Disp. (G) for a series of a-C:H films, the structural changes are reflected almost solely in variations in the sp^3 hybridisation of carbon atoms. In particular, this holds for all studied films with hydrogen contents lower than ~25 at.%.

The ta-C:H films, that are deposited with the ion beam source, show no macro-defects (droplets and/or particulates) and are ultra smooth as evidenced by RMS roughness of 0.1 nm. Due to the high hardness of these films as well as their excellent adhesion to many substrate materials and the possibility to achieve dense films even at low thicknesses, these films can be applied from the fields of data storage technology to gas barrier coatings or coating of artificial implants. The a-C:N films deposited by IR-PLD have been proven to excellently excel as electrodes in multi-reflection IR-ATR spectroelectrochemistry. The electrochemical activity of these a-C:N films was verified using the $Ru(NH_3)^{3+/2+}$ redox couple and demonstrated to be comparable with that of other conventional carbon-based electrodes. For applications where a tunable surface chemistry of the DLC films is mandatory, the deposited Si-a-C:H films would present a possible alternative to known films systems. Here it was found, that σ_s^P can be effectively tailored by variations in the C_2H_2 concentration in the process gas during reactive RF unbalanced magnetron sputtering of Si.

The developed process variants allow the deposition of films with unique properties, which can be effectively tailored by the deposition parameters. For ta-C:H and a-C:H films it was found, that the combination of multi-wavelengths Raman spectroscopy and ERDA/RBS is able to fully characterise the structure and chemistry of these film systems. Multi-wavelengths Raman spectroscopy is an excellent tool for both, process development and process control.

7. REFERENCES

[1] R. A. Haefer, Oberflächen- und Dünnschicht-Technologie/ R. A. Haefer (eds.), Berlin, Heidelberg, New York, London, Paris, Tokyo, Hong Kong, Barcelona, Teil 2: Oberfächenmodifikation durch Teilchen und Quanten, Springer, 1991.

[2] H. Gleiter, Nanostruct. Mater. 6 (1995) 3.

[3] H. Gleiter, Acta Mater. 48 (2000) 1.

[4] J. Robertson, Mater. Sci. Eng. R37 (2002) 129.

[5] A. Grill, Diamond Relat. Mater. 8 (1999) 428.

[6] Y. Lifshitz, Diamond Relat. Mater. 5 (1996) 388.

[7] Y. Lifshitz, Diamond Relat. Mater. 8 (1999) 1659.

[8] B. Druz, R. Ostan, S. Distefano, A. Hayes, V. Kanarov, V. Polyakov, Diamond Relat. Mater. 7 (1998) 965.

[9] Y. Lifshitz, G.D. Lempert, E. Grossman, Phys. Rev. Lett. 72 (1994) 2753.

[10] H.J. Scheibe, B. Schultrich, Thin Solid Films 246 (1994) 92.

[11] M. Chowalla, J. Robertson, C.W. Chen, S.R.P. Silva, G.A.J. Amaratunga, J. Appl. Phys. 81 (1997) 139.

[12] M. Chhowalla, A.C. Ferrari, J. Robertson, G.A.J. Amaratunga, Appl. Phys. Lett. 76 (2000) 1419.

[13] Y. Lifshitz, G.D. Lempert, E. Grossman, I. Avigal, C. Uzan-Saguy, R. Kalish, J. Kulik, D. Marton, J.W. Rabalais, Diamond Relat. Mater. 4 (1995) 318.

[14] J.A. Thornton, J. Vac. Sci. Technol. 11 (1974) 666.

[15] D.R. McKenzie, Rep. Prog. Phys. 59 (1996) 1611.

[16] P.J. Fallon, V.S. Veerasamy, C.A. Davis, J. Robertson, G.A.J. Amaratunga, W.I. Milne, J. Koskinen, Phys. Rev. B 48 (1993) 4777.

[17] J. Robertson, Pure Appl. Chem. 66 (1994) 1789.

[18] J. Robertson, Philos. Trans. R. Soc. A 342 (1993) 277.

[19] Y. Lifshitz, S.R. Kasi, J.W. Rabalais, W. Eckstein, Phys. Rev. B 41 (1990) 10468.

[20] H. Hofsass, H. Binder, T. Klumpp, E. Recknagel, Diamond Rel. Mater. 3 (1994) 137.

[21] H. Hofsass, C. Ronning, Beam Processing of Advanced Materials, ASME, Cleveland, 1995.

[22] J. Ishikawa, Y. Takeiri, K. Ogawa, T. Takagi, J. Appl. Phys. 55 (1987) 188.

[23] J.P. Hirvonen, R. Lappalainen, J. Koskinen, A. Antilla, Mater. Sci. Forum 52 (1990) 197.

[24] A.A. Voevodin, M.S. Donley, Surf. Coatings Technol. 82. (1996) 199.

[25] M.P. Siegal, L.J. Martinez-Miranda, J.N. DiNardo, D.R. Tallant, J.C. Barbour, P.N. Provencio, High Powered Laser Ablation, SPIE, 1998.

[26] F. Jansen, M. Mackonkin, S. Kaplan, S. Hark, J. Vac. Sci. Technol. A 3 (1985) 605.

[27] N. Savvides, J. Appl. Phys. 55 (1984) 4232.

[28] N. Savvides, J. Appl. Phys. 59 (1989) 4133.

[29] S.M. Rossnagel, M.A. Russak, J.J. Cuomo, J. Vac. Sci. Technol. A 5 (1987) 2150

[30] N.H. Cho, K.M. Krishnan, D.K. Vries, M.D. Rubin, C.B. Hopper, B. Brushan, D.B. Bogy, J. Mater. Res. 5 (1990) 2543.

[31] M. Rubin, C.B. Hopper, N.H. Cho, B. Bhushan, J. Mater. Res. 5 (1990) 2538.

[32] J. Schwan, S. Ulrich, H. Roth, H. Ehrhardt, S.R.P. Silva, J. Robertson, R. Samlenski, J. Appl. Phys. 79 (1996) 1416.

[33] J.J. Cuomo, J.P. Doyle, J. Bruley, J.C. Liu, Appl. Phys. Lett. 58 (1991) 466.

[34] W. Gissler, P. Hammer, J. Haupt, Diamond Rel. Mater. 3 (1994) 770.

[35] S. Logothetidis, Appl. Phys. Lett. 69 (1996) 158.

[36] G. Gassner, P.H. Mayrhofer, C. Mitterer, J. Kiefer, Surf. Coat. Technol. 200 1-4 (2005) 1147.

[37] G. Gassner, P.H. Mayrhofer, J. Patscheider, C. Mitterer, Thin Solid Films, 515, 13 (2007) 5411.

[38] Y.N. Kok, P.Eh. Hovsepian, R. Haasch, I. Petrov, Surf. Coat. Technol. 200 1-4 (2005) 1117.

[39] K. Bewilogua, C. V. Cooper, C. Specht, J. Schröder, R. Wittorf and M. Grischke, Surf. Coat. Technol. 127 2-3 (2000) 1117.

[40] J. M. Ting, H, Lee1, Diamond Relat. Mater. 11 (3-6) (2002) 1119.

[41] V.S. Veerasamy, H.A. Luten, R.H. Petrmichl, S.V. Thomsen, Thin Solid Films 442 (2003) 1.

[42] V.V. Zhurin, H.R. Kaufman, R.S. Robinson, Plasma Sources Sci. Technol. 8 (1999) R1.

[43] D.S. Knight, W.B. White, J. Mater. Res. 4 (1989) 385.

[44] R.J. Nemanich, S.A. Solin, Phys. Rev. B 20 (1979) 392.

[45] B.S. Elman, M. Shayegan, M.S. Dresselhaus, H. Mazurek, G. Dresselhaus, Phys. Rev. B 25 (1982) 4142.

[46] M.S. Dresselhaus, G. Dresselhaus, P.C. Eklund, Science of Fullerenes and Carbon Nanotubes, Academic Press, London, 1996.

[47] G.M.Pharr, D.L. Callahan, S.D. McAdams, T.Y. Tsui, S. Anders, A. Anders, J.W. Ager, I.G. Brown, C.S. Bhatia, S.R.P. Silva, J. Ropertson, Appl. Phys. Lett. 68 (1996) 779.

[48] M. Weiler, S. Sattel, K. Jung, H. Ehrhardt, V.S. Veerasamy, J. Robertson, Appl. Phys. Lett. 64 (1994) 2797.

[49] P. Koidl, C. Wagner, B. Dischler, J. Wagner, M. Ramsteiner, Mater. Sci. Forum 52 (1990) 41.

[50] W. Jakob, W. Moller, Appl. Phys. Lett. 63 (1993) 1771.

[51] A.C. Ferrari, J. Robertson, Phil. Trans. R. Soc. Lond. A, 362 (2004) 2477.

[52] A.C. Ferrari, Surf. Coat. Technol. 180-181 (2004) 190.

[53] A.H. Lettington, in: Y. Tzeng, M. Yoshikawa, M. Murakawa, A. Feldman (eds.), Applications of Diamond Films and Related Materials, Materials Science Monographs, Elsevier, New York, 1991, 703.

[54] A.C. Evans, J. Franks, P.J. Revell, Surf. Coat. Technol. 47 (1991) 662.

[55] W.J. Ma, A.J. Ruys, R.S. Mason, P.J. Martin, A. Bendavid, Z. Lui, M. Ionescu, H. Zreiqat, Biomaterials 28 (2007) 1620.

[56] J. Robertson, Diamond Rel. Mater. 2 (1993) 984.

[57] J. Robertson, Diamond Rel. Mater. 3 (1994) 361.

[58] J. Robertson, Radiat. Effect 142 (1997) 63.

[59] J. Robertson, in: S.R.P. Silva, et al. (Eds.) Amorphous Carbon: State of the Art, World Scientific, Singapore, 1998

[60] W. Moller, Appl. Phys. Lett. 59 (1991) 2391.

[61] H.P. Kaukonen, R.M. Nieminen, Phys. Rev. Lett. 68. 68 (1992) 620.

[62] H.P. Kaukonen, R.M. Nieminen, Phys. Rev. B 61 (2000) 2806.

[63] S. Uhlmann, T. Frauenheim, Y. Lifshitz, Phys. Rev. Lett. 81 (1998) 641.

[64] N.A. Marks, Phys. Rev. B56 (1997) 2441.

[65] K.J. Boyd, D. Marton, I.W. Rabalais, Y. Lifshitz, J. Vac. Sci. Technol. A16 (1998) 455.

[66] K. Kohary, S. Kugler, Phys. Rev. B 63 (2001) 193404.

[67] H.U. Jäger, K. Albe, J. Appl. Phys. 88, (2000) 1129.

[68] H. Hofsass, H. Feldermann, R. Merk, M. Sebastian, C. Ronning, Appl. Phys. A 153 (1998)

[69] N.M.J. Conway, A.C. Ferrari, A.J. Flewitt, J. Robertson, W.I. Wilne, A. Tagliaferro, W. Beyer, Diamond Rel. Mater. 9 (2000) 765.

[70] M. Chhowalla, J. Robertson, C.W. Chen, S.R.P. Silva, G.A.J. Amaratunga, J. Appl. Phys. 81 (1997) 139.

[71] J.P. Hirvonen, J. Koskinen, M. Kaukonen, R. Nieminen, J. Appl. Phys. 81 (1997) 7248.

[72] J. Koskinen, J.P. Hirvonen, J. Keranen, J. Appl. Phys. 84 (1998) 648.

[73] Veeco Instruments, Technical Manual to ALS340, 2003.

[74] J.J. Cuomo, D.L. Pappas, J. Bruley, J.P. Doyle, K.L. Saenger, J. Appl. Phys. 70 (1991) 1706.

[75] D.L. Pappas, K.L. Saenger, J. Bruley, W. Krakow, J.J. Cuomo, T. Gu, R.W. Collins, J. Appl. Phys. 71 (1992) 5675.

[76] J.J. Cuomo, D.L. Pappas, R. Lossy, J.P. Doyle, J. Bruley, G.W. Di Bello, W. Krakow, J. Vac. Sci. Technol. A 10 (6) (1992) 3414.

[77] R. Lossy, D.L. Pappas, R.A. Roy, J.P. Doyle, J.J. Cuomo, J. Bruely. J. Appl. Phys. 77 (9) (1995) 4750.

[78] M. Moseler, P. Gumbsch, C. Casiraghi, A.C. Ferrari, J. Robertson, Science, 309 (2005) 1545.

[79] Z.W. Zhao, B.K. Tay, L. Huang, G.Q. Yu, J. Phys. D. Appl. Phys. 37 (2004) 1701.

[80] E. Spiller, S. L. Baker, P. B. Mirkarimi, V. Sperry, E. M. Gullikson, and D. G. Stearns, Appl. Opt. 42 (2003) 4049.

[81] S. Aisenberg, R. Chabot, J. Appl. Phys. 42 (1971) 2953.

[82] H.R. Kaufman, J. Vac. Sci. Technol. 15 (1978) 272.

[83] D. Marton, in: J.W. Rabalais (eds.) Low energy ion-surface interactions, Wiley, Chichester, 1994, 481.

[84] D. Basting, G. Marowsky (eds.) Excimer Laser Technology, Berlin, Heidelberg, New York, Springer, 2005

[85] J. M. Lackner, C. Stotter, W. Waldhauser, R. Ebner, W. Lenz, M. Beutl, Surf. Coat. Technol. 174-175 (2003) 402.

[86] I. Petrov, V. Orlinov, I. Ivanov, J. Kourtev, Contrib. Plasma Phys. 28 (3) (1988) 265.

[87] J. Ganz, Metalloberfläche, 45, 1991, 11.

[88] B. Window, N. Savvides, J. Vac. Sci. Technol. A 4 (3) (1986) 453.

[89] B. Window, Surf. Coat. Technol. 81 (1996) 92.

[90] I. Petrov, F. Adibi, J.E. Greene, W.D. Sproul, W.D. Münz, J. Vac. Sci. Technol. A 10 (5) (1992) 3283.

[91] I. Ivanov, P. Kazansky, L. Hultman, I. Petrov, J.E. Sundgren, J. Vac. Sci. Technol. A 12 (2) (1994) 314.

[92] T.A. Friedmann, K.F. McCarty, J.C. Barbour, M.P. Siegal, D.C. Dibble, Appl. Phys. Lett. 68 (1996) 1643.

[93] A.C. Ferrari, J. Robertson, M.G. Beghi, C.E. Bottani, R. Ferulano, R. Pastorelli, Appl. Phys. Lett. 75 (1999) 1893.

[94] X. Shi, D. Flynn, B.K. Tay, S. Prawer, K.W. Nugent, S.R.P. Silva, Y. Lifshitz, W.I. Milne, Philos. Mag. B 76 (1997) 351.

[95] A.A. Voevodin, A.W. Phelps, J.S. Zabinski, M.S. Donley, Diamond Rel. Mater. 5 (1996) 1264.

[96] C. Casiraghi, A.C. Ferrari, J. Robertson, Phys. Rev. B, 72 (2005) 085401.

[97] A.C. Ferrari, A. Libassi, B.K. Tanner, V. Stolojan, J. Yuan, L.M. Brown, S.E. Rodil, B. Kleinsorge, J.Robertson, Phys. Rev. B 62 (2000) 11089.

[98] M. Grischke, K. Bewilogua, K. Trojan, H. Dimigen, Surf. Coat. Technol. 74/75 (1995) 739.

[99] M. Wang, K. Schmidt, K. Reichelt, H. Dimigen, H. Hubsch, J. Mater. Res. 7 (3) (1992) 667.

[100] C. Donnet, J. Fontaine, A. Grill, V. Pattel, C. Jahnes, M. Bellin, Surf. Coat. Technol. 94/95 (1997) 531.

[101] Papakonstantinou, P. Lemoine, J. Phys. Condens. Matter 13 (2001) 2971.

[102] A. Grill, IBM J. Res. Dev. Armonk 43 (1/2) (1998) 147.

[103] K. Yoo, B. Miller, R. Kalish, X. Shi, Electrochem. Solid-State Lett. 2 (5) (1999) 233.

[104] N.C. Yee, Q. Shi, W.B. Cai, D.A. Scherson, B. Miller, Electrochem. Solid-State Lett. 4 (10) (2001) E42.

[105] K.R. Lee, M.G. Kim, S.J. Cho, K.Y. Eun, T.Y. Seong, Thin Solid Films 308/309 (1997) 263.

[106] J. C. Damasceno, S.S. Camargo, F.L. Freire, R. Carius, Surf. Coat. Technol. 133/134 (2000) 247.

[107] S. Lee, D.S. Kim, S.G. Rhee, S.G. Oh, K.R. Lee, Thin Solid Films 341 (1999) 68.

[108] J.F. Zhao, P. Le moine, Z.H. Liu, J.P. Quinn, J.A. McLaughlin, J. Phys. Condens. Matter 12 (2000) 9201.

[109] J. Meneve, E. Dekempeneer, J. Smeets, Diamond Films Technol. 4 (1994) 23.

[110] A.K. Gangopadhyay, P.A. Willermet, M.A. Tamor, W.C. Vassell, Tribol. Int. 30 (1997) 9.

[111] X. Zhang, W.H. Weber, W.C. Vassell, T.J. Potter, M.A. Tamor, J. Appl. Phys. 83 (1998) 2820.

[112] C. De Martino, G. Fusco, G. Mina et al. Diamond Rel. Mater. 6 (1997) 559.

[113] K. Oguri, T. Arai, Surf. Coat. Technol. 47 (1991) 710.

[114] S. Miyake, R. Kaneko, Y. Kikuya, I. Sugimoto, Trans. ASME J. Tribol. 113 (1991) 384.

[115] X.M. He, K.C. Walter, M. Natasi, S.T. Lee, M.K. Fung, J. Vac. Sci. Technol. A 18 (2000) 2143.

[116] J. Robertson, Adv. Phys. 35 (1986) 317.

[117] J. Robertson, E.P. O'Reilly, Phys. Rev. B 35 (1987) 2946.

[118] J. Robertson, Mater. Sci. Forum 52 (1990) 125.

[119] C.H. Lee, W.R.L. Lambrecht, B. Segall, P.C. Kelires, T. Frauenheim, U. Stephan, Phys. Rev. B49 (1994) 11448.

[120] J. Robertson, Diamond Rel. Mater. 4 (1995) 297.

[121] J. Robertson, Phys. Rev. B53 (1996) 16302.

[122] S. Kaplan, F. Jansen, M. Machonkin, Appl. Phys. Lett. 47 (1985) 750.

[123] R. H. Jarman, G.J. Ray, R.W. Stadley, Appl. Phys. Lett. 49 (1986) 1065.

[124] A. Grill, B.S. Meyerson, V.V. Patel, J.A. Reimer, M.A. Petrich, J. Appl. Phys. 61 (1987) 2874.

[125] C. Jager, J. Gottwald, H.W. Spiess, R.J. Newport, Phys. Rev. B 50 (1994) 846.

[126] T. Blinc, D. Arcon, P. Cevc, I. Pocsik, M. Koos, Z. Trontelj, Z. Jaglicic, J. Phys. Condens. Mater. 10 (1998) 6813.

[127] M.A. Tamor, W.C. Vassel, K.R. Carduner, Appl. Phys. Lett. 58 (1991) 592.

[128] K.R. Carduner, M.J. Rokosz, M.A. Tamor, W.C. Vassel, Appl. Magn. Res. 2 (1991) 647.

[129] R. Kleber, K. Jung, H. Ehrhardt, I. Muhling, K. Breuer, H. Metz, F. Engelke, Thin Solid Films 205 (1991) 274.

[130] C. Donnet, J. Fontaine, F. Lefbvre, A. Grill, V. Patel, C. Jahnes, J. Appl. Phys. 85 (1999) 3264.

[131] M.v. Gradowski, A.C. Ferrari, R. Ohr, B. Jacoby, H. Hilgers, H.H. Schneider, H.Adrian Surf. Coat. Technol. 174-175 (2003) 246.

[132] C. Casiraghi, A.C. Ferrari, J. Robertson, R. Ohr, M.v. Gradowski, D. Schneider, H. Hilgers Diamond Relat. Mater. 13 (2004) 1480.

[133] J.B. Pethica, R. Hutchings, W.C. Oliver, Philos. Mag. A 48 (1983) 593.

[134] G. Pharr, W.C. Oliver, Mater. Res. Soc. Bull. 17 (1992) 28.

[135] X. Jiang, J.W. Zou, K. Reichelt, P. Grunberg, J. Appl. Phys. 66 (1989) 4729.

[136] X. Jiang, K. Reichelt, B. Stritzker, J. Appl. Phys. 66 (1990) 5805.

[137] H. Dimigen, Surf. Coatings Technol. 49 (1991) 453.

[138] F.M. Kimock, B.J. Knapp, Surf. Coatings Technol. 56 (1993) 273.

[139] A. Matthews, S.S. Eskildsen, Diamond Rel. Mater. 3 (1994) 902.

[140] S.J. Bull, Diamond Rel. Mater. 4 (1995) 827.

[141] J.P. Sullivan, T. Friedmann, Sandia Natl. Lab. MRS Bulletin, May 2001.

[142] A. Grill, Wear 168 (1993) 143.

[143] A. Gangopadhyay, Tribol. Lett. 5 (1998) 25.

[144] M.F. Doemer, R.L. White, MRS Bull. (1996) 28.

[145] B. Bhushan, Diamond Rel. Mater. 8 (1999) 1985.

[146] J. Robertson, Thin Solid Films 383 (2000) 81.

[147] P. Goglia, J. Berkowitz, J. Hoehn, A. Xidis, L. Stover, Diamond Rel. Mater. 10 (2001) 271.

[148] E. Martinez, J.L. Andujar, M.C. Polo, J. Esteve, J. Robertson, W.I. Milne, Diamond Rel. Mater. 10 (2001) 145.

[149] T. Staedler, K. Schiffmann, Surf. Sci. 482-485 (2001) 1125.

[150] W.D. Nix, H. Gao, J. Mech. Phys. Solids 46 (1998) 411.

[151] K. Durst, B. Backes, M. Göken, Scripta Mater. 52 (2005) 1093.

[152] D.K. Owens, R.C. Wendt, J. Appl. Polym. Sci. 13 (1969) 1741.

[153] W. Rabel, Farbe und Lacke, 77 (10) (1971) 997.

[154] L.Ecuyer, C. Brassard, C. Cardinal, J. Chabball, J. Appl. Phys. 47 (1976) 881.

[155] J. Tirira, P. Trocellier, Journal of Radioanalytical and Nuclear Chemistry, 130 (2) (1989) 311.

[156] P. Pelicon, A. Razpet, S. Markelj, I. Čadež, M. Budnar, Nucl. Instr. and Meth. B 227 (2005) 591.

[157] M. El Bouanani, P. Pelicon, A. Razpet, I. Cadez, M. Budnar, J. Simcic, S. Markelj, NIMB 243 (2006) 392.

[158] M. Mayer, SIMNRA User's Guide 6.05, Max-Planck-Institut für Plasmaphysik, Garching, Germany, 2009

[159] Nobel laureate C.V. Raman's work on light scattering, Singh, Rajinder. - Berlin : Logos-Verl., 2004

[160] P.Y. Yu, M. Cardona, Fundamentals of semiconductors, Springer, Berlin, 1996

[161] K.W. Gilkes, H.S. Sands, D.N. Batchelder, J. Robertson, W.I. Milne, Phys. Lett. 70 (1997) 1980.

[162] K.W. Gilkes, S. Prawer, K.W. Nugent, J. Robertson, H.S. Sands, Y. Lifshitz, X. Shi, J. Appl. Phys. 87 (2000) 7283.

[163] V.I. Merkulov, J.S. Lannin, C.H. Munro, S.A. Asher, V.S. Veerasamy, W.I. Milne, Phys. Rev. Lett. 78 (1997) 4869.

[164] A.C. Ferrari, J. Robertson, Phys. Rev. B64 (2001) 075414.

[165] F. Tuinstra, J.L. Koening, J. Chem. Phys. 53 (1970) 1126.

[166] A.C. Ferrari, J. Robertson, Phys. Rev. B 61 (2000) 14095.

[167] C. Castiglioni, F. Negri, M. Rigolio, G. Zerbi, J. Chem. Phys. 115 (2001) 3769.

[168] C. Castiglioni, E. Di Donato, M. Tommasini, F. Negri, G. Zerbi, Synth. Metals 139 (2003) 885.

[169] C. Castiglioni, M. Tommasini, G. Zerbi, Phil. Trans. R. Soc. Lond. A362 (2004) 2425.

[170] N. Wada, P.J. Gaczi, A. Solin, J. Non-cryst. Solids 35-36 (1980) 543.

[171] S.R. Salis, D.J. Gardiner, M. Bowden, J. Savage, D. Rodway, Diamond Relat. Mater. 5 589.

[172] F. Li, J.S. Lannin, Appl. Phys. Let. 61 (1992) 2116.

[173] G.P. Lopinski, V.I. Merkulov, J.S. Lannin, Appl. Phys. Lett. 69 (1996) 3348.

[174] A.C. Ferrari, B. Kleinsorge, N.A. Morrison, A. Hart, V. Stolojan, J. Robertson, J. Appl. Phys. 85 (1999) 7191.

[175] C. Casiraghi, A.C. Ferrari, D. Grambole, F. Piazza, J. Robertson, Diamond Relat. Mater. 3-7 (2005) 1098.

[176] W.C. Oliver, G.M. Pharr, J. Mater. Res. 1 (1992) 1564.

[177] G.G. Stoney, Proc. R. Soc. Lond. Ser. A82 (1909) 172.

8. OWN PUBLICATIONS

Contribution to the included scientific publications and unpublished results

Publication 1:

M. Kahn, M. Cekada, T. Schöberl, R. Berghauser, C. Mitterer, C. Bauer, W. Waldhauser, E. Brandstätter, Structural and mechanical properties of diamond-like carbon films deposited by an anode layer source, Thin Solid Films 517 (2009) 6502.

*Conception and Planning**	*Experiments*	*Analysis and Interpretation*	*Manuscript Preparation**
100	75	75	100

Publication 2:

M. Kahn, M. Cekada, R. Berghauser, W. Waldhauser, C. Bauer, C. Mitterer, E. Brandstätter, Accurate Raman spectroscopy of diamond-like carbon films deposited by an anode layer source, Diamond Relat. Mater. 17 (2008) 1647.

*Conception and Planning**	*Experiments*	*Analysis and Interpretation*	*Manuscript Preparation**
100	75	90	100

Publication 3:

M. Kahn, N. Menegazzo, B. Mizaikoff, R. Berghauser, J.M. Lackner, D. Hufnagel, W. Waldhauser, Properties of DLC and nitrogen-doped DLC films deposited by DC magnetron sputtering, Plasma Processes Polym. 4, S1 (2007) 200.

*Conception and Planning**	*Experiments*	*Analysis and Interpretation*	*Manuscript Preparation**
100	80	70	100

Publication 4:

M. Kahn, M. Cekada, T. Schöberl, H. Parizek, B. Raninger, R. Berghauser, W. Waldhauser, E. Brandstätter, DLC films deposited at room-temperature by reactive magnetron sputtering and by an anode layer source – a comparative study, Proceedings of the 17th Plansee Seminar 2009, Vol.2, HM 40/1.

*Conception and Planning**	*Experiments*	*Analysis and Interpretation*	*Manuscript Preparation**
100	70	70	100

Publication 5:

M. Kahn, S. Paskvale, M. Čekada, T. Schöberl, W. Waldhauser, C. Mitterer, E. Brandstätter, P. Pelicon, Relation between structural/topological disorder and mechanical properties of hydrogenated DLC films, *submitted*

*Conception and Planning**	*Experiments*	*Analysis and Interpretation*	*Manuscript Preparation**
100	90	70	100

Publication 6:

M. Kahn, W. Waldhauser, C. Mitterer, T. Koch, A. Pauschitz, E. Brandstätter, M. Roy, Nanoindentation and nanoscratch behaviour of room-temperature reactive pulsed magnetron sputtered DLC films-correlations with film structure, *submitted*

*Conception and Planning**	*Experiments*	*Analysis and Interpretation*	*Manuscript Preparation**
70	70	45	55

Unpublished Results:

N. Menegazzo, M. Kahn, R. Berghauser, W. Waldhauser, B. Mizaikoff, Application of nitrogen-doped diamond-like carbon films as novel optically transparent electrodes for multi-reflection IR-ATR spectroelectrochemistry, *Collaborative effort which generated preliminary data that showed a potential chemical application of nitrogen-doped diamond-like carbon films*

Conception and Planning	*Experiments*	*Analysis and Interpretation*	*Manuscript Preparation**
B. Mizaikoff/ N. Menegazzo	50	30	25

***…supervision not included**

PUBLICATION 1:

STRUCTURAL AND MECHANICAL PROPERTIES OF DIAMOND-LIKE CARBON FILMS DEPOSITED BY AN ANODE LAYER SOURCE

Markus Kahn, Miha Čekada, Thomas Schöberl, Roswitha Berghauser, Christian Mitterer, Christoph Bauer, Wolfgang Waldhauser, Elmar Brandstätter

Thin Solid Films 517 (2009) 6502.

STRUCTURAL AND MECHANICAL PROPERTIES OF DIAMOND-LIKE CARBON FILMS DEPOSITED BY AN ANODE LAYER SOURCE

Markus Kahn*[a], Miha Čekada[b], Thomas Schöberl[c], Roswitha Berghauser[a], Christian Mitterer[d], Christoph Bauer[e], Wolfgang Waldhauser[a], Elmar Brandstätter[a]

* Corresponding author, e-mail address: markus.kahn@joanneum.at, telephone: +43 3842 81260-2303, fax: +43 3842 81260-2310

[a] Joanneum Research, Laser Center Leoben, Leobner Strasse 94, A-8712 Niklasdorf, Austria

[b] Jožef Stefan Institute, Department of Thin Films and Surfaces, Jamova 39, 1000 Ljubljana, Slovenia

[c] Erich Schmid Institute of Materials Science of the Austrian Academy of Sciences, Jahnstrasse 12, A-8700 Leoben, Austria

[d] University of Leoben, Department of Physical Metallurgy and Materials Testing, Franz-Josef Strasse 18, A-8700 Leoben, Austria

[e] University of Graz, Institute of Earth Sciences, Department of Mineralogy and Petrology, Universitätsplatz 2, A-8010 Graz, Austria

ABSTRACT

An anode layer source is a special ion gun, which can be fed with carbon precursors like acetylene to deposit hard and highly defect-free hydrogenated diamond-like carbon films at room temperature. The present study focuses on the influence of the process parameters - discharge voltage, process pressure and acetylene flow - on structure and mechanical properties of the deposited films. Raman spectra show that an increased discharge voltage yields decreased structural disorder, *i.e.* a lower C–C sp^3 hybridised fraction of carbon atoms in the films. By an elevation of the discharge voltage from 1 to 3 kV the full width at half maximum of the G-band decreases from 194±0.2 cm^{-1} to 183±0.7 cm^{-1}. Films deposited at the lowest discharge voltage show in accordance to the spectroscopic data the highest nanohardness (36±1 GPa), stress (-2.34±0.2 GPa) and reduced elastic modulus (180±4 GPa).

KEYWORDS

Diamond-like carbon (DLC), linear ion beam source, mechanical properties, Raman spectroscopy

1. INTRODUCTION

Diamond-like carbon (DLC) films, which present a metastable form of carbon in an amorphous structure with a mixture of sp^2 and sp^3 hybridised bonds, have a wide range of applications. Initially, the films played an important role for tools or engineering components as wear resistant coatings, ensuring high hardness and low friction coefficients [1,2]. Wear protection is still one of the main implementations of DLC coatings, whereas in recent years these films have become more and more relevant as barrier coating on artificial implants, stents or applications in analytical chemistry, for example as corrosion resistant coating on zinc selenide infrared waveguides [3]. Moreover, biochemists have found DLC as a useful functional surface for cell biology or immobilisation experiments of proteins [4-6].

Depending on the mechanical and structural needs for application, these films can be deposited by pulsed laser deposition, sputtering, chemical vapour deposition and filtered cathodic vacuum arcs [2]. Each of these named deposition techniques has limitations in several important properties of DLC films, such as presence of defects, known as particulates and droplets or lacking adhesion on different substrates. For the application of DLC films as corrosion resistant coatings or coatings on artificial implants in contact with human serum and blood, defect-free layers are mandatory. Methods, where a solid target is sputtered or evaporated by a laser beam do not provide defect-free films. Macro-particles emitted from the target can hit the substrate, generating defects in the growing DLC coating. These macro-particles are also known as the origin of porosity and pinholes, due to shadowing effects and removal of initially adherent macro-particles during film growth. Deposition techniques, which use gaseous carbon containing precursors for film growth like chemical vapour deposition as well as ion beam methods, have the great advantage of growing basically defect-free films. Veerasamy et al. [7] reported in 2003 on a deposition technique using a closed drift linear ion beam source to deposit hydrogenated tetrahedral amorphous carbon films (ta-C:H) with sp^3 contents as high as 80 % directly onto glass substrates. They also claimed excellent adhesion of the ta-C:H coatings on the glass substrates, caused by the initial effect of implantation of carbon into the glass surface enabling the growth of a diffuse interfacial carbon-glass layer [7]. Zhurin et al. [8] have given a detailed review on physics of closed drift thrusters, another field of use and the primal application of linear beam ion sources. Depending on geometrical and material differences, these sources can be divided into magnetic layer thrusters and so called anode layer types. In general, the electric field that accelerates the ions is established by an electron current that passes through and is guided by a magnetic field [8]. These electrons follow a closed drift path, which is eponymous for these devices. The anode layer thruster has its origin in the acceleration of electrons from the cathode to the anode, increasing the electron temperature, which results in a sharp decrease in plasma potential, so that the ion generation and acceleration takes place in the form of a thin layer near the anode, giving the source its name - anode layer source [8]. The characteristics of an anode layer thruster are that the channel where the discharge takes place is short compared to the width of the channel. Thus, these types of ion sources are also called thrusters with short acceleration zone [8].

In thin film technology, anode layer sources are used for argon or oxygen plasma cleaning of substrates. Such a source can also be fed with hydrocarbon gases to deposit DLC films, as reported by Veerasamy et al. [7]. In this work, we applied a linear ion beam source for DLC deposition in a unique configuration, employing so

called contamination shielding plates installed at the cathodes of the ion source. These shielding plates are constructed to reduce the contaminant uptake from plasma erosion of the cathodes [9]. Using the described shielding plates it is possible to reduce contamination in the growing films for at least 50 % [9]. The aim of this study was to elucidate trends in the structure formation and mechanical property evolution of DLC films deposited by an anode layer source with varying discharge voltage, process pressure as well as different substrate manipulation in front of the ion beams using C_2H_2 as precursor gas.

2. EXPERIMENTAL DETAILS

2.1. FILM DEPOSITION

For deposition of DLC films, an ALS340L anode layer source from Veeco Instruments (Woodbury, NY, USA) was fed with acetylene (C_2H_2, nominal purity >99.96 %). Figure 1a shows a sketch of a cross-section of the anode layer source, and Figure 1b outlines its working principle [9]. The gas was directly introduced into the discharge channel. The anode layer source was powered with a high voltage DC power supply from Glassman High Voltage (High Bridge, NJ, USA) in the voltage controlled mode. Discharge voltages ranging from 1 to 3 kV were applied to the anode, providing ion energies of roughly 450 to 750 eV [9].

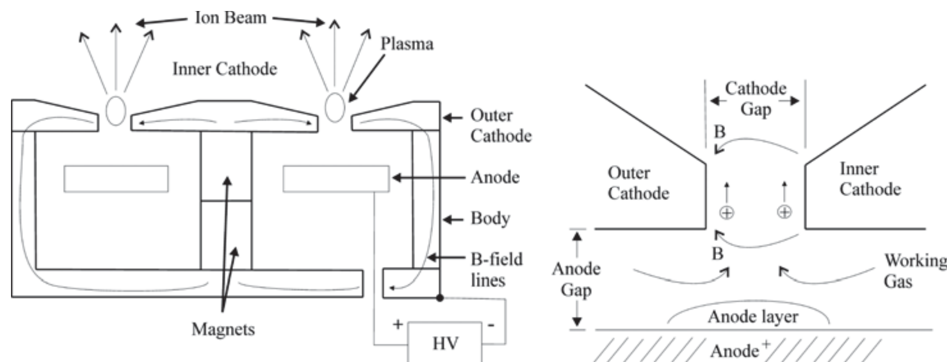

Figure 1. a) Cross-section of the anode layer source ALS340 from Veeco Instruments showing the main components of the source body and electrical circuit points [after 9]. **b)** Working principle of the anode layer source [after 9].

Silicon wafers (100) with a thickness of 525±25 μm were used as substrates. The wafers were chemically cleaned in an ultrasonic cleaner sequentially with acetone and ethanol, and were dried with nitrogen. The wafers were fixed on a grounded substrate holding carrousel situated at a distance of approximately 15 cm from the ion source. The diameter of this carrousel was 56 cm whereas the samples were fixed at a diameter of 40 cm on vertical static columns. No substrate bias was used during the depositions. For lateral mappings to investigate the film thickness uniformity as well as structural uniformity, 20 silicon wafers (1 cm broadness with a gap of ~0.9 cm) were mounted horizontally at a distance of 15 cm from the source. Films were deposited in three ways: in static mode, by oscillation of the carrousel with an amplitude of 9 cm (left-right), and by rotation around the vertical axis of the carrousel. The movement was in all cases one-dimensional and perpendicular to the ion beams of the linear anode layer source. The substrate temperature was monitored with an electrically insulated K-type thermocouple installed at the backside of the substrate holder. For plasma cleaning of the wafers prior to deposition, the ion source was operated at a voltage of 2 kV and an argon (Ar)

(nominal purity >99.999 %) flow rate of 20 sccm through the ion gun, resulting in a power density of 2.8 Wcm^{-1} (power on the anode layer source per cm of the discharge channel). For all depositions, the chamber was evacuated to a base pressure of $\leq 5 \cdot 10^{-3}$ Pa. During deposition, the pressure in the chamber ranged from 0.15 Pa to 0.3 Pa via introducing 10 to 30 sccm of C_2H_2.

2.2. FILM THICKNESS AND INTRINSIC STRESS

Thickness and internal stress of the films were determined using a stylus profilometer Form Talysurf Series 2 from Taylor Hobson Ltd. (Leicester, GB). Step size measurements were carried out at edges of coated and uncoated areas on the silicon substrates. For stress measurements, the wafers were checked for flatness prior to deposition. During deposition, these samples were fixed only on one end so that the wafer could follow the stress emerging during growth of the DLC film. Care was taken to avoid possible coating of these samples at the backside. After deposition of ~1 µm thick films, the curvature on the silicon wafers was measured with a stylus force of 1 mN. The stress in the films was calculated using the modified Stoney equation [10].

2.3. VICKERS MICROHARDNESS, NANOHARDNESS AND ATOMIC FORCE MICROSCOPY

Vickers microhardness of DLC films with ~1 µm thickness was measured with a Fischerscope H100C from Helmut Fischer (Sindelfingen-Maichingen, Germany) using a Vickers indenter and loads ranging from 3 to 10 mN. The indentation depth ranged from 10 to 20 % of the coating thickness for the applied loads. The hardness and elastic modulus showed relative standard deviations of less than 10 % for all loads used, so that in the following figures data from the 3 mN measurements are presented. In addition, on films with a thickness of ~200 nm, nanoindentation measurements were carried out on a Hysitron Triboscope (Hysitron Inc., Minneapolis, MN, USA) using a cube-corner indenter with a tip radius <50 nm. Quantitative hardness and reduced modulus values were determined from the unloading part of the load-displacement curves, applying the method introduced by Oliver and Pharr [11]. The reduced modulus takes into account the deformation of the indenter tip and the lateral deformation of the sample material via its Poisson’s ratio [11]. At constant indention depth on each film the relative standard deviation of hardness and modulus did not exceed 3 %. Effects like the influence from the substrate [12] and indentation size effect [13,14] were excluded by a careful choice of the indentation depth. In order to check a possible influence from the substrate, loads ranging from 200 to 750 µN were applied. For the determination of surface roughness, atomic force microscopy (AFM) imaging was performed using an ultra-sharp, high-aspect ratio tip in tapping mode with a scan size of 5×5 µm.

2.4. MICRO-RAMAN SPECTROSCOPY

A HR 800 high-resolution Raman microspectrometer from Jobin-Yvon (Villeneuve d'Ascq, France) was used to characterise the structure of carbon bonds in the DLC films. The instrument was operated with lasers at excitation wavelengths of 325, 532 and 633 nm, respectively. Olympus 40× (for 325 nm) and 100× objectives (for 532 and 633 nm) were used to focus the beams on the sample, where in all cases the power of the laser was kept well below 0.25 mW. The entrance slit to the spectrometer was set to 100 µm and holographic gratings with 1800 grooves mm^{-1} were used for 532 and 633 nm and 2400 grooves mm^{-1} for 325 nm

excitation. A standard (100) orientated silicon wafer with a Si-peak position of 520 cm^{-1} was used as drift standard for all excitation wavelengths. A resolution of 0.3 cm^{-1} could be achieved with the spectrometer. Mathematical spectrum fitting for the D and G-bands with Gaussian functions was performed with "Peak-Fit" 4.11 from Systat (Point Richmond, CA, USA). Additionally, Raman spectra of films deposited at the lowest ion energy were fitted with a Breit-Wigner-Fano function (BWF) for the G-band and a Lorentzian for the D-band. The G-band in Raman spectra from amorphous carbon phases taken at visible excitation has its origin in the effect of bond stretching of all carbon atoms in sp^2 hybridisation in rings and chains. The D-band occurs from the breathing mode of carbon atom rings [15-17]. I_D/I_G ratios were calculated by using peak heights. Since this work focuses on the spectral features of the D and G-bands, other Raman active modes have been neglected.

3. RESULTS AND DISCUSSION

3.1. GENERAL FILM PROPERTIES

In order to investigate the influence of C_2H_2 flow and discharge voltage on the deposition rate of the DLC films, we performed experiments by varying the C_2H_2 flow from 10 to 30 sccm while keeping the discharge voltage constant at 3 kV. In addition, investigations were carried out by varying the discharge voltage from 1 to 3 kV while working with constant C_2H_2 flow of 20 sccm (at constant substrate oscillation). The results show an increased deposition rate with higher discharge voltage (Figure 2a): A deposition rate of 3.7±0.3 nm min^{-1} was found for 1 kV and 9.5±0.5 nm min^{-1} for 3 kV. Besides this, elevating the C_2H_2 flow through the source by a factor of three resulted in a fourfold increase of the deposition rate (Figure 2b).

Static deposition experiments with the standard C_2H_2 flow of 20 sccm and an applied discharge voltage of 3 kV showed the expected spikes of deposition rate in front of the two plasma beams of the anode layer source (Figure 2c). The observed profile of the deposition rate corresponds to the particle density of the two beams. Working with oscillation amplitude of 9 cm showed a symmetric and homogeneous deposition rate of 9.5±0.5 nm min^{-1} over a horizontal distance of approximately 10 cm using similar process conditions.

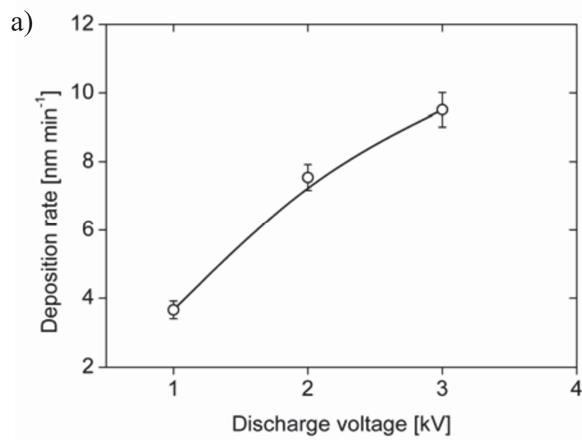

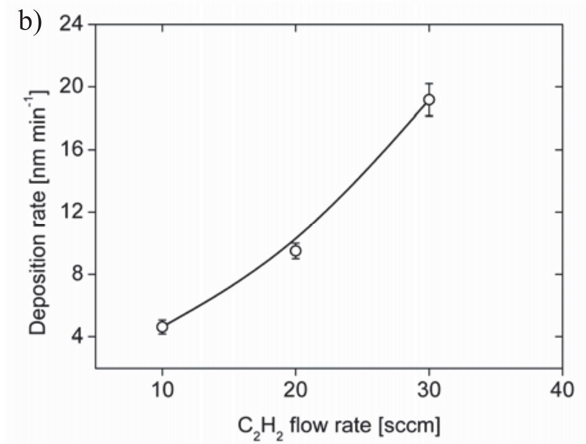

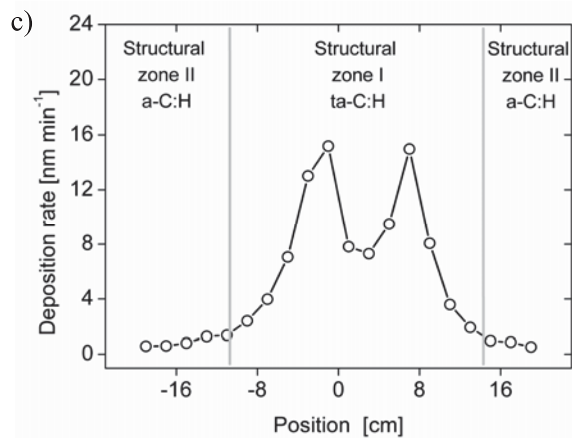

Figure 2. Deposition rate as function of a) discharge voltage at constant C_2H_2 flow of 20 sccm, **b)** C_2H_2 flow rate at constant discharge voltage of 3 kV, **c)** the horizontal position perpendicular to the beam major axis. Additionally, structural zones I and II are shown, which are discussed in the text.

A great advantage of this deposition process is the low temperature of the substrates of less than 70°C after runs for several hours with the highest possible discharge voltage of 3 kV. Depositions at 1 kV discharge voltage showed an equilibrium temperature of less than 40°C on the substrates. Hence, this technique of depositing DLC films is very versatile and can be applied also on temperature-sensitive substrates.

Another advantage is the smooth and defect-free DLC surface obtained by this method. AFM studies on our deposited films showed a roughness of the DLC surfaces of 0.1-1 nm. Figure 3 shows an AFM image of the smooth and homogeneous surface. With such highly defect-free films it is possible to realize much thinner and compact coatings compared for example to sputtered DLC coatings. It might thus be assumed that our coatings are comparable to those applied in semiconductor industry, where DLC films with thicknesses as thin as 1 nm are used for protective coatings of data storage materials, deposited with gridless ion source technology [1].

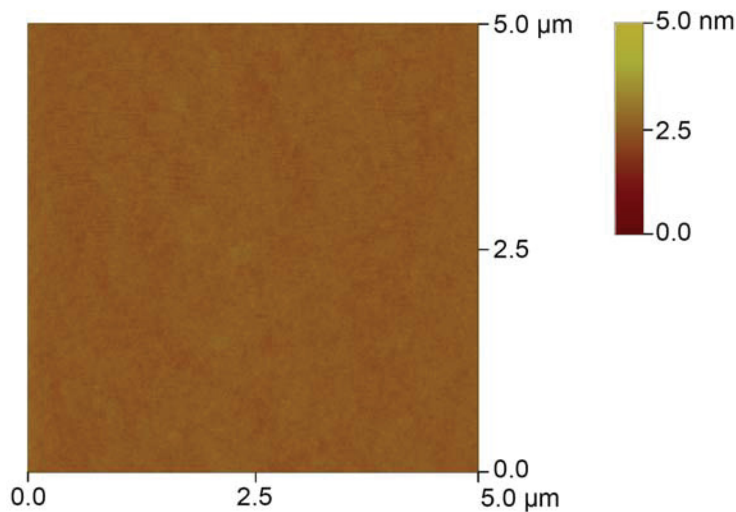

Figure 3. AFM image of the DLC surface.

3.2. STRUCTURAL PROPERTIES

Figure 4 shows an exemplary Raman spectrum (with additional Gaussian function fits for the D and G-band), taken from a film deposited with 20 sccm C_2H_2 at a discharge voltage of 1 kV (at constant substrate oscillation). The bands were found to be at spectral positions of 1358±2 cm^{-1} (D-band) and 1541±1 cm^{-1} (G-band).

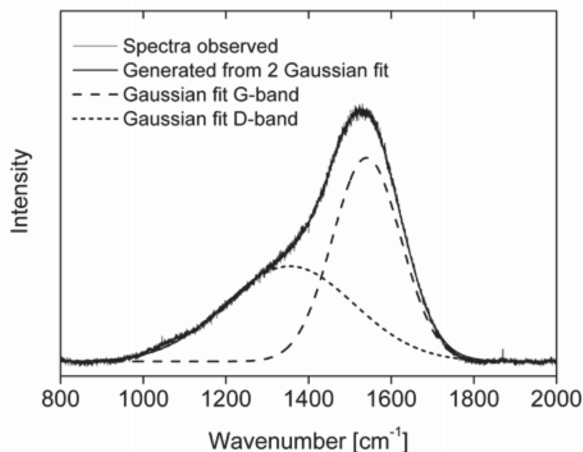

Figure 4. Exemplary Raman spectrum recorded with 532 nm for an a-C:H coating deposited with 20 sccm C_2H_2 at a discharge voltage of 1 kV.

In order to describe the structure of the films it is necessary to discuss the intensity ratio I_D/I_G, the full width at half maximum of the G-band (FWHM (G)), the position of the G-band and the dispersion of the G-band with excitation wavelength. First, it has to be considered, that the intensity ratio I_D/I_G is a measure of the size of the sp^2 phase organized in rings [18]. If the intensity ratio I_D/I_G becomes lower or zero, the sp^2 phase is organised rather in chains, whereas a higher intensity ratio I_D/I_G is an indication of an increase of the sp^2 phase in aromatic rings. Thus, if no D-band is visible, no sp^2 carbon rings exist in the material [15].

For hydrogenated amorphous carbon films (a-C:H), where the sp^2 phases and the sp^3 phases are linked together, the visible Raman parameters (532 nm) can be used to reveal information about the sp^3 hybridisated carbon fraction of the films. A lower intensity ratio I_D/I_G is connected with higher overall sp^3 content [15,16].

Since carbon is sp^3 bonded in a-C:H films also to hydrogen, an increase in sp^3 content does not always mean an increase in density, hardness and other mechanical properties [15, 18]. For a-C:H with hydrogen contents over 25 at.% the overall sp^3 content can increase, but not the C–C sp^3 content. Such polymeric films have the lowest hardness, stress and density. The ta-C:H films represent a class of hydrogenated DLC in which the C–C binding content can be increased while keeping a fixed hydrogen content (25 to 30 at.%) [18]. Therefore ta-C:H have much more C–C sp^3 bonding than a-C:H, enabling a higher hardness and density while having a similar sp^3 content as an a-C:H film [15, 18]. Thus, utilizing the intensity ratio I_D/I_G only, it is difficult to estimate the bonding regimes in amorphous carbons. To investigate the structure of the deposited films in more detail it is necessary to focus also on the FWHM (G). The FWHM of the G-band is a key parameter of monitoring structural disorder in DLC films [18]. This structural disorder arises from the bond angle and bond length distortions in DLC. The FWHM (G) is small when sp^2 clusters are more defect-free and ordered and a higher FWHM (G) is thus indicative for an increase in disorder [18]. The effect originates in the higher bond length and higher bond angle in more disordered material [18]. The increase in disorder is here linked to an increase in C–C sp^3 content, density, and hardness [18]. Casiraghi et al. [18] stated, that this concept holds for hydrogen free carbons as well as for a-C:H with hydrogen contents around 20-30 at.%. At higher hydrogen contents, FWHM (G) as an indicator for structural disorder decreases for a-C:H with hydrogen contents higher than the prementioned 30 at.% [18].

An I_D/I_G ratio of 0.48±0.02 was calculated with peak amplitudes of the bands shown in Figure 4. Intensities from D and G-bands taken from samples deposited at higher discharge voltages of 2 and 3 kV at similar process parameters show enhanced I_D/I_G ratios of 0.53±0.01 and 0.59±0.01, respectively. Figure 5 shows the discussed increase in D-band intensity induced by a higher discharge voltage and Figure 6 depicts graphically the rise in I_D/I_G ratios when increasing the discharge voltage. The position of the G-band shows no significant shifts while increasing the discharge voltage and remains at a constant position of 1541±0.7 cm^{-1}. From these data, a trend of an increased clustering of sp^2 phases in rings for higher discharge voltages can be deduced [15-18]. We did not investigate films deposited at lower discharge voltages since the anode layer source is only stable at a minimum discharge voltage of 0.6 kV. In order to confirm the trends derived from the intensity ratios, the FWHM of the G-band is used to reveal information about the structural variance induced by changes in the process parameters. For films deposited at a discharge voltage of 1 kV, a FWHM (G) of 194±0.2 cm^{-1} was derived from the Gaussian fits, which decreases linearly to 183±0.7 cm^{-1} for a discharge voltage of 3 kV (Figure 6). The trends in FWHM (G) completely confirm the observed behaviour that the films at the lowest discharge voltage have increased structural disorder. The increase in disorder can here be linked to an increase in C–C sp^3 content in the material [18].

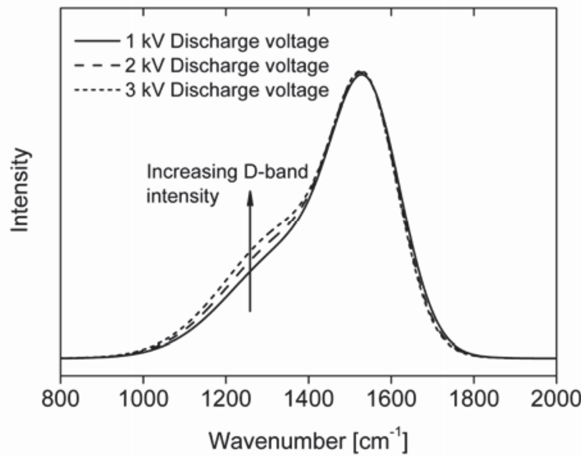

Figure 5. Raman spectral shape as function of discharge voltage measured at 532 nm.

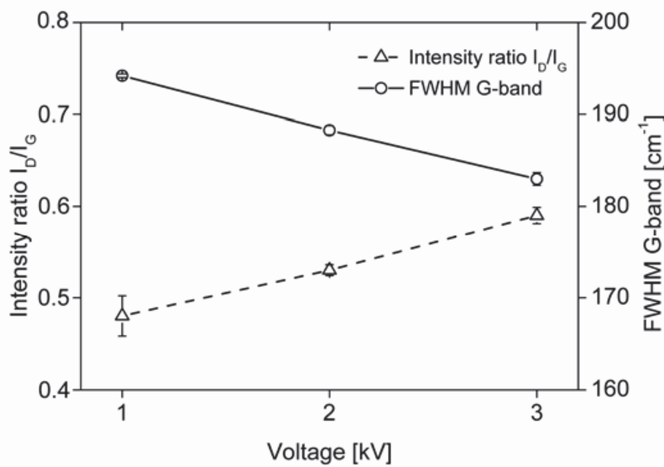

Figure 6. Intensity ratio I_D/I_G and FWHM (G) as function of discharge voltage (measured at 532 nm).

The high FWHM (G) of 194±0.2 cm^{-1} (fitted with a Gaussian function) for the most disordered film deposited at the lowest ion energy suggests the classification of the deposited film to the structural class of ta-C:H. Additional fitting of the obtained spectra with a BWF function for the G-band and a Lorentzian for the D-band showed a FWHM (G) of 249 cm^{-1} with an I_D/I_G ratio of 0.06. This allows the comparison of our measured data with results from Conway et al., where I_D/I_G ratios of ~0.05 were reported for ta-C:H films [19].

The topological disorder of the deposited DLC films can be probed by Raman measurements with more than one excitation wavelength [18]. The topological disorder arises from the size and shape distribution of the sp^2 clusters. Only a carbon material with disorder shows G-band dispersion, because the dispersion has its origin in the resonant selection of sp^2 chains of different sizes (conjugation length) at different excitation energies [18]. A hydrogenated amorphous carbon film, deposited by using a C_2H_2 flow rate of 20 sccm at a voltage of 3 kV (at constant substrate oscillation), was investigated with excitation wavelengths of 633, 532 and 325 nm, respectively. The position of the G-band increases from ~1516 cm^{-1} to ~1588 cm^{-1} while lowering the excitation wavelength. The dispersion is 0.23 $cm \cdot nm^{-1}$ for the investigated film, which fits well the results in literature for dispersion of a-C:H [18].

Evolution of the background slopes arising in the spectra showed unaffected backgrounds with no increasing photoluminescence caused by elevated hydrogen contents in DLC films when using a relatively high excitation wavelength of 532 nm in Raman spectroscopy [15]. The Raman spectra indicate a hydrogen content of

roughly ≤25 at.%, which could be estimated from the ratio of the fitted background slope (m) per intensity of the G-band (I_G) [15] of ~0 µm. This result authenticates that the anode layer source is able to decompose the C_2H_2 molecule for growing a-C:H films with roughly ≤25 at.% hydrogen when using the described experimental setup.

We want to highlight, that a deposition with a static mapping, where 20 silicon wafers were mounted perpendicular to the major beam axis of the source, showed increased m/I_G ratios up to 10 µm at a horizontal distance of approximately 10 to 12 cm (measured with 532 nm excitation) from the axis of the source. This indicates a higher hydrogen concentration in the films, which causes the increased m/I_G ratio in the Raman spectrum [15]. These films are authentic a-C:H films which showed a decreased FWHM (G) down to ~140 cm^{-1}. Figure 2c depicts the zones (zones II (a-C:H)), where these strongly hydrogenated films can be found. It can be assumed, that these films have lower structural disorder which is estimated by the decreased FWHM (G). Samples mounted to the prementioned distance of up 10 to 12 cm showed no increased slope of the Raman spectra background which gives values for m/I_G of ~0 µm. This structural zone (zone I (ta-C:H)) is shown as well in Figure 2c. Oscillation as well as complete rotation of the samples through the plasma beams showed in all cases ratios for m/I_G of ~0 µm.

Further Raman investigations showed also a dependence of the FWHM (G) and the I_D/I_G ratio of the films as a function of the horizontal position perpendicular to the major beam axis. A discharge voltage of 3 kV and a C_2H_2 flow of 20 sccm were applied for this investigation. A FWHM (G) of 190±0.5 was detected for samples which were installed between the two plasma beams. A lower FWHM (G) of 182±1 cm^{-1} measured for samples installed directly in front of the two beams evidenced the proposed behaviour, that higher ion energy yields less tetrahedral character films with less disordering. Additionally, the I_D/I_G ratio was used to verify the structural trends derived from the FWHM (G) for these experiments. An I_D/I_G ratio of 0.48±0.07 was detected for samples installed in front of the center of the source, whereas an I_D/I_G ratio of 0.6±0.02 was observed for samples positioned directly under the beams. This observation confirmed that higher ion energies on samples immediately in front of the two beams result in an increased clustering of sp^2 phases in the DLC films, also known as an ordering process. Furthermore, this guarantees the described overall behaviour that films grown with generally higher discharge voltages of 3 kV show less C–C sp^3 fractions. The I_D/I_G ratio of 0.48±0.07 in the lower ion energy region in the center of the source between the two plasma beams is similar to the results observed for processes with oscillating movement of the substrates where the discharge voltage was set to 1 kV.

We also investigated the influence of mixing Ar to the process gas in order to find further improved deposition parameters. These experiments were carried out with the standard procedure of oscillating the silicon wafers with an amplitude of 9 cm through the ion beams. The total gas flow was 20 sccm and the discharge voltage for these experiments was set to 1 and 3 kV, respectively. With a mixture of 15 sccm C_2H_2 and 5 sccm Ar, an I_D/I_G ratio of ~0.60 was detected for a discharge voltage of 1 kV. A discharge voltage of 3 kV with similar conditions showed a further increased I_D/I_G ratio of ~0.80. The FWHM (G) decreased from ~190 to ~176 cm^{-1} when increasing the discharge voltage from 1 to 3 kV. Introducing mixtures of Ar and C_2H_2 into the anode layer source showed an ordering process in the DLC films. This behaviour can be interpreted as the result of

the high energy ion bombardment by heavy Ar-ions during film growth, reducing the disordered character and C–C sp^3 content. It can be concluded that highly disordered films can be achieved by using exclusively C_2H_2 as process gas. It is also reported by Conway et al. [19] that C_2H_2 is the favoured precursor for growing ta-C:H with plasma beam methods. They report, that depositions, where methane as carbon source is used, do not grow authentic ta-C:H and the character is less tetrahedral [19].

3.3. MECHANICAL PROPERTIES

In order to validate the structural trends derived from Raman spectra, we applied the nanoindentation method to 200 nm thick films. The nanohardness increased with decreasing discharge voltage and ion energy (Figure 7). A nanohardness of 36±1 GPa and a reduced modulus of 180±4 GPa are indicative for a highly disordered film deposited in our study using the lowest possible ion energy. [2]. It can be concluded that the mean ion energy in our deposition process has the most important influence on the structure of the films.

The results of our study agree well with the results from Weiler et al. [20]; they showed that films deposited with an ion energy of ~ 90 eV per carbon ion using the plasma beam source have the highest C–C sp^3 content. However, Veerasamy et al. [7] found the highest hardness values for mean ion energies of ~ 750 eV per carbon atom for films deposited on soda-lime glass. They did not observe any drop in hardness and tetrahedral character of the deposited films when working with ion energies up to 1 keV per carbon atom. The ta-C:H films in their study were deposited with a linear ion beam source which is constructed according to the principles of an anode layer source, having a short discharge channel compared to the width of the channel. This source belongs to the short acceleration zone ion guns, as well as the anode layer source we used. Veerasamy et al. [7] report a completely inverse trend of the hardness as a function of the mean ion energy per carbon atom compared to other studies [2, 20] as well as our data reported in this paper. They named two possible reasons for higher disordered character of the DLC films deposited at elevated ion energies: First, the presence of H during the film growth may delay the onset of graphitisation which is caused by thermal spikes at high energies, and second, the charging of the film surface can also reduce the effective energy of the incident ions. In contrast, our films show highest hardness and disordered character when working with the lowest possible ion energy.

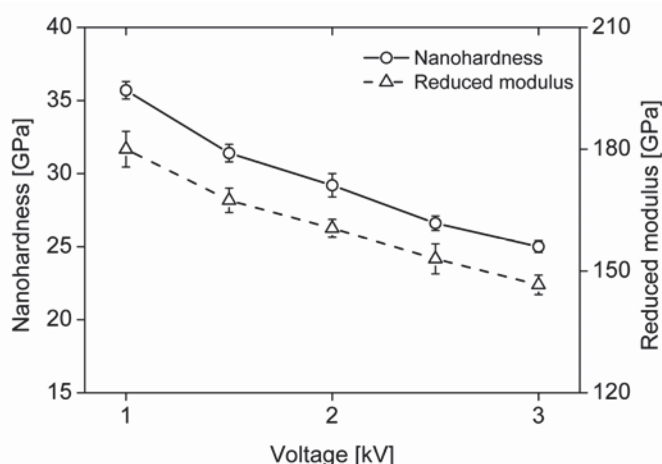

Figure 7. Nanohardness and reduced modulus as function of discharge voltage.

In order to establish further evidence of our results from nanohardness measurements, we applied the Vickers microhardness method to films with enhanced thicknesses of ~1 µm. The results are plotted in Figure 8. A Vickers microhardness of 2900±80 HV could be detected for the film deposited by the lowest discharge voltage of 1 kV. The Vickers microhardness also confirmed the trend derived from our nanohardness results that increased ion energy yields less disordered character and less hardness.

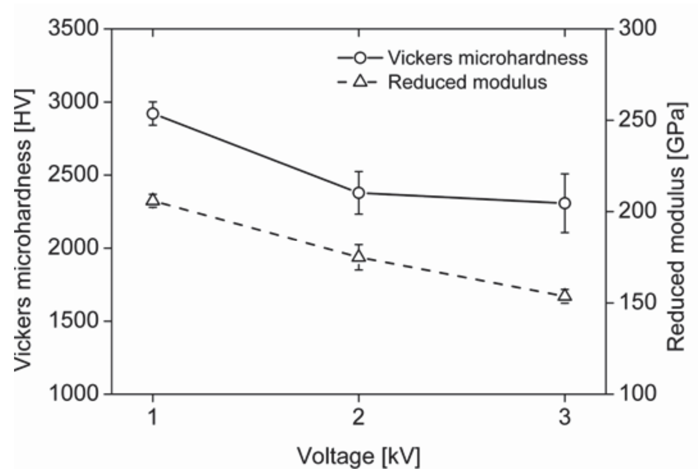

Figure 8. Vickers microhardness and reduced modulus as a function of discharge voltage.

The trends derived from Raman spectroscopy and nanoindentation could also be fully evidenced by the determination of stress in our films. The stress in DLC is known to increase with increasing C–C sp^3 binding content [2]. The measured values showed the expected drop in compressive stress when increasing the discharge voltage. For a discharge voltage of 3 kV, a compressive stress of -0.85±0.02 GPa was detected, whereas the films deposited at 2 and 1 kV showed -0.89±0.3 and -2.34±0.2 GPa, respectively.

4. CONCLUSIONS

The present paper demonstrates the unique properties of an anode layer source for the direct deposition of hard a-C:H films. Raman spectra indicate an increasing disorder of the film structure when applying the lowest ion energy for film growth. This behaviour is confirmed by elevated hardness, reduced modulus and intrinsic stresses in films deposited at the lowest ion energy. Due to the very smooth and defect-free nature of the deposited a-C:H films, these films are assumed to be excellent candidates for applications as corrosion-resistant coatings or coatings of artificial implants. Another important benefit of this coating technique is a low substrate temperature of <70°C, which makes the method very versatile for coating of temperature-sensitive surfaces. We want to highlight the simple and robust working principle of the anode layer source, which enables the use of the source for plasma-cleaning of substrates as well as for deposition of a-C:H films for industrial applications.

ACKNOWLEDGEMENTS

Financial support of this work by the Austrian Federal Ministry of Traffic, Innovation and Technology, the Austrian Industrial Research Promotion Fund (FFG), the Government of Styria, Forschung Austria and the European Union is highly acknowledged.

REFERENCES

[1] A.C. Ferrari, Surf. Coat. Technol. 180-181 (2004) 190.

[2] J. Robertson, Mater. Sci. Eng. R37 (2002) 129.

[3] M. Janotta, D. Rudolph, A. Kueng, C. Kranz, H.S. Voraberger, W. Waldhauser, B. Mizaikoff, Langmuir 20 (2004) 8634.

[4] F.Z. Cui, D.J. Li, Surf. Coat. Technol. 131 (2000) 481.

[5] T. Yokota, T. Terai, T. Kobayashi, M. Iwaki, Nucl. Instrum. Methods Phys. Res. Sect. B 242 (2005) 48.

[6] C. Lim, S. Slack, S. Ufer, E. Lindner, Pure Appl. Chem. 76 (2004) 753.

[7] V.S. Veerasamy, H.A. Luten, R.H. Petrmichl, S.V. Thomsen, Thin Solid Films 442 (2003) 1.

[8] V.V. Zhurin, H.R. Kaufman, R.S. Robinson, Plasma Sources Sci. Technol. 8 (1999) R1.

[9] Veeco Instruments, Technical Manual to ALS340, 2003.

[10] G.G. Stoney, Proc. R. Soc. Lond. Ser. A82 (1909) 172.

[11] W.C. Oliver, G.M. Pharr, J. Mater. Res. 1 (1992) 1564.

[12] T. Staedler, K. Schiffmann, Surf. Sci. 482-485 (2001) 1125.

[13] W.D. Nix, H. Gao, J. Mech. Phys. Solids 46 (1998) 411.

[14] K. Durst, B. Backes, M. Göken, Scripta Mater. 52 (2005) 1093.

[15] A.C. Ferrari, J. Robertson, Phil. Trans. R. Soc. Lond. A, 362 (2004) 2477.

[16] A.C. Ferrari, J. Robertson, Phys. Rev. B, 61 (2000) 14095.

[17] A.C. Ferrari, J. Robertson, Phys. Rev. B, 64 (2001) 075414.

[18] C. Casiraghi, A.C. Ferrari, J. Robertson, Phys. Rev. B, 72 (2005) 085401.

[19] N.M.J. Conway, A.C. Ferrari, A.J. Flewitt, J. Robertson, W.I. Wilne, A. Tagliaferro, W. Beyer, Diamond Rel. Mater. 9 (2000) 765.

[20] M. Weiler, S. Sattel, T.Giessen, K. Jung, H. Ehrhardt, V.S. Veerasamy, J. Robertson, Phys. Rev. B, 53 (1996) 1594.

PUBLICATION 2:

ACCURATE RAMAN SPECTROSCOPY OF DIAMOND-LIKE CARBON FILMS DEPOSITED BY AN ANODE LAYER SOURCE

M. Kahn, M. Cekada, R. Berghauser, W. Waldhauser, C. Bauer, C. Mitterer, E. Brandstätter

Diamond Relat. Mater. 17 (2008) 1647.

ACCURATE RAMAN SPECTROSCOPY OF DIAMOND-LIKE CARBON FILMS DEPOSITED BY AN ANODE LAYER SOURCE

M. Kahn[1]*, M. Cekada[1,2], R. Berghauser[1], W. Waldhauser[1], C. Bauer[3], C. Mitterer[4], E. Brandstätter[1]

[1]Joanneum Research, Laser Center Leoben, Leobner Straße 94, 8712-Niklasdorf, Austria

[2]Jozef Stefan Institute, Department of Thin Films and Surfaces, Jamova 39, 1000 Ljubljana, Slovenia

[3]University of Graz, Institute of Earth Sciences, Department of Mineralogy and Petrology, Universitaetsplatz 2, 8010-Graz, Austria

[4]University of Leoben, Department of Physical Metallurgy and Materials Testing, Franz-Josef Straße 18, 8700-Leoben Austria

ABSTRACT

Diamond-like carbon (DLC) films deposited by a new room-temperature deposition method were critically investigated by Raman spectroscopy. A gridless, linear anode layer source was fed with acetylene at different flow rates at varying applied voltages producing highly adhesive and transparent DLC films. Raman spectra showed a correlation between the intensity ratio I_D/I_G and the voltage applied to the ion source. When increasing the voltage from 1 to 3 kV, the intensity ratio increased from 0.48±0.02 to 0.59±0.01 (measured at an excitation wavelength of 532 nm and fitted with Gaussian functions). These observations were confirmed by stress measurements, where an increase of the voltage from 1 to 3 kV resulted in a decrease of the compressive stress from -2.34±0.17 to -0.85±0.02 GPa, indicating a decreased sp^3-hybridised carbon fraction at elevated voltage. Under the described conditions we observed maximum substrate temperatures of 70°C after deposition processes for several hours which clearly show the unique features of this relatively new deposition technique for hydrogenated tetrahedral DLC films.

KEYWORDS

Diamond-like carbon; chemical vapour deposition; vibrational properties characterisation

1. INTRODUCTION

The properties of DLC films can be tailored by deposition techniques as well as deposition parameters. DLC films are smooth and have many other remarkable properties such as high wear resistance, high hardness and chemical inertness, resulting in their application in several fields ranging from tribology to biochemistry [1-4].

However, the occurrence of particulates and droplets on DLC films typically produced with DC magnetron sputtering or pulsed laser deposition, can diminish the fields of application where highly defect- and pinhole-free films are of major importance. Such defects are caused by macro-particles from the applied carbon target which do not undergo the vapour state and were therefore found as defects on the DLC surface. Droplets are melted aggregates from the target material which also do not undergo any vapour state. These defects have their origin in the use of a solid carbon source as a target together with exposure of the material to intense ion-bombardment or intense laser light. The use of gaseous carbon-containing precursors together with high energy dissociation and ionisation by an anode layer source can overcome these problems providing high purity and basically defect-free films. This technique was originally reported in the early 1970`s as a auxiliary propulsion system for space satellites [5]. Such sources are commercially available for plasma cleaning, whereas the use for deposition of DLC is relatively new. In fact there is sparse literature about the direct use for the deposition of DLC with an anode layer source. Veerasamy et al. [6] reported about the deposition of hydrogenated tetrahedral DLC with a similar source as described in this study. They proved the possibility of depositing hydrogenated tetrahedral DLC films with hardness up to 55 GPa on glass substrates, not exceeding temperatures of 60°C during deposition.

The present work focuses on Raman spectroscopy in order to achieve a refinement of the deposition parameters by considering information on the chemical composition and binding state of the films. For this purpose, the two main bands of the DLC films were investigated by means of their position, intensity and peak shape.

2. EXPERIMENTAL DETAILS

2.1. SAMPLE PREPARATION AND DEPOSITION OF DLC FILMS

DLC films were deposited by employing an ALS340L anode layer source from Veeco Instruments (Woodbury, NY, USA) fed with 10 to 30 sccm acetylene (nominal purity <99.96 %) on (100) orientated silicon wafers with a thickness of 525±25 µm. We used no other carbon precursors during the experiments. Figure 1a shows a sketch of a cross section of the anode layer source and Figure 1b outlines the working principle of such a source [7].

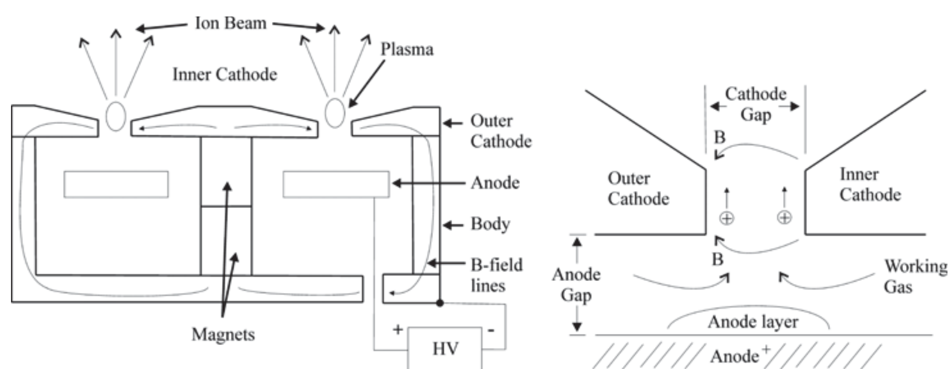

Figure 1. a) Cross-section of the anode layer source ALS340 from Veeco Instruments. **b)** Working principle of the anode layer source [7].

The anode layer source was powered with a high voltage DC power supply from Glassman High Voltage (High Bridge, NJ, USA) in the voltage regulation mode. Samples were pre-cleaned in an ultrasonic cleaner sequentially with acetone and ethanol, and were dried with nitrogen. The silicon wafers were fixed on a grounded substrate holding device situated at a distance of approximately 15 cm from the ion source. During deposition, no substrate bias was used. Films were deposited in three ways: in static mode, by oscillation with an amplitude of 9 cm, and by rotation around the vertical axis of the grounded plate from the substrate-holder. The diameter of this plate is 56 cm whereas the samples were fixed at a diameter of 40 cm on vertical columns. The movement was in all cases one-dimensional and orthogonal to the plasma-beams of the linear anode layer source. Substrate temperature was monitored with an electrically insulated K-type thermocouple installed at the backside of the substrate holder. Prior to deposition, the substrates were plasma-cleaned from residual surface contaminants with the use of the anode layer source operated at a voltage of 2 kV and an argon (nominal purity <99.999 %) flow rate of 20 sccm through the ion gun, resulting in a power density of 2.8 Wcm^{-1}. For deposition the chamber was evacuated to a base pressure of $5 \cdot 10^{-5}$ mbar. Discharge voltages in the range of 1 to 3 kV between anode and cathode of the ion gun were used for deposition with acetylene. These discharge voltages correspond to ion energies between 450 to 750 eV [7].

2.2. FILM THICKNESS AND STRESS

Thickness and internal stress of the films were determined using a mechanical stylus profilometer Form Talysurf Series 2 from Taylor Hobson Ltd. (Leicester, GB). Prior to the deposition, parts of the sample were covered by a mask to get locally uncoated areas. Film thickness was obtained by measuring step-size at the edges between coated and uncoated areas. For stress measurements, the used wafers were checked prior to deposition for flatness. During deposition, these samples were fixed only on one end so that the wafer could follow the applied stress of the growing DLC film. Care was taken to avoid possible coating of these samples at the backside. After deposition, the curvature on the silicon wafers was measured with a stylus force of 1 mN. The stress in the films was calculated using the Stoney equation [8].

2.3. RAMAN SPECTROSCOPY

The film structure was characterised by using a LabRam-HR 800 Raman micro-spectrometer from Jobin Yvon (Villeneuve d'Ascq, France). Lasers with excitation wavelength of 325, 532 and 633 nm were used at constant

room temperature with an Olympus 40× (for 325 nm) and an Olympus 100× objective (for 532 and 633 nm). The power of the laser was kept in all cases well below 0.25 mW at the sample in order to avoid possible film damage caused by light absorption and subsequent annealing of the films. The entrance slit to the spectrometer was set to 100 µm. Light was dispersed by holographic gratings with 1800 grooves mm^{-1} (532 and 633 nm) and 2400 grooves mm^{-1} (325 nm). The spectral resolution of the instrument was about 0.6 cm^{-1}. The dispersed light was collected with a 2048×512 back illuminated low noise UV CCD detector. During analysis, the spectrometer was checked for correct wavenumber calibration by periodic measurement of a standard (100) orientated silicon wafer with a Si-peak position of 521.3±0.6 cm^{-1}. The spectrum fitting was performed using "Peak-Fit" 4.11 from Systat (Point Richmond, CA, USA) using two Gaussian functions together with a linear base line correction. The I_D/I_G ratios being a measure for the sp^2 binding content of DLC coatings were calculated using the peak amplitudes from the D-and G-lines, where the G-peak results from the bond stretching of all pairs of sp^2 sites in rings and chains; the D-peak has its origin in the breathing modes of rings [9-11].

3. RESULTS AND DISCUSSION

3.1. DEPOSITION RATE AS A FUNCTION OF THE APPLIED VOLTAGE AND ACETYLENE FLOW

DLC deposition experiments with an anode layer source were carried out at varying voltages applied to the source and at different acetylene flow rates (at constant substrate oscillation in front of the source with an amplitude of 9 cm).

Deposition of a film with an applied voltage of 1 kV at a constant acetylene flow of 20 sccm yields a deposition rate of 3.7±0.3 nm min^{-1}. Enhancement of the voltage to 2 and 3 kV results in higher deposition rates of 7.5±0.4 and 9.5±0.5 nm min^{-1}, respectively. The presented data show a clear relationship between applied voltage and deposition rate for the DLC films. The higher deposition rates with elevated voltage are interpreted as a higher degree of ionisation caused by the higher power density which increased from 0.5 Wcm^{-1} for 1 kV to 5.3 Wcm^{-1} for 3 kV. A clear relationship between the acetylene flow and grow rate was observed when increasing the flow from 10 to 30 sccm at constant applied voltage. The deposition rate increased from 4.6±0.5 to 19.2±1.0 nm min^{-1} with increasing acetylene flow. This simple relation is caused by the anode layer source's ability to decompose acetylene molecules in a linear fashion to the flow rate within the investigated area. We observed substrate temperatures of not even 70°C after depositions for several hours which show the real room-temperature capability of this technique.

3.2. RAMAN SPECTROCOPY

3.2.1. Raman band parameters as a function of the applied voltage

This work focuses on the spectral features of the D and G signals neglecting other Raman active modes present at 1100 to 1200 cm^{-1} or 1400 to 1500 cm^{-1}. Additionally, the position of the G-peak will be evaluated in detail because of its indirect relationship to variations in sp^3 bonded carbon fraction in the films.

Raman spectra recorded with an excitation wavelength of 532 nm showed a correlation of the intensity ratio I_D/I_G and the voltage applied to the anode layer source. For these experiments with a constant acetylene flow rate of 20 sccm (at constant substrate oscillation in front of the source with an amplitude of 9 cm), I_D/I_G ratios of 0.48±0.02 for a film deposited at 1 kV and 0.59±0.01 for 3 kV were observed. The position of the G-band is relatively constant at 1541±0.7 cm^{-1} when modifying the voltage. Figure 2 shows a Raman spectrum with the deconvoluted Gaussian peaks for a DLC film deposited at a voltage of 1 kV. The D- and G-bands shown in the spectrum are due to the inelastic scattering of sp^2 sites. Low sp^2 contents in films are expressed by a low intensity ratio I_D/I_G, whereas a higher ratio points to a clustering of sp^2 sites, *i.e.* the formation of aromatic rings [9-11].

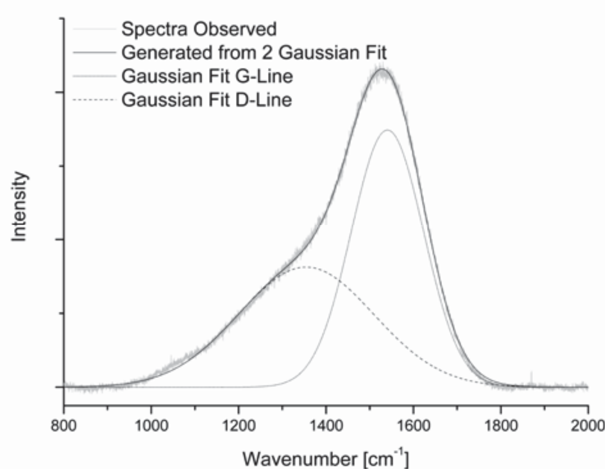

Figure 2. Raman spectra of a DLC film recorded with 532 nm. The film was deposited with an applied voltage of 1 kV at an acetylene flow rate of 20 sccm (at constant substrate oscillation in front of the source with an amplitude of 9 cm).

Comparing the spectral shape as well as the band parameters to other studies, the films show a typical spectrum of hydrogenated tetrahedral DLC. It is also known from Ferrari and Robertson [10] that for tetrahedral amorphous carbon as well as for hydrogenated amorphous carbon, where the sp^2 clustering is controlled by the sp^3 fraction, the visible Raman parameters can be used to reveal information about the sp^3-hybridisated carbon fraction of the films. For hydrogenated tetrahedral amorphous carbon, a lower intensity ratio I_D/I_G is connected with higher sp^3 content [9, 10]. From this, an increasing voltage during the experiments yields lower sp^3 content. These findings were further evidenced by the determination of stress in the films. The stress in DLC is known to increase with increasing sp^3 content [1]. The determined values of the intensity ratio I_D/I_G and the compressive stress as a function of the applied voltage are shown in Figure 3.

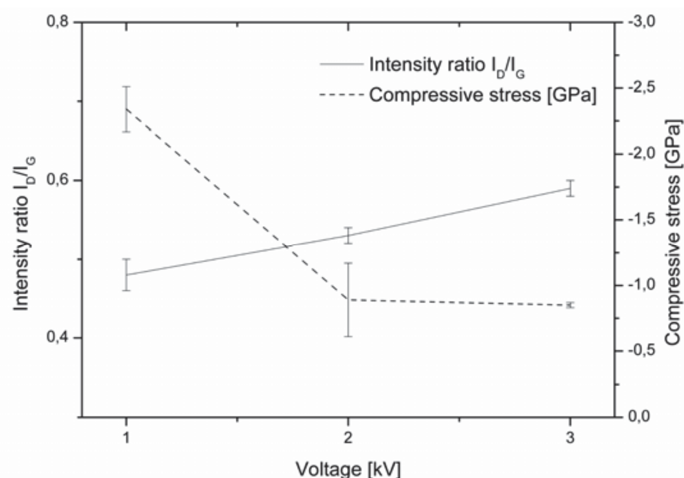

Figure 3. Intensity ratio I_D/I_G and compressive stress as a function of the applied voltage. The intensity ratio was calculated using the peak amplitude of the D- and G-line observed with 532 nm. The films were deposited with an applied voltage of 1 to 3 kV at an acetylene flow rate of 20 sccm (at constant substrate oscillation in front of the source with an amplitude of 9 cm).

The stress values are rather low but show the expected drop in compressive stress when increasing the voltage. For a voltage of 3 kV, a compressive stress of -0.85±0.02 GPa was detected, whereas the films deposited at 2 and 1 kV showed -0.89±0.28 and -2.34±0.17 GPa, respectively.

3.2.2. Dispersion of the G and D-line with excitation wavelengths

Our goal was to prove the well known peak dispersion of the D- and G-bands in the deposited DLC films with varying the laser excitation wavelengths, as reported in various articles by Ferrari and Robertson [9,10] and Robertson [1]. A hydrogenated tetrahedral amorphous carbon film, deposited by using an acetylene flow rate of 20 sccm at a voltage of 3 kV (at constant substrate oscillation in front of the source with an amplitude of 9 cm), was investigated with excitation wavelengths of 633, 532 and 325 nm (Figure 4).

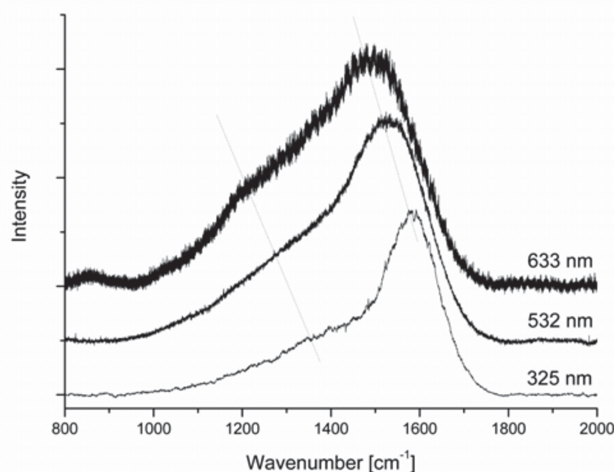

Figure 4. Dispersion of the D- and G-line for hydrogenated tetrahedral DLC. The dispersion is indicated with dotted lines. The film was deposited with an applied voltage of 3 kV at an acetylene flow rate of 20 sccm (at constant substrate oscillation in front of the source with an amplitude of 9 cm).

Dispersion of the D- and G-band for the varying excitation wavelength is indicated with dotted lines. A G-band position of ~1516 cm^{-1} was observed for the highest used wavelength of 633 nm which rises to higher wavenumbers of ~1541 cm^{-1} and ~1588 cm^{-1}, when using the green and blue excitation wavelength at 532 and 325 nm. The same trends of increasing peak position with lower excitation wavelength could also be shown for the D-line. These observations are in good agreement with the results of Ferrari and Robertson [9, 10] and Robertson [1]. It is reported that this dispersion could only occur in disordered carbon because of a range of configurations with different local band gaps and phonon modes [11] in this material. Corresponding to these

observations, Ferrari and Robertson [11] reported a resonant selection of sp^2 configurations or clusters with wider π band gaps which are the origin of this effect.

3.2.3. Lateral chemical distribution of carbon species

The lateral chemical distribution of carbon species formed during static deposition on an amplitude of 19 cm from the centre of the anode layer source was investigated. This experiment was performed by mounting 20 silicon wafers horizontally at a distance of 15 cm from the source. The film on each wafer was measured with 532 nm excitation wavelength. It is shown that at a distance of approximately 10 to 12 cm from the centre of the anode layer source, the films show a higher hydrogen concentration, which causes the increased ratio of slope/intensity of the G-line in the Raman spectrum [9] expressed as µm (Figure 5). It is known that this characteristic phenomenon of an increased ratio of slope/intensity of the G-line has its origin in an increasing photoluminescence when using a relatively high excitation wavelength of 532 nm in Raman spectroscopy [9]. Raman spectra from samples which were mounted up to a distance of 10 to 12 cm from the centre of the source indicate a hydrogen content lower than 20 at.%, which could be estimated from ratio slope/intensity of the G-line of ~0 µm (Figure 5) [9].

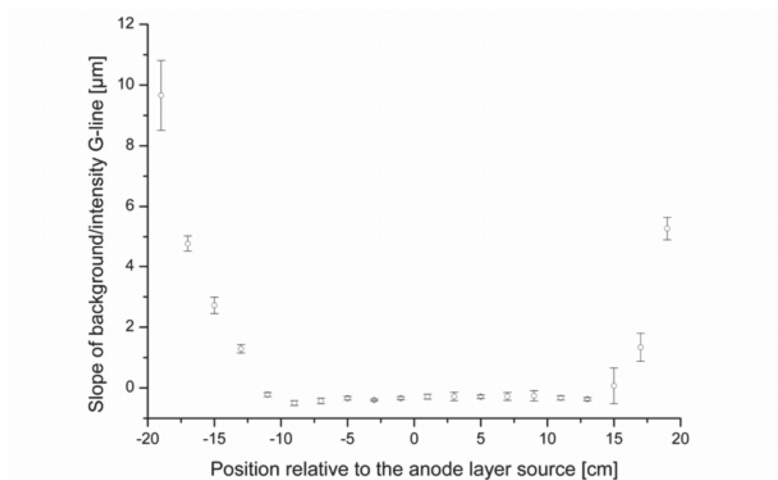

Figure 5. Ratio of the slope of the fitted linear background to the amplitude of the G-line as a function of the position relative to the centre of the anode layer source. Raman spectra of the hydrogenated tetrahedral DLC films were recorded with 532 nm. The films were deposited with an applied voltage of 3 kV at an acetylene flow rate of 20 sccm.

At both ends of the horizontally investigated area, the ratio slope/intensity of the G-line increased to ~10 µm at the highest, which demonstrates a hydrogen content higher than 20 at.% [9]. These results indicate that the anode layer source is able to decompose the acetylene molecule with growing hydrogenated tetrahedral amorphous carbon with less than 20 at.% hydrogen over a horizontal distance of 20 cm when the source is situated 15 cm away from the samples. Oscillating the samples with an amplitude of 9 cm as well as complete rotation of the substrates through the plasma beams showed in all cases Raman spectra that were similar to the spectral shape observed in the centre of the two beams from the anode layer source, as also shown in Figure 2.

4. CONCLUSIONS

We have demonstrated the unique properties of a linear, gridless anode layer source for the deposition of hydrogenated tetrahedral diamond-like carbon films. Raman spectroscopy is a powerful tool to investigate the structure of the deposited films, which can be tailored by the deposition parameters of this method. Careful analysis of the Raman band features indicate a higher fraction of sp^3 bonded carbon in the films when using a relatively low working voltage of 1 kV on the anode of the anode layer source. The major benefit of this deposition technique is the moderate substrate temperature of not even 70°C which was observed for deposition times of several hours. Moreover, we want to highlight the simple and robust working principle of the anode layer source, which enables the use of the source for plasma-cleaning of substrates as well as for deposition of DLC films for industrial applications.

ACKNOWLEDGEMENTS

Financial support of this work by the Austrian Federal Ministry of Traffic, Innovation and Technology, the Austrian Industrial Research Promotion Fund (FFG), the Government of Styria, and the European Union is highly acknowledged.

REFERENCES

[1] J. Robertson, Mater. Sci. Engin. R37 (2002) 129.

[2] T. Yokota, T. Terai, T. Kobayashi, M. Iwaki, NIM B. 242 (2005) 48.

[3] C. Lim, S. Slack, S. Ufer, E. Lindner, Pure Appl. Chem. 76 (2004) 753.

[4] A. Lagrini, S. Charvet, M. Benlahsen, C. Debiemme-Chouvy, C. Deslous, H. Cachet, Thin Solid Films. 41 (2005) 482.

[5] A.L. Morozov, Y.V. Esipchuk, A.M. Kapulkin, V.A. Smirnov, Sov. Phys. Tech. Phys. 17 (1972) 482.

[6] V.S. Veerasamy, H.A. Luten, R.H. Petrmichl, S.V. Thomsen, Thin Solid Films 442 (2004) 1.

[7] Veeco Instruments, Technical Manual to ALS340, 2003

[8] G.G. Stoney, Proc. R. Soc. Lond. Ser. A82 (1909) 172.

[9] A.C. Ferrari, J. Robertson, Phil. Trans. R. Soc. Lond. A, 362 (2004) 2477.

[10] A.C. Ferrari, J. Robertson, Phys. Rev. B, 61 (2000) 14095.

[11] A.C. Ferrari, J. Robertson, Phys. Rev. B, 64 (2001) 075414.

PUBLICATION 3:

PROPERTIES OF DLC AND NITROGEN-DOPED DLC FILMS DEPOSITED BY DC MAGNETRON SPUTTERING

Markus Kahn, Nicola Menegazzo, Boris Mizaikoff, Roswitha Berghauser, Jürgen M. Lackner, Daniel Hufnagel, Wolfgang Waldhauser

Plasma Processes Polym. 4, S1 (2007) 200.

PROPERTIES OF DLC AND NITROGEN-DOPED DLC FILMS DEPOSITED BY DC MAGNETRON SPUTTERING

Markus Kahn*[1], Nicola Menegazzo[2], Boris Mizaikoff[2], Roswitha Berghauser[1], Jürgen M. Lackner[1], Daniel Hufnagel[1], Wolfgang Waldhauser[1]

[1] Joanneum Research, Laser Center Leoben, Leobner Strasse 94, A-8712 Niklasdorf, *e-mail: markus.kahn@joanneum.at

[2] Georgia Institute of Technology, School of Chemistry and Biochemistry, Atlanta GA 30332 0400

ABSTRACT

Diamond-like carbon (a-C) and nitrogen-doped amorphous carbon (a-C:N_x) films were synthesised by direct current (DC) magnetron sputtering. Films were characterised for their chemical structure and nitrogen content by applying Raman spectroscopy and X-ray photoelectron spectroscopy (XPS). The data collected demonstrates that sputtering power densities in the range of ~ 6.7 W · cm^{-2} to ~20 W · cm^{-2} have no apparent influence on the film structure. The ratio of the intensities of the D- and G-bands (I_D/I_G) in the Raman spectra resulted in a value of 1.56±0.04 for a film deposited at power density of ~ 6.7 W · cm^{-2} indicating a high sp^3-hybridized carbon fraction at low sputtering power. Sputtering with pure nitrogen as the plasma gas resulted in a nitrogen concentration of 25.7±1.6 at.% in the film. Moreover it was shown that the total pressure in the deposition chamber ranging from 1.8 · 10^{-3} mbar to 3.5 · 10^{-3} mbar did not adversely affect the chemical structure and growth rate of the films.

KEYWORDS

Diamond-like carbon (DLC), nitrogen-doped amorphous carbon, sputtering, Raman spectroscopy

1. INTRODUCTION

Diamond-like amorphous carbon thin films are typically characterized by high hardness and wear resistance, chemical inertness, and optical transparency in the infrared region, and increased electrical conductivity upon doping with nitrogen or boron. It's remarkable properties have generated a lot of interest, resulting in the application of diamond-like amorphous carbon films to several commercial fields as protective coatings for magnetic and optical disks, wear-resistant coatings for abrasive applications and for semiconductor uses [1 and references therein]. Moreover diamond-like carbon coatings play an increasingly important role for biological and biochemical applications. Recently Yokota et. al demonstrated cell adhesion to nitrogen-doped diamond-like carbon [2] and Lim et. al reported on protein adsorption at modified amorphous carbon coatings [3]. The properties of amorphous carbon can be tailored by varying the deposition parameters. Therefore the goal of the present work is to investigate the structure and the surface quality of DC sputtered amorphous carbons and nitrogen-doped amorphous carbon with varying deposition parameters. The study focuses on the influence of sputtering power density, nitrogen content in the deposition plasma and coating pressure on the properties of the carbon based films.

2. EXPERIMENTAL

2.1. SAMPLE PREPARATION AND DEPOSITION PARAMETERS

For DC magnetron sputtering a unbalanced three inch cathode from AJA (AJA International, North Scituate, MA, USA) equipped with a high purity graphite target (nominal purity >99.999 %) (Alfa Aesar, Ward Hill, MA, USA) was used. The cathode was powered with a ten kilowatt DC power supply (Advanced Energy Industries, Fort Collins, CO, USA) in power regulation mode. Power densities between ~ 6.7 $W \cdot cm^{-2}$ and ~ 20 $W \cdot cm^{-2}$ were applied to the carbon sputtering target resulting in voltages between ~ 600 V and ~700 V. Argon 5.0 (nominal purity >99.999 % argon) and nitrogen 5.0 (nominal purity >99.999 % nitrogen) from Air Liquide (Air Liquide, Paris, France) were used as sputtering gases. Silicon wafers (111) (ON Semiconductor, Phoenix, AZ, USA) and glass plates were used as substrate materials. The samples were cleaned in an ultrasonic cleaner (Bandelin, Berlin, Germany) sequentially with acetone (Herba Chemosan, Vienna, Austria) and ethanol (Herba Chemosan, Vienna, Austria) and were dried with nitrogen. The substrates were fixed on a static, floating potential substrate holding device kept at approximately ten centimetres away from the sputtering target. The substrate temperature was consequently monitored with an electrically insulated K-type thermocouple (Jumo, Fulda, Germany) installed at the backside of the substrate holder. In order to clean the substrates from residual surface contaminants a mild plasma etching procedure was applied (using 20 $cm^3 min^{-1}$ of argon and a voltage of 600 V) with a DC bias power supply (Advanced Converters, Zielonka, Poland). For the deposition the chamber was pumped down to a base pressure of $4 \cdot 10^{-5}$ mbar. Argon and nitrogen were introduced into the vacuum chamber with varying percentages (*v/v*) resulting in pressures between $1.3 \cdot 10^{-3}$ mbar and $3.4 \cdot 10^{-3}$ mbar which correspond to a total gas flow of 20 and 65 $cm^3 \cdot min^{-1}$.

2.2. SURFACE CHARACTERISATION AND FILM THICKNESS

Contact angle measurements were performed using a fixed CCD digital camera (Philips, Amsterdam, Netherlands) equipped with a Tokina ATX objective (Tokina, Saitamo, Japan) and a one microliter pipette (Brand, Wertheim, Germany). To determine the hydrophilic character of the films distilled water was used. All measurements were done at 22 ºC at constant room humidity. Three seconds after displacement of the droplet pictures were recorded and transferred to the analysing software. Film thickness was determined with a Dektak^3 ST mechanical stylus profilometer (Veeco/Sloan Technologies, Santa Barbara, CA, USA).

2.3. CHEMICAL CHARACTERISATION

The film structure was characterised using Raman spectroscopy and X-ray photoelectron spectroscopy (XPS) on silicon wafers. Raman analysis were done with a LABRAM (ISA, Horiba Jobin Yvon, Villeneuve d'Ascq, France) spectrometer using a frequency doubled Nd-YAG laser operating at λ=532 nm. The power of the laser system was kept at 0.8mW and 8mW in order to avoid film damage. Prior to analysis, the system was internally calibrated using silicon (520 cm^{-1}), polyethylene (1062, 1128, 1169, 1295, 1487, 1439, 2848, 2881 cm^{-1}), calcite (156, 283, 713, 1087, 1437 cm^{-1}) and diamond (1332 cm^{-1}). All spectra were normalized to these positions. The spectra were collected with a 100x magnification objective. The spectrum fitting was performed on the peak fitting software 4.11 for windows (SYSTAT, Point Richmond, CA, USA) using two Gaussian functions together with a linear base line correction. The I_D/I_G ratios were calculated using the integrated peak areas from the D-and G-lines. The nitrogen content of nitrogen-doped amorphous carbon films was determined with an XPS spectrometer model SSX-100 from Surface Science Labs (Surface Science Labs, Mountain View, CA, USA) equipped with a small spot monochromatic Al K_α source (1486.6eV). General survey scans from 0 to 1100 eV (1 eV steps with a 800 µm spot size) were performed to verify the surface constituents. Additionally, high resolution scans (0.1 eV steps with a 400 µm spot size) of the carbon and nitrogen 1s photoemission peaks were recorded for the nitrogen quantification.

3. RESULTS AND DISCUSSION

3.1. GROWTH RATE AND SURFACE PROPERTIES OF CARBON BASED COATINGS

Amorphous carbon deposition experiments with a three inches DC magnetron at varying power densities were carried out. During deposition the pressure was $2.7 \cdot 10^{-3}$ mbar resulting from an argon flow of 50 cm$^3 \cdot$ min^{-1}. Sputtering with a power density of ~ 6.7 W · cm^{-2} resulted in a film growth rate of 5±1 nm · min^{-1}. In order to achieve a higher growth rate, the power density on the target was increased stepwise to ~ 20 Wcm^{-2} yielding a maximum growth rate of 16±1 nm · min^{-1}. Figure 1 depicts graphically the linear relationship between sputtering power and growth rate for the a-C films, enabling the prediction of the growth rate for power densities between ~ 6.7 W · cm^{-2} and ~ 20 W · cm^{-2}. Additionally the substrate temperature was monitored during the deposition process. For low sputtering powers, substrate temperatures of ~ 40 ºC were observed, whereas ~ 50 ºC were recorded for the highest power density for depositions yielding 100 nm thin films. The effect of the growth rate of the sputtering process in mixed argon/nitrogen deposition atmospheres were also investigated. The experiments were carried out at a nearly constant pressure of $2.7 \cdot 10^{-3}$ mbar for pure argon

and 2.0 · 10^{-3} mbar for pure nitrogen resulting from the introduction of 50 $cm^3 \cdot min^{-1}$ of plasma gas and a constant power density of ~ 11 W · cm^{-2}. The growth rates for the varying nitrogen concentration in the deposition chamber are plotted in Figure 2.

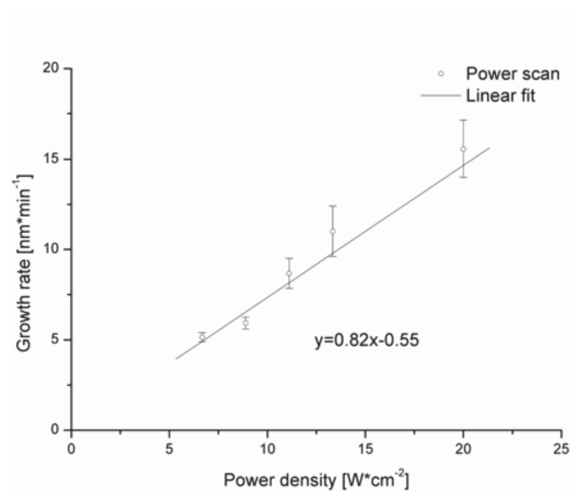

Figure 1. Change of growth rate with varying power densities applied on the carbon sputtering target.

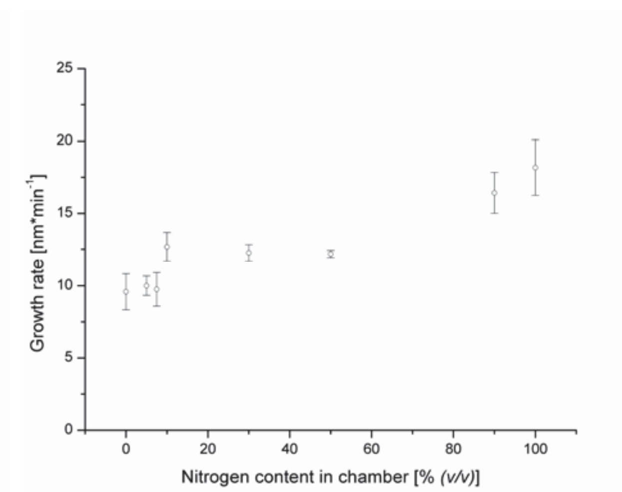

Figure 2. Change of growth rate with varying nitrogen concentration in the deposition chamber

The growth rate of the carbon based films increases with increasing nitrogen concentration in the argon/nitrogen mixture. A growth rate of 9.6±1 nm · min^{-1} was measured for the nitrogen-free layers. An increase to 13±1 nm · min^{-1} was observed upon addition of 10 % nitrogen gas to the total gas flow of 50 $cm^3 \cdot min^{-1}$. For nitrogen gas concentrations between 10 % to 50 %, the growth rate stabilized at 12±1 nm · min^{-1}, while at very high nitrogen concentration (100 %) the films show a growth rate of 18±2 nm · min^{-1}. It is postulated that one reason for the observed accelerated growth with nitrogen as plasma gas is an increase in disordered carbon in the films [4]. From this discussion it could be derived that an increase in disordered carbon results in a decrease of the density of the material deposited. Additionally it is known that a sputtering gas with an atomic mass, which is very close to the atomic mass of the target material, will increase the sputtering yield [5,6]. A total pressure scan with argon as plasma gas at constant sputtering power density (~ 20 W · cm^{-2}) revealed no relevant influence on the growth rate for the a-C carbon films. Introducing 20 $cm^3 \cdot min^{-1}$ of argon in the chamber resulted in a growth rate of 15±0.3 nm · min^{-1}. Increasing the argon flow rates to 30 $cm^3 \cdot min^{-1}$ and 50 $cm^3 \cdot min^{-1}$ resulted in nearly identical growth rates of 14±0.3 nm · min^{-1} and 16±1 nm · min^{-1}, respectively. We also observed no significant changes in growth rate when a maximum amount of 65 $cm^3 \cdot min^{-1}$ of argon was used for sputtering. The surface quality of the films was characterized further since it's homogeneity will have a direct impact on the utilization the films to commercial products. The thin films were found to be dense and well adherent on silicon wafers and glass substrates without pin holes. Water contact angle measurements on the as-deposited films indicate a difference in hydrophilic character of nitrogen-doped and nitrogen-free films. Analysis of a freshly deposited DLC film surface sputtered with a power density of ~11 W · cm^{-2} results in a contact angle for water of θ=49±1° in contrast to a contact angle of θ=43±2° for a nitrogen-doped layer sputtered in a 5 % nitrogen/argon mixed atmosphere at a total gas flow of 50 $cm^3 \cdot min^{-1}$. When using nitrogen as additional sputtering gas the hydrophilicity of the surface is further increased resulting in a lower water contact angle. Chen et. al reported on a similar change in

hydrophilic properties upon doping of amorphous carbon with nitrogen and has been attributed to the formation of carbon-nitrogen bonds [7]. Finally, the stability of the surface with time was determined. The as-deposited samples were stored in the atmosphere and in a dessicator filled with silica. Approximately sixty minutes after deposition the water contact angle was increased to θ=65±2º for the nitrogen-free films. The same behaviour was observed for the nitrogen-doped film where θ=61±2º after one hour of exposure to the atmosphere. Slightly lower values for the contact angle were observed for the samples which were stored in the dessicator revealing θ=60±1º for the nitrogen-free layer and θ=49±1º for the nitrogen-doped layer. Additional storage (at atmosphere) of the samples showed that the water contact angle further increased after three hours to θ=73±1º for the nitrogen-free layer and θ=63±1º for the nitrogen-doped amorphous carbon layer showing a significant loss in hydrophilic properties of the films. After ~ 24 hours similar water contact angles were observed for both samples. However, we cannot verify this behaviour at the moment but future studies will answer these questions.

3.2. CHEMICAL PROPERTIES

Depending upon the ratio of sp^2 (graphitelike) to sp^3 (diamondlike) the physical properties of amorphous carbon layers can vary significantly. The spectra of amorphous carbon obtain via visible Raman spectroscopy corresponds to the ordering of sp^2 clusters. The fraction of sp^3-hybridized carbon atoms may only be derived indirectly by careful analysis of the sp^2-carbon spectral features. The Raman spectrum of amorphous carbon is typically composed of a band at approximately 1550 cm^{-1} (G-band) and a band at approximately 1355 cm^{-1} (D-band). The two bands can be deconvoluted in several ways [8,9,10], with Gaussian fits being amongst the most popular. Detailed analysis of the peak positions, the full width at half maximum and the integrated intensity ratio of the disordered and graphite bands (I_D/I_G) gives information about the composition of the amorphous carbon films [11,12]. Comparison of the nitrogen doped amorphous carbon with the nitrogen-free layers reveals that a general decrease in sp^3 content is observed with increasing nitrogen content. It has been reported that upon substitution of carbon with nitrogen, the long-range order of graphite structure is broken and the clustering of sp^2 sites is promoted [13,14]. It is also reported that the vibration frequencies of nitrogen-doped amorphous carbon lie close to the modes of their nitrogen free analogues [15,16,17]. Therefore it is difficult to distinguish between C–C and C–N modes. Alternatively it enables the analysis of the trends for the D- and G-bands in a similar fashion to the nitrogen free samples [18]. Figure 3a shows at typical Raman spectra with the deconvoluted Gaussian peaks for an amorphous carbon sputtered at a power density of ~ 20 $W \cdot cm^{-2}$ using 50 $cm^3 \cdot min^{-1}$ of argon. Analysis of the Raman spectra recorded for amorphous carbon films deposited with power densities between ~ 6.7 $W \cdot cm^{-2}$ and ~ 20 $W \cdot cm^{-2}$ did not reveal a significant change in the intensity ratio I_D/I_G (Figure 3b).

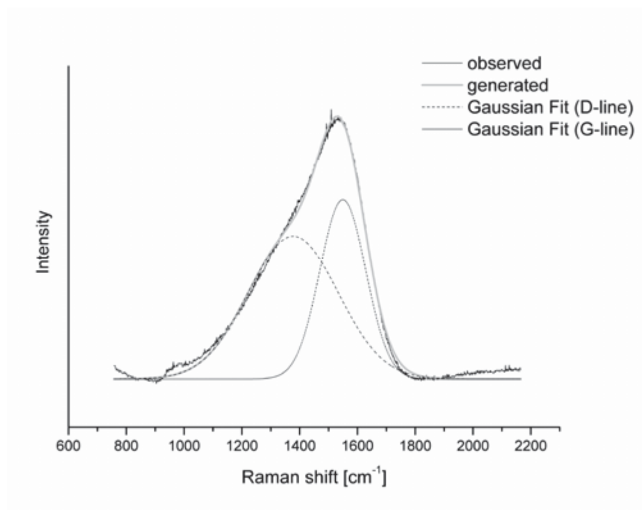

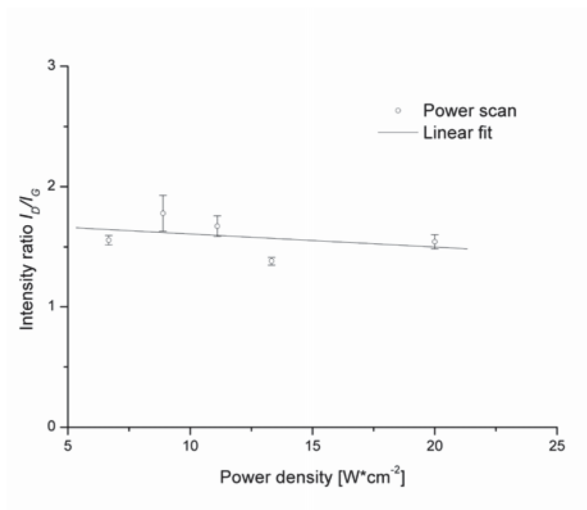

Figure 3a. Raman spectra were fitted into two Gaussian peaks together with linear base line correction.

Figure 3b. Change of intensity ratio I_D/I_G with varying power densities.

The full width at half maximum and the peak positions for D- and G-bands also did not change substantially in the sputtering power range mentioned. Zeng et. al reported I_D/I_G ratios between ~ 2 and ~ 2.5 for sputtering power densities of approximately 10 and 17 W · cm^{-2}, respectively [19]. For comparison, I_D/I_G ratios between 1.38±0.03 and 1.77±0.15 were observed in approximately the same power density range. Zeng et. also reported on a sharp decrease in I_D/I_G at sputtering power densities above 17 W · cm^{-2}. The lower I_D/I_G ratio, caused by a decreased intensity of the D-band, suggests high sp^3 content in the DLC films [17]. In addition, the argon flow rate was changed to 30 cm^3 · min^{-1} and to 65 cm^3 · min^{-1}, resulting in I_D/I_G ratios of 1.62±0.3 and 1.61±0.1, respectively (power density was ~20 W · cm^{-2}). No significant changes in the peak positions provided further evidence that the argon flow rate does not appear to affect the structure of DC sputtered amorphous carbon films. The Raman spectra obtained for a-C and a-C:N$_x$ films deposited at constant pressure and constant power density showed a significant increase of the intensity ratio I_D/I_G with increasing nitrogen content in the chamber (Figure 4).

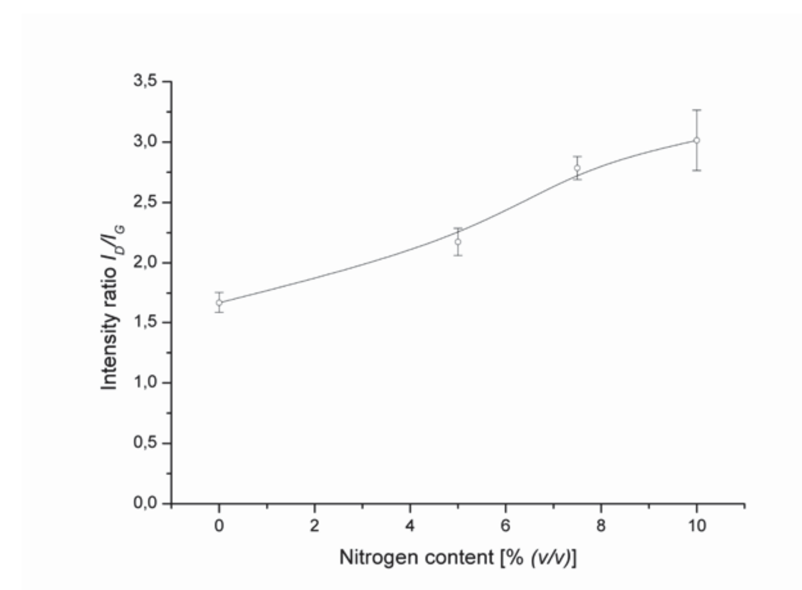

Figure 4. Change of intensity ratio I_D/I_G with varying nitrogen content in the deposition chamber. Raman spectra were fitted into two Gaussian peaks together with linear base line correction.

As was mentioned previously, this behaviour indicates that the incorporation of nitrogen induces an increase and clustering of sp^2 sites [14]. However, the position of the G-band to higher frequency was not observed with increasing nitrogen content in the chamber up to a concentration of 10 %. Finally the nitrogen incorporation efficiency in amorphous carbon was investigated at constant power density and total pressure. For these studies, X-ray photoelectron spectroscopy (XPS) was employed to determine the nitrogen concentration in the nitrogen-doped amorphous carbon films. Figure 5 shows schematically the changes in nitrogen concentrations in the layers with changing nitrogen content in the deposition atmosphere.

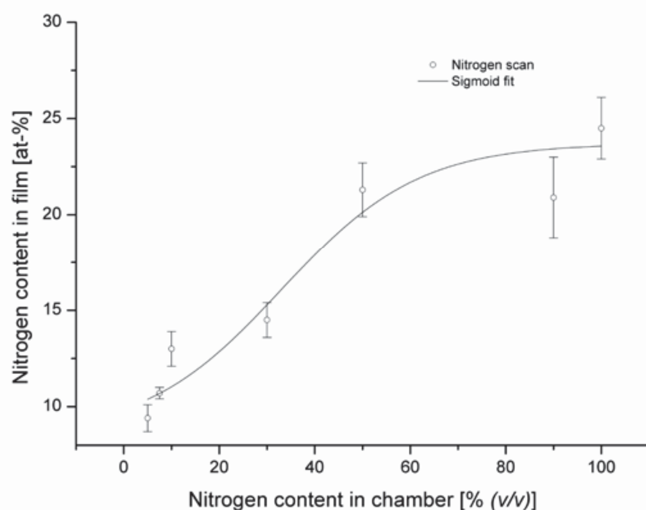

Figure 5. Authentic nitrogen concentration (determined by XPS) in nitrogen-doped amorphous carbon films as a function of varying nitrogen concentration in the deposition chamber.

Introducing a mixture of 5 % nitrogen in argon resulted in a nitrogen concentration of 8.6±0.7 at.% in the film. A six-fold increase in nitrogen (30 %) in the deposition chamber results in double the nitrogen incorporation (14.4±0.9 at.%). Sputtering in pure nitrogen revealed only a concentration of 25.7±1.6 at.%. The data indicates a sigmoid shape like incorporation efficiency for nitrogen when using DC magnetron sputtering for growing nitrogen-doped amorphous carbon films.

4. CONCLUSIONS

It was demonstrated that amorphous carbon and nitrogen-doped amorphous carbon films can be deposited with DC magnetron sputtering at low power density while still providing high sp^3 content and unique properties. In order to detect the efficiency of nitrogen incorporation in amorphous carbon XPS was employed. The data suggests a sigmoidal behaviour for the incorporation of nitrogen in the films with concentrations of nitrogen up to 25.7±1.6 at.% in the film sputtered in a pure nitrogen atmosphere. Additionally, the growth rate of amorphous carbon films as a function of nitrogen content in the deposition chamber was established.

ACKNOWLEDGEMENTS

Financial support of this work by the Austrian Federal Ministry of Traffic, Innovation and Technology, the Austrian Industrial Research Promotion Fund (FFG), the Government of Styria, and the European Union is highly acknowledged.

REFERENCES

[1] N.H. Cho et. al, *J. Mater. Res.* **1990**, *5*, 2543.

[2] T. Yokota, T. Terai, T. Kobayashi, M. Iwaki, *NIM B*, **2005**, *242*, 48.

[3] C. Lim, S. Slack, S. Ufer, E. Lindner, *Pure Appl. Chem.* **2004**, *76*, 753.

[4] A. Lagrini, S. Charvet, M. Benlahsen, C. Debiemme-Chouvy, C. Deslous, H. Cachet, *Thin Solid Films.* **2005**, *41*, 482.

[5] *"Oberflächen- und Dünnschicht-Technologie, Teil 1: Beschichtung von Oberflächen",* R.A. Haefer, Springer, Berlin 1987.

[6] *"Deposition Technologies for Films and Coatings",* R. F. Bunshah (ed), Noyes Publications, Park Ridge 1982.

[7] L.Y. Chen, F.C.N. Hong, *Diamond Relat. Mater.* **2003**, *12*, 968.

[8] S. Zhang, B. Wang, J.Y. Tang, *Surf. Eng.* **1997**, *13*, 303.

[9] M. Yoshikawa, *Mater. Sci. Forum.* **1989**, *5253*, 365.

[10] S.F. Yoon, J. Rusli, J. Ahn, Q. Zang, Y.S. Wu, H. Yang, *Diamond Relat. Mater*. **1998**. *7*, 1213.

[11] D. Beeman, J. Silverman, R. Lynds, M.R. Anderson*, Phys. Rev. B*, **1984**, *30*, 870.

[12] F. Tunistra, J.L. Koenig, *J. Chem. Phys.* **1970**, *53*, 1126.

[13] M. Lejeune, O. Durand-Drouhin, S. Charvet, A. Grosman, C. Ortega, M. Behnlahsen, *Thin Solid Films*, **2003**, *444*, 1.

[14] A.C. Ferrari, S.E. Rodil, J. Robertson, *Phys. Rev. B*, **2003**, *67*, 155306.

[15] *"Characteristic Raman frequencies of organic molecules",* F.R. Dollish, W.G. Fateley, F.F. Bentley, Wiley, Berlin 1974.

[16] *"Physical methods in heterocyclic chemistry",* A.R. Katkritzki (ed), 1963.

[17] *"Physical methods in heterocyclic chemistry",* A.R. Katkritzki (ed), 1971.

[18] A.C. Ferrari, J. Robertson, *Phil. Trans. R. Soc. Lond. A*, **2004**, *362*, 2477.

[19] A. Zeng, E. Lui, S. Zhang, S.N. Tan, P. Hing, I.F. Annergren, J. Gao, *Thin Solid Films*, **2003**, *426*, 258.

PUBLICATION 4:

DLC FILMS DEPOSITED AT ROOM TEMPERATURE BY REACTIVE MAGNETRON SPUTTERING AND BY AN ANODE LAYER SOURCE – A COMPARATIVE STUDY

M. Kahn, M. Čekada, T. Schöberl, H. Parizek, B. Raninger, R. Berghauser, W. Waldhauser, E. Brandstätter

Proceedings of the 17th Plansee Seminar 2009, Vol 2, HM 40/1

DLC FILMS DEPOSITED AT ROOM TEMPERATURE BY REACTIVE MAGNETRON SPUTTERING AND BY AN ANODE LAYER SOURCE – A COMPARATIVE STUDY

M. Kahn[*], M. Čekada[**], T. Schöberl[***], H. Parizek[*], B. Raninger[*], R. Berghauser[*], W. Waldhauser[*], E. Brandstätter[*]

[*] Joanneum Research Forschungsgesellschaft, Laser Center Leoben, Leobner Strasse 94,

8712 Niklasdorf, Austria

[**] Jožef Stefan Institute, Department of Thin Films and Surfaces, Jamova 39, 1000 Ljubljana,

Slovenia

[***] Erich Schmid Institute of Materials Science of the Austrian Academy of Sciences, Jahnstrasse 12, 8700 Leoben, Austria

ABSTRACT

We report on the structural, mechanical and surface properties of diamond-like carbon films (DLC) deposited by employing reactive pulsed DC magnetron sputtering of graphite in argon/acetylene atmosphere and by the use of a special ion gun working with acetylene as carbon precursor. The goal of this study was to work out and discuss the most promising advantages of the two named DLC deposition techniques, in order to cover the needs for practical applications of these films. It was found, that the ion beam process using the anode layer source allows the deposition of defect-free films with high hardness (36±1 GPa) and reduced elastic modulus values (180±4 GPa). However, the disadvantage of this method is the very low deposition rate of the coatings of ~4 - 10 nm · min^{-1}. Sputtering is the favoured process when higher deposition rates as well as not completely defect-free films are necessary. A highest hardness of 23.3±0.3 GPa and a reduced elastic modulus of 161±4 GPa were found for the sputtered films. Deposition rates of a-C:H coatings could be tuned up to ~33 nm · min^{-1} for the sputtering processes. Film properties could be mainly varied by the discharge voltage when using the anode layer source or by adjustment of the acetylene/argon-ratio and the bias voltage during sputter deposition. Sputtered a-C:H films with a higher overall sp^3 binding content (C–C, C–H) show lower diamond-like character (less disordering), whereas films deposited with the anode layer source show a higher overall sp^3 content and thus higher diamond-like character. In general, the films deposited by the anode layer source were found to be ultra-smooth which was derived from an averaged roughness of the film surfaces of down to ~0.1 nm, whereas the sputtered films showed minimum roughness values of ~1 nm.

KEYWORDS

Diamond-like carbon (DLC), linear ion beam source, mechanical properties, Raman spectroscopy, reactive magnetron sputtering, residual stress, surface energy

1. INTRODUCTION

Diamond-like carbon (DLC) is an amorphous, metastable form of carbon in sp^2 and sp^3 hybridisation. Since DLC films have superior properties with a unique combination of high hardness, good thermal conductivity, low friction coefficients, excellent wear resistance, ultra-smoothness and chemical inertness [1,2], the films have found a wide range of applications. DLC films are used for example as protective coatings on magnetic hard discs and on engineering components as wear resistant coatings, or as reported in recent years, as biocompatible or barrier coatings [1-6].

DLC films can be deposited by pulsed laser deposition, sputtering, chemical vapour deposition and filtered cathodic vacuum arcs [2]. Each of the deposition techniques named has its advantages but several disadvantages like a high defect density in the deposited films or a too high process temperature which limits the field of applications of the coatings. For example, the application of DLC films as barrier coatings requires absolutely defect-free films. In particular, pulsed laser deposition shows a high defect density in the grown films. Micro particles and droplets emitted from the target can hit the substrate, generating defects in the growing DLC coating. Deposition techniques, which use gaseous carbon containing precursors for film growth like chemical vapour deposition as well as ion beam methods, have the great advantage of growing basically defect-free films. However, the combination of techniques and clever use of the unique advantages of each coating process can be satisfactory in practical applications. Therefore, the focus of the present study was to find out the most promising advantages of films deposited by an ion beam deposition process working with acetylene as precursor gas and of films deposited by reactive magnetron sputtering of carbon in argon/acetylene atmosphere.

In this work, we applied a linear ion beam source of the anode layer type and a pulsed DC magnetron cathode equipped with a graphite target for DLC deposition. The anode layer thruster has its origin in the acceleration of electrons from the cathode to the anode, increasing the electron temperature, which results in a sharp decrease in plasma potential, so that the ion generation and acceleration takes place in the form of a thin layer near the anode, giving the source its name - anode layer source [7]. In thin film technology, anode layer sources are used for substrate pre-treatment via argon or oxygen plasma cleaning. Such a source can also be fed with hydrocarbon gases to deposit DLC films [7,8]. Sputtering is widely used due to advantages like low cost, simplicity and control of the process and film homogeneity. These films can vary from diamond-like structures to graphite-like dominated structures, having a high amount of sp^2 bonds in the DLC matrix [2]. The desired properties of the films can be varied by careful adjustment of the process parameters: deposition pressure, sputtering and reactive gas flow, sputtering power and bias voltage [2].

2. EXPERIMENTAL DETAILS

2.1. FILM DEPOSITION

For ion beam deposition of DLC films, an ALS340L anode layer source from Veeco Instruments (Woodbury, NY, USA) was fed with acetylene (C_2H_2, nominal purity >99.96 %). The gas was directly introduced into the

discharge channel. Discharge voltages ranging from 1 to 3 kV were applied to the anode, providing ion energies of roughly 450 to 750 eV [10].

For deposition of quasi non-hydrogenated (a-C) and hydrogenated amorphous carbon films (a-C:H), an balanced industrial-sized magnetron cathode from AJA (Type: ST-30; AJA International, North Scituate, MA, USA) was equipped with a graphite target (target dimensions: 432 × 74 mm × 7 mm^3; nominal purity >99.95 %). A power density of ~10 Wcm^{-2} was applied on the carbon target for all depositions. The pulsing unit was set to 80 kHz, where a reverse voltage of 15 % with a reverse time of 1 µs was used. For deposition of a-C:H films, C_2H_2 was introduced into the coating chamber together with argon (Ar) (nominal purity >99.999 %) resulting in C_2H_2/Ar ratios from 0 to 0.43. For deposition of the a-C coatings, an Ar flow of 30 sccm was used.

Boron-doped silicon wafers (100) with a thickness of 525±25 µm were used as substrates. The wafers were fixed to a grounded substrate holding carrousel situated at a distance of approximately 10 cm from the sputtering source and 15 cm from the anode layer source. The diameter of this carrousel was 56 cm whereas the samples were fixed at a diameter of 40 cm on vertical columns. In order to study the influence of substrate bias during sputtering, a Heiden (Pürgen, Germany) bias power supply was connected to the carrousel. Films were deposited by oscillation of the carrousel with an amplitude of 9 cm (left-right) symmetrically through the sputtering and ion gun plasma. The movement was in all cases one-dimensional and perpendicular to the longitudinal axis of the magnetron cathode and the anode layer source. The substrate temperature was monitored by an electrically insulated K-type thermocouple installed at the backside of the substrate holder.

For plasma cleaning of the wafers prior to deposition, the anode layer source was operated at a voltage of 2 kV and an Ar flow rate of 20 sccm. For all depositions, the chamber was evacuated to a base pressure of $\leq 5 \cdot 10^{-5}$ mbar. During deposition and plasma etching, the pressure in the chamber ranged from $1 \cdot 10^{-3}$ mbar to $7 \cdot 10^{-3}$ mbar. The substrate temperature did not exceed 80 °C for the sputtering processes and 70 °C for the ion beam processes.

2.2. FILM CHARACTERISATION

Thickness and internal stress of the films were determined using a stylus profilometer Form Talysurf Series 2 from Taylor Hobson Ltd. (Leicester, GB). For stress measurements, the wafers in use were checked for flatness prior to deposition. After deposition of ~200 nm thick films, the resulting curvature of the silicon wafers was measured with a stylus force of 1 mN. The stress in the films was calculated using the modified Stoney equation [11].

On films with a thickness of ~200 nm deposited by applying the anode layer source, nanoindentation measurements were carried out on a Hysitron Triboscope (Hysitron Inc., Minneapolis, MN, USA) using a cube-corner indenter with a tip radius < 50 nm. Quantitative hardness and reduced modulus values were determined from the unloading part of the load-displacement curves, applying the method introduced by Oliver and Pharr [12]. The reduced modulus takes into account the deformation of the indenter tip and the lateral

deformation of the sample material via its Poisson's ratio [12]. Effects like the influence from the substrate [13] and indentation size effect [14,15] were excluded by a careful choice of the indentation depth. The hardness and the reduced modulus of the films deposited by pulsed reactive magnetron sputtering were determined with an instrumented depth sensing indenter without atomic force microscopy (AFM) attachment equipped with a Berkovich three sided pyramidal diamond indenter. The surface roughness was determined by AFM using an ultra-sharp, high-aspect ratio tip in tapping mode with a scan size of 5×5 µm.

A Raman microspectrometer from Jobin-Yvon (Villeneuve d'Ascq, France) was used to characterize the hybridization of carbon atoms in the DLC films. The instrument was operated with a laser working at an excitation wavelength of 532 nm. An Olympus 100× objective was used to focus the beam on the sample, where in all cases the power of the laser was kept well below 0.25 mW. The entrance slit to the spectrometer was set to 100 µm and a holographic grating with 1800 grooves mm^{-1} was used. A standard (100) orientated silicon wafer with a Si-peak position of 520 cm^{-1} was used as drift standard. A resolution of ~0.3 cm^{-1} could be achieved with the spectrometer. Mathematical spectrum fitting for the D and G-bands with Gaussian functions was performed with "Peak-Fit" 4.11 from Systat (Point Richmond, CA, USA). Additionally, Raman spectra of films deposited at the lowest ion energy applying the ion beam process were fitted with a Breit-Wigner-Fano function (BWF) for the G-band and a Lorentzian for the D-band. The G-band in Raman spectra from amorphous carbon phases taken at visible excitation has its origin in the effect of bond stretching of all carbon atoms in sp^2 hybridisation in rings and chains. The D-band occurs from the breathing mode of carbon atom rings [16-18]. I_D/I_G ratios were calculated by using peak heights.

Surface energy of the deposited films was determined by the sessile droplet method [19,20] using droplets of 2 µl of water (18.2 $M\Omega cm^{-1}$), ethylenglycole (≥99.98 %), bromnaphtaline (≥95 %) and diiodomethane (≥98 %). All measurements were carried at 22 ºC at constant room humidity of ~30 %.

3. RESULTS AND DISCUSSION

3.1. GENERAL FILM PROPERTIES

For the anode layer source process increased deposition rates with increased discharge voltages from 1 to 3 kV were noticed. A deposition rate of ~4 nm min^{-1} was found for 1 kV and ~10 nm min^{-1} for 3 kV when using a C_2H_2 flow of 20 sccm.

An important advantage of the ion beam deposition process is the low temperature of the substrates of less than 70 °C after runs for several hours with the highest possible discharge voltage of 3 kV. Depositions at 1 kV discharge voltage showed an equilibrium substrate temperature of less than 40 °C. Hence, this technique of depositing DLC films is very versatile and can be applied on temperature-sensitive substrates as well. Another advantage is the smooth and defect-free DLC surface obtained. However, also the arising temperatures during sputtering were found to be not exceeding 80 °C. Therefore, in our case also balanced magnetron sputtering is applicable on temperature-sensitive substrates.

AFM studies on films deposited by employing the anode layer source showed a roughness of the DLC surfaces of down to ~0.1 nm. This roughness is comparable to those films applied in semiconductor industry, where DLC layers with thicknesses as low as 1 nm are used for protective coatings on data storage materials, deposited by ion source technology [1].

Deposition rates of sputtering processes were found to be generally remarkable higher compared to those obtained by the anode layer source process. Sputtering in pure argon showed a deposition rate of ~21 nm min^{-1} which could be linearly increased to 33 nm min^{-1} when increasing the C_2H_2/Ar-rate from 0 to 0.43. Applied bias voltages of up to -100 V did not adversely affect the deposition rate, when using Ar as process gas only. Here it has to be noted that substrate manipulation was similar for ion beam and sputtering processes. Therefore, direct comparison of data is possible.

AFM studies of the films deposited by applying pulsed DC magnetron sputtering showed roughness values between ~0.9 and ~1.4 nm. However, since sputtering of graphite can result in the generation of defects, which originate from the solid target, a limited number of spikes in the AFM image were found. We were able to prevent arcing and particle emission from the porous target by pulsing the magnetron discharge in the kHz range. Therefore, the defect density was reduced significantly in the investigated films presented here compared to films which were deposited by the use of conventional DC sputtering. From the measured data no dependence between process conditions and roughness values could be identified.

Surface energy measurements revealed average values in the range of 46 mN m^{-1} for films deposited by magnetron sputtering. The polar component did not exceed 2.5 mN m^{-1}. Therefore, the surface energy showed high dispersive character. The measured values agree well to literature, and were found to be typical for a-C:H coatings [2]. Focusing on the wettability only, the contact angles for water were ~80° for films deposited by using C_2H_2/Ar-ratios between 0 and 0.43 during sputtering. Additional biasing of the substrates during deposition with -100 V showed increased contact angles of ~90° for our films. To our knowledge the influence of bias voltage on the water contact angle is not yet reported in literature. Usually it is reported, that a-C:H has a water contact angle of 55 to 70° and was found to be independent of bias voltage [2]. The surface energy measurements on films deposited by applying the anode layer source revealed average values in the range of 41 mN m^{-1}, where the polar component did not exceed 4.3 mN m^{-1}. Therefore, also here the surface energy showed high dispersive character for all films deposited. No dependence of process parameters on surface energy and wetting properties were found. Comparing the results to the measured values obtained for sputtered DLC coatings, a slightly lower surface energy for the ion beam deposited films is noted.

3.2. STRUCTURAL PROPERTIES

Figure 1a shows an exemplary Raman spectrum, taken from a film deposited by the anode layer source applying 20 sccm C_2H_2 at a discharge voltage of 1 kV. The bands were found to be at spectral positions of 1358±2 cm^{-1} (D-band) and 1541±1 cm^{-1} (G-band). Figure 1b shows a spectrum of a sputtered a-C film, deposited with pure Ar as sputtering gas. Here, the bands were found to be at spectral positions of 1356±8 cm^{-1} (D-band) and 1550±4 cm^{-1} (G-band).

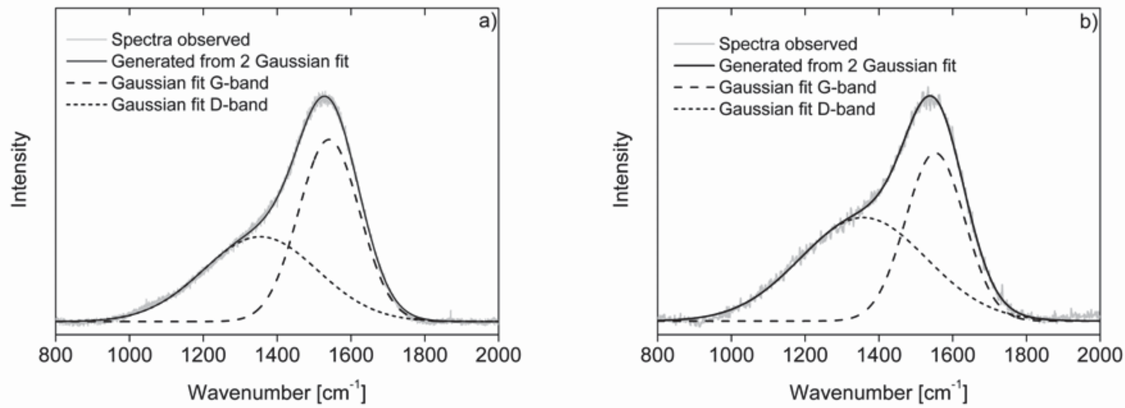

Fig. 1: **a)** Raman spectrum of an a-C:H coating deposited by using the anode layer source (20 sccm C_2H_2 at a discharge voltage of 1 kV), **b)** spectrum of a sputtered a-C coating (power density ~10 W cm^{-2} , 30 sccm Ar).

In order to describe the variations in films structure induced by different process parameters it is necessary to discuss the intensity ratio I_D/I_G, the full width at half maximum of the G-band (FWHM (G)) and the position of the G-band [16-18]. Figures 2a and 2b show the variation of the intensity ratio I_D/I_G and the FWHM (G) with varied process parameters applied during our study. The films were deposited with the anode layer source by varying the discharge voltage (ion energy varied from ~450 to ~750 eV) and by varying the C_2H_2/Ar-ratio in the coating chamber for sputter deposition.

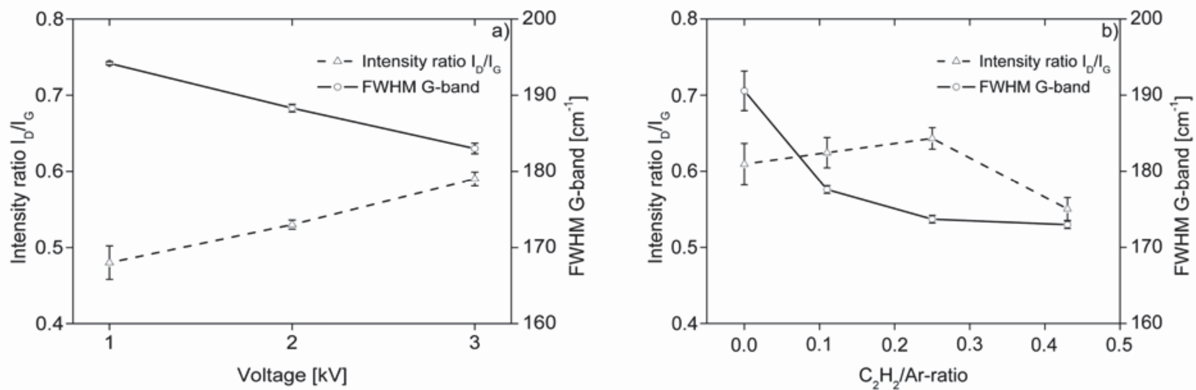

Fig. 2: **a)** Intensity ratio I_D/I_G and FWHM (G) as a function of the discharge voltage of films deposited with the anode layer source, **b)** Intensity ratio I_D/I_G and FWHM (G) as a function of the C_2H_2/Ar-ratio of sputtered films.

It was found, that film properties could be mainly varied by the discharge voltage when using the anode layer source process or by adjustment of the C_2H_2/Ar-ratio and the bias voltage during deposition of sputtered DLC films. An I_D/I_G ratio of 0.48±0.02 was calculated with peak amplitudes of the bands shown in Figure 1a. Intensities from D and G-bands taken from samples deposited at higher discharge voltages of 2 and 3 kV at similar process parameters show enhanced I_D/I_G ratios of 0.53±0.01 and 0.59±0.01, respectively. From these data, a trend of an increased clustering of sp^2 phases in rings for higher discharge voltages can be deduced for our coatings [21]. The intensity ratio I_D/I_G is a measure of the size of the sp^2 phase organized in rings [21]. If the intensity ratio I_D/I_G is low or even zero, the sp^2 phase is organised rather in chains, whereas a higher intensity ratio I_D/I_G is an indication of an increase of the sp^2 phase in aromatic rings [21].

The position of the G-band shows no significant shifts while increasing the discharge voltage and remains at a constant position of 1541±0.7 cm^{-1}. For films deposited at a discharge voltage of 1 kV, a FWHM (G) of 194±0.2 cm^{-1} was derived from the Gaussian fits, which decreases linearly to 183±0.7 cm^{-1} for a discharge voltage of 3 kV (Figure 2a). The trend of FWHM (G) shows an increased structural disorder at the lowest ion energy when using the described experimental setup. The increase in disorder can be linked to an increase in C–C sp^3 content in the material [21]. The FWHM (G) is small when sp^2 clusters are more defect-free and ordered and a higher FWHM (G) is thus indicative for an increase in disorder [21]. The high FWHM (G) of 194±0.2 cm^{-1} (fitted with a Gaussian function) and the low I_D/I_G ratio of 0.48±0.02 found for the film deposited at a discharge voltage of 1 kV suggests the classification of the deposited film to the structural class of hydrogenated tetrahedral amorphous carbon films (ta-C:H) [21]. Additional fitting of the obtained spectra with a BWF function for the G-band and a Lorentzian for the D-band showed a FWHM (G) of 249 cm^{-1} with an I_D/I_G ratio of 0.06. This allows the comparison of our measured data with results from Conway et al. [22], where I_D/I_G ratios of ~0.05 were reported for ta-C:H films.

Focusing on the structure of the pulsed DC sputtered DLC films an I_D/I_G ratio of 0.61±0.03 was calculated with peak amplitudes of the bands shown in Figure 1b. Here, the significantly higher I_D/I_G ratio compared to the films deposited with a discharge voltage of 1 kV using the anode layer source clearly identifies the sputtered films as more ordered films, having a higher amount of ring-like aromatic sp^2 hybridised carbon clusters. In fact the consideration of the high FWHM (G) together with a low I_D/I_G ratio found in the films grown with the anode layer source is indicative for higher diamond-like character there. Intensities from D and G-bands in spectra taken from samples deposited at higher C_2H_2/Ar-ratios of 0.11 to 0.25 at similar process parameters show slightly enhanced I_D/I_G ratios of 0.62±0.04 and 0.64±0.01, respectively (Figure 2b). Therefore, the size of graphitic clusters is slightly increased in this process area. Sputtering at the highest used C_2H_2/Ar-ratio of 0.43 resulted in a film structure with an I_D/I_G ratio of 0.55±0.05. Here, the FWHM (G) was found to be 173±0.5 cm^{-1}. This observed behaviour clearly identified the sputtered coatings deposited in our study as authentic a-C:H coatings, showing less disordering derived from decreased FWHM (G) while having at the same time lower I_D/I_D ratios. The finding implies that the increase in sp^3 binding content is mainly formed by C–H bonds in our deposited coatings [21]. This observation separates the sputtered films structurally from the films deposited by the anode layer source. Since with the I_D/I_G ratio one cannot distinguish between C–C and C–H sp^3 bonds, the FWHM (G) as a parameter for structural disordering has always to be taken into account when using Raman spectroscopy for structural investigations. Structurally, a-C:H films are a more highly ordered material, having a high amount of chain-like organised (C–H) clusters in its matrix [21]. Additionally, the trend of a decreased clustering of sp^2 phases in aromatic rings in the film deposited with the highest C_2H_2/Ar-ratio can be deduced for the sputtering processes [21].

3.3. CORRELATION OF STRUCTURAL WITH MECHANICAL PROPERTIES

In order to evaluate the influence of the film structure on the film properties, the mechanical properties of the coatings deposited are plotted as a function of the FWHM (G) in Figures 3a and 3b. Since the FWHM (G) is a key parameter for structural disordering in DLC films, it allows the correlation of film properties with the C–C sp^3 binding content. Figures 3a and 3b show the variation of the nanohardness and the reduced modulus as a

function of the FWHM (G) for our coatings. The distinct correlation between the mechanical properties and the trends obtained by the FWHM (G) from the Raman spectra is remarkable for films deposited by the anode layer source (Figure 3a). A higher FWHM (G) derived from the Gaussian fits is accompanied with a higher hardness, indicating an increased amount of C–C sp^3 bonds in the deposited film. Also the intensity ratio I_D/I_G is in our case directly linked to mechanical properties (Figure 3c), since for ta-C:H films the C–C sp^3 binding content is increased while having a decreased intensity ratio. A nanohardness of 36±1 GPa and a reduced modulus of 180±4 GPa are indicative for a highly disordered film deposited in our study using the lowest possible ion energy of ~450 eV [2]. From the variation in mechanical data it can be concluded that the mean ion energy in our ion beam deposition process has the most important influence on the properties of the films. The variation of nanohardness and reduced elastic modulus of sputtered films as a function of the FWHM (G) and the C_2H_2/Ar-ratio is shown in Figure 3b. It can be seen, that the variation in nanohardness and reduced modulus follows the trends derived by Raman spectroscopy (FWHM (G)). An ordering effect in the films induced by elevated C_2H_2 concentration in the process gas atmosphere as well as a higher degree of polymerisation seen in the film deposited with a C_2H_2/Ar-ratio of 0.43, showed slightly lower nanohardness and reduced modulus values. Therefore, the variation of the FWHM (G) can be directly correlated with our measured mechanical properties of the films. The values ranged from a nanohardness of 18±0.4 GPa to 15±0.2 GPa when increasing the C_2H_2/Ar-ratio in the chamber.

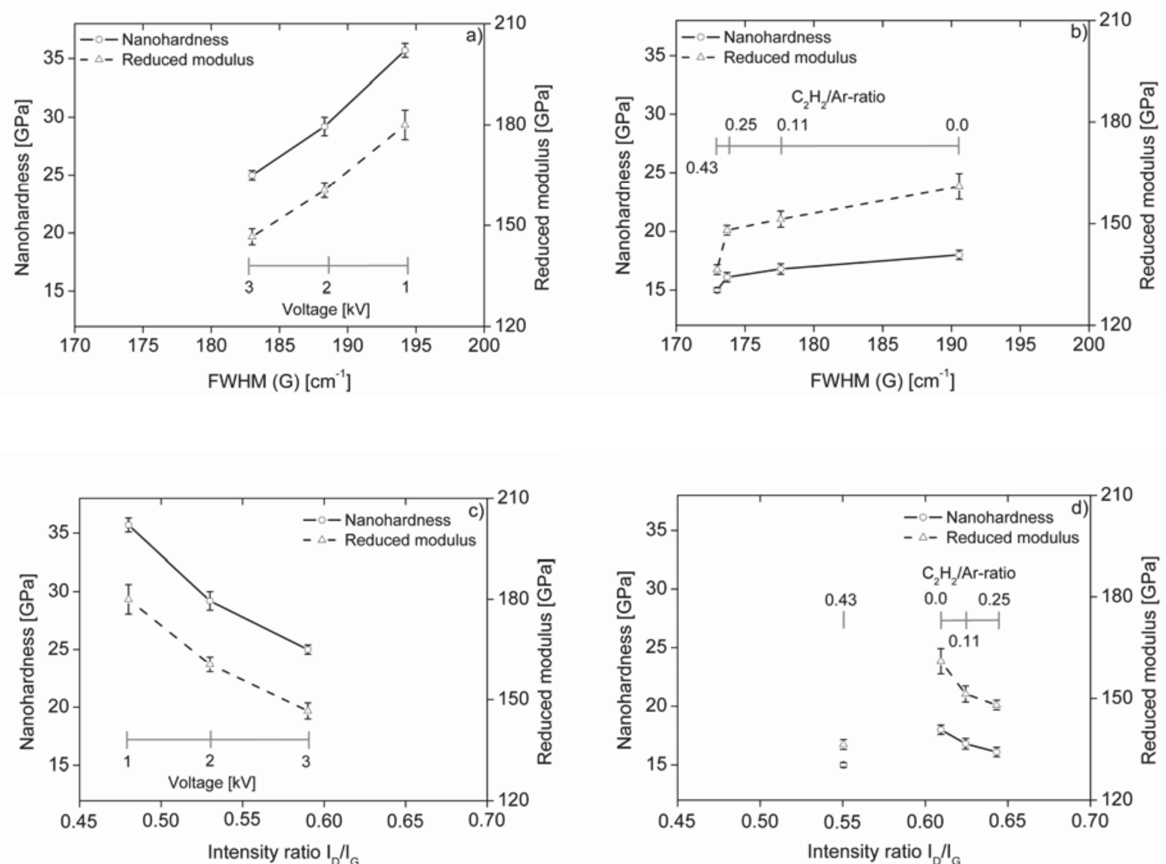

Fig. 3: Nanohardness and reduced modulus as a function of the **a)** FWHM (G) of films deposited by the anode layer source, **b)** FWHM (G) for sputtered films, **c)** intensity ratio I_D/I_G of films deposited by the anode layer source, **d)** intensity ratio I_D/I_G for sputtered films.

The correlation of the mechanical properties with the FWHM (G) and the intensity ratio I_D/I_G shows one additional interesting detail for the sputtered films (Figure 3d). Films deposited with the highest C_2H_2/Ar-ratio in the process gas atmosphere showed as already mentioned a drop in the intensity I_D/I_G ratio down to 0.55. Figure 3 d shows, that the mechanical properties are hardly influenced by a decreased intensity ratio. This behaviour is the consequence of slight polymerisation (formation of C–H bonds) of the film structure when sputtering with the highest C_2H_2/Ar-ratio.

We investigated the influence of biasing the substrates during sputter deposition, too. We found that highest hardness and reduced modulus values can be achieved with an additional applied bias voltage of -100 V. Here a hardness of 23.3±0.3 GPa and a reduced modulus of 161±4 GPa were found. It can be concluded, that the Ar bombardment induced by additional biasing helped to encourage the C–C sp^3 binding content in the film [2].

For the ion beam deposition process we also investigated the influence of mixing Ar to the process gas in order to find further improved deposition parameters. These experiments where carried out with the standard procedure of oscillating the silicon wafers with an amplitude of 9 cm through the ion beams. The total gas flow was 20 sccm and the discharge voltage for these experiments was set to 1 and 3 kV, respectively. With a mixture of 15 sccm C_2H_2 and 5 sccm Ar, an I_D/I_G ratio of ~0.60 was detected for a discharge voltage of 1 kV. A discharge voltage of 3 kV with similar conditions showed a further increased I_D/I_G ratio of ~0.80. The FWHM (G) decreased from ~190 to ~176 cm^{-1} when increasing the discharge voltage from 1 to 3 kV. Introducing mixtures of Ar and C_2H_2 into the anode layer source showed an ordering process in the DLC films. This behaviour can be interpreted as a result of the high energy ion bombardment by heavy Ar-ions during film growth in the range of ~450 to ~750 eV, reducing the disordered character and C–C sp^3 content. It can be concluded that highly disordered films can be achieved by using exclusively C_2H_2 as process gas.

Stress measurements revealed increased compressive stress values when decreasing the discharge voltage applied to the anode layer source. For a discharge voltage of 3 kV, a compressive stress of -2.4±0.2 GPa was detected for films with a thickness of ~200 nm. The stress increased to -4±0.1 GPa for the hardest film deposited at the lowest discharge voltage of 1 kV.

For the sputtered films deposited without bias support it was found, that the compressive stress decreases from -1.91±0.02 GPa to -0.61±0.02 GPa when increasing the C_2H_2/Ar-ratio from 0.11 to 0.43. The DLC film which was deposited in pure Ar atmosphere with an additional biasing of -100 V showed a high stress value of -1.89±0.01 GPa, respectively.

4. CONCLUSIONS

In the present paper we have shown that it is possible to deposit DLC coatings with promising and application relevant properties at substrate temperatures below 80 °C by employing (1) pulsed DC magnetron sputtering and (2) an ion beam technique. The most important process parameters were identified, and the structure and properties of the deposited films were investigated in detail. It was found, that during sputtering, the structure and the properties of the coatings can be tuned by adjustment of the C_2H_2/Ar-ratio process gas mixture and the

bias voltage. For the ion beam technique the discharge voltage represent the most important process parameter. DLC films deposited with 1 kV discharge voltage are so-called ta-C:H films with remarkable mechanical properties whereas films from sputter deposition can be clearly classified as authentic a-C:H coatings with lower hardness and stress values.

ACKNOWLEDGEMENTS

Financial support of this work by the Austrian Federal Ministry of Traffic, Innovation and Technology, the Austrian Industrial Research Promotion Fund (FFG), the Government of Styria, Forschung Austria and the European Union is highly acknowledged. The authors are grateful to Prof. C. Mitterer from the Department of Physical Metallurgy and Materials Testing, University of Leoben, for fruitful discussions. We would like to thank Dr. M. Roy from the Defence Metallurgical Research Laboratory in India and Dr. T. Koch and from the Institute of Materials Science and Technology, Vienna University of Technology for nanoindentation and AFM investigations of the films from sputter deposition.

REFERENCES

1. A.C. Ferrari, *Surf. Coat. Technol.* **180-181**, 190-206, (2004)

2. J. Robertson, *Mater. Sci. Eng.* **R37**, 129-281, (2002)

3. M. Janotta, D. Rudolph, A. Kueng, C. Kranz, H.S. Voraberger, W. Waldhauser, B. Mizaikoff, *Langmuir.* **20**, 8634-8640, (2004)

4. F.Z. Cui, D.J. Li, *Surf. Coat. Technol.* **131**, 481-487, (2000)

5. T. Yokota, T. Terai, T. Kobayashi, M. Iwaki, *NIM B.* **242**, 48-50, (2006)

6. C. Lim, S. Slack, S. Ufer, E. Lindner, *Pure Appl. Chem.* **76**, 753-764, (2004)

7. V.S. Veerasamy, H.A. Luten, R.H. Petrmichl, S.V. Thomsen, *Thin Solid Films*. **442**, 1-10, (2003)

8. M. Kahn, M. Cekada, R. Berghauser, W. Waldhauser, C. Bauer, C. Mitterer, E. Brandstätter. *Diamond Relat. Mater.* **17**, 1647-1651, (2008)

9. V.V. Zhurin, H.R. Kaufman, R.S. Robinson, *Plasma Sources Sci. Technol.* **8**, R1-R20, (1999)

10. Veeco Instruments, Technical Manual to ALS340, 2003.

11. G.G. Stoney, Proc. R. Soc. Lond. Ser. **A82**, 172-175, (1909)

12. W.C. Oliver, G.M. Pharr, *J. Mater. Res.* **1**, 1564-1583, (1992)

13. T. Staedler, K. Schiffmann, Surf. Sci. **482-485**, 1125-1129, (2001)

14. W.D. Nix, H. Gao, *J. Mech. Phys. Solids.* **46**, 411-425, (1998)

15. K. Durst, B. Backes, M. Göken, *Scripta Mater*. **52**, 1093-1097, (2005)

16. A.C. Ferrari, J. Robertson, *Phil. Trans. R. Soc. Lond. A*, **362**, 2477-2512, (2004)

17. A.C. Ferrari, J. Robertson, *Phys. Rev. B*, **61**, 14095-14107, (2000)

18. A.C. Ferrari, J. Robertson, *Phys. Rev. B*, **64**, 075414-075414-13, (2001)

19. D.K. Owens, R.C. Wendt, *J. Appl. Polym. Sci.* **13**, 1741-1747, (1969)

20. W. Rabel, Farbe und Lacke, **77** [10], 997-1005, (1971)

21. C. Casiraghi, A.C. Ferrari, J. Robertson, *Phys. Rev. B*, **72**, 085401-1-085401-14, (2005)

22. N.M.J. Conway, A.C. Ferrari, A.J. Flewitt, J. Robertson, W.I. Wilne, A. Tagliaferro, W. Beyer, *Diamond Relat. Mater.* **9**, 765-769, (2000)

PUBLICATION 5:

RELATION BETWEEN STRUCTURAL/TOPOLOGICAL DISORDER AND MECHANICAL PROPERTIES OF HYDROGENATED DLC FILMS

M. Kahn, S. Paskvale, M. Čekada, T. Schöberl, W. Waldhauser, C. Mitterer, E. Brandstätter

Submitted

RELATION BETWEEN STRUCTURAL/TOPOLOGICAL DISORDER AND MECHANICAL PROPERTIES OF HYDROGENATED DLC FILMS

M. Kahn[1], S. Paskvale[2], M. Čekada[2], T. Schöberl[3], W. Waldhauser[1], C. Mitterer[4], P. Pelicon[2], E. Brandstätter[1]

[1] Joanneum Research, Laser Center Leoben, Leobner Strasse 94, A-8712 Niklasdorf, Austria

[2] Jožef Stefan Institute, Jamova 39, SI-1000 Ljubljana, Slovenia

[3] Erich Schmid Institute of Materials Science of the Austrian Academy of Sciences, Jahnstrasse 12, A-8700 Leoben, Austria

[4] Department of Physical Metallurgy and Materials Testing, University of Leoben, Franz-Josef-Strasse 18, A-8700 Leoben, Austria

ABSTRACT

There is an increasing interest in the relations between Raman band parameters and mechanical properties of diamond-like carbon films. The present work describes consequently these relations in hydrogenated diamond-like carbon films (a-C:H) deposited by an ion beam source operated at varied discharge voltages, *i.e.* kinetic carbon species energies. Several highly distinct relations between Raman band parameters and mechanical properties are identified for the a-C:H films investigated: The nanohardness (H) and reduced elastic modulus (E) increase almost linearly with increasing full width at half maximum of the G-band (FWHM (G)). The film elasticity expressed as H^3/E^2 increases in an exponential fashion with increasing FWHM (G). H and E increase linearly with decreasing intensity ratio of the D-band and the G-band (I_D/I_G). H and E increase with the G-band dispersion (Disp. (G)), *i.e.* the rate of change of the G-band position with excitation energy. Hydrogen contents were found to be approximately equal and are constant at 22.2±1.2 at.% over the whole series of investigated a-C:H films.

KEYWORDS

Diamond-like carbon (DLC), elastic modulus, Elastic Recoil Detection Analysis (ERDA), hydrogen content, nanohardness, nanoindentation, Raman spectroscopy, structural disorder, topological disorder

1. INTRODUCTION

Diamond-like carbon (DLC) films present a meta-stable amorphous form of carbon with a significant amount of sp^3 hybridisation [1]. Due to the broad range of possible physical and chemical properties, structure/property relationships play an important role in DLC research. Within this regard, Raman spectroscopy is the most direct way to determine the carbon structure in all forms of carbon materials ranging from crystalline to amorphous carbon. DLC films show two prominent features in their Raman spectra, the so-called D-band around 1360 cm^{-1} and the G-band which lies around 1560 cm^{-1}. The D-band is due to the breathing modes of all sp^2 atoms in rings and the G-band is due the bond stretching of all pairs of sp^2 atoms in rings and chains [2 and references therein].

In order to describe the structure of hydrogenated diamond-like carbon films (a-C:H) it is necessary to discuss the intensity ratio of the D-band and the G-band (intensity ratio I_D/I_G), the full width at half maximum of the G-band (FWHM (G)) and the dispersion of the G-band with excitation wavelength (Disp. (G)) [2]. The intensity ratio I_D/I_G, which varies with the overall sp^3 content (Csp^3–Csp^3 + Csp^3–H1s) in a-C:H films, is almost zero for tetrahedral amorphous carbon films (ta-C) and for polymer-like amorphous carbon films (polymeric a-C:H) [2]. Since the intensity ratio I_D/I_G is a parameter which probes the amount of ring-like sp^2 clusters in a-C:H films, it enables the prediction that in ta-C and polymeric a-C:H films almost no sp^2 rings are present. The presence of hydrogen causes the overall sp^3 content of a-C:H and hydrogenated tetrahedral amorphous carbon films (ta-C:H) to be equal at 60 to 70 at.%. The hardness values of these two types of films are very different. The ta–C:H films may reach a hardness up to 50 GPa [3], whereas polymeric a-C:H films with the same overall sp^3 bonding content have a hardness of less than 10 GPa [4]. From these data, it is clear, that mechanical properties of a-C:H films cannot in general relate to the intensity ratio I_D/I_G.

The FWHM (G), as a parameter of structural disordering of sp^2 phases, has to be taken into account when a relation between Raman band parameters and mechanical properties should be found [2]. Structural disorder arises from the bond angle and bond length distortions in DLC. The FWHM (G) is small when sp^2 clusters are more defect-free and ordered, and a higher FWHM (G) is indicative of an increase in disorder. This effect originates from the higher bond length and higher bond angle in more disordered materials. Since Csp^3–Csp^3 bonds are responsible for the structural disorder in the probed sp^2 hybridisated carbon fraction of the films, this parameter is in direct relation with the Csp^3–Csp^3 bonding content.

Disp. (G) is a measure of the topological disorder [2]. Topological disorder arises from the size and shape distribution of sp^2 clusters. Samples with a sp^2 phase entirely constituted of fully π delocalised rings do not show any Disp. (G) and therefore Disp. (G) is zero. The Disp. (G) arises from the resonant selection of sp^2 chains of different sizes at different excitation energies. Highest values for Disp. (G) are around 0.35 for ta-C and polymeric a–C:H. Therefore, the Disp. (G) is proportional to the overall sp^3 content (Csp^3–Csp^3 + Csp^3–H1s) in a-C:H films. Depending on the hydrogen content, two different structural regimes can be observed for a-C:H films [2]:

(1) At hydrogen contents <25-30 at.%, the structural and topological disorder vary parallel to the amorphisation trajectory and are related to the Csp^3–Csp^3 bonding content.

(2) If the hydrogen content is >25-30 at.%, structural and topological disorder have opposite trends, meaning at higher hydrogen concentrations the overall sp^3 content can still increase but not the Csp^3−Csp^3 content. In this case, Csp^3−H1s bonds are formed to enhanced amounts in the polymeric a-C:H films.

The present work provides an insight in the structural evolution of a–C:H films deposited with varied kinetic carbon ion energies. The gained films with tailored properties were investigated by means of dual wavelength Raman spectroscopy for structural analysis, Elastic Recoil Detection Analysis (ERDA) for hydrogen content determination and nanoindentation for mechanical properties characterisation. The structure of the films is correlated with their nanomechanical properties.

2. EXPERIMENTAL DETAILS

2.1. FILM DEPOSITION

For deposition of a–C:H films, an ALS340L linear anode layer source from Veeco Instruments (Woodbury, NY, USA) was operated with 20 sccm acetylene (nominal purity >99.96%), which was flushed directly into the discharge channel. A detailed description of the ion beam source in use is given in references [5] and [6]. Discharge voltages ranging from 1 to 3 kV were applied to the anode for deposition. The discharge voltage relates in a linear fashion to the effective kinetic energy of accelerated species, being typically 25-45% of the discharge voltage. Boron doped silicon wafers (100) with a thickness of 500 µm were used as substrates. The wafers were fixed on a grounded substrate holding carrousel situated at a distance of 15 cm from the anode layer source. For plasma cleaning of the wafers prior to deposition, the ion source was operated at a discharge voltage of 2 kV with 20 sccm argon. Plasma cleaning and film deposition was carried out by oscillation of the carrousel in front of the anode layer source, providing homogeneous cleaning and films deposition over the whole substrate holder. The movement of the samples was perpendicular to the major ion beam axis of the anode layer source. For all depositions, the chamber was evacuated to a base pressure of $\leq 5\cdot10^{-5}$ mbar, whereas the process pressure was $1.3\cdot10^{-3}$ mbar. The substrate temperature ranged between 40 and 70°C.

2.2. FILM CHARACTERISATION

Two Raman micro-spectrometers from Jobin-Yvon (Villeneuve d'Ascq, France) were used to characterise the structure of carbon bonds in the DLC films. The instruments were operated with lasers at excitation wavelengths of 325 and 532 nm. Olympus 40× (for 325 nm) and 100× objectives (for 532 nm) were used to focus the beams on the sample, where in all cases the power of the laser was kept well below 0.25 mW. The entrance slit to the spectrometer was set to 100 µm. A holographic grating with 1800 grooves mm^{-1} was used for 532 nm excitation wavelength, for 325 nm excitation wavelength a grating with 2400 grooves mm^{-1} was chosen. Spectrum fitting for the Raman bands described in the introduction was carried out with symmetric Gaussian functions. Nanoindentation measurements were carried out on a Hysitron Triboscope (Hysitron Inc.,

Minneapolis, MN, USA) using a cube-corner indenter with a tip radius <50 nm. Quantitative hardness and reduced modulus values were determined from the unloading part of the load-displacement curves, applying the method introduced by Oliver and Pharr [7]. The reduced modulus takes into account the deformation of the indenter tip and the lateral deformation of the sample material via its Poisson's ratio [7]. Influence from the substrate [8] and indentation size effect [9,10] were excluded by careful choice of the indentation depth. Hydrogen contents were determined by ERDA with a 2 MV tandetron accelerator using a beam of 4.2 MeV ^{7}Li ions [11]. The beam was collimated by a 1×2 mm rectangular shaped slit placed in front of the entrance of the experimental chamber which was equipped with two silicon detectors; the Rutherford backscattering spectroscopy (RBS) detector at the scattering angle of θ=150° and the ERDA detector at the recoil angle φ=30°. The incident beam angle and the exit angle as measured from the normal to the sample surface were both 75°. An 11 µm thick aluminium absorber foil was inserted in front of the ERDA detector to block the scattered ^{7}Li ions. The measured RBS and ERDA spectra were analyzed using SIMNRA [12] code.

3. RESULTS AND DISCUSSION

In previous papers [5,6], we have shown, how a-C:H films can be deposited with a rather new method, employing a so-called anode layer source. There it was found, that the structure and the mechanical properties of the deposited films can be tailored effectively by the discharge voltage applied to the source, *i.e.* the kinetic energy of carbon species. In the present paper we enlight the relations between structural and chemical properties of the deposited films and their nanomechanical properties.

Figure 1 shows Raman spectra taken at 325 and 532 nm excitation wavelength from an a–C:H film deposited at 3 kV discharge voltage. Disp. (G) is indicated with a dashed line in Figure 1 and was found to be 0.16 cm^{-1}nm^{-1}. From these results it can be concluded, that this film has an intermediate topological disorder assigned to be typical for DLC films with a high degree of amorphisation. The lowest applied discharge voltage of 1 kV resulted in a significantly increased Disp. (G) of 0.23, being in line with intermediate discharge voltages showing a systematic variation with Disp. (G) (Figure 2).

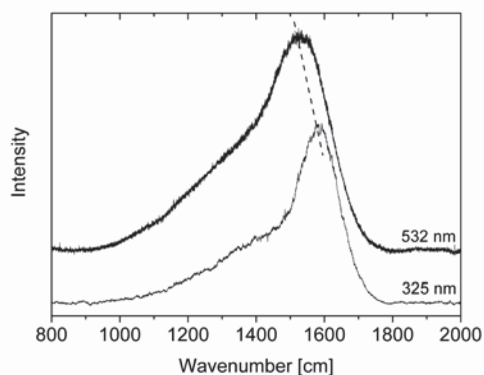

Figure 1. Raman spectra recorded with 325 and 532 nm excitation wavelengths taken from an a-C:H film deposited with a discharge voltage of 3 kV. Disp. (G) is indicated with a dashed line.

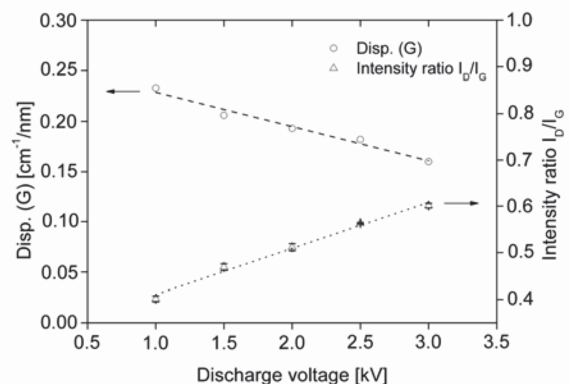

Figure 2. Disp. (G) and intensity ratio I_D/I_G (532 nm excitation wavelength) as a function of the discharge voltage.

Such a strong increase in Disp. (G) can be attributed to a significant increase in topological disorder where an increase in Disp. (G) is associated with an increase of Csp^3–Csp^3 and/or Csp^3–H1s bonds in the films [1]. A similar trend was denoted for the intensity ratio $I_D/I_G^{532\ nm}$ as a function of the discharge voltage (Figure 2). The overall sp^3 content is highest in films deposited with the lowest discharge voltage and decreases almost in a linear fashion with the discharge voltage (Figure 2).

Observation of the nanohardness (H) and reduced elastic modulus (E) values of these samples showed, that FWHM $(G)^{532\ nm}$, being a measure of the Csp^3–Csp^3 bonding content, as well as Disp. (G) influence the mechanical properties in a systematic fashion. Figure 3a shows, that a H of 25±0.4 GPa and an E of 147±2 GPa is connected with the lowest FWHM $(G)^{532\ nm}$ of 179±1 cm^{-1}. Highest values of H of 36±1 GPa and E of 180±4 GPa are observed for a FWHM $(G)^{532\ nm}$ of 196±1 cm^{-1}. Furthermore, highest values of H and E are observed for highest Disp. (G) of 0.23 (Figure 3b). In addition, H and E decrease with increasing intensity ratio $I_D/I_G^{532\ nm}$ (Figure 3c).

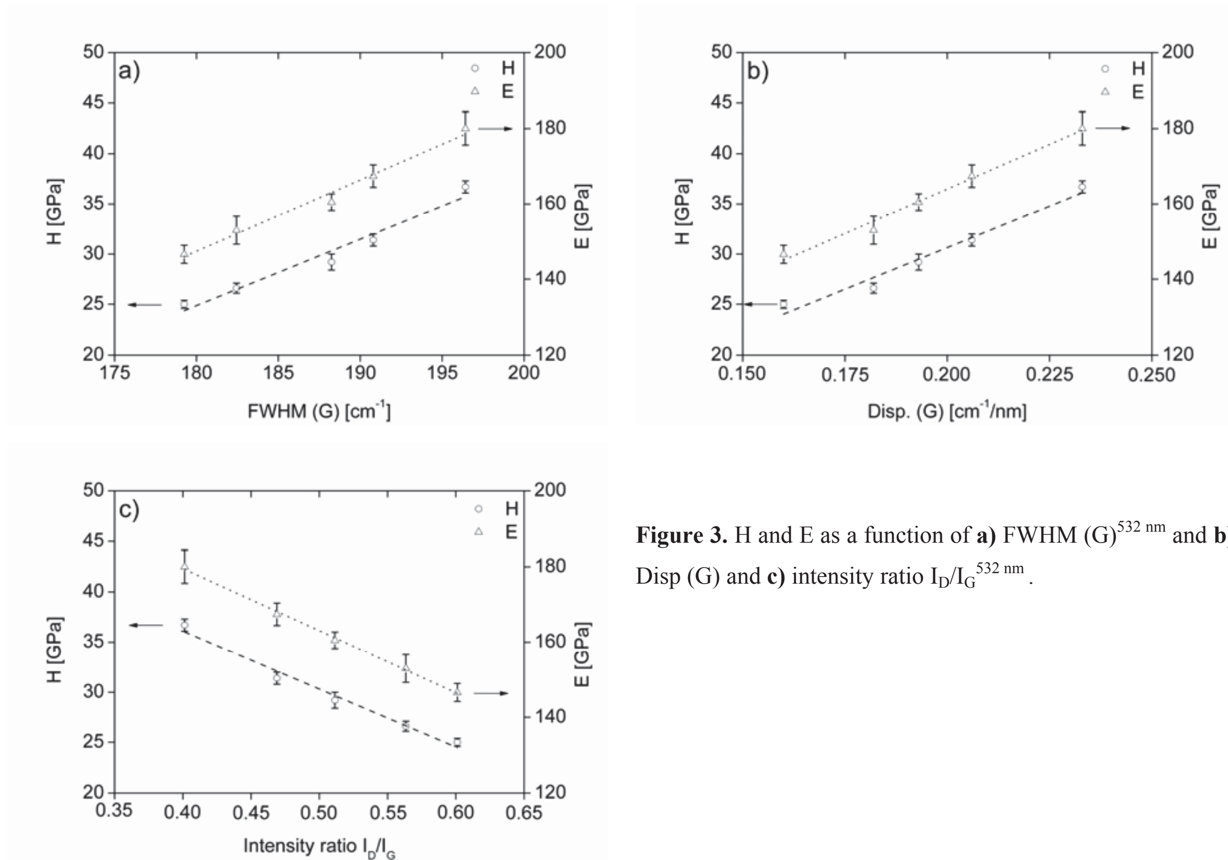

Figure 3. H and E as a function of **a)** FWHM $(G)^{532\ nm}$ and **b)** Disp (G) and **c)** intensity ratio $I_D/I_G^{532\ nm}$.

The expression H^3/E^2 is a measure of the elasticity exhibited by a film [13]. A high value of H^3/E^2 is an indicator of a highly elastic behaviour and a low value of H^3/E^2 suggests a more pronounced plastic behaviour of the investigated film. Within this context, we studied the elasticity of our films and found, that it increases in an exponential fashion with FWHM $(G)^{532nm}$ (Figure 4).

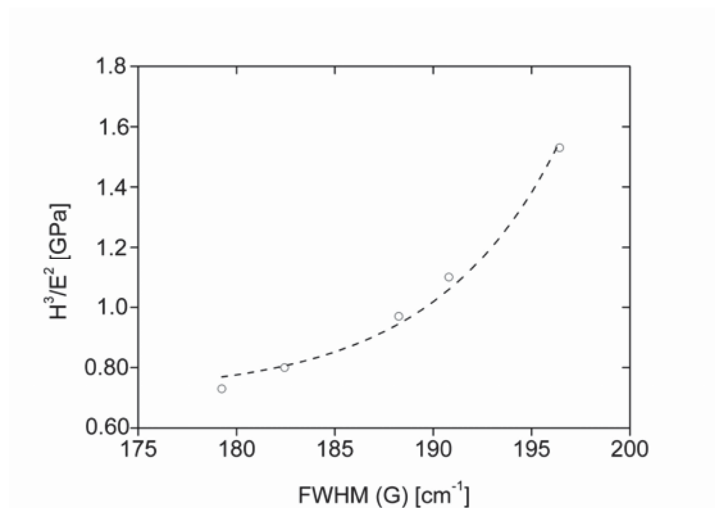

Figure 4. H^3/E^2 as a function of FWHM (G) determined with an excitation wavelength of 532 nm.

An important relation is the FWHM (G) as a function of the Disp. (G), since this indicates if a-C:H films follow structural trends in the polymeric or the tetrahedral regime as shown by Casiraghi et al. [2]. For tetrahedral films with high Csp^3–Csp^3 contents, an increasing FWHM (G) is associated with an increasing Disp. (G), whereas in the polymeric regime, trend inversion occurs, *i.e.* a decreasing FWHM (G) is associated with an increasing Disp. (G) [2]. The favoured formation of Csp^3–H1s bonds is responsible for this behaviour noted for polymeric a-C:H films. Figure 5 shows, that for both applied Raman excitation wavelengths an increasing FWHM (G) is in line with an increasing Disp. (G). With these data one can assume, that the hydrogen content must be rather similar in all of our investigated films and changes of the overall sp^3 content are caused by augmented formation of Csp^3–Csp^3 bonds.

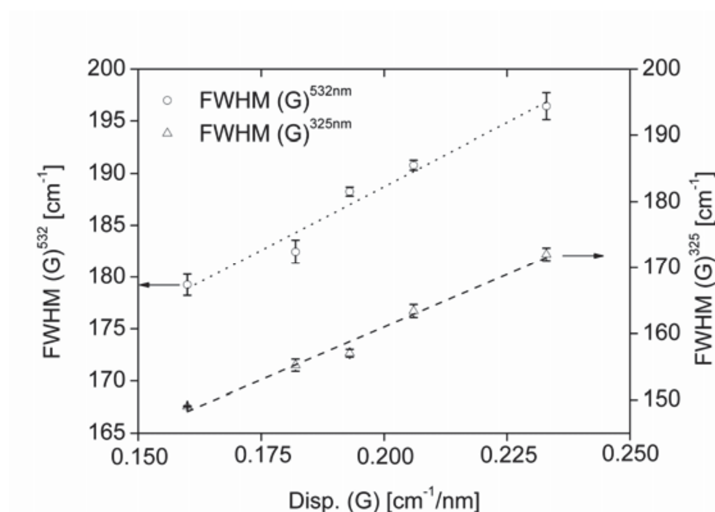

Figure 5. Correlation between Disp. (G) and FWHM (G) for excitation wavelengths of 532 nm and 325 nm.

Indeed, the hydrogen contents in the films investigated do not vary significantly with the discharge voltage applied to the anode layer source and were found to be constant at 22.2±1.2 at.% over the whole series of samples. Our data show, that in special cases, *i.e.* in the tetrahedral structural evolution regime (Figure 5), changes in Csp^3–Csp^3 bonding contents occur at similar hydrogen contents. In this regime, Raman band parameters usually associated with the overall sp^3 bonding content (intensity ratio I_D/I_G and Disp. (G)) are

related to the mechanical properties of the films. The relation between Disp. (G)/intensity ratio I_D/I_G and mechanical properties for a-C:H films was discussed theoretically by Casiraghi et al. [2]. Gradowski et al. [14] and Casiraghi et al. [15] studied the mechanical properties as a function of the Disp. (G) for ta-C and nitrogenated amorphous carbon films; however, to the best of our knowledge it has not yet been shown practically for a-C:H films.

4. CONCLUSION

We studied the relation between structural and mechanical properties of a-C:H films deposited by a rather new method employing the so-called anode layer source. The identified relations between structure and nanomechanical properties are highly accurate and allow an insight in the structural formation of a-C:H films as a function of the kinetic carbon ion energy during growth. In special cases, where H and E are proportional to Disp. (G) and are inversely proportional to the intensity ratio I_D/I_G in a *linear* fashion, one can assume that changes in the overall sp^3 content are only reflected by changes in the Csp^3–Csp^3 bonding content of the a-C:H films. A proportionality of FWHM (G) and Disp. (G) gives further evidence of such a behaviour. We see the reason for the distinct relations by the fact, that the hydrogen content is similar in all investigated films, allowing the Csp^3–Csp^3 bonding fraction to emerge independently from Csp^3–H1s bonds.

ACKNOWLEDGEMENTS

Financial support of this work by the Austrian Federal Ministry of Traffic, Innovation and Technology, the Austrian Industrial Research Promotion Fund (FFG), the Government of Styria, and the European Union is highly acknowledged.

REFERENCES

[1] J. Robertson, Mater. Sci. Eng. R37 (2002) 129.

[2] C. Casiraghi, A.C. Ferrari, J. Robertson, Phys. Rev. B 72 (2005) 085401.

[3] M. Weiler, S. Sattel, K. Jung, H. Ehrhardt, V.S. Veerasamy, J. Robertson, Appl. Phys. Lett. 64 (1994) 2797.

[4] P. Koidl, C. Wagner, B. Dischler, J. Wagner, M. Ramsteiner, Mater. Sci. Forum 52 (1990) 41.

[5] M. Kahn, M. Čekada, T. Schöberl, R. Berghauser, C. Mitterer, C. Bauer, W. Waldhauser, E. Brandstätter, Thin Solid Films 517 (2009) 6502.

[6] M. Kahn, M. Cekada, R. Berghauser, W. Waldhauser, C. Bauer, C. Mitterer, E. Brandstätter, Diamond Relat. Mater. 17 (2008) 1647.

[7] W.C. Oliver, G.M. Pharr, J. Mater. Res. 1 (1992) 1564.

[8] T. Staedler, K. Schiffmann, Surf. Sci. 482-485 (2001) 1125.

[9] W.D. Nix, H. Gao, J. Mech. Phys. Solids 46 (1998) 411.

[10] K. Durst, B. Backes, M. Göken, Scripta Mater. 52 (2005) 1093.

[11] P. Pelicon, A. Razpet, S. Markelj, I. Čadež, M. Budnar, Nucl. Instr. and Meth. B 227 (2005) 591.

[12] M. Mayer, SIMNRA User's Guide 6.05, Max-Planck-Institut für Plasmaphysik, Garching, Germany, 2009.

[13] C.A. Charitidis, S. Logothetidis, Diamond Relat. Mater. 14 (2005) 98.

[14] M.v. Gradowski, A.C. Ferrari, R. Ohr, B. Jacoby, H. Hilgers, H.H. Schneider, H.Adrian, Surf. Coat. Technol. 174-175 (2003) 246.

[15] C. Casiraghi, A.C. Ferrari, J. Robertson, R. Ohr, M. v. Gradowski, D. Schneider, H. Hilgers, Diamond Relat. Mater. 13 (2004) 1480.

PUBLICATION 6:

NANOINDENTATION AND NANOSCRATCH BEHAVIOUR OF ROOM-TEMPERATURE REACTIVE PULSED MAGNETRON SPUTTERED DLC FILMS-CORRELATIONS WITH FILM STRUCTURE

M. Kahn, W. Waldhauser, C. Mitterer, T. Koch, A. Pauschitz, E. Brandstätter, M. Roy

Submitted

NANOINDENTATION AND NANOSCRATCH BEHAVIOUR OF ROOM-TEMPERATURE REACTIVE PULSED MAGNETRON SPUTTERED DLC FILMS-CORRELATIONS WITH FILM STRUCTURE

M. Kahn[1], W. Waldhauser[1], C. Mitterer[2], T. Koch[3], A. Pauschitz[4], E. Brandstätter[1], Manish Roy[5]

[1] Joanneum Research Forschungsgesellschaft mbH, Laser Center Leoben, Leobner Strasse 94, 8712 Niklasdorf, Austria

[2] Department of Physical Metallurgy and Materials Testing, University of Leoben, Franz-Josef Strasse 18, A-8700 Leoben, Austria

[3] Institute of Materials Science and Technology, Vienna University of Technology, 1040 Vienna, Austria

[4] Austrian Center of Competence for Tribology, Viktor Kaplan-Strasse 2, 2700 Wiener Neustadt, Austria

[5] Defence Metallurgical Research Laboratory, PO: Kanchanbagh, Hyderabad: 500 058, India

ABSTRACT

The nanoindentation and nanoscratch behaviour of quasi non-hydrogenated and hydrogenated diamond-like carbon films (a-C:H) deposited by reactive pulsed direct current magnetron sputtering were investigated in detail. The study focused on the influence of the process parameters: acetylene/argon-ratio (C_2H_2/Ar-ratio) and bias voltage on the structural, nanomechanical and nanotribological properties of the deposited films. Raman spectra show that C_2H_2/Ar-ratios up to 0.25 favoured a decreased structural disorder in the a-C:H matrix gained by an increasing graphitisation of the films, and the highest used C_2H_2/Ar-ratio of 0.43 resulted in a structural trend inversion from graphitisation to slight polymerisation. Highest nanohardness (H) (23.3±03 GPa) and elastic modulus (E) values (173±2 GPa) were found to be accompanied with highest friction coefficients of ~0.06, whereas rather soft films with H = 15±0.2 GPa and an E = 142±1.5 GPa provide the lowest friction coefficients of ~0.04. The elasticity of the films expressed as H^3/E^2 decreased with increasing C_2H_2/Ar-ratios in the deposition chamber.

1. INTRODUCTION

Diamond-like carbon (DLC) is an amorphous, metastable form of carbon in sp^2 and sp^3 hybridisation. Since DLC films have superior properties with a unique combination of high hardness, good thermal conductivity, low friction coefficients, excellent wear resistance, ultra-smoothness and chemical inertness [1,2], these films have found a wide range of applications. DLC films are used for example as protective coatings on magnetic hard discs and on engineering components as wear resistant coatings, or as reported in recent years, as biocompatible or barrier coatings [1-6]. DLC films can be deposited by chemical vapour deposition, sputtering, pulsed laser deposition and filtered cathodic vacuum arcs [2]. Sputtering is widely used due to advantages like good process control and film homogeneity. These films can vary from diamond-like structures to graphite-like dominated structures, having a high amount of sp^2 bonds in the DLC matrix [2]. The desired properties of the films can be varied by careful adjustment of the process parameters: deposition pressure, reactive gas flow and bias voltage [2].

The friction properties of DLC films have been reviewed by Grill [7, 8], Donnet [9] and Gangopadhyay [10]. It is reported, that the friction coefficient of hydrogenated diamond-like carbon (a-C:H) depends on the relative humidity [11]. Friction coefficients as low as 0.05 of a-C:H films were found in vacuum and increased to 0.1 to 0.15 when rising atmospheric humidity of ~30 % [11]. It was found, that the elevated friction coefficients in air were caused by the higher humidity and not by oxygen in the atmosphere. However, Erdemir *et al.* [12, 13] found a dependence of friction coefficients measured at low humidity on the carbon precursor, which was used for the deposition of DLC films. The friction coefficients were found to vary with the C/H-ratio in the process gas atmosphere. Higher hydrogen concentrations in films deposited with methane and hydrogen as precursor for plasma enhanced chemical vapour deposition resulted in the lowest friction coefficients [12]. Moreover, Riedo and Brune [14] suggest a correlation of friction coefficients and reciprocal of the elastic modulus for hard coatings, as exemplified for DLC, diamond and CrN coatings.

A variety of methods have been employed to study the nanotribological properties of DLC films. The durability of carbon films have been assessed by several investigators by means of nanoindentation to measure nanohardness [15-19] and scratch testing to measure scratch resistance [20-23]. Mate [24,25] and Perry *et al.* [26] investigated friction and adhesion properties of a-C:H films by scanning probe microscopy. Nanotribology of carbon-based films is also reported by several investigators based on studies using atomic force microscopy (AFM) [27-30].

The basic understanding and influence of the sputtering process conditions on the nanotribological properties of DLC films is far from satisfactory. Therefore, the present investigation provides a detailed study on the structural, nanoindentation and nanoscratch properties of ~200 nm thin DLC films deposited by pulsed DC reactive magnetron sputtering of graphite. Films deposited by application of varied acetylene/argon mixtures were investigated. Additionally, the effect of bias voltage on structure, mechanical and friction properties will be discussed. The gained DLC structures will be correlated with mechanical and tribological properties.

2. EXPERIMENTAL DETAILS

2.1. FILM DEPOSITION

For deposition of quasi non-hydrogenated (a-C) and a-C:H films, a balanced magnetron cathode from AJA (AJA International, North Scituate, MA, USA) equipped with a graphite target (size: 432×74×7 mm^3, nominal purity >99.95 %) was used. The magnetron cathode was powered with a 10 kW power supply from Advanced Energy (Advanced Energy Industries, Fort Collins, CO, USA) in the power regulation mode. The pulsing unit was set to 80 kHz, where a reverse voltage of 15 % with a reverse time of 1 µs was used. A power density of ~10 Wcm^{-2} was applied on the carbon target for all depositions. For deposition of a-C:H films, acetylene (C_2H_2) (nominal purity >99.96 %) was introduced in the coating chamber together with argon (Ar) (nominal purity >99.999 %) resulting in C_2H_2/Ar ratios from 0 to 0.43. For deposition of the a-C coatings, a total flow of 30 sccm Ar was used. Boron doped silicon wafers (100) with a thickness of 525±25 µm were used as substrates. The wafers were cleaned in an ultrasonic cleaner sequentially with acetone and ethanol, and were dried with nitrogen. The wafers were fixed on a grounded substrate holding carrousel situated at a distance of approximately 10 cm from the sputtering source. The diameter of this carrousel was 56 cm whereas the samples were fixed at a diameter of 40 cm on vertical columns. In order to study the influence of substrate bias, a Heiden (Pürgen, Germany) bias power supply was connected to the carrousel for some additional experiments. Films were deposited by oscillation of the carrousel with amplitude of 9 cm (left-right) symmetrically through the sputtering plasma. The movement was in all cases one-dimensional and perpendicular to the major axis of the rectangular magnetron cathode. The substrate temperature was monitored with an electrically insulated K-type thermocouple installed at the backside of the substrate holder. For plasma cleaning of the wafers prior to deposition, an ALS 340 linear ion beam source from Veeco (Woodbury, NY, USA) was operated at a discharge voltage of 2 kV with an Ar flow rate of 20 sccm through the ion gun. For all depositions, the chamber was evacuated to a base pressure of <5 x 10^{-5} mbar. During deposition and plasma etching, the pressure in the chamber ranged from 1 x 10^{-3} to 5 x 10^{-3} mbar. No heating was applied to the substrates. The coating temperature did not exceed 80°C for all depositions and was found to be stable at that value also for depositions for several hours.

2.2. FILM CHARACTERISATION

2.2.1. Structure

A Raman microspectrometer from Jobin-Yvon (Villeneuve d'Ascq, France) was used to characterize the hybridization of carbon atoms in the DLC films. The instrument was operated with a laser working at an excitation wavelength of 532 nm. An Olympus 100× objective was used to focus the beam on the sample, while in all cases the power of the laser was kept well below 0.25 mW. The entrance slit to the spectrometer was set to 100 µm and a holographic grating with 1800 grooves mm^{-1} was used. A standard (100) orientated silicon wafer with a Si-peak position of 520 cm^{-1} was used as drift standard. A resolution of ~2 cm^{-1} could be achieved with the spectrometer. Mathematical spectrum fitting for the D and G-bands with Gaussian functions was performed with “Peak-Fit” 4.11 from Systat (Point Richmond, CA, USA). The G-band in Raman spectra from amorphous carbon phases taken at visible excitation has its origin in the effect of bond stretching of all carbon atoms in sp^2 hybridisation in rings and chains. The D-band occurs from the breathing mode of carbon

atom rings [31-33]. I_D/I_G ratios were calculated by using peak heights. Since this work focuses on the spectral features of the D and G-bands, other Raman active modes have been neglected.

2.2.2. Surface topography

Atomic force microscope (AFM) images of the deposited films were obtained with an AFM MFP-3D instrument (Asylum Research, Santa Barbara, CA) in air at ambient condition. Silicon nitride tips, triangular cantilevers with a spring constant of 0.1 Nm^{-1} were used. The scan area was 5 x 5 μm^2. Images were recorded in the 'constant-force' mode (feedback electronics and the corresponding software were used to keep the cantilever at constant deflection and to measure the sample topography).

2.2.3. Nanohardness

The nanohardness and the elastic modulus of the deposited films were determined with an instrumented depth sensing indenter equipped with a Berkovich three sided pyramidal diamond indenter with a nominal angle equal to 63.5^o. The instrument was placed in a vibration isolated chamber. A maximum load of 4 mN was applied for the indentations. The load was selected in a fashion to keep the deformation confined within the film. The holding time during indentation was 5 seconds for all measurements. Loading and unloading was performed within 10 seconds for all measurements. The experimental results were corrected for the thermal drift of the equipment and for the uncertainty in the zero position. The reported nanohardness and elastic modulus were averaged of 10 indentations for each sample on different surface positions separated by ~50 µm. The elastic modulus (E_r) was determined using the procedure described in ref. [34] and was calculated employing the equation (1) as given below.

$$\frac{1}{E_r} = \frac{(1-\upsilon^2)}{E} + \frac{(1-\upsilon_i^{\,2})}{E_i} \tag{1}$$

E_r is given by

$$E_r = \frac{0.89S}{\sqrt{A}} \tag{2}$$

There, S is the slope of the initial part of the unloading curve (in N/m) and A is the contact area between the indenter and the substrate (in m^2). E and E_i are the elastic moduli and ν and ν_i are the Poisson ratios of the film and the indenter, respectively. The nanoindenter was calibrated by indenting on a fused silica sample with nanohardness and elastic modulus of approximately 10 and 73 GPa, respectively. Measurements were performed in a clean air environment with a relative humidity of ~40 % while the testing temperature was ~22°C.

2.2.4. Nanoscratch performance

Nanoscratch tests were performed on the deposited films by using a conical diamond tip of a nominal radius of approximately 2 µm for scratching. The scratch velocity was set to 1 µm s^{-1}, while scratching was carried out with constant normal loads of 25 and 500 µN. To avoid effects from neighbouring scratches, the distance between sequential scratches was set to 10 µm.

3. RESULTS AND DISCUSSION

3.1. CORRELATION OF FILM SURFACE TOPOGRAPHY WITH PROCESS PARAMETERS

The root mean square (RMS) roughness values of these films vary from 0.6 nm to 1.4 nm. Figure 1 shows a representative AFM image, recorded for a film deposited with a C_2H_2/Ar-ratio of 0.25. No dependence between process conditions and roughness values could be identified when depositing on grounded substrates.

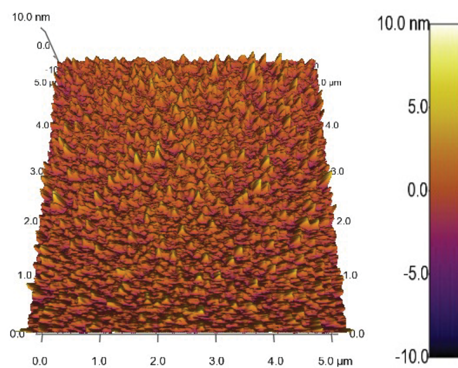

Figure 1. Representative AFM image for a film deposited with a C_2H_2/Ar-ratio of 0.25.

Films deposited under grounded conditions show a mean RMS roughness of 1.2±0.2 nm (C_2H_2/Ar-ratios from 0 to 0.43). Working with a bias voltage of -100 V resulted in a reduction of the RMS roughness value down to ~0.6 nm. This smoothening effect can be attributed apparently to two possible origins:

(1) A so-called impact induced downhill current originating from the additional bombardment of the growing film with carbon ions can give a smoothing effect [35]. However, since the rate of carbon neutrals is reported to be very high in sputtering plasmas [2], this effect might not be dominating.

(2) An impact induced downhill current can also be fostered by the bombardment of the growing film with Ar^+ ions. Moseler *et al.* [35] found by simulations and AFM studies, that these downhill currents cause an erosion of hills into neighbouring hollows at the top layer during growth and thus reduces roughness.

Impact induced downhill currents originating from highly energetic species bombarding the DLC surface are the generally most accepted reason for the ultra-smoothness of DLC films with roughness values down to 0.1 nm [35].

Sputtering of graphite targets results in the generation of defects, which originate from the solid target. It can be noted, that arcing and particle emission from the porous target can be almost prevented by pulsing in the

kHz range. Therefore, the occurrence of defects in the films originating by particulates is reduced significantly compared to films which were deposited by the use of conventional DC magnetron sputtering during process development.

3.2. CORRELATION OF PROCESS PARAMETERS WITH FILM STRUCTURE

Figure 2 shows a Raman spectrum of a quasi a-C film structure, deposited with pure Ar as sputtering gas. The bands were found to be located at spectral positions of 1356±8 cm^{-1} (D-band) and 1550±4 cm^{-1} (G-band). All deposited films represent structurally a highly disordered carbon phase verified by Raman studies. Comparing the spectral shape as well as the band parameters with literature revealed rather an a-C:H structure than a-C also for films which were deposited with Ar as sputtering gas only. Therefore, under room temperature deposition conditions, an introduction of hydrogen from the residual gas background of the vacuum chamber into the film structure cannot be prevented when only working with Ar as sputtering gas.

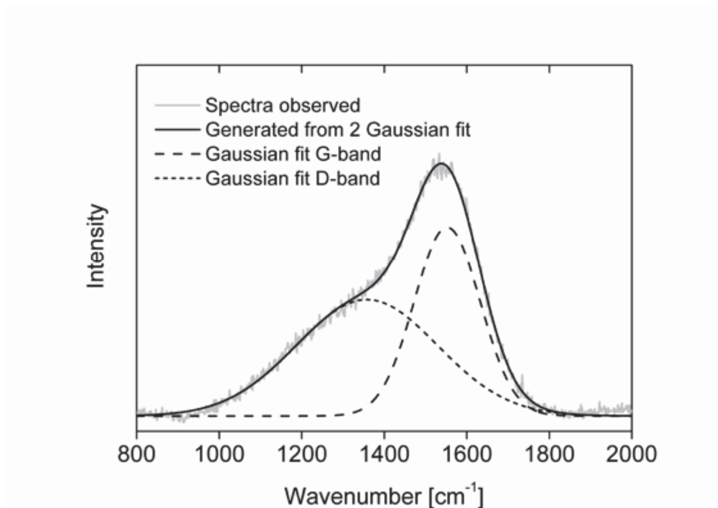

Figure 2. Raman spectrum recorded from a DLC film deposited with 30 sccm Ar at a process pressure of $5 \cdot 10^{-3}$ mbar.

On the following, it is attempted to enlighten the role of the varied process gas mixtures as well as the role of a bias voltage of -100 V on the structural, nanomechanical and nanotribological properties of the deposited films. Since the evaluation of Raman spectra is rather complex, the following rules have to be taken into account when interpreting them [31-33,36]:

(1) The intensity ratio I_D/I_G is a measure of the size of the sp^2 phase organized in rings. If the intensity ratio I_D/I_G becomes lower or zero, the sp^2 phase is organized rather in chains, whereas a higher intensity ratio I_D/I_G is an indication of an increase of the sp^2 phase in aromatic rings.

(2) For a-C:H films, the Raman parameters can be used to reveal information about the sp^3-hybridisated carbon fraction of the films. A lower intensity ratio of I_D/I_G is connected with higher overall (C–C, C–H) sp^3 content.

(3) The trends in the C–C sp^3 bonding content can be interpreted by using the full width at half maximum of the G-band (FWHM (G)). An increase in the FWHM (G) is connected directly with an increase in the C–C sp^3 bonding content.

Focusing on the structure of the a-C:H films deposited in pure Ar atmosphere onto grounded substrates, an I_D/I_G ratio of 0.61±0.03 was calculated with peak amplitudes of the bands shown in Figure 2. Intensities from D and G-bands in spectra taken from samples deposited at higher C_2H_2/Ar-ratios of 0.11 to 0.25 at similar process parameters show slightly enhanced I_D/I_G ratios of 0.62±0.04 and 0.64±0.01, respectively (Figure 3).

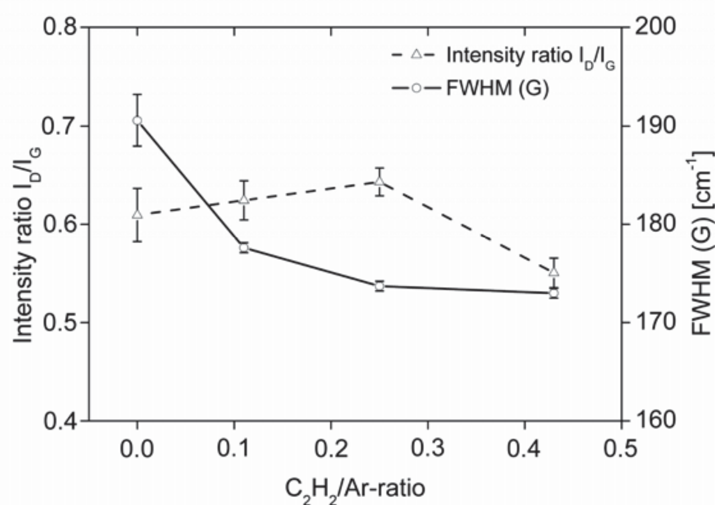

Figure 3. Intensity ratio I_D/I_G and FWHM (G) as a function of the C_2H_2/Ar-ratio of the deposited films.

Therefore, the size of graphitic clusters is slightly increased in this process area. Sputtering at the highest C_2H_2/Ar-ratio of 0.43 resulted in a film structure with an I_D/I_G ratio of 0.55±0.05. Here, the FWHM (G) was found to be 173±0.5 cm^{-1} (Figure 3). This observed behaviour clearly identifies the film deposited with a C_2H_2/Ar-ratio of 0.43 as an authentic a-C:H film, showing less disordering derived from decreased FWHM (G) while having at the same time a low I_D/I_G ratio. The finding implies, that the increase in overall sp^3 content is mainly formed by C–H bonds in coatings deposited at a C_2H_2/Ar-ratio of 0.43 [36].

3.3. CORRELATION OF FILM STRUCTURE WITH MECHANICAL PROPERTIES

The variation of nanohardness and elastic modulus of the deposited films as a function of the FWHM (G) and the C_2H_2/Ar-ratio is shown in Figure 4. The values ranged from a nanohardness of 18±0.4 GPa to 15±0.2 GPa when increasing the C_2H_2/Ar-ratio in the chamber. The variation in nanohardness and elastic modulus follows the trends derived by Raman spectroscopy. An ordering effect in the films induced by elevated C_2H_2 concentrations in the process gas atmosphere as well as a higher degree of polymerisation seen in the film deposited with a C_2H_2/Ar-ratio of 0.43, results in slightly lower nanohardness and elastic modulus values. Therefore, the variation of the FWHM (G) can be correlated with the measured mechanical properties of the films.

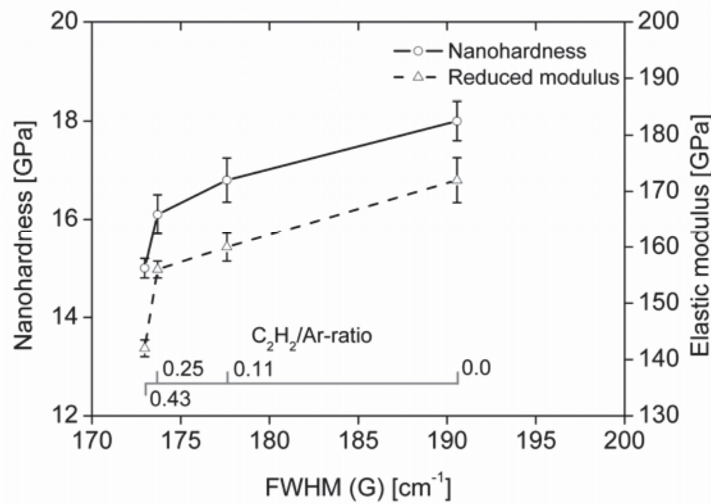

Figure 4. Nanohardness and elastic modulus as a function of the FWHM (G) and the C_2H_2/Ar-ratio of the deposited films.

An applied bias voltage of -100 V resulted in a film with a nanohardness of 23.3±0.3 GPa and an elastic modulus of 173±2 GPa (deposited in pure Ar atmosphere). The FWHM (G) as well as the intensity ratio I_D/I_G were found to be different compared to the film sputtered onto grounded substrates. A FWHM (G) of 179±1 cm^{-1} and an intensity ratio I_D/I_G of 0.86±0.1 were found for this film. The spectral shape indicates the occurrence of a stronger a-C structure [31] with less hydrogen saturated carbon atoms. This observation indicates that the increase in nanohardness induced by -100 V bias was not necessarily gained by an increase in C–C sp^3 content in the film. Instead, the Ar^+ bombardment during deposition helped to lower the hydrogen content, reducing the occurrence of polymeric chains in the film, showing subsequently a higher nanohardness. Interestingly, the bias support did not help to encourage the elastic modulus compared to unbiased samples. However, it is to be stressed that application of a DC bias voltage is limited to conductive substrates and will influence the film structure as a function of the conductivity of the used substrates. It has been reported [37] that DLC films are sensitive to very high energy Ar^+ ion bombardment, showing graphitisation due to energy transfer of the incident heavy Ar^+ ions to the growing DLC film, reducing the disordered and diamond-like character of the films.

3.4. EVALUATION OF FILM ELASTICITY AND FILM COHESIVE STRENGTH

The load versus displacement curves of these films obtained at an applied load of 500 µN are smooth and none of the curves show the presence of pop-in or pop-out events. Each curve is obtained by averaging ten measured curves. Figure 5a shows an exemplary load versus displacement curve for the film deposited in pure Ar atmosphere on grounded substrates.

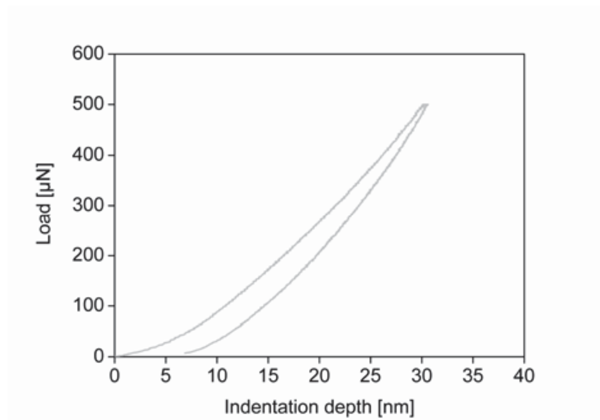

Figure 5a. Exemplary load versus displacement curve for the film deposited in pure Ar atmosphere at a grounded substrate.

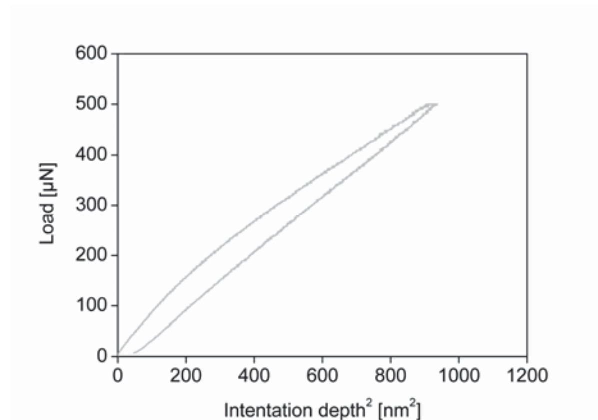

Figure 5b. Exemplary load versus square of displacement for the film deposited in pure Ar atmosphere at a grounded substrate.

The highest depth of penetration of 33.6 nm and the highest residual depth of 7.21 nm were obtained for the film deposited at a C_2H_2/Ar-ratio of 0.43, whereas the lowest depth of penetration of 28.12 nm and the lowest residual depth of 2.6 nm pertain to the film obtained by an applied bias voltage of -100 V. Table 1 summarizes the depth of penetration, residual depth, percentage of elastic and plastic deformation of the films studied in the present work.

Table 1. Elastic and plastic deformation of the films during indentation. Substrates are grounded if not mentioned otherwise.

	Depth of penetration (nm)	**Residual depth of penetration (nm)**	**% of elastic deformation**	**% of plastic deformation**
C_2H_2/Ar: 0	30.8	6.5	78.9	21.1
C_2H_2/Ar: 0.11	31.7	6.8	78.5	21.5
C_2H_2/Ar: 0.25	31.8	7.2	77.4	22.6
C_2H_2/Ar: 0.43	33.6	7.2	78.6	21.4
C_2H_2/Ar: 0, Bias: -100 V	28.1	2.6	90.7	9.35

The smooth load versus displacement curves is an indication that there was no fracture of the film during the indentation process. The least depth of penetration is around 28 nm. Given the fact that the RMS values of most of the films are around 1 nm, the indentation process fulfils roughness criteria [38]. The maximum depth of penetration is around 33 nm which represents 17 % of the film thickness. Table 1 show that the highest percentage of plastic deformation is around 22 % indicating that the films are quite brittle. Thus, the total deformed zone due to indentation should be confined within the film. Hence, the nanohardness evaluated in the present work is a true representation of the nanohardness of the investigated films. During holding at maximum load, the displacement increases in all the films indicating drift due to creep as the load versus displacement curves are plotted after incorporating the correction due to thermal drift. The extent of this drift is, however, independent of the process conditions. The load versus square of the penetration depth curves did not show presence of any step. Thus, the films possess high cohesive strength and high fracture

toughness [39]. Figure 5b shows an exemplary load versus square of the displacement curve for the film deposited in pure Ar atmosphere on grounded substrates. With in the range of applied load, there is no cracking in these films. Typically, these curves show an initial straight line during loading and a turning point at an intermediate loading. This initial stage can be identified as coating only behaviour.

As the coating deforms in response to the maximum Hertzian shear stress lying within the coating depth, it is apparent that the maximum shear stress experienced by the substrate at the initial straight line portion of the load displacement square curve is not enough for substrate yielding. Beyond the turning point, sufficiently high shear stress is experienced and the subsurface undergoes plastic yielding.

This in turn requires the coating to flex and bend to confirm to this subsurface deformation. The shear stress in the coating is large enough to cause plastic flow in an area immediately around the axis of the contact and along the indenter edges. At the same time, significant tensile stresses are generated in a circular pattern around the outer periphery of the contact zone, as the coating is forced to bend to conform to subsurface deformation and pile up.

The expression H^3/E^2, that contains nanohardness and elastic modulus, is a measure of the elasticity exhibited by a film [40]. A high value of H^3/E^2 is an indicator of a highly elastic behaviour and a low value of H^3/E^2 suggests a more pronounced plastic behaviour of the investigated film. Table 2 lists the H^3/E^2-ratios, the elastic modulus and the nanohardness of all films tested in this work.

Table 2. Nanohardness, elastic modulus and H^3/E^2-ratios of the investigated films. Substrates are grounded if not mentioned otherwise.

	Nanohardness [GPa]	**Elastic Modulus [GPa]**	**H^3/E^2 (GPa)**
C_2H_2/Ar: 0	18±0.4	172±4	0.197
C_2H_2/Ar: 0.11	16.8±0.45	160±2.5	0.185
C_2H_2/Ar: 0.25	16.1±0.4	156±1.5	0.171
C_2H_2/Ar: 0.43	15±0.2	142±1.5	0.167
C_2H_2/Ar: 0, Bias: -100 V	23.3±0.3	173±2	0.423

The significant gain in elasticity induced by -100 V bias can be interpreted as the result of a loss of hydrogen in the film structure, as evidenced by Raman spectroscopy. Perusal of nanohardness and elastic modulus of this film indicates that this film has a high nanohardness and the elastic modulus is comparable to the film deposited in pure Ar atmosphere without bias support.

3.5. NANOSCRATCH PERFORMANCE

The variation of friction coefficient as a function of the scratch distance under a nanoscratch load of 25 µN is shown in Figures 6a to 6e. Two different behaviours are noted.

(1) Films deposited at a C_2H_2/Ar-rate of 0 and 0.11 show a constant and very low friction coefficient of ~0.05 (Figure 6a and 6b).

(2) The friction coefficients of films deposited at higher C_2H_2/Ar-rates of 0.25 and 0.43, and also the film deposited with -100 V bias under pure Ar, initially decrease with increasing scratch distance and then start to increase after attaining a minimum friction coefficient of ~0.05.

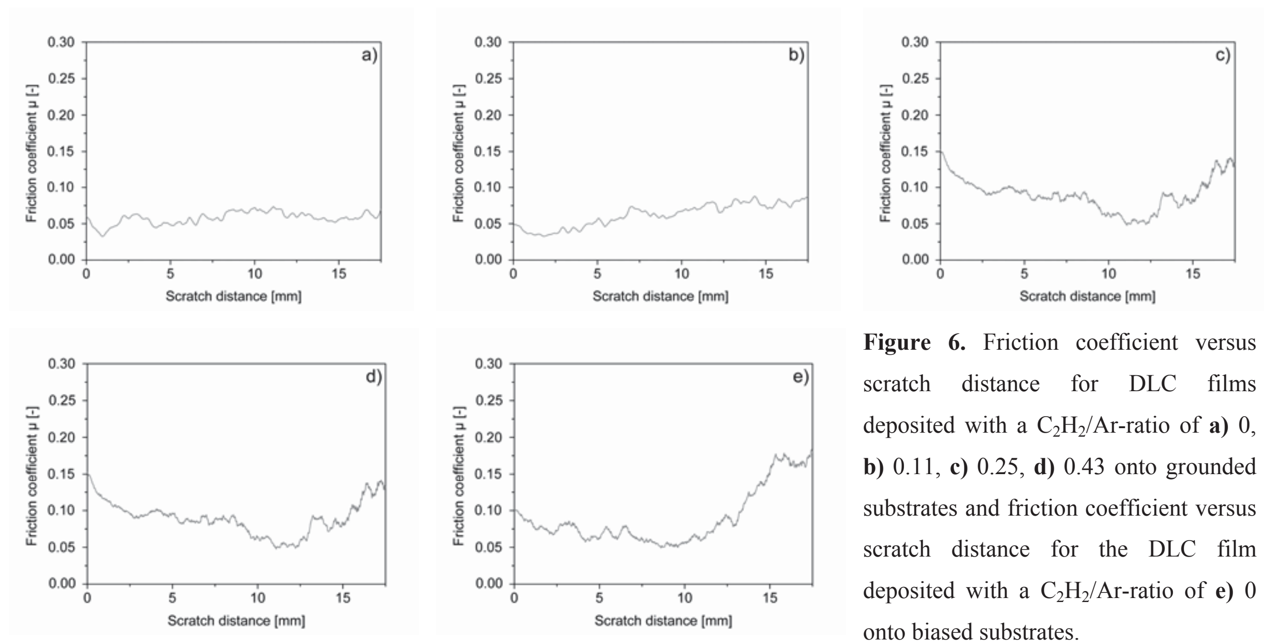

Figure 6. Friction coefficient versus scratch distance for DLC films deposited with a C_2H_2/Ar-ratio of **a)** 0, **b)** 0.11, **c)** 0.25, **d)** 0.43 onto grounded substrates and friction coefficient versus scratch distance for the DLC film deposited with a C_2H_2/Ar-ratio of **e)** 0 onto biased substrates.

The friction response of these films under 25 µN and 500 µN load is different. For the test with 500 µN, almost all films show constant friction coefficients with scratch distance. Films deposited in pure Ar atmosphere onto grounded substrates show friction coefficients of ~0.04 (C_2H_2/Ar-ratios of 0.11, 0.25 and 0.43). The film, which was deposited under biased conditions in pure Ar atmosphere show a slightly increased friction coefficient of ~0.06.

The rather systematic decrease and following increase of friction coefficients at low load test conditions with scratch distance for the films shown in Figures 6c to 6e is not explainable with the current results. However, we would like to point out, that friction coefficients of films sputtered at C_2H_2/Ar-ratios of 0 and 0.11 show constant and very low frictions coefficients of ~0.05 over the whole sliding distance.

3.6. COMPARISON OF THE NANOMECHANICAL RESULTS WITH EXISTING MODELS

In order to discuss the relation between friction and mechanical properties in more detail, the results will be compared to existing models. When contact between two bodies with surface asperities takes place, the real (A_r) contact area is a small fraction of the apparent contact area (A_p) [41]. According to Greenwood and

Williamson [42], the real contact area is proportional to the normal load. Based on the classical theory of adhesion, the frictional force is defined as [42]:

$$F = \tau_a A_r \quad \text{and} \quad \frac{F}{(L)} = \frac{\tau_a A_r}{(L)} = \mu_a \tag{3}$$

where τ_a is the average shear strength during sliding and (L) is the applied load. μ_a is adhesion induced friction coefficient. For elastic contact of a spherical indenter and a homogenous half-space, the contact area A_r can be estimated as:

$$A_r = \pi \left(\frac{3(L)R}{4E} \right)^{\frac{2}{3}} \tag{4}$$

where E is the effective elastic modulus and R is the effective radius of curvature. Combining equations (3) and (4), the friction coefficient corresponding to pure elastic adhesion is given by

$$\mu_a = \pi\tau \left(\frac{3R}{4E} \right)^{\frac{2}{3}} L^{-\frac{1}{3}} \tag{5}$$

Following the model of Greenwood and Williamson [42] for a finite asperity height distribution, in the presence of adhesion forces, equation (5) can be written as

$$\mu_a = \tau \left(\frac{\pi}{2} \right)^{1/2} \left(\frac{3R^{1/2}}{4E\lambda^{1/2}} \right) \tag{6}$$

or $$\mu_a = \frac{3}{4}\tau \left(\frac{\pi R}{2\lambda} \right)^{1/2} \frac{1}{E} \tag{7}$$

where λ is the root-mean-square (rms) width of the height distribution on the surfaces, which is assumed to be Gaussian. Thus, as per equation (7), the friction coefficients of various films will be inversely proportional to the effective elastic modulus of the film and the nanoscratch indenter system. In the present investigation, λ can be assumed to be constant as all the films have more or less equal roughness. Contrary to investigations of Riedo and Brune [14] we observed a slight decrease of the friction coefficients with increasing reciprocal of elastic modulus for our studied films.

4. CONCLUSIONS

We have studied the structural and mechanical properties of room-temperature reactive pulsed DC magnetron sputtered DLC films. Raman spectroscopy suggests that the addition of C_2H_2 to the process gas atmosphere results in the formation of clustered sp^2 phases in the deposited films, whereas a very high C_2H_2/Ar-ratio of 0.43 results in the formation of C–H sp^3 bonds in the film structure. Structural variations are reflected

systematically in hardness, elastic modulus and elasticity values. Application of a bias voltage of -100 V provides further improved film quality with respect to roughness and mechanical properties. Friction coefficients are very low and range between 0.4 and 0.6 and are almost independent of structural and mechanical properties. Under nanoscratch conditions, a relation between friction coefficients and reciprocal of the elastic modulus is hardly noticeable for the studied DLC films. We would like to highlight, that structural and mechanical properties of the films can be tailored effectively with the applied process parameters.

ACKNOWLEDGEMENTS

Financial support of this work by the Austrian Federal Ministry of Traffic, Innovation and Technology, the Austrian Industrial Research Promotion Fund (FFG), the Government of Styria, Forschung Austria and the European Union is highly acknowledged.

REFERENCES

[1] A.C. Ferrari, Surf. Coat. Technol. 180-181 (2004) 190.

[2] J. Robertson, Mater. Sci. Eng. R37 (2002) 129.

[3] M. Janotta, D. Rudolph, A. Kueng, C. Kranz, H.S. Voraberger, W. Waldhauser, B. Mizaikoff, Langmuir. 20 (2004) 8634.

[4] F.Z. Cui, D.J. Li, Surf. Coat. Technol. 131 (2000) 481.

[5] T. Yokota, T. Terai, T. Kobayashi, M. Iwaki, Nucl. Instrum. Methods Phys. Res. B 242 (2005) 48.

[6] C. Lim, S. Slack, S. Ufer, E. Lindner, Pure Appl. Chem. 76 (2004) 753.

[7] A. Grill, Wear 168 (1993) 143.

[8] A. Grill, Surf. Coat. Technol. 94 (1997) 507.

[9] C. Donnet, Surf. Coat. Technol. 100 (1998) 180.

[10] A. Gangopadhyay, Tribol. Lett. 5 (1998) 25.

[11] C. Donnet, T. LeMogne, L. Ponsonnet, M. Belin, A. Grill, V. Patel, C. Jahnes, Tribol. Lett. 4 (1998) 259.

[12] A. Erdemir, O.L. Eryilmaz, I.B. Nilhufer, G.R. Fenske, Diamond Rel. Mater. 9 (2000) 632.

[13] A. Erdemir, O.L. Eryilmaz, G.R. Fenske, J. Vac. Sci. Technol. A 18 (200) 1987.

[14] E. Riedo, H. Brune, Appl. Phys. Lett. 83 (2003) 1986.

[15] K.J. Grannen, X. Ma, R. Thangaraj, J. Gui, G.C. Rauch, IEEE Trans. Magn. 26 (2000) 120.

[16] R.C. Hsiao, D.B. Bogy, IEEE Trans. Magn. 34 (1998) 1720.

[17] S. Sundararajan, B. Bhushan, Wear 225-229 (1999) 678.

[18] D.B. Bogy, Z. Jiang, Proc. Mater. Res. Soc. Symp. 356 (1995) 737.

[19] S. Logothetidis, C. Charitidies, Thin Solid Films 353 (1999) 208.

[20] E.R. Kral, K. Komvopoulos, D.B. Bogy, J. Tribol. 118 (1996) 1.

[21] X. Li, B. Bhushan, Wear 220 (1998) 51.

[22] H. Deng, T.W. Scarf, J.A. Barnard, IEEE Trans. Magn. 33 (1997) 3151.

[23] B. Bhushan, B.K. Gupta, M. Azarian, Wear 181-183 (1995) 743.

[24] C.M. Mate, Surf. Coat. Technol. 62 (1993) 373.

[25] C.M. Mate, Wear 168 (1993) 373.

[26] S.S. Perry, C.M. Mate, G.A. Somojai, Tribol. Lett. 1 (1995) 233.

[27] T. Hua Fang, C. I. Weng, J.G. Chang, C.C. Hwang, Thin Solid Films 396 (2001) 166.

[28] B.D. Beake, I.U. Hassan, C.A. Rego, W. Ahmed, Diamond Rel. Mater. 9 (2000) 1421.

[29] S. Kavasnica, J. Schalko, C. Eisenmenger-Sittner, J. Bernardi, G. Vorlaufer, A. Pauschitz, M. Roy, Diamond Rel. Mater. 15 (2006) 1743.

[30] A. Bogus, I.C. Gebeshuber, A. Pauschitz, M. Roy, R. Haubner, Diamond Rel. Mater. 17 (2008) 1998.

[31] A.C. Ferrari, J. Robertson, Phil. Trans. R. Soc. London A, 362 (2004) 2477.

[32] A. C. Ferrari, J. Robertson, Phys. Rev. B 61 (2000) 14095.

[33] A.C. Ferrari, J. Robertson, Phys. Rev. B 64 (2001) 075414.

[34] W.C. Oliver, G.M. Pharr, J. Mater. Res. 7 (1992) 1564.

[35] M. Moseler, P. Gumbsch, C. Casiraghi, A.C. Ferrari, J. Robertson, Science 309 (2005) 1545.

[36] C. Casiraghi, A.C. Ferrari, J. Robertson, Phys. Rev. B, 72 (2005) 085401.

[37] M. Kahn, M. Čekada, T. Schöberl, R. Berghauser, C. Mitterer, C. Bauer, W. Waldhauser, E. Brandstätter, Thin Solid Films 517 (2009) 6502.

[38] C. Walter, C. Mitterer, Surf. Coat. Technol. 203 (2009) 3286.

[39] J. Ding, Y. Meng, S. Wen, Thin Solid Films 371 (2000) 178.

[40] C.A. Charitidis, S. Logothetidis, Diamond Relat. Mater. 14 (2005) 98.

[41] B. Bhushan, Introduction to Tribology, Wiley, New York, 2002.

[42] J.A. Greenwood, J.B.P. Williamson, Proc. Royal. Soc. London A 295 (1966) 300.

UNPUBLISHED RESULTS:

APPLICATION OF NITROGEN-DOPED DIAMOND-LIKE CARBON FILMS AS NOVEL OPTICALLY TRANSPARENT ELECTRODES FOR MULTI-REFLECTION IR-ATR SPECTROELECTROCHEMISTRY

N. Menegazzo, M. Kahn, R. Berghauser, W. Waldhauser, B. Mizaikoff

Collaborative effort which generated preliminary data that showed a potential chemical application of nitrogen-doped diamond-like carbon films

APPLICATION OF NITROGEN-DOPED DIAMOND-LIKE CARBON FILMS AS NOVEL OPTICALLY TRANSPARENT ELECTRODES FOR MULTI-REFLECTION IR-ATR SPECTROELECTROCHEMISTRY

Nicola Menegazzo[1], Markus Kahn[2], Roswitha Berghauser[2], Wolfgang Waldhauser[2], Boris Mizaikoff[1]

[1] School of Chemistry and Biochemistry, Georgia Institute of Technology, Atlanta, Georgia, 30332-0400.

[2] Joanneum Research, Laser Center Leoben, Niklasdorf, Austria, A-8712.

ABSTRACT

This contribution describes the development of nitrogen-doped diamond-like carbon (a-C:N) thin films for multi-reflection mid-infrared attenuated total reflectance (IR-ATR) spectroelectrochemistry. A-C:N coatings were deposited using pulsed laser deposition (PLD), involving the ablation of a high purity graphite target in the presence of nitrogen gas. This technique offers the advantage, that the deposition can be performed at room temperature, enabling coating of temperature-sensitive substrates, such as mid-IR waveguides. Nitrogen was found to induce clustering of graphite-like carbon phases which gained enhanced conductivity of the films. The clustering of graphite-like phases induced by the addition of nitrogen was monitored with Raman spectroscopy. A percentage of 33 % nitrogen in process gas mixture resulted in films with highest structural order and highest graphite-like cluster size, while still remaining typical diamond-like character. The resulting films deposited at the highest nitrogen flow contain approx. 9 at.% nitrogen, as well as adventitious oxygen in addition to carbon and were chosen for the spectroelectrochemical studies. The electrochemical activity of PLD fabricated a-C:N films was verified using the $Ru(NH_3)^{3+/2+}$ redox couple and demonstrated to be comparable with that of other conventional carbon-based electrodes. In-situ spectroelectrochemical studies involving a-C:N coated ZnSe waveguides provide evidence concerning oxidation of a-C:N at anodic potentials in 1 M $HClO_4$. Finally, the electropolymerization of polyaniline was performed at the modified waveguides, which enabled spectroscopic monitoring of the electro-polymerization as well as conversion between different redox states of polyaniline.

KEYWORDS

Pulsed laser deposition (PLD), nitrogen-doped diamond-like carbon (a-C:N), electrochemistry, infrared spectroscopy (IR)

1. INTRODUCTION

During an electrochemical reaction, information about the rearrangement of the electrochemical double layer, changes in electrode composition (e.g. surface oxidation) and mechanistic pathways concerning the formation of electrochemical products is not directly accessible by electrochemical means alone. Several in- and ex-situ spectroscopic configurations have been combined with electrochemistry in an effort to obtain further details about electrochemical phenomena.[1] Approaches based on optical spectroscopies are particularly advantageous due to in-situ capabilities,[2] yielding real-time monitoring while suppressing potential artifacts rising from exposure of electrode surfaces to atmospheric conditions, common to ex-situ spectroscopic analysis.[1]

In particular, mid-infrared (mid-IR) spectroscopy (2-20 μm) provides spectral signatures corresponding to fundamental vibrational and rotational modes of molecular bonds, and therefore offers extensive bonding rearrangement information related to electrochemical processes. IR spectroelectrochemical analysis in highly absorbing media (e.g. water) requires thin electrolyte layers (typically ≤ 30 μm), inducing high solution resistance and distorting the electrochemical signal.[3,4] Spectroscopic configurations based on attenuated total reflectance (ATR) circumvent this limitation since the interaction of incident radiation with the sample is restricted to the penetration depth (d_p) of the evanescent field (generally ≤ 2 μm).[5] Electrolyte present over the d_p is not probed and therefore does not further attenuate the spectroscopic signal.

Highly doped germanium (Ge) waveguides were initially proposed as an attractive approach to mid-IR-ATR spectroelectrochemistry, however, chemical lability of the waveguiding material resulted in its restricted application.[6,7] Alternatively, metallic electrodes in the form of grids[8,9] or ultra-thin films (≤10 nm)[10,11] have been utilized as optically transparent electrodes (OTEs) on waveguide surfaces. Yet, both strategies have experienced a limited adoption due to localized formation of electrochemical products with metallic grids, and therefore decreased sensitivity, or high electrical resistivity and insufficient adhesive properties displayed by ultra-thin films.[12] Similarly, mid-IR-ATR OTEs based on thin graphitic films evaporated onto Ge waveguides have been investigated for their potential. Despite electrochemical behavior comparable to typical sp^2-carbon electrodes, films deposited yielded limited optical throughput. Finally, boron doped diamond (BDD) deposited onto silicon substrates has also been proposed for spectroelectrochemical applications.[13,14] BDD electrodes offer several advantageous electrochemical properties due to the inert sp^3-hybridized carbon network. However, limited IR transparency due to boron doping and high growth temperatures (up to 800 °C) preclude coating of temperature-sensitive multi-reflection IR ATR waveguide substrates, such as zinc selenide (ZnSe) and thallium bromo-iodide (KRS-5).

Diamondlike carbon (DLC) is a metastable allotrope of carbon composed of both sp^2- and sp^3-hybridization states mixed in an amorphous matrix[15]. Incorporation of a high fraction of sp^3-hybridized carbon result in unique mechanical qualities resembling those of diamond. Likewise, DLC thin films are also chemically inert and optically transparent in the mid-IR range, as confirmed by Janotta et al.[16,17] The authors utilized thin (< 100 nm) hydrogen-free DLC coatings deposited onto multi-reflection ZnSe IR-ATR waveguides to directly monitor aqueous solutions containing chemically aggressive agents in high concentrations (0.5 – 10 % hydrogen peroxide), without adverse affects to the waveguide substrate.

Electrochemically, the application of non-doped DLC thin films as electrode materials has recently been reported.[18-22] Electrical conductivity in non-doped layers typically originates from the incorporation of a large fraction of sp^2-hybridized carbon (> 60 %). However, graphitic layers are softer, mechanically labile, and more prone to chemical degradation compared to electrically insulating layers containing a higher sp^3-carbon fraction. Introducing modifiers into the DLC matrix typically yields films with improved electrical conductivity while maintaining the superior mechanical and chemical properties of films with high sp^3-carbon contents. Current modification strategies include co-deposition of metallic nanoparticles (e.g. platinum[23], hafnium[24], nickel[25]) or dopants (e.g. nitrogen[26,27]). Introductory reports concerning metal-DLC nanocomposites suggest films containing a high fraction of metal display favorable electrochemical properties.[23] However, use of metal-DLC nanocomposites is deferred if chemical and electrochemical properties associated with sp^3-hybridized carbon electrodes is principally desired.

Application of nitrogen-doped DLC (N-DLC) as thin film electrodes was initially reported by Miller and co-workers[28,29], who demonstrated that tetrahedral amorphous carbon (ta-C) films, doped with ~ 10 % nitrogen, displayed electrochemical properties similar to those of highly boron doped diamond (BDD). In addition, Zeng et al.[30,31] and Lagrini et al.[32,33] independently evaluated the electrochemical properties of hydrogen-free N-DLC, and in their contributions, the $Fe(CN)_6^{4-/3-}$ redox couple exhibited a peak potential separation (ΔE_p) of < 80 mV ($\nu = 0.1$ V/s) for nitrogen concentrations ranging from 5-12 %, confirming the potential of a-C:N films for electrochemical applications. Therefore, favorable electrochemical and spectroscopic properties indicate that hydrogen-free a-C:N thin films can be applied to waveguide substrates as working electrodes for multi-reflection mid-IR-ATR spectroelectrochemistry.

Coating of ZnSe waveguides with a-C:N films can also be performed by pulsed laser deposition (PLD). With this technique laser pulses ablate small sections of a carbon target in a vacuum chamber. The resulting plume is composed of carbon ions, atoms, and clusters, which are projected towards the substrate and condense as a thin film at the substrate surface. This technique provides a straightforward method of incorporating additional elements, resulting in DLC films with tailored properties (e.g. improved hardness[34] or electrical conductivity[27]). Modifiers are included via the ablation of the carbon source in the presence of a reactive gas,[35] by sequentially focusing the laser beam onto different targets[36], or by intimately mixing the carbon source with the desired modifier.[37] Most importantly, substrates are maintained at room temperature, enabling deposition onto temperature sensitive materials, including mid-IR waveguiding materials.

In this contribution, a detailed characterization of the physical and electrochemical properties of a-C:N films deposited via the PLD technique is presented. Implementation of a-C:N thin films as working electrodes is further expanded by coating multi-reflection ZnSe IR-ATR waveguides for improved sensitivity in mid-IR spectroelectrochemical analysis. The potential of N-DLC-based spectroelectrochemistry is finally demonstrated by confirming the formation of carbon-oxygen bonds at anodic potentials as well as monitoring the electro-polymerization process of polyaniline (PANI).

2. EXPERIMENTAL SECTION

2.1. DLC DEPOSITION

A-C:N films were deposited in an industrial scale vacuum chamber which has been described in detail elsewhere.[38] Prior to deposition, the chamber was evacuated to a base pressure of $\sim 4 \times 10^{-5}$ Torr, and then raised to a working pressure $\sim 5 \times 10^{-3}$ Torr as the pre-selected gas mixture (10 sccm N_2 combined with 20 sccm Ar) was flushed through the chamber for the deposition process. Additionally, depositions were performed at varied nitrogen flows from 2.5 to 7.5 sccm N_2 at a total gas flow of 30 sccm. All substrates including reference silicon samples were cleaned by sequential sonication in acetone and ethanol. The samples were fixed on a grounded substrate holding carrousel situated at a distance of approximately 10 cm from the graphite targets. The diameter of this carrousel was 56 cm whereas the samples were fixed at a diameter of 40 cm on vertical columns. Films were deposited by oscillation of the carrousel with an amplitude of 9 cm (left-right) through the PLD plasma. The movement was one-dimensional and perpendicular to the rotating axis of the graphite target. Prior to deposition, the substrates were Ar-plasma-cleaned from residual surface contaminants with the use of an anode layer source from Veeco instruments (Woodbury, NY, USA). The anode layer source was operated at a discharge voltage of 2 kV and an argon flow rate of 20 sccm. A-C:N deposition was achieved by ablation of a graphite target (99.99 %, GfE, Gesellschaft für Elektrometallurgie, Nürnberg, Germany) with a 1064 nm Nd:YAG laser from Continuum (Santa Clara, CA) operating at a repetition rate of 50 Hz with a pulse duration of 10 ns. The film thickness was fixed to 40 nm. For the electrochemical and compositional characterization, a-C:N thin films were deposited onto n-type doped silicon substrates from Nova Electronics (Carrollton, TX, As-doped, $< 0.01\ \Omega$/cm), which were previously backside sputter coated with titanium and gold (total film thickness ~ 300 nm). For spectroelectrochemical analysis, zinc selenide (ZnSe) trapezoidal attenuated total reflectance ATR waveguides (MacroOptica, Moscow, Russia) with dimensions of 50 mm × 20 mm × 2 mm and a 45 ° coupling angle (25 nominal reflections), were coated simultaneously to the doped silicon substrates. The waveguides were appropriately masked to prevent coating of in- and out-coupling facets.

2.2. PHYSICAL AND CHEMICAL CHARACTERISATION

Film thicknesses were determined using a Dektak^3 ST stylus profilometer (Veeco/Sloan Technologies, Santa Barbara, CA). X-ray photoelectron spectroscopy (XPS) data were acquired using a SSX-100 ESCA spectrometer (Surface Science Labs, Mountain View, CA) equipped with a small spot monochromatic Al Kα source (1486.6 eV). General survey spectra (0 to 1100 eV, 1 scan at 1 eV steps, 800 µm spot size, 150 eV pass energy) were recorded to verify surface constituents. High resolution spectra (10 scans at 0.1 eV steps, 400 µm spot size, 50 eV pass energy) were obtained for the carbon and nitrogen 1s peaks. Compositional information about the a-C:N films was obtained via the Analysis 2000 software package (Service Physics Inc., Bend, OR). Infrared spectra were recorded with an Equinox 55 FT-IR spectrometer (Bruker Optics, Billerica, MA) equipped with a broadband liquid nitrogen-cooled mercury-cadmium-telluride (MCT) detector (Infrared Associates, Stuart, FL). Spectra were recorded at a 4 cm^{-1} resolution, and a total of 100 scans were averaged for each collected spectrum.

The film structure was characterized by using a Raman micro-spectrometer from Jobin Yvon (Villeneuve d'Ascq, France) using a frequency doubled Nd-YAG laser operating at an excitation wavelength of λ=532 nm. The power of the laser was maintained below ~1 mW to prevent thermal degradation of the samples. The entrance slit to the spectrometer was set to 100 µm. Light was dispersed by a holographic grating with 1800 grooves mm^{-1}. During analysis, the spectrometer was checked for correct wavenumber calibration by periodic measurement of silicon (520 cm^{-1}), polyethylene (1062, 1128, 1169, 1295, 1487, 1439, 2848, 2881 cm^{-1}), calcite (156, 283, 713, 1087, 1437 cm^{-1}) and diamond (1332 cm^{-1}).

The spectrum fitting was performed using "Peak-Fit" 4.11 from Systat (Point Richmond, CA, USA) using two Gaussian functions for the D- and G-band together with a linear base line correction. The G-peak results from the bond stretching of all pairs of sp^2 sites in rings and chains and the D-peak has its origin in the breathing modes of sp^2 atoms in rings[39]. I_D/I_G ratios were calculated by using band heights. For data treatment, we focused on the spectral features of the D and G-bands neglecting other Raman active modes present at 1100 to 1200 cm^{-1} or 1400 to 1500 cm^{-1} [39].

The vibration frequencies of carbon nitrides lie close to the modes of their nitrogen free analogues, since C–N, and C–C modes have rather similar frequencies [39]. Therefore it is difficult to distinguish between C–C and C-N modes. Instead, an analysis of the trends in the G-band positions and the full width at half maximum of the G-band (FWHM (G)) similar to the nitrogen free analogous is possible in order to derive structural changes in a-C:N films. Following rules are applied for the interpretation of the collected Raman spectra[39]:

(1) The position of the G-band is a probe of the clustering of sp^2 hybridisated phases. For room-temperature deposited a-C:N films, an up-shift of the G-band is indicative for clustering of sp^2 phases when using visible excitation.

(2) The intensity ratio I_D/I_G is a measure of the size of the sp^2 phase organized in rings. If the intensity ratio I_D/I_G becomes lower or zero, the sp^2 phase is organised rather in chains, whereas a higher intensity ratio I_D/I_G is an indication of an increase of the sp^2 phase in aromatic rings.

(3) The FWHM (G) is a key parameter of monitoring structural disorder in any amorphous carbon system for any excitation energy. Structural disorder arises from the bond angle and bond length distortions in DLC. The FWHM (G) is small when sp^2 clusters are more defect-free and ordered and a higher FWHM (G) is thus indicative for an increase in structural disorder.

2.3. ELECTROCHEMICAL CHARACTERISATION

The electrochemical properties of a-C:N films were evaluated using a custom-made three-electrode Teflon cell using a potentiostat (440A CH Instruments, Austin, TX). A 3 M KCl Ag|AgCl reference electrode (+210 mV vs. SHE) was used for studies involving redox mediator, and a saturated Hg|$HgSO_4$ reference electrode (+640 mV vs. SHE) for determining the potential window of the metal-DLC electrodes. The electrochemical cell was completed with a segment of platinum foil as counter electrode, and DLC-coated silicon substrates as the working electrode. A-C:N films were pressed onto the bottom portion of the cell with

the solution being contained by a Viton o-ring, resulting in an exposed geometric area of 0.068 cm^2. 5 mM hexaammineruthenium(III) trichloride/hexaammineruthenium(II) dichloride ($Ru(NH_3)_6^{3+/2+}$) in 0.1 M potassium chloride as supporting electrolyte (Aldrich, St. Louis, MA) were used as reversible redox mediator couples. The working potential windows were determined in 0.5 M solution of sulfuric acid, and 1 M hydrochloric acid (both acids from Fisher Scientific, Fair Lawn, NJ). A-C:N films display semiconducting properties,[40] therefore, all electrochemical experiments were performed in the absence of light, limiting photoconductive effects. All solutions were prepared with deionized water (Millipore Milli-Q, Billerica, MA) with a resistance of 18.2 MΩ·cm at 25ºC, and were sparged with Ar (Airgas, Marietta, GA) for >15 min prior to electrochemical analysis. All chemicals were used as received without further purification. Heterogeneous electron transfer rate constants (k_s), and transfer coefficients (α) were obtained from mathematical fitting of the experimental data using the DigiElch software package[41-43]. Diffusion coefficients used for the oxidized and reduced species were 5.5×10^{-6} cm/s^2 and 9.2×10^{-6} cm/s^2, respectively.[23] Automatic IR compensation, available through the potentiostat software interface, was applied to all voltammetric measurements.

Unless otherwise noted, all potentials herein are presented with respect to a chloridized silver quasi-reference electrode (AgQRE). The ATR spectroelectrochemical experiments were performed in the sample compartment of the infrared spectrometer equipped with a vertical ATR module (Specac, Norcross, GA). The front portion of the flow cell was custom built from poly ether-ether ketone (PEEK) in order to accommodate the AgQRE reference electrode and the platinum foil counter electrode (Figure 1).

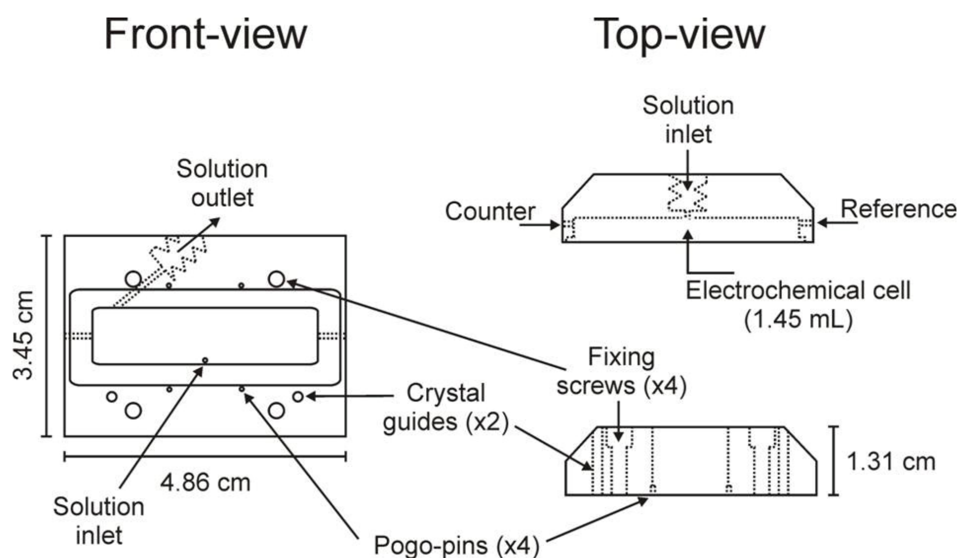

Figure 1. Front- and top-view schematics for multi-reflection ATR spectro-electrochemical cell.

Electrical contact to the a-C:N coated waveguide was achieved by sputtering a thin titanium|gold strip (approx. 1 mm wide, ~ 300 nm total thickness) on the top and bottom portions of the waveguide. Four gold-coated pogo-pins (Emulation Technology, Santa Clara, CA) were then used to connect the sputtered gold contact to the potentiostat. The cell volume is approx. 1.45 mL. Aqueous solutions containing 1.0 M perchloric acid or 0.2 M aniline and 1.0 M perchloric acid were flushed through the PEEK cell for spectroelectrochemical analysis. Electropolymerization of aniline was performed via cyclic voltammetry sweeping from the open circuit potential (+0.015 V) to +1.0 V at a scan rate of 0.002 V/s for a total of 10 cycles.

IR spectra were acquired at 0.2 V intervals simultaneous to the potential sweeping. Acquisition of 100 scans (*i.e.* one spectrum) requires 20 s, therefore, each collected spectrum represents the cumulative spectroscopic signal over a 0.04 V potential range (Figure 2).

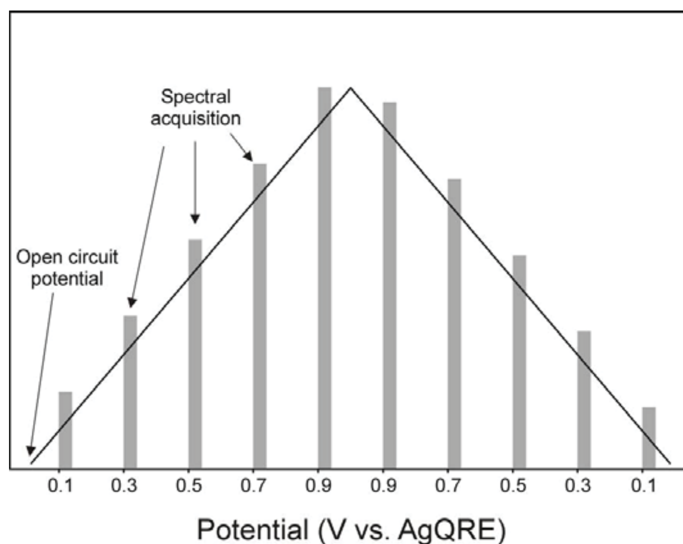

Figure 2. Graphical representation of the triangular potential waveform coupled to spectral acquisition. Each spectrum collected corresponds to the average spectroscopic signal acquired over a 0.040 V potential range.

3. RESULTS AND DISCUSSION

3.1. COMPOSITIONAL ANALYSIS

X-ray photoelectron spectroscopy provides a non-destructive, semi-quantitative approach to the determination of constituents and their oxidation states within the top ~ 5 nm of a material.[44] Scanning the typical binding energy range (*i.e.* 0 to 1100 eV) provides information about the presence of elements in a material's surface. For the deposited a-C:N films, only carbon, nitrogen and adventitious oxygen are detectable (Figure 3). A-C:N films, applied for further spectroelectrochemical studies deposited at 10 sccm N_2 and 20 sccm Ar, typically contain 9.2 ± 0.9 at. % nitrogen.

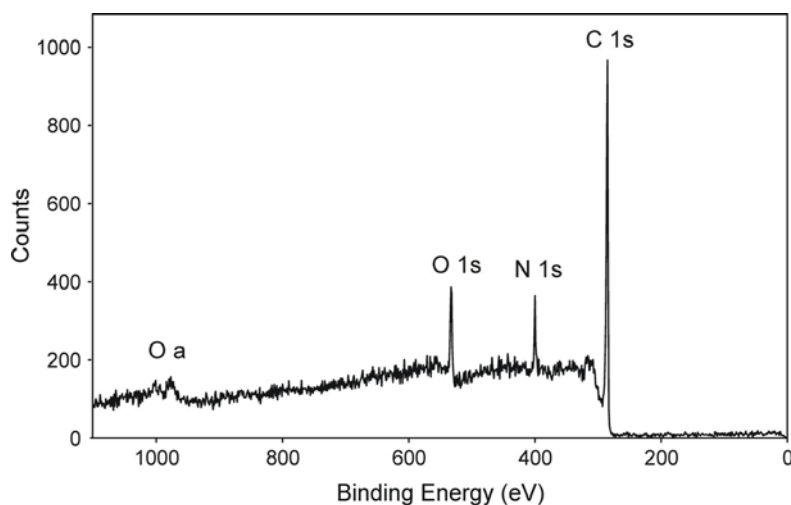

Figure 3. Exemplary XPS general survey scan of a-C:N films. Peaks corresponding to detectable elements have been labeled for clarity.

XPS has also been widely adopted as a means of quantifying the hybridization state of the carbon matrix, as the physical and chemical properties displayed by DLC films are intimately related to the fraction of

sp^3-hybridized carbon.[45] The carbon 1s photoemission peak of non-doped DLC is commonly deconstructed into sp^2- (BE = 284.4 ± 0.1 eV) and sp^3-hybridization (BE = 285.2 ± 0.1 eV), and carbon bonded to adventitious oxygen (BE ~ 286.5 eV).[45,46] However, contributions from bonding of nitrogen to both sp^2- and sp^3-carbon further complicates deconvolution of the carbon peak, resulting in ambiguous values.[48-50]

Our observation of an increasing G-band position (for 532 nm excitation wavelength) from 1543±2 cm^{-1} for the film deposited without N_2 to 1557±1 cm^{-1} for the film synthesized in the highest N_2 concentration in the PLD plasma can be interpreted as an ordering effect of sp^2 phases. The up-shift of the G-band is indicated with a dotted line in Figure 4a. An I_D/I_G ratio of 0.66 was calculated for the films deposited without N_2 in the deposition plasma. Increasing the N_2 concentration in the PLD plasma stepwise to 33 %, yields an increased size of the sp^2-phase in the film matrix, verified by an increased I_D/I_G-ratio of 1.0. Figure 4a shows the increase in the D-band intensity with increasing N_2 concentration in the deposition plasma. Additionally, ordering of the sp^2-phases with increasing nitrogen concentration in the deposition plasma was evidenced by the decreasing FWHM (G). Structural ordering induced the FWHM (G) to decrease from 184±0.1 cm^{-1}, indicative of a higher sp^3 content, to 159±0.1 cm^{-1} indicative of a higher percentage of sp^2-hybridized carbons and higher structural order in the films. The systematic variation of the G-band position as well as the variation of the FWHM (G) with the nitrogen concentration in the chamber is remarkable (Figure 4b).

The a-C:N films with highest structural order and highest nitrogen content were used in the spectroelectrochemical studies, due to their combination of high diamond-like character while maintaining a significant fraction of electrically conductive sp^2-hybridized carbon clusters.

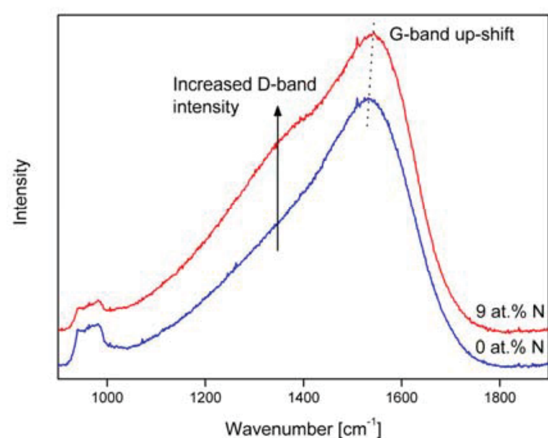

Figure 4a. Raman spectra as a function of the nitrogen concentration in the films. The used N_2 concentrations in the chamber were 0 and 33 %. The small features around 900 cm^{-1} originate from the silicon substrate.

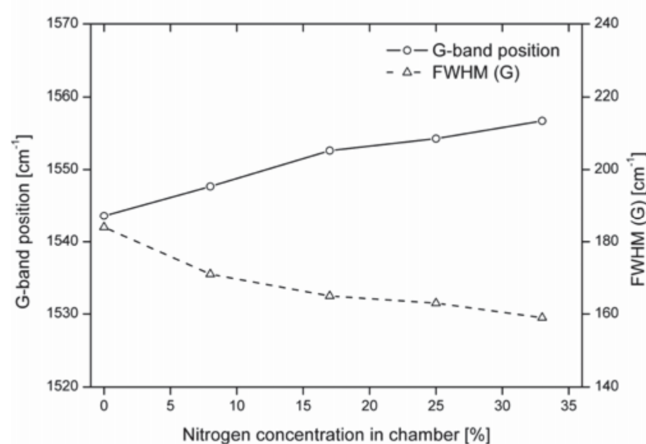

Figure 4b. Position of the G-band and FWHM (G) as a function of the N_2 concentration in the PLD carbon plasma.

3.2. ELECTROCHEMICAL ANALYSIS

Working potential windows measured at a-C:N films in different media are summarized graphically in Figure 5. Selection of the potential range between current density limits of ±200 μA/cm^2 yields potential

windows of 2.8 V and 1.9 V for 0.5 M H_2SO_4 and 1 M HCl, respectively. These values are larger than those reported for purely sp^2-hybridized materials, such as glassy carbon[51], highly oriented pyrolitic graphite[52] and pyrolized photoresist films.[53] In contrast, electrode materials containing very high fractions of sp^3-hybridized carbon (e.g. BDD, ta-C) are commonly characterized by working potential windows in excess of 3 V.[28,54] Gas evolution at carbon-based electrodes involves adsorption of reaction intermediates onto sp^2-sites,[52,55] hence, the narrower potential range displayed by the a-C:N films is indicative of a comparatively higher sp^2-hybridized carbon content. Finally, potential sweeping in 1 M HCl reveals the electrocatalytic Cl_2/Cl^- redox couple wave at approx. +0.7 V, similar to previous reports on a-C:N films.[28,31]

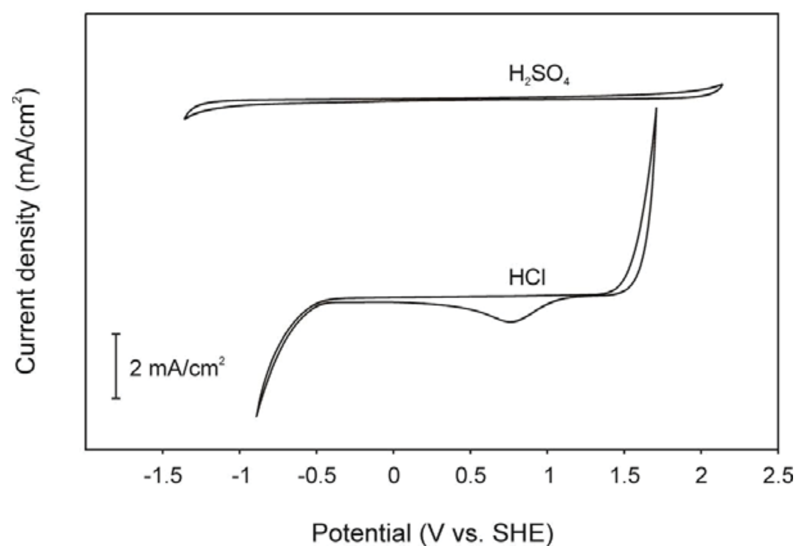

Figure 5. Cyclic voltammograms depicting the working potentials windows obtained at a-C:N electrodes in 0.5 M H_2SO_4 and 1 M HCl.

Additional evidence regarding sp^2-content is presented by the measured charging currents during cyclic voltammetric analysis. Several sp^2-hybridized carbon electrodes display values that range between 20 and 120 $\mu F/cm^2$,[56-58] depending on the type of electrode. In contrast, BDD electrodes are routinely reported to exhibit charging currents of approx. 5 $\mu F/cm^2$.[54] A-C:N films display charging currents of approx. 17 $\mu F/cm^2$ in 0.1 M KCl (ν = 100 V/s) over the potential range between +0.11 V and +0.91 V, suggesting that the a-C:N surface contains a significant amount of sp^2-hybridized carbon. Slightly higher background current values (approx. 29 $\mu F/cm^2$) are recorded over the same potential range in 0.5 M H_2SO_4. Increased current values at carbon electrodes in acidic media are commonly attributed to the formation of additional superficial carbon-oxygen moieties.[56]

Testing the electrochemical performance of novel electrode materials typically involves the use of quasi-reversible redox couples. $Fe(CN)_6^{4-/3-}$ is among the most widely utilized redox couples, however, despite its electron transfer being commonly attributed to an outer-sphere mechanism, at carbon electrodes electron transfers are complicated by changes in electrolyte and electrode history.[59-61] Instead, a-C:N films presented here are evaluated versus $Ru(NH_3)^{2+/3+}$, since this redox couple does not display electrode dependencies to the same extent as $Fe(CN)_6^{4-/3-}$.[56,61] Under ideal conditions, fully reversible heterogeneous electron transfer reactions are characterized by a potential separation between the anodic and cathodic peaks (ΔE_p) of 59 mV/n, where n equals the number of moles of electrons transferred. In addition, the rate at which heterogeneous electron transfers (k^o) occur can be derived from ΔE_p values, where values larger than 59 mV/n are indicative

of hindered electron transfers and commonly reported for carbon-based electrodes.[61, 62] ΔE_p and k^o values measured at a-C:N films for the $Ru(NH_3)^{2+/3+}$ couple are 72 ±2 mV (scan rate, $\nu = 0.1$ V/s, $N = 3$) and $2.3 \pm 0.5 \times 10^{-2}$ cm/s, respectively, suggesting that electron transfers occur at rates comparable to those reported for other carbon electrodes.[62]

3.3. SPECTROCHEMICAL ANALYSIS

Coating of a-C:N films onto pristine multi-reflection zinc selenide (ZnSe) attenuated total reflection (ATR) waveguides resulted in a decrease of approx. 40 % of the propagated radiation. Deposition of the titanium|gold strips on the top and bottom portions of the waveguide resulted in only a minor additional reduction of the optical throughput, as radiation is mostly confined to the central portion of waveguide.[63] Hence, despite substantial modification of the waveguide surface, its optical transparency remains sufficient for spectroelectrochemical measurements (Figure 6).

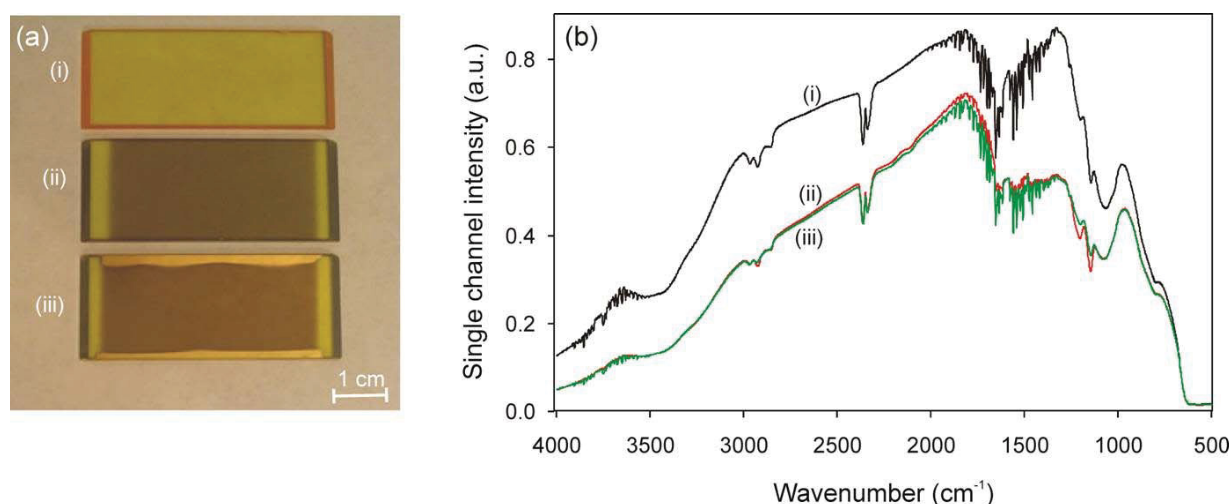

Figure 6. (a) Optical photograph of (i) bare, (ii) a-C:N coated and (iii) a-C:N coated with titanium|gold strip ZnSe waveguides. **(b)** Mid-infrared transparency of bare and modified ZnSe waveguides.

IR spectra of coated waveguides are characterized by a broad absorption feature ranging from approx. 1650 to 1000 cm^{-1}. This band is characteristic of a-C:N films with higher sp^2-carbon fractions, and is commonly assigned to the delocalization of π electron density of conjugated C=C bonds in sp^2-carbon clusters in combination with C=N bonds, which display absorption features in the similar wavelengths range.[64-66]

Upon filling the spectroelectrochemical cell with 1 M $HClO_4$, absorption bands related to water (3330 cm^{-1}, 1637 cm^{-1}, shoulder < 950 cm^{-1}) and ClO_4^- (1103 cm^{-1}) are easily identified. Potential sweeping from the open circuit potential (+0.015 V) to +1.0 V resulted in an increased ClO_4^- absorption band and a concomitant decrease in the water bands. Although it is anticipated that charge compensation by the anion will induce a change in the spectral signature,[67] potential sweeping in the reverse direction does not yield the initial IR spectrum. Ex-situ XPS analysis of carbon electrodes has shown that additional carbon-oxygen bonds form at surfaces exposed to anodic potentials in acidic media.[68, 69] Continuous collection of IR spectra over several cyclic voltammograms shows that additional bands ranging between 1750 cm^{-1} and 1250 cm^{-1} increase in intensity, ultimately stabilizing after approx. ten cycles. Absorbance features in this spectroscopic range are

characteristic of carbon-oxygen functionalities (Figure 7), thereby confirming previous XPS analysis. Spectral contributions from nitrogen-oxygen functionalities may also be present, since NO groups absorb in the same wavelength region as CO groups.[70] Hence, spectral evidence indicates that the observed rearrangement of the electrochemical double layer which resulted in the influx of anions within the d_p, is also related to superficial changes at the carbon electrode.

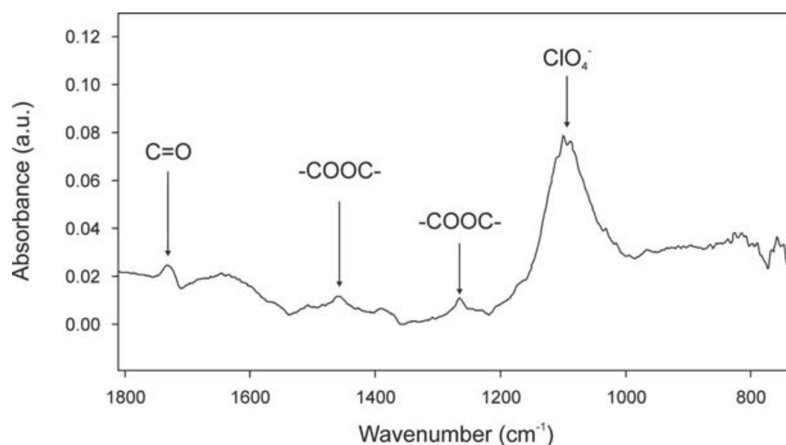

Figure 7. IR-ATR absorption spectrum of a-C:N coated waveguide after potential cycling in 1.0 M $HClO_4$ between +0.015 V and +1.0 V for 10 cycles.

The spectroelectrochemical capabilities of the N-DLC-IR-ATR configuration was further verified by monitoring the electropolymerization process of 0.2 M aniline in 1.0 M $HClO_4$. Polymer growth can be achieved by repetitive cycling between the open circuit potential to +1.0 V.[70] Immediately upon completion of the first cycle, several absorption bands appear, with subsequently increasing in intensity with each voltammetric cycle (Figure 8).

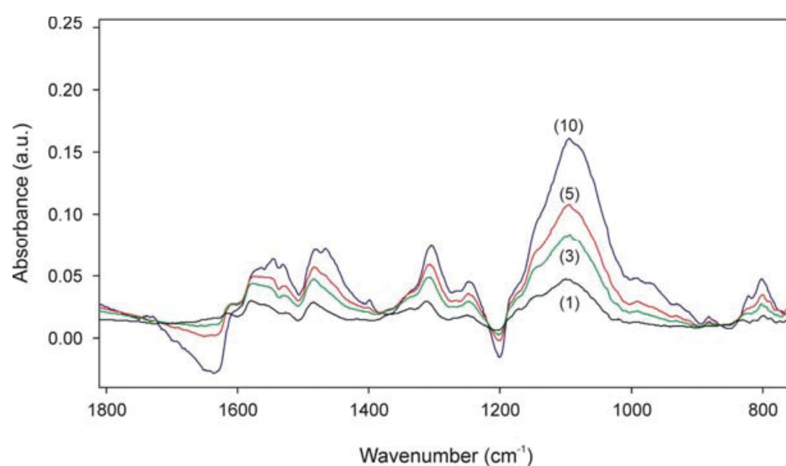

Figure 8. IR-ATR absorption spectrum depicting several peaks associated with the electropolymerization of PANI increasing in intensity with each voltammetric cycle.

Other potential-dependent changes to the polymer are shown in Figure 9. The most evident spectroscopic changes correspond to water (centered at approx. 3340 cm^{-1}, Figure 9 (a)) and the combination $ClO_4^-/C{=}N_{quinoid}$ (1103 cm^{-1}, with a shoulder at 1140 cm^{-1} Figure 9 (b))[71] bands. Increasing intensities for these bands are observed at potentials above +0.5 V and are subsequently decreasing during the reverse sweep. The measured trend for the combination $ClO_4^-/C{=}N_{quinoid}$ band is related to the uptake and expulsion of the anion into the PANI matrix (*i.e.* doping and de-doping) occurring at high potentials.[73] However, decreasing negative absorbances of water appears to be counterintuitive if the polymer grows. Therefore displacement of water molecules from the d_p is considered.

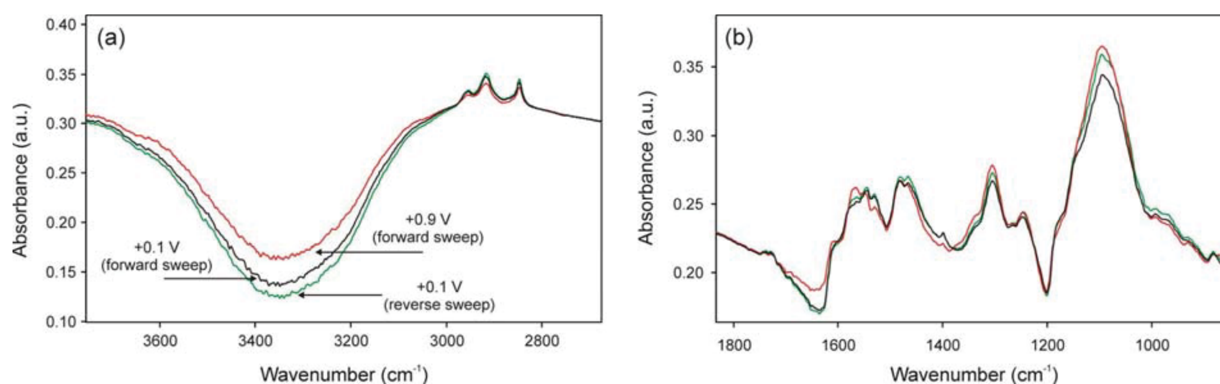

Figure 9. IR-ATR absorption spectrum illustrating spectral changes of **(a)** water and aromatic C-H stretching modes and **(b)** ClO_4^- as well as additional bands assigned to PANI during the 10th potential cycle.

The observed effect can be attributed to (1) oxidation-induced swelling of the polymer, thereby facilitating diffusion of water molecules,[74] and (2) the hydration sphere associated with dissolved anions and cations, hence, as anions are incorporated by the polymer, water is also included.[75,76] Swelling of PANI in its oxidized form (pernigraniline) is additionally confirmed through the decreasing intensity of the aromatic C–H stretching modes (2980 – 2830 cm^{-1}, Figure 9 (a)), which originates from a decreased interaction of the swollen polymer with the evanescent field. Furthermore, oxidation of PANI also results in additional clearly identifiable spectral changes, such as the conversion of benzenoid (1530 cm^{-1}) to quinoid groups (1565 cm^{-1}, 1304 cm^{-1}).[71,73,77] The relative spectral intensity of the bands associated with each group cycles in relation to the applied potential. That is, greater benzenoid contributions are measured at +0.1 V whereas quinoid contributions become dominant at +0.9 V (Figure 9 (b)). Spectral features corresponding to N–H stretching modes (approx. 3300 cm^{-1}), commonly used for determination of doping level,[73] are buried by the broad water band, and are not currently accessible. In addition, consistent with the ongoing electropolymerization process, and therefore polymer growth, the spectral features described typically display higher intensities at the end of each potential cycle, indicating that a-C:N films can be applied as OTEs to monitor electrochemical events via multi-reflection IR-ATR spectroelectrochemistry.

4. CONCLUSIONS

Laser ablation of high-purity graphite targets in the presence of nitrogen gas yields electrically conducting films, while maintaining favorable optical qualities in the mid-IR range. XPS analysis indicated that films deposited following the conditions described contain approx. 9 at.% nitrogen, while Raman spectroscopy suggests that the addition of nitrogen as reactive gas resulted in a clustering of sp^2 sites in the films. Measurements with the $Ru(NH_3)^{3+/2+}$ redox couple confirm that an electrochemical activity comparable to other carbon electrodes is achieved. Finally, the formation of carbon-oxygen functionalities at anodic potentials in acidic media was demonstrated by in-situ spectroelectrochemical studies, providing confirmation to previously reported ex-situ XPS analysis. The spectroelectrochemical potential of the setup described was further investigated by monitoring the electropolymerization process (*i.e.* growth) of polyaniline, as well as the reversible changes associated with conversion between the different forms of polyaniline. In particular, this study demonstrates that thin a-C:N films can be applied as novel electrode materials to multi-reflection IR-ATR spectroelectrochemistry.

ACKOWLEDGEMENTS

H. Shin, J.-S. Moon and G. Dobbs are gratefully acknowledged for assistance in deposition of titanium|gold films and fruitful scientific discussions. Financial support from the ExxonMobil Research and Engineering Company in Annandale, NJ (B.M. and N.M.) and financial support by the Austrian Federal Ministry of Traffic, Innovation and Technology, the Austrian Industrial Research Promotion Fund (FFG), the Government of Styria, Forschung Austria and the European Union is highly acknowledged.

REFERENCES

(1) Gale, R. J.; Editor, *Spectroelectrochemistry: Theory and Practice*. Plenum Press: New York, 1988; p 450.

(2) Christensen, P. A., *Encyclopedia of Electrochemistry* **2003,** *3*, 530-571.

(3) Flowers, P. A.; Callender, S.-A., *Anal. Chem.* **1996,** *68 (1)*, 199-202.

(4) Korzeniewski, C.; Pons, S., *Journal of Vacuum Science & Technology, B: Microelectronics and Nanometer Structures* **1985,** *3 (5)*, 1421-4.

(5) Harrick, N. J., *Internal Reflection Spectroscopy*. 1967; p 327 pp.

(6) Higashiyama, T.; Takenaka, T., *J. Phys. Chem.* **1974,** *78 (9)*, 941-7.

(7) Reed, A. H.; Yeager, E., *Electrochim. Acta* **1970,** *15 (8)*, 1345-54.

(8) Zimmermann, A.; Kunzelmann, U.; Dunsch, L., *Synth. Met.* **1998,** *93 (1)*, 17-25.

(9) Ping, Z.; Neugebauer, H.; Neckel, A., *Synth. Met.* **1995,** *69 (1-3)*, 161-2.

(10) Neugebauer, H.; Moser, A.; Strecha, P.; Neckel, A., *J. Electrochem. Soc.* **1990,** *137 (5)*, 1472-5.

(11) Bae, I. T.; Sandifer, M.; Lee, Y. W.; Tryk, D. A.; Sukenik, C. N.; Scherson, D. A., *Anal. Chem.* **1995,** *67 (24)*, 4508-13.

(12) Zippel, E.; Kellner, R.; Breiter, M. W., *J. Electroanal. Chem. Interfac.* **1990,** *289 (1-2)*, 297-8.

(13) Mattson, J. S.; Smith, C. A., *Anal. Chem.* **1975,** *47 (7)*, 1122-5.

(14) Martin, H. B.; Morrison, P. W., Jr., *Electrochem. Solid-State Lett.* **2001,** *4 (4)*, E17-E20.

(15) Robertson, J., *Adv. Phys.* **1986,** *35 (4)*, 317-74.

(16) Janotta, M.; Rudolph, D.; Kueng, A.; Kranz, C.; Voraberger, H.-S.; Waldhauser, W.; Mizaikoff, B., *Langmuir* **2004,** *20 (20)*, 8634-8640.

(17) Janotta, M.; Vogt, F.; Voraberger, H.-S.; Waldhauser, W.; Lackner Jurgen, M.; Stotter, C.; Beutl, M.; Mizaikoff, B., *Anal. Chem.* **2004,** *76 (2)*, 384-91.

(18) Schnupp, R.; Kuhnhold, R.; Temmel, G.; Burte, E.; Ryssel, H., *Biosens. Bioelectron.* **1998,** *13 (7-8)*, 889-894.

(19) Bouamrane, F.; Kautek, W.; Sahre, M.; Tadjeddine, A.; Rzepka, E.; Levy-Clement, C., *Proc. - Electrochem. Soc.* **1998,** *97-32 (Proceedings of the International Symposium on Diamond Materials, 5th, 1997)*, 309-323.

(20) Moon, J.-M.; Park, S.; Lee, Y.-K.; Sook Bang, G.; Hong, Y.-K.; Park, C.; Cheol Jeon, I., *J. Electroanal. Chem.* **1999,** *464 (2)*, 230-237.

(21) Niwa, O.; Jia, J.; Sato, Y.; Kato, D.; Kurita, R.; Maruyama, K.; Suzuki, K.; Hirono, S., *J. Am. Chem. Soc.* **2006,** *128 (22)*, 7144-7145.

(22) You, T.; Niwa, O.; Horiuchi, T.; Tomita, M.; Iwasaki, Y.; Ueno, Y.; Hirono, S., *Chem. Mater.* **2002,** *14 (11)*, 4796-4799.

(23) Menegazzo, N.; Jin, C.; Narayan, R. J.; Mizaikoff, B., *Langmuir* **2007,** *23 (12)*, 6812-6818.

(24) Sunkara, M. K.; Chandrasekaran, H.; Koduri, P., *New Diamond Front. Carbon Technol.* **1999,** *9 (6)*, 407-415.

(25) Maalouf, R.; Chebib, H.; Saikali, Y.; Vittori, O.; Sigaud, M.; Garrelie, F.; Donnet, C.; Jaffrezic-Renault, N., *Talanta* **2007,** *72 (1)*, 310-314.

(26) Liu, L. X.; Liu, E., *Surf. Coat. Technol.* **2005,** *198 (1-3)*, 189-193.

(27) Arena, C.; Kleinsorge, B.; Robertson, J.; Milne, W. I.; Welland, M. E., *Diamond Relat. Mater.* **1999,** *8 (2-5)*, 435-439.

(28) Yoo, K.; Miller, B.; Kalish, R.; Shi, X., *Electrochem. Solid-State Lett.* **1999,** *2 (5)*, 233-235.

(29) Yee, N. C.; Shi, Q.; Cai, W.-B.; Scherson, D. A.; Miller, B., *Electrochem. Solid-State Lett.* **2001,** *4 (10)*, E42-E44.

(30) Zeng, A.; Liu, E.; Tan, S. N.; Zhang, S.; Gao, J., *Electroanalysis* **2002,** *14 (18)*, 1294-1298.

(31) Zeng, A.; Liu, E.; Tan, S. N.; Zhang, S.; Gao, J., *Electroanalysis* **2002,** *14 (15-16)*, 1110-1115.

(32) Lagrini, A.; Charvet, S.; Benlahsen, M.; Cachet, H.; Deslouis, C., *Diamond Relat. Mater.* **2007,** *16 (4-7)*, 1378-1382.

(33) Lagrini, A.; Charvet, S.; Benlahsen, M.; Debiemme-Chouvy, C.; Deslouis, C.; Cachet, H., *Thin Solid Films* **2005,** *482 (1-2)*, 41-44.

(34) Voevodin, A. A.; Zabinski, J. S., *Diamond Relat. Mater.* **1998,** *7 (2-5)*, 463-467.

(35) Voevodin, A. A.; Jones, J. G.; Back, T. C.; Zabinski, J. S.; Strel'nitzki, V. E.; Aksenov, I. I., *Surf. Coat. Technol.* **2005,** *197 (1)*, 116-125.

(36) Narayan, R. J., *Diamond Relat. Mater.* **2005,** *14 (8)*, 1319-1330.

(37) Rusop, M.; Soga, T.; Jimbo, T.; Umeno, M.; Sharon, M., *Surf. Rev. Lett.* **2005,** *12 (4)*, 579-586.

(38) Lackner, J. M., *Surf. Coat. Technol.* **2005,** *200 (5-6)*, 1439-1444.

(39) A.C. Ferrari, J. Robertson, Phil. Trans. R. Soc. Lond. A, 362 (2004) 2477.

(40) Robertson, J., *Semicond. Sci. Technol.* **2003,** *18 (3)*, S12-S19.

(41) Rudolph, M., *J. Electroanal. Chem.* **2003,** *543 (1)*, 23-39.

(42) Rudolph, M., *J. Electroanal. Chem.* **2004,** *571 (2)*, 289-307.

(43) Rudolph, M., DigiElch 2.0, http://www.elchsoft.com/ accessed on May 15, 2007.

(44) Briggs, D.; Seah, M. P.; Editors, *Practical Surface Analysis by Auger and X-ray Photoelectron Spectroscopy*. 1983; p 533.

(45) Robertson, J., *Materials Science & Engineering, R: Reports* **2002,** *R37 (4-6)*, 129-281.

(46) Merel, P.; Tabbal, M.; Chaker, M.; Moisa, S.; Margot, J., *Appl. Surf. Sci.* **1998,** *136 (1/2)*, 105-110.

(47) Diaz, J.; Paolicelli, G.; Ferrer, S.; Comin, F., *Phys. Rev. B: Condens. Matter* **1996,** *54 (11)*, 8064-8069.

(48) Tabbal, M.; Merel, P.; Moisa, S.; Chaker, M.; Ricard, A.; Moisan, M., *Appl. Phys. Lett.* **1996,** *69 (12)*, 1698-1700.

(49) Riedo, E.; Comin, F.; Chevrier, J.; Bonnot, A. M., *J. Appl. Phys.* **2000,** *88 (7)*, 4365-4370.

(50) Xu, W.; Fujimoto, T.; Wang, L.; Ohchi, T.; Kojima, I., *J. Vac. Sci. Technol., B: Microelectron. Nanometer Struct.--Process., Meas., Phenom.* **2004,** *22 (1)*, 6-11.

(51) Barbero, C.; Silber, J. J.; Sereno, L., *J. Electroanal. Chem. Interfac.* **1988,** *248 (2)*, 321-40.

(52) Martin, H. B.; Argoitia, A.; Landau, U.; Anderson, A. B.; Angus, J. C., *J. Electrochem. Soc.* **1996,** *143 (6)*, L133-L136.

(53) Donner, S.; Li, H.-W.; Yeung Edward, S.; Porter Marc, D., *Anal. Chem.* **2006,** *78 (8)*, 2816-22.

(54) Swain, G. M., Electrically Conducting Diamond Thin Films: Advanced Electrode Materials for Electrochemical Technologies. In *Electroanalytical Chemistry*, Bard, A. J., Ed. Marcel Dekker, Inc.: New York, 2004; Vol. 22, pp 181-277.

(55) Bennett, J. A.; Wang, J.; Show, Y.; Swain, G. M., *J. Electrochem. Soc.* **2004,** *151 (9)*, E306-E313.

(56) McCreery, R. L., *Carbon Electrodes: Structural Effects on Electron Transfer Kinetics*. Marcel Dekker, Inc.: New York, 1991; Vol. 17, p 221-374.

(57) Jia, J.; Kato, D.; Kurita, R.; Sato, Y.; Maruyama, K.; Suzuki, K.; Hirono, S.; Ando, T.; Niwa, O., *Anal. Chem.* **2007,** *79 (1)*, 98-105.

(58) Ranganathan, S.; McCreery, R. L., *Anal. Chem.* **2001,** *73 (5)*, 893-900.

(59) Jordan, J.; Ewing, G. J., *Inorg. Chem.* **1962,** *1*, 587-91.

(60) Compton, R. G.; Foord, J. S.; Marken, F., *Electroanalysis* **2003,** *15 (17)*, 1349-1363.

(61) Chen, Q.; Swain, G. M., *Langmuir* **1998,** *14 (24)*, 7017-7026.

(62) Granger, M. C.; Witek, M.; Xu, J.; Wang, J.; Hupert, M.; Hanks, A.; Koppang, M. D.; Butler, J. E.; Lucazeau, G.; Mermoux, M.; Strojek, J. W.; Swain, G. M., *Anal. Chem.* **2000,** *72 (16)*, 3793-3804.

(63) Dobbs, G. T.; Mizaikoff, B., *Appl. Spectrosc.* **2006,** *60 (6)*, 573-583.

(64) Ferrari, A. C.; Rodil, S. E.; Robertson, J., *Phys. Rev. B: Condens. Matter Mater. Phys.* **2003,** *67 (15)*, 155306/1-155306/20.

(65) Victoria, N. M.; Hammer, P.; dos Santos, M. C.; Alvarez, F., *Phys. Rev. B: Condens. Matter Mater. Phys.* **2000,** *61 (2)*, 1083-1087.

(66) Lazar, G.; Zellama, K.; Vascan, I.; Stamate, M.; Lazar, I.; Rusu, I., *Journal of Optoelectronics and Advanced Materials* **2005,** *7 (2)*, 647-652.

(67) Bard, A. J.; Faulkner, L. R., *Electrochemical Methods: Fundamentals and Application*. 2nd ed.; John Wiley & Sons, Inc.: New York, 2001.

(68) Kozlowski, C.; Sherwood, P. M. A., *Journal of the Chemical Society, Faraday Transactions 1: Physical Chemistry in Condensed Phases* **1984,** *80 (8)*, 2099-107, 4 plates.

(69) Ilangovan, G.; Pillai, K. C., *Langmuir* **1997,** *13 (3)*, 566-575.

(70) Pavia, D.; Lampman, G.; Kriz, G., *Introduction to Spectroscopy*. 2nd ed.; Saunders College Publishing: 1996; p 512.

(71) Zimmermann, A.; Dunsch, L., *J. Mol. Struct.* **1997,** *410-411*, 165-171.

(72) Sariciftci, N. S.; Kuzmany, H.; Neugebauer, H.; Neckel, A., *J. Chem. Phys.* **1990,** *92 (7)*, 4530-9.

(73) Hatchett, D. W.; Josowicz, M.; Janata, J., *J. Phys. Chem. B* **1999,** *103 (50)*, 10992-10998.

(74) Pile, D. L.; Zhang, Y.; Hillier, A. C., *Langmuir* **2006,** *22 (13)*, 5925-5931.

(75) Jencks, W. P., Catalysis in Chemistry and Enzymology. In *Mcgraw-hill series in advanced chemistry*, McGraw-Hill: New York, 1969; pp 351-392.

(76) Wei, Z.-F.; Zhang, Y.-H.; Zhao, L.-J.; Liu, J.-H.; Li, X.-H., *J. Phys. Chem. A* **2005,** *109 (7)*, 1337-1342.

(77) Neugebauer, H.; Neckel, A.; Sariciftci, N. S.; Kuzmany, H., *Synth. Met.* **1989,** *29 (1)*, E185-E192.

9. APPENDIX-EXPERIMENTAL DETAILS

9.1. DLC FILM DEPOSITION

9.1.1. Ion beam deposition of ta-C:H films

For deposition of ta-C:H and ta-C:H:N films, an ALS340L anode layer source from Veeco Instruments (Fort Collins, CO, USA) was fed with 10, 20 or 30 sccm C_2H_2 (nominal purity >99.96 %). The gas was directly introduced into the discharge channel. The anode layer source was powered with a high voltage DC power supply from Glassman High Voltage (High Bridge, NJ, USA) in the voltage controlled mode. Discharge voltages ranging from 1 to 3 kV were applied to the anode. Samples were fixed on a grounded substrate holding carrousel situated at a distance of approximately 15 cm from the ion source. The diameter of this carrousel was 56 cm whereas the samples were fixed at a diameter of 40 cm on vertical static columns. No substrate bias was used during the depositions. For lateral mappings to investigate the film thickness uniformity as well as structural uniformity, 20 silicon wafers (1 cm broadness with a gap of ~0.9 cm) were mounted horizontally at a distance of 15 cm from the source. For angle of incidence investigations, 10 wafers were mounted from 0 (perpendicular to the beam) to 90° (parallel to the beam) on a substrate holding device. The substrate holder was kept static in front of one beam of the anode layer source. In general, films were deposited in three ways: in static mode, by oscillation of the carrousel with an amplitude of 9 cm (left-right), and by rotation around the vertical axis of the carrousel. The movement was in all cases one-dimensional and perpendicular to the ion beams of the linear anode layer source. The substrate temperature was monitored with an electrically insulated K-type thermocouple installed at the backside of the substrate holder. For plasma cleaning of the wafers prior to deposition, the ion source was operated at a voltage of 2 kV and an Ar (nominal purity >99.999 %) flow rate of 20 sccm through the ion gun, resulting in a power density of 2.8 Wcm^{-1} (power on the anode layer source per cm of the discharge channel). For all depositions, the chamber was evacuated to a base pressure of $\leq 5 \cdot 10^{-5}$ mbar. During deposition, the pressure in the chamber ranged from $1 \cdot 10^{-3}$ mbar to $1.5 \cdot 10^{-3}$ mbar via introducing 10 to 30 sccm C_2H_2.

9.1.2. Magnetron sputtering deposition of a-C and a-C:H films

For deposition of quasi non-hydrogenated (a-C) and a-C:H films, a balanced magnetron cathode from AJA (AJA International, North Scituate, MA, USA) equipped with a graphite target (size: 432×74×7 mm^3, nominal purity >99.95 %) was used. The magnetron cathode was powered with a 10 kW power supply from Advanced Energy (Advanced Energy Industries, Fort Collins, CO, USA) in the power regulation mode. The pulsing unit was set to 80 kHz, where a reverse voltage of 15 % with a reverse time of 1 µs was used. A power density of ~10 Wcm^{-2} was applied on the carbon target for all depositions. For deposition of a-C:H films, C_2H_2 (nominal purity >99.96 %) was introduced in the coating chamber together with Ar (nominal purity >99.999 %) resulting in C_2H_2 concentrations between 0 and 30 % (v/v). For deposition of the a-C coatings, a total flow of 30 sccm Ar was used. Samples were fixed on a grounded substrate holding carrousel situated at a distance of approximately 10 cm from the sputtering source. The diameter of this carrousel was 56 cm whereas the samples were fixed at a diameter of 40 cm on vertical columns. In order to study the influence of substrate bias, a Heiden (Pürgen, Germany) bias power supply was connected to the carrousel. Films were deposited by

oscillation of the carrousel with an amplitude of 9 cm (left-right) symmetrically through the sputtering plasma. The movement was in all cases one-dimensional and perpendicular to the major axis of the rectangular magnetron cathode. The substrate temperature was monitored with an electrically insulated K-type thermocouple installed at the backside of the substrate holder. For plasma cleaning of the wafers prior to deposition, an ALS 340 linear ion beam source from Veeco (Fort Collins, CO, USA) was operated at a discharge voltage of 2 kV with an Ar flow rate of 20 sccm through the ion gun. For all depositions, the chamber was evacuated to a base pressure of $<5\cdot10^{-5}$ mbar. During deposition and plasma etching, the pressure in the chamber ranged from $1\cdot10^{-3}$ to $5\cdot10^{-3}$ mbar.

9.1.3. Reactive magnetron sputtering deposition of Si-a-C:H films

For deposition of Si-a-C:H films an unbalanced three inch magnetron from AJA (North Scituate, MA, USA) was powered with a RF power supply working at 13.56 MHz type CESAR model 136 from Dressler (Dressler, Germany). A slightly boron doped silicon target (100) was used for all depositions. For sputtering, the power density on the target was set to 6.7 Wcm^{-2}. As process gases C_2H_2 (nominal purity <99.96 %) and Ar (nominal purity <99.999 %) were used. The total flow was in all cases 50 sccm, whereas the C_2H_2 concentration in the chamber was varied from 0 to 10 %. During deposition, the pressure in the chamber was $\sim2\cdot10^{-3}$ mbar. Samples were fixed on a grounded substrate holding device situated at a distance of 10 cm from the magnetron. Films were deposited on the wafers by rotation around the vertical axis of the grounded plate from the substrate-holder. The diameter of this plate was 30 cm whereas the samples were fixed at a diameter of 20 cm. The movement was in all cases one-dimensional and in plane to the sputtering magnetron. The substrate temperature was monitored with a K-type thermocouple immediately after each run. For plasma cleaning the wafers from contaminants, a discharge voltage of -450 V was applied to the substrate holding device at an Ar flow of 30 sccm. For all depositions the chamber was evacuated to a base pressure of $\leq3\cdot10^{-5}$ mbar.

9.1.4. Reactive magnetron sputtering deposition of a-C and a-C:N films

For DC magnetron sputtering an unbalanced three inch cathode from AJA (AJA International, North Scituate, MA, USA) equipped with a high purity graphite target (nominal purity >99.999 %) (Alfa Aesar, Ward Hill, MA, USA) was used. The cathode was powered with a DC power supply (Advanced Energy Industries, Fort Collins, CO, USA) in power regulation mode. Power densities between ~6.7 Wcm^{-2} and ~20 Wcm^{-2} were applied to the carbon sputtering target resulting in voltages between -600 V and -700 V. Ar (nominal purity >99.999 %) and N_2 (nominal purity >99.999 % nitrogen) from Air Liquide (Air Liquide, Paris, France) were used. The substrates were fixed on a static, floating potential substrate holding device kept at approximately 10 centimetres away from the sputtering target. The substrate temperature was consequently monitored with an electrically insulated K-type thermocouple installed at the backside of the substrate holder. In order to clean the substrates from residual surface contaminants, a mild plasma etching procedure was applied (using 20 sccm of Ar and a voltage of -600 V) with a DC bias power supply (Advanced Converters, Zielonka, Poland). For the deposition the chamber was pumped down to a base pressure of $4\cdot10^{-5}$ mbar. Ar and N_2 were introduced into the vacuum chamber with varying percentages resulting in pressures between $1.3\cdot10^{-3}$ mbar and $3.4\cdot10^{-3}$ mbar which correspond to a total gas flow of 20 and 65 sccm.

9.1.5. UV-PLD of ta-C films

A-C and ta-C films were deposited by KrF excimer laser PLD at 248 nm using a Coherent LPX Pro 305i laser (Coherent Incorporated, Santa Clara, CA, USA). The maximum pulse energy was 1100 mJ and the applied repetition rate was set to 50 Hz. The pulse duration was set to 25 ns. A graphite cylinder (nominal purity >99.99 %) with a diameter of 5 cm and a height of 5 cm was rotated in a fashion to provide homogeneous ablation in the focus of the laser beam. The laser pulse fluence was varied between ~3 and ~11 Jcm^{-2}. Substrates were fixed on a static, grounded substrate holding device kept at approximately 5 cm away from the laser spot on the graphite target. In order to clean the substrates from residual surface contaminants, a glow discharge plasma etching procedure was applied (using 20 sccm of Ar and a voltage of -600 V) with a DC bias power supply (Advanced Converters, Zielonka, Poland). For the deposition the chamber was pumped down to a base pressure of $4 \cdot 10^{-5}$ mbar. Depositions were carried out at base pressure.

9.1.6. IR-PLD of a-C and a-C:N films

a-C and a-C:N deposition was achieved by ablation of a graphite target (99.99 %, GfE, Gesellschaft für Elektrometallurgie, Nürnberg, Germany) with a 1064 nm Nd:YAG laser from Continuum (Santa Clara, CA, USA) operating at a repetition rate of 50 Hz with a pulse duration of 10 ns. Samples were fixed on a grounded substrate holding carrousel situated at a distance of approximately 10 cm from the graphite targets. The diameter of this carrousel was 56 cm whereas the samples were fixed at a diameter of 40 cm on vertical columns. Films were deposited by oscillation of the carrousel with an amplitude of 9 cm (left-right) through the PLD plasma. The movement was one-dimensional and perpendicular to the rotating axis of the graphite target. Prior to deposition, the substrates were Ar-plasma-cleaned from residual surface contaminants with the use of an anode layer source from Veeco instruments (Fort Collins, CO, USA) The anode layer source was operated at a discharge voltage of 2 kV and an argon flow rate of 20 sccm. As process gases Ar (nominal purity <99.999 %) and N_2 (nominal purity <99.999 %) were used. Prior to deposition the chamber was pumped down to a base pressure of $3 \cdot 10^{-5}$ mbar. The total flow was in all cases 30 sccm, whereas the N_2 concentration in the chamber was varied from 0 to 33 %. During deposition, the pressure in the chamber was ~$2 \cdot 10^{-3}$ mbar.

9.2. EXPERIMENTAL – CHARACTERISATION

9.2.1. Structure and chemistry

9.2.1.1. Raman spectroscopy

Raman spectrometers from HORIBA, Jobin Yvon S.A.S. (Villeneuve d'Ascq, France) were used to characterise the structure of carbon bonds in the DLC films. The instruments were operated with lasers at excitation wavelengths of 325, 532 and 633 nm, respectively. Olympus 40× (for 325 nm) and 100× objectives (for 532 and 633 nm) were used to focus the beams on the sample, where in all cases the power of the laser was kept well below 0.25 mW. The entrance slit to the spectrometers was set to 100 µm and holographic gratings with 1800 grooves mm^{-1} were used for 532 and 633 nm and 2400 grooves mm^{-1} for 325 nm excitation. A standard (100) orientated silicon wafer with a Si-peak position of 520 cm^{-1} was used as drift standard for all excitation wavelengths. A resolution of 0.3 cm^{-1} could be achieved with the spectrometer. Mathematical spectrum fitting for the D and G-bands with Gaussian functions was performed with "Peak-Fit" 4.11 from Systat (Point Richmond, CA, USA). Additionally, Raman spectra of films deposited with the ion beam source were fitted with a Breit-Wigner-Fano function (BWF) for the G-band and a Lorentzian for the D-band.

9.2.1.2. XPS (a-C:N)

X-ray photoelectron spectroscopy (XPS) data were acquired using a SSX-100 ESCA spectrometer (Surface Science Labs, Mountain View, CA, USA) equipped with a small spot monochromatic Al Kα source (1486.6 eV). General survey spectra (0 to 1100 eV, 1 scan at 1 eV steps, 800 µm spot size, 150 eV pass energy) were recorded to verify surface constituents. High resolution spectra (10 scans at 0.1 eV steps, 400 µm spot size, 50 eV pass energy) were obtained for the carbon and nitrogen 1s peaks. Compositional information about the a-C:N films was obtained via the Analysis 2000 software package (Service Physics Inc., Bend, OR).

9.2.1.3. ERDA/RBS

Hydrogen contents were determined by ERDA with a 2 MV tandetron accelerator using a beam of 4.2 MeV ^{7}Li ions [156]. The beam was collimated by a 1×2 mm rectangular shaped slit placed in front of the entrance of the experimental chamber which was equipped with two silicon detectors; the Rutherford backscattering spectroscopy (RBS) detector at the scattering angle of θ=150° and the ERDA detector at the recoil angle φ=30°. The incident beam angle and the exit angle as measured from the normal to the sample surface were both 75°. An 11 µm thick aluminium absorber foil was inserted in front of the ERDA detector to block the scattered ^{7}Li ions. Data treatment was performed according to chapter 4.3.1 of the present thesis.

9.2.2. Bulk properties

9.2.2.1. Nanoindentation (ta-C:H)

Nanoindentation measurements were carried out on a Hysitron Triboscope (Hysitron Inc., Minneapolis, MN, USA) using a cube-corner indenter with a tip radius <50 nm. Quantitative hardness and reduced modulus

values were determined from the unloading part of the load-displacement curves, applying the method introduced by Oliver and Pharr [176]. The reduced modulus takes into account the deformation of the indenter tip and the lateral deformation of the sample material via its Poisson's ratio [176]. Influence from the substrate [149] and indentation size effect (ISE) [150,151] were excluded by careful choice of the indentation depth. ISE, the effect that the hardness values increase with decreasing penetration depth cannot be excluded for hard coatings. Thus, for comparison of hardness values, results only from measurements with similar indentation depths were used. Loads ranging from 200 to 750 µN were applied which were held for 8 seconds at the maximum. The resulting indentation depths varied from 5 to 30 % of the film thickness. For indentation depths up to ~60 nm on the 250 nm thick films no significant decrease in modulus, *i.e.* no remarkable influence from the substrate was obtained. Substrate effects on the hardness can be excluded within this range of penetration depths.

9.2.2.2. Nanoindentation (a-C:H)

The nanohardness and the elastic modulus of the deposited films were determined with a Hysitron TriboIndenter TI 900 (Hysitron Inc., Minneapolis, MN, USA) equipped with a Berkovich three sided pyramidal diamond indenter with a nominal angle equal to 63.5^{o}. The instrument was placed in a vibration isolated chamber. A maximum load of 4 mN was applied for the indentations. The load was selected in a fashion to keep the deformation confined within the film. The holding time during indentation was 5 seconds for all measurements. Loading and unloading was performed within 10 seconds for all measurements. The experimental results were corrected for the thermal drift of the equipment and for the uncertainty in the zero position. The reported nanohardness and elastic modulus were averaged of 10 indentations for each sample on different surface positions separated by ~50 µm. The nanoindenter was calibrated by indenting on a fused silica sample with nanohardness and elastic modulus of approximately 10 and 73 GPa, respectively. Measurements were performed in a clean air environment with a relative humidity of ~40 % while the testing temperature was ~22°C.

9.2.2.3. Vickers microhardness (ta-C:H)

Vickers microhardness of DLC films with ~1 µm thickness was measured with a Fischerscope H100C (Helmut Fischer, Sindelfingen-Maichingen, Germany) using a Vickers indenter and loads ranging from 3 to 10 mN. The indentation depth ranged from 10 to 20 % of the coating thickness for the applied loads. The hardness and elastic modulus showed relative standard deviations of less than 10 % for all loads used.

9.2.2.4. Film thickness and intrinsic stress

Thickness and internal stress of the films were determined using stylus profilometers Form Talysurf Series 2 from Taylor Hobson Ltd. (Leicester, GB) and Veeco (Veeco Instruments, Tucson, AZ, USA). Step size measurements were carried out at edges of coated and uncoated areas on the silicon substrates. For stress measurements, the wafers were checked for flatness prior to deposition. During deposition, these samples were fixed only on one end so that the wafer could follow the stress emerging during growth of the DLC film. Care

was taken to avoid possible coating of these samples at the backside. After deposition of ~1 µm thick films, the curvature on the silicon wafers was measured with a stylus force of 1 mN. The stress in the films was calculated using the modified Stoney equation [177].

9.2.2.5. Nanoscratch behaviour (a-C:H)

Nanoscratch tests were performed on the deposited films by using a conical diamond tip of a nominal radius of approximately 2 µm for scratching using a Hysitron TriboIndenter TI 900 (Hysitron Inc., Minneapolis, MN, USA). The scratch velocity was set to 1 µm s^{-1}, while scratching was carried out with constant normal loads of 25 and 500 µN. To avoid effects from neighbouring scratches, the distance between sequential scratches was set to 10 µm.

9.2.3. Surface properties

9.2.3.1. AFM

AFM images of a-C:H and Si-a-C:H films were obtained with an AFM MFP-3D instrument (Asylum Research, Santa Barbara, CA, USA) in air at ambient condition. Silicon nitride tips, triangular cantilevers with a spring constant of 0.1 Nm^{-1} were used. The scan area was 5×5 $µm^2$. Images were recorded in the 'constant-force' mode (feedback electronics and the corresponding software were used to keep the cantilever at constant deflection and to measure the sample topography). Additionally, AFM images of ta-C:H and ta-C:H:N films were obtained with an Dimension 3100 instrument (Veeco, Santa Barbara, CA, USA) in air at ambient condition. The scan area was 5×5 $µm^2$. Images were recorded in tapping mode.

9.2.3.2. Surface Energy

Surface energy of the deposited films was determined by the sessile drop method [152,153] using 2 µl drops of water (18.2 $MΩcm^{-1}$), ethylenglycole (≥99.98 %), bromnaphtaline (≥95 %) and diiodomethane (≥98 %). All measurements were carried out at 22 ºC at constant room humidity of ~30 %. Data treatment was performed according to chapter 4.3.2 of the present thesis.